Integrated *in vitro* and *in silico* studies for optimisation of broad-spectrum antibiotic combination therapy

Inaugural-Dissertation
to obtain the academic degree
Doctor rerum naturalium (Dr. rer. nat.)

submitted to the Department of Biology, Chemistry and Pharmacy
of Freie Universität Berlin

by
Sebastian Georg Wicha
from Erlenbach am Main

2015

II

Diese Dissertation wurde von 2011 bis 2015 unter der Leitung von Prof. Dr. Charlotte Kloft am Institut für Pharmazie der Freien Universität Berlin angefertigt.

1. Gutachter: Prof. Dr. Charlotte Kloft

2. Gutachter: Prof. Dr. Hartmut Derendorf

Disputation am: 12. November 2015

IV

Für Silvia.

Abstract

Emergence of bacterial resistance renders our antimicrobial armamentarium progressively ineffective and requires increasing use of antibiotics that display broad antibiotic activity including drug-resistant organisms. Particularly in hospital-acquired infections, patients very often receive empiric broad-spectrum combination therapy for the first days of therapy until the infective pathogen is identified and the antibiotic spectrum can be tailored accordingly. However, the consequences of combining antibiotics on the pharmacodynamics (PD) are hardly explored yet.

The present thesis aimed at a systemic investigation of the PD consequences of broad-spectrum antibiotic combination therapy using either linezolid (LZD) or vancomycin (VAN) combined with meropenem (MER) on the pathogen methicillin-susceptible *Staphylococcus (S.) aureus*, the most-abundant *S. aureus* strain in Germany and other countries in the EU.

In the experimental part, the single and combined effects of the antibiotics were explored by performance of conventional and dynamic *in vitro* checkerboard and time-kill curve studies. Quantification assays were developed and validated for determination of *S. aureus* (viable plate count assay) and the studied antibiotics (high-performance liquid chromatography) in the growth medium (Mueller-Hinton broth) in order to have a quantitative basis for characterisation of the influence of (changing) drug concentrations of the antibiotic effect. The growth state at drug exposure as a currently neglected influential factor on the determined antibiotic effect, i.e. if bacteria were exponentially replicating (log-phase) or resting (lag-phase) was identified – independently of the inoculum size – with unpredictable consequences which ranged from a higher kill rate (MER), more intense killing (LZD), or, conversely, more rapid regrowth after initial killing (VAN) if in log-phase compared to lag-phase.

In the mathematical Modelling and Simulation part, an adaptive optimal experimental design assessment accompanied the performance of the experiments to exploit the experimental data utmost. Based on the quantified singe-drug effects, a response surface analysis was further developed that allowed for statistical, quantitative assessment of the nature and extent of the pharmacodynamic interaction of the combinations: In combination, LZD fully antagonised the rapid (4-6 h) bactericidal effect of MER alone at ≥0.25 mg/L to bacteriostasis if LZD exceeded its minimal inhibitory concentration (MIC) of 2 mg/L. This interaction was invisible in the conventional, turbidity-based checkerboard analysis (insensitive turbidity threshold) and was solely revealed if bacteria were quantified. VAN and MER interacted partly synergistic (subinhibitory, i.e. below the MICs of VAN of 1 mg/L and MER of 0.125 mg/L) or additive (inhibitory combinations) being bactericidal after 24 h.

Based on the experimental *in vitro* data, a mathematical, semi-mechanistic PD model was developed and extensively evaluated that simultaneously predicted the time-course of bacterial growth and killing under single and combined exposure of LZD, MER and VAN. The semi-mechanistic PD model was linked to published population pharmacokinetic (PK) models of the antibiotics LZD, MER and VAN. The resulting PK/PD models proved their value to translate into the clinical setting by successful

prediction of PK/PD indices for *S. aureus* determined from animal and clinical studies. Hence, a clinical trial simulation with a virtual patient population was performed that indicated that the observed antagonism between LZD and MER might also translate into the clinical setting, whereas the comparator regimen between VAN and MER was even superior with respect to bacterial killing and suppression of adaptive resistance compared to either monotherapy.

The PK/PD model was also used to evaluate currently used and newly recommended alternative dosing regimens for monotherapy with LZD, MER or VAN against *S. aureus*-related infections in dependence of PK covariates using as evaluation criterion a probability of target attainment analysis for bactericidal and/or bacteriostatic effect after 24 h of therapy, respectively: For MER, the standard dosing regimen of 1000 mg TID administered as short-term infusion was reliable up to a creatinine clearance (CLCR) of 140 mL/min (bacteriostatic) or 100 mL/min (bactericidal). Yet, continuous infusion of 1500 mg MER over 24 h was superior to intermittent dosing and provided sufficient bactericidal target attainment up to the highest studied CLCR value of 160 mL/min. For LZD, the standard dosing regimen of 600 mg BID as 1 h infusion was solely bacteriostatic and target attainment was sufficient up to CLCR of 120 mL/min. The present work identified 'front-loaded' therapy with 1200 mg LZD followed by 600 mg as BID being beneficial to augment the antibacterial effect of LZD to a bactericidal effect in a fraction of patients (up to 23% depending on CLCR). For VAN, standard dosing with 1000 mg BID was found unreliable for the majority of the virtual patients. The present work underlines the value of a loading dose of 30 mg/kg total body weight which substantially increased the bacteriostatic PTA which was sufficient for CLCR <80 mL/min. However, the use of intensified dosing intervals (500 mg VAN QID) or continuous infusion of 2000 mg VAN over 24 h was comparable to the therapy with the loading dosing, or superior (sufficient bacteriostatic PTA up to CLCR of 160 mL/min), respectively, at a lower total daily dose than the regimen with the loading doses. Prospective clinical trials that evaluate the efficacy and safety of the proposed alternative dosing regimens based on the present translational approach for LZD, MER and VAN are highly warranted.

Zusammenfassung

Der rasante Anstieg von Antibiotikaresistenzen schwächt unser antibiotisches Arzneistofffarsenal zunehmend und erfordert vermehrt den Einsatz von Antibiotika mit einem breiten antibiotischen Wirkspektrum. Besonders bei im Krankenhaus erworbenen Infektionen erhalten die Patienten häufig empirische Breispektrum-Kombinationstherapien in den ersten Therapietagen bis der infektiöse Erreger identifiziert wird und das antibiotische Spektrum angepasst werden kann. Die Konsequenzen dieser verabreichten Kombinationen von Antibiotika auf die Pharmakodynamik (PD) sind jedoch bisher noch kaum erforscht.

Das Ziel der vorliegenden Doktorarbeit war eine systematische Untersuchung der Folgen einer Breitspektrum-Antibiotikatherapie aus entweder Linezolid (LZD) oder Vancomycin (VAN) in Kombination mit Meropenem (MER) auf den pharmakodynamischen Effekt gegen Methicillin-sensitiven *Staphylococcus (S.) aureus*, der in Deutschland und den meisten EU-Staaten häufigste *S. aureus*-Stamm.

Im experimentellen Teil der Arbeit wurden die individuellen und kombinierten Effekte der o.g. drei Antibiotika in konventionellen und dynamischen *In-Vitro*-‚Checkerboard'-Experimenten und Studien zur bakteriellen Absterbekinetik untersucht. Quantifizierungsmethoden zur Bestimmung von *S. aureus* (Lebendkeimzahlbestimmung) und den o.g. Antibiotika (Hochleistungs-Flüssigkeits-Chromatographie) in bakteriellem Nährmedium (Müller-Hinton Boullion) wurden entwickelt und validiert, um den Einfluss (veränderlicher) Antibiotikakonzentrationen auf den antibiotischen Effekt mittels quantitativer Größen charakterisieren zu können. Die Wachstumsphase zum Zeitpunkt der Anitbiotikaexposition, d.h. ob sich die Bakterien exponentiell teilten (Log-Phase) oder ruhten (Lag-Phase) wurde – unabhängig von der initialen Bakterienkonzentration – als ein bisher vernachlässigter Einflussfakor auf den antibiotischen Effekt charakterisiert, wobei kein einheitliches Muster feststellbar war: In der Log-Phase tötete MER schneller, LZD zu einem höheren Ausmaß, wohingegen für VAN ein deutlich ausgeprägteres Wiederanwachsen nach initialem Absterben im Vergleich zur Lag-Phase sichtbar war.

Mathematische Modellierung und Simulation einschließlich adaptiver Optimierung des Versuchsaufbaus wurden parallel zur experimentellen Durchführung angewendet, um die experimentelle Datenbasis bestmöglich zu verwerten. Basierend auf den individuellen Effekten wurde eine ‚Response-Surface-Analyse' entwickelt, mit welcher die Art und das Ausmaß der PD-Wechselwirkung zwischen den Antibiotika statistisch quantifiziert werden konnte. In Kombination antagonisierte LZD den raschen (4-6 h) bakteriziden Effekt von MER allein ab MER ≥ 0.25 mg/L auf einen bakteriostatischen Effekt für LZD-Konzentrationen oberhalb der minimalen Hemmkonzentration (MHK) von 2 mg/L. Diese Interaktion war im konventionellen, trübungsbasierten Checkerboard-Experiment aufgrund der unempfindlichen Trübungsschwelle nicht erkennbar, sondern nur, wenn die Bakterienkonzentration quantifiziert wurde. Die Wechselwirkung zwischen VAN und MER war tendenziell synergistisch für subinhibitorische Konzentrationen von VAN und MER

unterhalb der MHK (VAN: 1 mg/L; MER: 0.125 mg/L), oder additiv im Falle von inhibitorischen Konzentrationen, wobei dabei ein bakterizider Effekt nach 24 h beobachtet wurde.

Ein mathematisches, semi-mechanistisches PD-Modell wurde basierend auf den erhobenen experimentellen Daten entwickelt und umfangreich evaluiert. Auf dieser Basis konnte der Zeitverlauf des bakteriellen Wachstums und Absterbens unter alleiniger und kombinierter Exposition von LZD, MER und VAN vorhergesagt werden konnte. Dieses semi-mechanistische PD Modell wurde mit publizierten Populations-pharmakokinetischen (PK)-Modellen der Antibiotika LZD, MER und VAN verknüpft. Das resultierende PK/PD Modell bildete die klinische Situation korrekt ab, da es die bestehenden klinisch-genutzten PK/PD-Indices aus Tierexperimenten und klinischen Studien für *S. aureus* erfolgreich vorhersagen konnte. Daher wurde es im nächsten Schritt zur *In-Silico*-Simulation von klinischen Studien genutzt, welche darauf hindeuteten, dass der beobachtete Antagonismus zwischen LZD und MER auch im klinischen Umfeld relevant sein kann, wohingegen das Vergleichs-Therapieregime mit VAN und MER der Monotherapie mit den beiden Einzelsubstanzen sogar hinsichtlich Abtötung der Bakterien und Unterdrückung von adaptiver Resistenzentwicklung überlegen war.

Weiterhin wurde das PK/PD Modell genutzt, um die derzeit klinisch etablierten und alternativen Dosierungsschemata von LZD, MER und VAN für Infektionen mit *S. aureus* in Abhängigkeit von PK-Covariaten zu untersuchen, wobei die Wahrscheinlichkeit eines bakteriziden und/oder bakteriostatischen Effekts nach 24 h Therapie als Bewertungskriterium herangezogen wurde: Für MER war für das Standardtherapieschema von 1 g alle 8 h, verabreicht als Kurzinfusion, zuverlässig bis zu einer Kreatinin-Clearance (CLCR) von 140 mL/min (bakteriostatisch) oder 100 mL/min (bakterizid). Mittels kontinuierlicher Gabe von 1500 mg MER konnte hingegen ein verlässlicher bakterizider Effekt bis zur höchsten untersuchten CLCR von 160 mL/min erreicht werden. Für LZD wurde für die Standarddosierung von 600 mg alle 12 h als einstündige Infusion bis zu einer CLCR von 120 mL/min ein verlässlicher bakteriostatischer Effekt bestimmt. Mithilfe einer Initialdosis von 1200 mg LZD, gefolgt von 600 mg alle 12 h konnte in einem Teil der Patienten (8-23%, abh. von CLCR) sogar ein bakterizider Effekt erzielt werden. Für VAN war die Standarddosierung von 1000 mg alle 12 h, als einstündige Infusion verbreicht, unzuverlässig in der Mehrzahl der virtuellen Patienten. Eine Initialdosis von 30 mg/kg Gesamtkörpergewicht erhöhte die Wahrscheinlichkeit einer zuverlässigen bakteriostatischen Therapie bis zu einer CLCR <80 mL/min. Ein verkürztes Dosierungsintervall (500 mg VAN alle 6 h) oder kontinuierliche Infusion von 2000 mg VAN über 24 h waren der Therapie mit Initialdosis gleichwertig bzw. überlegen (zuverlässige bakteriostatische Therapie bis zu einer CLCR von 160 mL/min) – bei niedrigerer Gesamttagesdosis. Als nächster Schritt sollten prospektive klinische Studien die auf Basis des vorliegenden translationalen Ansatzes vorgeschlagenen Dosierungsregime hinsichtlich ihrer Wirksamkeit und Sicherheit untersuchen.

Acknowledgements

Table of contents

Abbreviations

ACN	Acetonitril
AIC	Akaike's information criterion
AICc	corrected Akaike's information criterion for small sample sizes
AR	Adaptive resistance
ARI	Adaptive resistance interaction
ATCC	American type culture collection
ATP	Adenosine triphosphate
AUC	Area under the concentration-time profile
BI	Bliss independence
BID	Twice daily
CaMHB	Cation-adjusted Mueller Hinton broth
CFU	Colony forming unit
CI	Confidence interval
CIR	Liver cirrhosis
CL	Total clearance
CLCR	Creatinine clearance
CLSI	Clinical Laboratory Standards Institute
C_{max}	Maximum concentration
C_{min}	Minimum concentration
CV	Coefficient of variation
DAD	Diode array detector
E	Effect
EC_{50}	Concentration at which 50% of the maximum effect were obtained
Emax	Maximum effect
GC	Growth control
GRO	Growing state
H	Hill factor accounting for the steepness of the concentration-effect relationship

HPLC	High performance liquid chromatography
IC	Initial condition
IE	intensity of the antibacterial effect
LL	Log likelihood
LLOQ	Lower limit of quantification
log	Natural logarithm
log10	Decadic logarithm
LRT	Likelihood ratio test
LZD	Linezolid
MBC	Minimum bactericidal concentration
McF	McFarland turbidity standard
MeOH	Methanol
MER	Meropenem
MHB	Mueller-Hinton broth
MIC	Minimal inhibitory concentration
MRSA	Methicillin-resistant *Staphylococcus aureus*
MSSA	Methicillin-susceptible *Staphylococcus aureus*
NaCl	Sodium chloride
NCA	Non-compartimental analysis
NLME	Nonlinear mixed-effects modelling
ODE	Ordinary differential equation
OLS	Ordinary least squares
PBPK	Physiologically-based pharmacokinetics
PBSP	Phosphate buffered saline with peptone
PCR	Polymerase chain reaction
PD	Pharmacodynamics
PER	Persisting state
PI	Prediction interval

PK	Pharmacokinetics
PTA	Probability of target attainment
QC	Quality control
QID	Four times daily
REP	Replicating state
RNA	Ribonucleic acid
RSE	Relative standard error
SCR	Serum creatinine
SD	Standard deviation
TFA	Trifluoroacetic acid
TID	Three times daily
t_{max}	Time at which maximum concentration is attained
ULOQ	Upper limit of quantification
VAN	Vancomycin
V	Volume of distribution
Vss	Volume of distribution at steady-state
WT	Total body weight

Symbols

∇	Hessian matrix
$E(y)$	Expectation of y
J	Jacobian matrix
J^T	Transpose of the Jacobian matrix
$P_{k,i}$	k'th model parameter for the i'th individual
σ^2	Variance
$t_{1/2}$	Half-life
$t_{1/2,z}$	Terminal half-life
η	Individual random effects parameter
$\eta_{k,i}$	Vector of individual random effects
θ	Typical parameter
λ_z	Terminal elimination rate constant
Σ	Variance-covariance matrix of θ
Ω	Variance-covariance matrix in of η
ω^2	Variance of η

1 Introduction

1.1 Infectious diseases and anti-infective therapy

Infectious diseases are a leading cause of death in the world. The Global Disease Burden Report 2013 identified lower respiratory tract infections as the second-most abundant cause of death worldwide with ca. 2,652,600 deaths in 2013 [1]. The burden of death for infections is yet not equally distributed around the world: Whereas lower respiratory tract infections are even the leading cause of death in the so called 'developing countries', they are less abundant in the 'developed world' and rank ninth as cause of death [1]. Amongst other factors such as the facile availability of potable water and high hygienic standards, medical personnel have access to an armamentarium of anti-infective agents to treat various infections rendering infections 'manageable' in the developed world. The first 'modern' antibiotic, penicillin, discovered by Alexander Fleming in 1929 [2] being still in clinical use revolutionised the management of infections. For instance, the decrease in mortality rate from combat wounds from 8% to 4.5% from World War I to World War II is attributed to a major part to the use of wound management and antimicrobial therapy [3]. The area between 1940 and 1962 is often referred to as the 'Golden-Age of antibacterial drug discovery' [4], in which the lead structures of sulphonamides, beta-lactams, tetracyclines, aminoglycosides, macrolides, glycopeptides, quinolones and streptogramins were discovered [5]. The following innovation gap in discovery of new drug classes lasted until the year 2000 and is often referred to as the 'Golden-Age of Medicinal Chemistry' in which the lead structures were continuously modified to improve their antibacterial effect [5]. Figure 2 illustrates the availability of anti-infective agents since the 1940's.
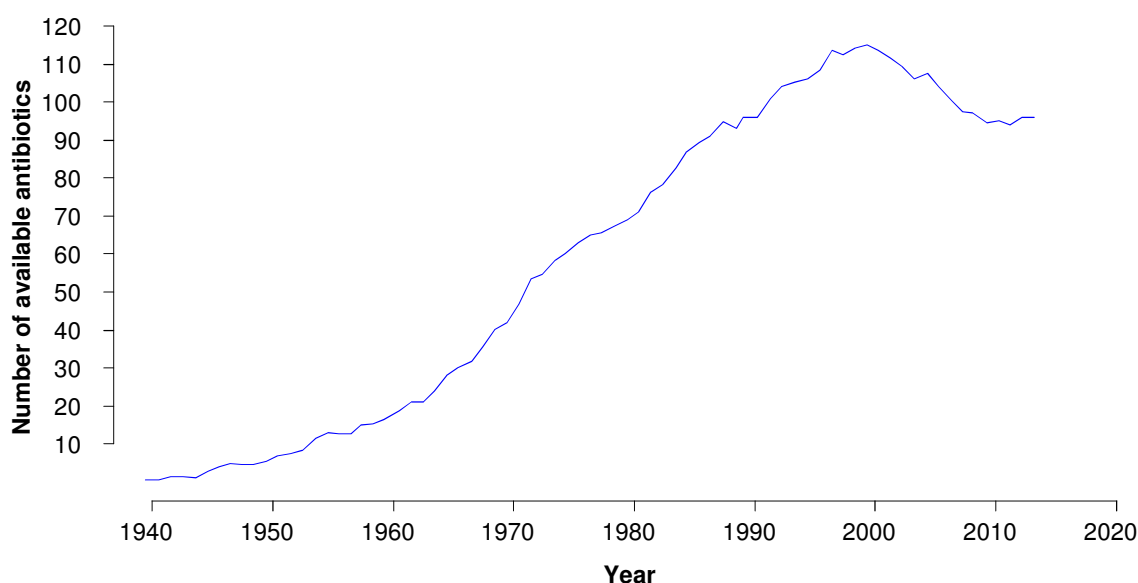
Figure 1: Number of available antibiotics approved for clinical use by the US Food and Drug Administration. Changes over time result from both approval and withdrawal of antibiotic form the market. Modified from [6].

1.2 "No new drugs for bad bugs"

Although there is some loss of 'old' antibiotics in the last years from the market (Figure 1), the treasure trove of anti-infective agents is still richly filled for the time being. Yet, mankind begins to face a situation of increasing resistance of bacteria and a decreasing rate of approval of new anti-infectives – referred to as a "perfect storm" by Cooper and Shlaes [7,8] illustrating this unfavourable development in Figure 2.
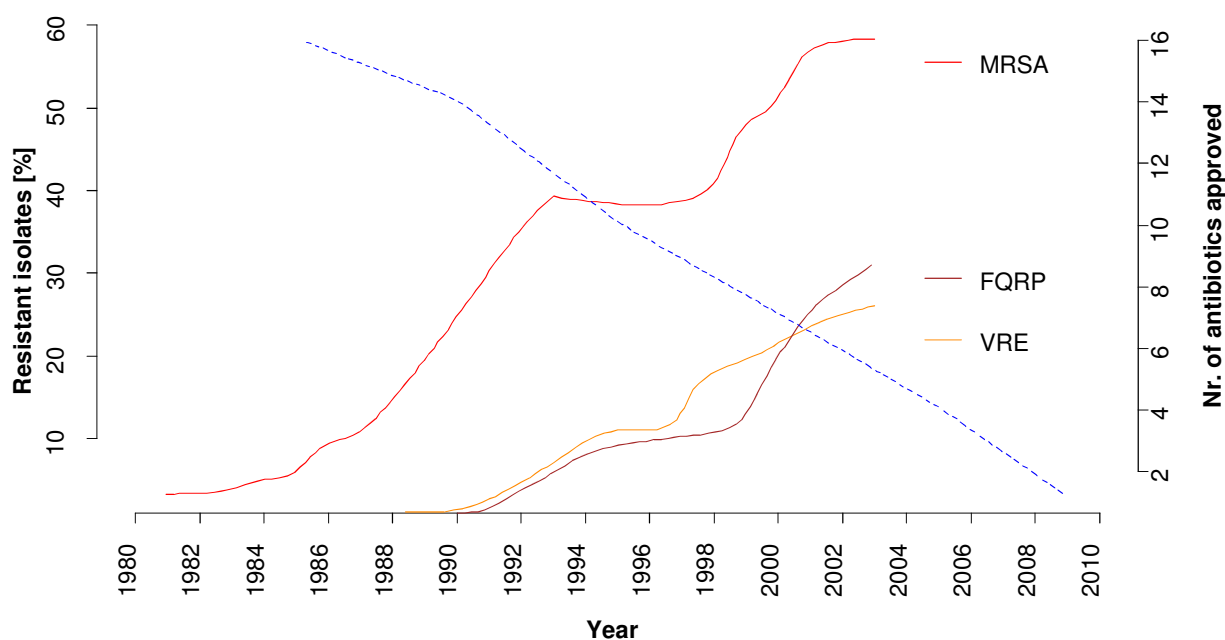
Figure 2: Proportion of antibiotic-resistant clinical isolates of methicillin-resistant *Staphylococcus aureus* (MRSA, solid red line), vancomycin-resistant *Enterococcus* (VRE, solid brown line) and fluoroquinolone-resistant *Pseudomonas aeruginosa* (FQRP, solid orange line) and number of newly approved antibiotics (dashed blue line) from [7].

Cooper stressed the issue of raising cost in drug development accompanied by considerably low financial revenues for antibiotics developed by pharmaceutical industry as a key driving force of this development and calls for both new incentives for industry and governmental leadership [7]. Until new therapies become available, as advocated by the WHO [9], rational use of existing antibiotics under consideration of pharmacokinetic (PK) and pharmacodynamic (PD) principles is imperative to preserve our antimicrobial armamentarium for future use [10]. In particular, deliberate use of ultima-ratio antibiotics is highly important, which are often applied too generous [11].

1.3 Pharmacokinetic/pharmacodynamic analysis in anti-infective therapy

In the following chapter, the conventionally utilised analysis methods as well as the their limitations are presented. Thereafter, the science of pharmacometrics is introduced and the potential benefits of applying pharmacometric techniques in antimicrobial PK/PD analyses is summarised.

1.3.1 Conventional approaches for PK/PD assessment

1.3.1.1 Minimal inhibitory concentration

The minimal inhibitory concentration (MIC) represents the lowest concentration of an antibiotic that inhibits visible growth of a bacterium after incubation for 16 - 20 h at 35° C [12]. The inoculum is usually standardised to $5 \cdot 10^5$ colony forming units (CFU)/mL (see 1.3.1.2). This inoculum is typically prepared with a turbidity-meter using the so called McFarland (McF) turbidity standards [13]. The inoculum is either adjusted by direct suspension of colonies into the growth medium or by growing few colonies to a defined turbidity value before addition of the antibiotic [12]. The MIC is typically determined in liquid growth media such as Mueller-Hinton broth (MHB) [14] and drug concentrations are added to the medium in geometric dilutions in base 2 logarithmic increments centred around a drug concentration of 1 mg/L [12]. Other methods for MIC determination are based on diffusion of an antibiotic into solid agar media: For the disk diffusion method, the diameter of inhibition around an antibiotic-containing disk on an inoculated agar plate is measured. The radius of inhibition is related to the susceptibility of the strain [15]. The same principle of diffusion of the antibiotic into agar is used for the E-test: Hereby, a gradient with increasing antibiotic concentration is applied along a carrier strip, which has the advantage that the MIC is directly readable at the strip where bacterial growth of the strain meets the strip [16]. It is acknowledged that different methods for MIC determination can generate different results [17]. The MIC determination has an inherent uncertainty of ±1 MIC tier [18] and the MIC, as a binary measure, does not reflect the continuity of the antibacterial effect in time and magnitude [19]. Yet, the MIC has proven useful as routine measure of the antibacterial effect in clinical practice, and based on the determined MIC value the bacteria are classified into susceptible, intermediate and resistant to the antibiotic [20].

1.3.1.2 Time-kill curve studies and *in vitro* infection models

In so called time-kill curve studies, the antibacterial effect is measured over time. In principle, a time-kill curve study is performed under similar experimental conditions as MIC determination, but usually in cell culture flasks with larger volumes of the growth medium [21]. In addition, a growth curve is recorded in which the unperturbed growth of the bacteria over time is obtained. In contrast to standard time-kill curve studies, in which drug concentrations are static, i.e. constant over the entire experiment,

dynamic time-kill curve studies are performed in *in vitro* infection models that allow for alteration of drug concentrations to mimic the PK of the antibiotic in the human body [22].

The read-out for the antibacterial effect in MIC experiments is the binary turbidity measure at a single end (time) point. Instead, for time-kill curve studies, a continuous effect measure at several time points is used. This continuous effect measure is most commonly CFU/mL as a surrogate for viable bacteria [21]. For determination of CFU/mL, an aliquot is removed from the cell culture flask, diluted and transferred onto an agar plate which is incubated at bacterium-specific conditions until colonies become visible. Subsequently, colonies are counted and CFU/mL are calculated. Other, much less frequently used, methods to determine viable bacteria include measurement of phosphatase activity [23] and intracellular adenosine-triphosphate (ATP) [24] or the 'Thoma cell counting chamber' [25] to count the total number of bacteria.

In contrast to MIC determination, time-kill curve studies are up-to-date less strictly standardised e.g. with respect to the inoculum size: For many antibiotics, including beta-lactam antibiotics such as meropenem (MER) [21] or glycopeptides such as vancomycin (VAN) [26], the rate of bacterial killing is drastically reduced at higher inocula. Moreover, many investigators aim to assess the antibacterial effect against an inoculum of exponentially growing bacteria. Therefore, a pre-incubation step of the bacteria in drug-free growth medium is performed before addition of the antibiotic. Published studies, e.g. for the oxazolidinone linezolid (LZD), vary largely (0-2 h) with respect to the pre-incubation time [27–31], and the impact of the potential time-dependency of this pre-incubation step on the antibacterial effect has not yet been explored to the author's knowledge.

1.3.1.3 Investigation of the effect of antibiotic combinations

The combined effects of antibiotics are typically assessed with respect to interactions on the level of antibacterial killing and/or resistance development. For assessment of the potential interaction of antibiotics on the level of antibiotic killing, a 'checkerboard' study is performed [32], typically in a well plate format. Two antibiotics are diluted on the x- and y-axis of the well-plate, in similar dilution steps as MIC experiments. Hence, the outermost wells in x- and y-direction, i.e. the rows on the bottom and left of the well plate represent MIC experiments, whereas the inner area of the well plate contains the combinations. For assessment of the interaction, the MIC of the combination experiment, also referred to as fractional inhibitory concentration (FIC), is compared to the MIC of the single antibiotic, based on turbidity [33]. The ratio of FIC to MIC is referred to as the FIC index. If the sum of both $FIC_{drug\ A\ (in\ presence\ of\ B)}/MIC_{drug\ A}$ and $FIC_{drug\ B\ (in\ presence\ of\ A)}/MIC_{drug\ B}$ is smaller than 0.25, a synergistic, for 0.25-4 and indifferent and for >4 and antagonistic interaction is assumed [34]. Due to the considerable simple design and interpretation, the turbidity-based checkerboard study is the most commonly used method to evaluate antibiotic combinations [32]. Yet, as there are different ways to calculate the FIC index [33] and the checkerboard is – as the MIC – prone to reproducibility issues

[35] and the other limitations (1.3.1.1), the checkerboard approach has been criticised [34]. Another approach to determine the FIC index relies on E-test. With this method, the MIC of the single drug experiment, obtained from one E-test strip is related to the FIC of the combination, which is determined by two overlaying E-test strips [36]. Yet, this approach is also inherently variable and limited to a binary read-out.

As advancement, the use of the 'dynamic checkerboard', i.e. a checkerboard experiment with quantification of bacteria [37,38] can explore the effect of antibiotics beyond the binary turbidity-threshold and provides a continuous measure of an interpretation. However, interpretation of the nature of the interaction and discrimination between synergy, additivity and antagonism from unprocessed continuous data possesses challenges due to the unavailability of a standardised interpretation method.

Finally, the kinetics of an interaction between antibiotics can be explored by time-kill curve studies. A usual design for an interaction study using the time-kill curve approach combines antibiotics at concentrations around their MIC value [32]. If an itself inactive antibiotic enhances or diminishes the killing of another antibiotic, synergism and antagonism, respectively is concluded. Discrimination from additivity is yet not standardised, and as for the 'dynamic checkerboard', interpretation of unprocessed data is challenging.

1.3.2 Pharmacometrics for assessment of antimicrobial PK/PD

The term 'pharmacometrics' appeared first in the 1970's indicating the relatively recent history of the research area [39]. Pharmacometrics comprises quantitative methods related to basic and clinical pharmacology, pharmacy and medicine from the field of life-sciences, and statistics, engineering and computational methods from mathematical sciences [39]. Pharmacometric techniques are applied in the characterisation of the PK, PD and PK/PD relationship of a drug.

1.3.2.1 Analysis of PK

The concentration-time course of an intravenously applied drug in the human body is determined by the processes of distribution, metabolism and excretion. For extravascular, e.g. oral or cutaneous administration, also the liberation of the drug from the galenic vessel and subsequent resorption shape the kinetic profile of a drug in the human body [40].

Non-compartmental analysis. A model-independent analysis method of the PK is the non-compartmental analysis (NCA) [41]. The NCA uses log-linear regression for determination of the (terminal) slope of the concentration time-profile (λ_z) and the trapezoidal rule to calculate the area under the concentration-time profile (AUC) for computation of the PK parameters total clearance (CL) and volume of distribution in steady state (V_{ss}). Additionally, the time t_{max} at which the maximum

concentration C_{max} is observed, and the elimination half-life $t_{1/2,z}$ are often reported. The application of NCA is limited to rich PK data and assumes linear PK of first-order processes.

Compartmental analysis. Compartmental analysis represents a model-dependent analysis method to describe the PK of a drug [42]. Thereby, the distribution of a drug in the human body is approximated by a number of compartments (typically one to three-compartment models) and a considerably low number of model parameters such as compartment volumes, transfer rates between the compartments and elimination rate constants. Those models are capable to describe the entire concentration-time profile of a drug in a continuous manner, but due to their empiric nature, the physiological interpretation of the parameter estimates is limited. To overcome such limits, 'physiologically-based pharmacokinetic' (PBPK) models aim at assigning a physiological meaning to model compartments [43]. For instance, in PBPK models each organ is represented by an individual compartment and physiological organ volumes as well as perfusion properties are considered. Yet, this level of detail in the parameterisation is hardly supported solely from conventional clinical trial data, in which the PK of the drug is usually exclusively determined in plasma. Hence, for PBPK models other data sources such as physicochemical properties of the drug or further *in vitro* investigations have to be taken into account. Yet, in spite of the unavailability of clinically-evaluated PBPK models for the investigated antibiotics LZD, MER and VAN, the PBPK approach was not used in the present work.

Variability. As PK data in clinical studies originates from several patients, numerous methods to determine the PK parameters in the study population and to quantify variability in the PK have evolved. In the naïve pooling approach, the study data is pooled if it originated form a single individual [44]. Hence, solely point estimates of the PK in the population can be derived and variability between patients (inter-individual variability) is neglected.

The 'two-stage' approach is capable to quantify variability between patients [45]. In 'stage one', the individual PK parameters are obtained from the individual PK profiles. In 'stage two', descriptive statistics on the obtained individual PK parameters is employed to derive point estimates and dispersion parameters to describe the population of interest. The advantage of the computational and mathematical simplicity of the two-stage approach is accompanied by several disadvantages such as the requirement of a balanced, rich sampling study design and systematic overestimation of inter-individual variability as solely a single dispersion parameter is calculated and further sources of variability such as residual variability within an individual are neglected.

Application of nonlinear mixed-effects modelling (NLME) in the 'population approach' is to-date the most elaborated methodology to quantify variability in PK in a study population [42], which has numerous advantages: Population PK models are hierarchical and can accommodate different levels of variability. Usually, a distinction between intra-individual and inter-individual variability of the PK parameters and residual variability in the PK profile is made. Moreover, the population approach allows for estimation of the point and various dispersion estimates from sparse or unbalanced study

designs, as all data is analysed simultaneously applying the Bayesian methodology. The population approach enables to include patient characteristics (covariates) into the mathematical model aiming at explaining parts of the observed, unexplained inter-individual variability. Moreover, other sources of variability (study arm, study site, inter-occasion) can be quantified. Population PK models hence are the most reliable basis to perform simulations, e.g. to develop dosing regimens that are tailored to patient characteristics. Consequently, population PK models of the investigated antibiotics were to be utilised as PK basis for the PK/PD investigations in the present thesis.

1.3.2.2 Analysis of PD

The PD studies the drug action and effect in a quantitative fashion. In the field of antibiotics, an experimental measure for the PD is the bacterial load, expressed by turbid growth or inhibition of growth in the MIC, as binary effect measure (1.3.1.1) or CFU/mL (1.3.1.2) as a continuous effect measure [21]. In a clinical setting, also inflammatory biomarkers, mortality or duration of hospitalisation are considered as PD surrogates [46].

Empiric PD modelling. If a time-independent effect measure per antibiotic concentration is considered, empiric mathematical models can be employed to quantify the concentration-effect relationship. Linear regression can be used to describe simple linear concentration-effect relationships, whilst non-linear regression is employed for more complex concentration-effect curves utilising e.g. the sigmoidal Michaelis-Menten model [47]. However, frequently several, time-dependent effect measures per antibiotic concentration, e.g. in time-kill curve studies (1.3.1.2), are available. In order to analyse such data with empiric concentration-effect models, summary PD endpoint measures such as the area between growth and kill curves in time-kill curve studies [48], the initial slope of the time-kill curve [49], the time until nadir bacterial load [50] or simply the bacterial load at the end of the time-kill curve [51,52] are utilised.

Response surface analysis for antibiotic combinations. For quantification of combined drug effects and assessment of the nature of potential drug interactions, a response surface analysis can be performed [53]. As the empiric models, the response surface analysis relies on a time-independent effect measure per antibiotic concentration. The observed single-drug effect is either processed directly (non-parametric) or computed by the previously obtained empiric mathematical concentration-effect relationship (parametric). Those single-drug effects of two antibiotics are utilised to predict an anticipated combined additive effect by means of various 'null-interaction' models [53], of which 'Loewe Additivity' [54] and Bliss Independence (BI) [55] are most frequently used. The difference between the anticipated additive and the observed effect is calculated to assess deviation from additivity: Positive deviation (i.e. a greater than anticipated additive effect) indicates synergy whilst negative deviation (i.e. a smaller than anticipated additive effect) indicates antagonism.

Time-kill curve modelling. To mathematically model the time course of the antibacterial effect, e.g. data originating from time-kill curve studies, more complex mathematical models have to be employed. Time-kill curve modelling usually relies on (systems of) ordinary differential equations (ODEs) capturing the change in bacterial load over time [56]. The complexity of such ODE systems is very heterogeneous: Time-kill curves models can be considerably simple and consist of a single differential equation [57]. In the recent years, more complex models have been developed [56] and due to their mechanistically-motivated elements, are referred to as semi-mechanistic models [58]. Those models go beyond pure description of the observed experimental data, but aim at characterising the underlying system in a qualitative and quantitative way.

1.3.2.3 Integrating PK and PD

Pharmacokinetic/pharmacodynamic indices. If summary endpoints for the PK and PD are used, the efficacy of an antibacterial drug and the suitability of a dosing regimen are assessed by PK/PD indices that relate a PK to a PD parameter. Thereby, the PK parameter is derived from the PK profile of the antibiotic, whilst the PD parameter is conventionally the MIC in this approach [59].

The impact of the dosing regimen on the effectiveness of an antibiotic treatment has already been noted in very early times of antibiotic research: Harry Eagle et al. reported for penicillin in 1950 that lower total doses are required if the dosing interval was decreased and serum concentrations should exceed the MIC [60]. Yet, this knowledge on the time- and concentration-independent effect (if above the MIC) for penicillin was not further exploited during the following 'Golden Age' of antibiotic discovery until Craig and co-workers started their seminal studies to systematically evaluate the PK/PD relationship of various antibiotic drug classes in the late 1980's [61]. They realised that some antibiotics such as aminoglycosides displayed 'concentration-dependent' killing whilst other drugs, such as beta-lactams, exhibited 'time-dependent' killing [59]. Moreover, some drugs such as macrolides or aminoglycosides stimulate moderate or long 'postantibiotic effects' up to ca. 10 h [62,63], i.e. a persistent antibacterial effects after removal of the antibiotic. When the antibacterial effects were explored, it was noted that solely unbound drug concentrations stimulated an antibacterial effect [64], Hence, PK/PD indices should be based upon unbound drug concentrations [59].

Craig integrated those findings and proposed three MIC-based PK/PD indices: (i) $f\mathrm{C_{max}}/\mathrm{MIC}$, i.e. the unbound ($f$) peak concentration divided by the MIC for concentration-dependent drugs with long perstistent effects, (ii) $f\mathrm{AUC}/\mathrm{MIC}$, i.e. the unbound AUC divided by the MIC for drugs being both concentration and time-dependent to some degree with moderate persistent effects and (iii) $f\mathrm{T_{>MIC}}$, i.e. the time or the percentage of the dosing interval that unbound drug concentrations exceed the MIC for drugs that display time-dependent killing and no or very short persistent effects [59]. PK/PD indices and breakpoints, that are associated with an adequate antibacterial effect can be derived *in vitro*, animal models and clinical studies [65].

Figure 3 displays the PK/PD relationship of the beta-lactam antibiotic cefotaxime against the Gram-negative bacterium *Klebsiella pneumoniae*, derived from a dose-fractionation study in a neutropenic mouse infection model of pneumonia [66]. In is apparent, that $T_{>MIC}$ is the most suitable PK/PD index for cefotaxime in this setting.
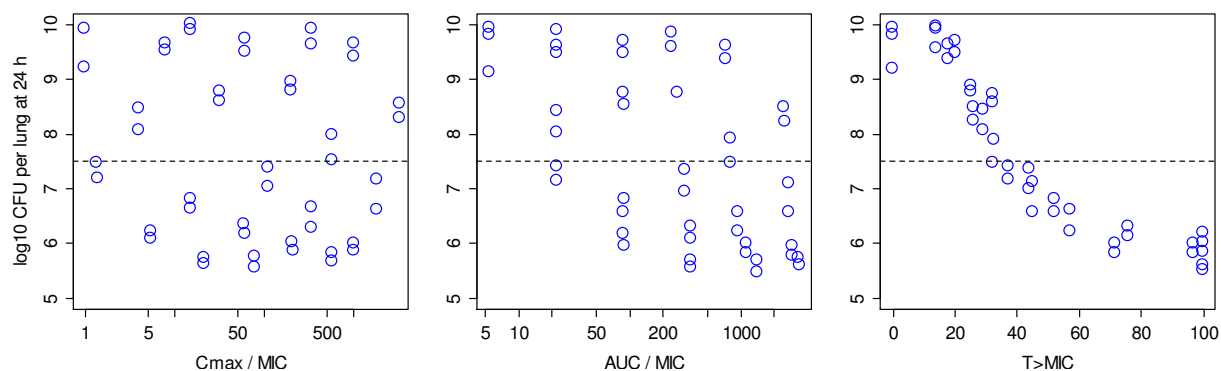
Figure 3: Relationship between CFU of *Klebsiella pneumoniae* in the lungs of neutropenic mice after 24 h of therapy with cefotaxime and the three PK/PD indices (see text). PK/PD indices were derived from total drug concentrations due to the low (<20 %) protein binding of cefotaxime to mouse serum [59]. Each point reflects number of bacteria at 24 h from one mouse. The dashed line represents the number of bacteria at the initiation of therapy. Data redrawn from [66,67].

Time-continuous PK/PD modelling. Although, PK/PD indices have been proven as useful tools for dosing decision making, also in clinical practice [68], this concept simplifies both PK and PD to summary endpoint measures. In continuous PK/PD modelling, the entire concentration-time profile of the antibiotic (PK) is linked to a mathematical time-kill curve model (PD). This approach captures the entire time course of the effect-time curve [56]. Depending on the experimental data, both single drug and combinatory time-kill curve studies can be described by mathematical models. Hence, *in vitro* results can be translated into a clinical perspective if human PK data is used for PK input.

Clinical trial simulation. If population PK models are employed as PK component of the PK/PD model, also inter-individual variability can be considered in PK/PD modelling, leading to virtual clinical trials which allow for assessment of the effectiveness of various dosing regimens or drug combinations. Moreover, if population PK models are employed that include patient-specific characteristics, the impact of those PK-related covariates on the PD can be quantified. Yet, due to the requirement of population PK models and experimentally labour-intense time-kill curve data for PD, and maybe also due to the complexity of the mathematical PK and PD models in this setting, this approach is currently rarely used in the PK/PD assessment of antibiotics.

1.3.2.4 Optimal study design

As outlined above, time-kill curve studies are labour- and personnel-intense as being non-automated. Moreover, if time-kill curve studies are analysed by complex mathematical models, usually many scenarios (e.g. drug concentrations) and frequent sampling is required to support all parameters of the mathematical model with sufficient information. Hence, efficient planning of time-kill curve studies is required to reduce the workload to a reasonable extent. Mathematical optimal design strategies have evolved as useful tools to support study planning [69]: Under the assumption of a mathematical model with defined parameter values which is capable to describe the experiment, optimal design approaches can be used to minimise the variance of the model parameters as a function of the study design variables such as the investigated drug concentration or the number and precise timing of sampling points to determine the bacterial load. Minimal parameter variance may lead to less biased and more precise parameter estimates of the mathematical model, which is a prerequisite to perform reliable simulations. Frequently, a lower number of 'optimal' scenarios have to be experimentally performed to obtain the same parameter precision as with conventional study designs.

In clinical drug development the concept of 'learning and confirming' was introduced by Sheiner in 1997 [70]. In the learning step, data from earlier stages of clinical development are analysed to generate hypotheses, which are prospectively evaluated. Such prospective trials can be confirmatory if the original hypothesis was confirmed or can be a learning study if previously undetected effects were elucidated. Finally, learning steps should converge to confirming steps. Optimal study design can streamline such repetitive circles of 'learning and confirming' and is referred to as 'adaptive optimal design' as the study design is iteratively optimised [71]. Application of adaptive optimal design techniques in parallel to the experimental conduct in pre-clinical time-kill curve experiments may be associated with similar benefits as mentioned above, but is – to the author's knowledge – very infrequently done in preclinical research.

1.4   Antibiotic therapy

The following chapter introduces the clinical profiles of key antibiotics that represent the backbone of therapeutic regimens in treating infections in hospitalised patients, frequently being critically ill [72]. Moreover, the rationales behind antibiotic combination therapy are reviewed. Finally, the microbiological properties of one of the most-abundant pathogens in the hospital, *Staphylococcus aureus*, as well as its typical infections are introduced.

1.4.1   Key antibiotics and their clinical profiles

1.4.1.1 Meropenem

MER is a beta-lactam antibiotic belonging to the chemical subgroup of the 'carbapenems' [73], formerly also called 'thienamycins' named after the chemical lead structure isolated from *Streptomyces cattleya* [74]. The antibacterial target of MER is located in the bacterial cell-wall at so called 'penicillin-binding proteins', since they were originally discovered by labelling experiments with radioactive penicillin G [75]. One of those penicillin-binding proteins is the transpeptidase which cross-links peptidoglycan precursors of the bacterial cell-wall [76]. MER inhibits the transpeptidase and also stimulates secretion of autolysins which eventually cause lysis of the bacterium [77]. This mode of action frequently stimulates a rapid bactericidal effect, i.e. a reduction of the initial bacterial load (inoculum) by ≥99.9%. MER displays a very broad antibacterial spectrum ranging from Gram-negative to Gram-positive organisms. MER is not susceptible to degradation by a wide variety of beta-lactamases [73], including recently emerged extended-spectrum-beta-lactamases [78], to which beta-lactams of earlier generations are substrates. Yet, the antibacterial spectrum of MER has a gap for MRSA [73]; the minimal inhibitory concentrations (MIC, see 1.3.1) of MER against MRSA is frequently >8 mg/L. *S. aureus* isolates with MIC values ≤2 mg/L are methicillin-susceptible and hence commonly also considered susceptible to MER [79].

After a standard dose of 1000 mg administered as 30 min i.v. infusion, MER reached a maximum mean plasma concentration of 55 mg/L in healthy volunteers [80]. As a considerably hydrophilic molecule, MER displays a low volume of distribution of ca. 20 L [80]. Plasma protein binding of MER is 2% [81]. The area under the (unbound) concentration time curve (AUC) in the interstitial fluid of the lung or muscle in steady state was 41% or 60%, respectively, of the AUC in serum indicating adequate tissue distribution of MER [82]. The only metabolite of MER is produced by hydrolysis of the beta-lactam ring which displays no antibacterial activity. 60-80% of MER is excreted unchanged via urine; 15%-25% are recovered from urine as open-ring metabolite [73]. The renal clearance of MER is 219 mL/min [80], being higher than the glomerular filtration rate of 120 mL/min which indicates tubular secretion of MER. The elimination half-life of MER is ca. 1 h [73] which requires three times daily (TID) dosing of the standard dose of 1000 mg to achieve sufficient exposure in patients with normal renal function. The label suggests less intensified twice-daily (BID) dosing with 1000 mg MER for a creatinine clearance ≤50 mL/min [81]. Continuous infusion of MER is an alternative dosing strategy gaining more and more popularity to treat infections with elevated MIC values close to the susceptibility breakpoint [72,83]. MER displays a favourable safety profile and even high doses of 2000 mg TID are generally well tolerated [81,84].

1.4.1.2 Linezolid

LZD is the first-in-class antimicrobial agent of the comparably young antibiotic drug class of the 'oxazolidinones' being introduced into the market in the year 2000 [5]. The mode of action of LZD is found in inhibition of bacterial protein synthesis. In contrast to other protein-synthesis inhibitors, such as macrolides or aminoglycosides, LZD acts at an early stage of this vital process in the bacterial metabolism and inhibits the formation of the ribosomal initiation complex, i.e. the transfer-(t)-ribonucleic acid (RNA)-ribosome-messenger-(m)RNA ternary complex [85]. LZD displays an antibacterial effect against Gram-positive bacteria, including MRSA [86,87]. The magnitude of the antibacterial effect of LZD is mostly bacteriostatic in nature, i.e. the reduction of the inoculum is <99.9%. Solely against streptococci, LZD can exert a slow bactericidal effect at high concentrations [87]. Gram-positive bacterial isolates with a MIC of ≤4 mg/L are considered susceptible to LZD [20]. Gram-negative bacteria are generally resistant towards the effect of oxazolidinones [88], possibly due to the presence of efflux pumps that decrease intracellular LZD concentrations [89].

The standard dosing regimen for LZD is flat-dosing of 600 mg BID [90]. Both intravenous and oral formulations of LZD are available and are considered equivalent due to the bioavailability of LZD of 100% [90]. After a standard dose of 600 mg administered as intravenous infusion over 0.5 h, a mean maximum serum concentration of ca. 13 mg/L is obtained. The volume of distribution is 30-50 L, which approximates total body water [91]. LZD is moderately bound to plasma proteins and reported values for concentration-independent plasma protein binding range from 12.4% [92] to 31% [90]. LZD displays good penetration into interstitial fluid of well-perfused tissues [92,93] and the epithelial lining fluid of the lung [94] and LZD concentrations were similar to concomitant plasma concentrations in steady state. LZD is metabolised into two inactive metabolites, which contributes to a non-renal clearance of 65% of the total body clearance [91]. This leads to an elimination half-life of LZD in serum at steady-state of ca. 3.4-7.4 h [95]. The safety profile of LZD is favourable. Yet, the label limits use of LZD to <28 days due to an increased likelihood of myelosuppression for longer treatment durations [90].

1.4.1.3 Vancomycin

VAN is an antibiotic belonging to the group of 'glycopeptides' [96]. VAN exhibits its antibacterial effect in the cell-wall of the bacterium by forming a complex with C-terminal D-alanine residue of the peptidoglycan precursors [76]. This interruption of the cell-wall synthesis stimulates a bactericidal effect, which has often been reported to be less rapid than that of beta-lactams [97]. VAN displays its antibacterial effect solely against Gram-positive bacteria including MRSA. *S. aureus* isolates are considered susceptible to VAN if MIC values are ≤2 mg/L [20]. The considerably large molecular mass of 1450 Da [96] renders VAN inactive against Gram-negative bacteria, as it is believed that VAN cannot penetrate the outer membrane of the Gram-negative cell-wall [76].

The standard dosing regimen of VAN reported in the label is 1000 mg BID as 1 h intravenous infusion [98,99]. With this dosing regimen, a mean maximum concentration of 65.7 mg/L was attained in steady state in healthy volunteers, which declined to 7.9 mg/L in mean before the next dose [98]. The volume of distribution in steady-state was ca. 0.6 L/kg [98]. Protein binding of VAN is variable and values from 10% to 50% are reported [96]. Distribution of unbound VAN into soft tissue was assessed under continuous infusion and steady-state concentrations were ca. 30% of simultaneous plasma concentrations [100]. Trough concentrations in epithelial lining fluid were between 1.4 and 2.8 mg/L whereas concomitant plasma concentrations ranged between 20.9 and 23.3 mg/L [101]. 80% - 90% of VAN are eliminated unchanged via the kidney. The elimination half-life is reported to be within 6 – 12 h [96]. To achieve sufficiently high VAN exposure in presence of the partly hindered tissue distribution, alternative dosing regimens of 15 mg/kg BID with a loading dose of up to 30 mg/kg have been suggested [102]. VAN use is associated with several adverse events including infusion-related anaphylactic reactions, nephrotoxicity and ototoxicity [99]. However, those adverse reactions were stimulated by impurities in early formulations of VAN and their rate appears to be much lower today [102]. Yet, to ascertain safe and effective VAN exposure, therapeutic drug monitoring of VAN is recommended and trough concentrations between 10 and 20 mg/L are targeted [102].

1.4.2 Antibiotic combination therapy

Antibiotics are combined in an effort to enhance their antibacterial spectrum, to benefit from a synergistic effect, to decelerate the development of resistance and to potentially also select against emerging resistant strains [103].

Enhancement of the antibacterial spectrum. As a single 'full-spectrum' antibiotic is not available, extending the antibacterial spectrum by combining different antibiotics is a vital option in initial empiric treatment of severe infections when the causative pathogen and its inherent susceptibility pattern are unidentified yet. Microbiological results and pathogen susceptibility are available at earliest after 1-2 days after sampling. Beforehand, a broad antibacterial spectrum with high antibacterial activity is the most important reason to apply combination therapy in this critical situation, as no coverage of the infective organism is equivalent to no treatment of the infection with potentially deleterious consequences [104]. Combinatory regimens of MER with either LZD or VAN are most frequently employed initial treatment regimens of severe nosocomial infections (e.g. pneumonia), because they provide considerably large and partly complementary antibacterial spectra including multi-drug resistant Gram-positive and Gram-negative pathogens [105].

Synergy. Synergism on the level of PD, i.e. the rate and extent of bacterial killing is the number two reason for combining antibiotics. Despite a manifold of synergistic interactions between antibiotics described *in vitro* [106], only few combination regimens prove their value on the level of reduced mortality rates in clinical practice, such as the combination of beta-lactams and aminoglycosides

against *Pseudomonas aeruginosa* bacteraemia [46]. Both the fact that the clinical setting is much more variable than well-controlled *in vitro* studies [32] and that the PD interaction is frequently strain- or even isolate-specific [107] might explain this translational gap.

Reduction of the emergence of resistance. Thirdly, antibiotic combinations are used to minimise resistance development. The rationale behind this concept is that a bacterium being resistant to one antibiotic is still susceptible to the other combination partner and it is unlikely to observe simultaneous resistance development to both antibiotics [103]. Yet, the selection for resistance is also a function of the selective pressure which might also be influenced by the nature of the PD interaction on the rate and extent of bacterial killing [108,109].

Risk factors. In contrast to these potential benefits, the risks of combination therapy are frequently neglected, namely a potentially enhanced spectrum of adverse events or even antagonistic interactions between the combined drugs [32]. Particularly, the latter might possess an uncontrollable risk in empiric therapy and both favourable and unfavourable PD interactions may occur, dependent on the bacterial isolate. Therefore, profiling of the PD interactions of empiric combination regimens and *likely suspected* bacterial strains is required to guide healthcare personnel to select the most favourable combinatory regimen for initial empiric therapy.

1.4.3 *Staphylococcus aureus* as a major problematic pathogen

Staphylococcus (S.) aureus is a Gram-positive, round-shaped coccal bacterium associated in bunches similar to grapes [110]. *S. aureus* grows on agar in 'golden', haemolytic colonies and can be rapidly distinguished from other staphylococci using the coagulase- and catalse-reaction for clumping factor and catalase activity, respectively, being specific for *S. aureus* [110]. *S. aureus* is frequently isolated as part of the commensal normal skin flora [110,111], but can become infectious in presence of a compromised host immune system, a defect in the skin or insertion of a (contaminated) foreign body [110]. Once an infection is established, *S. aureus* has developed several immune evasion mechanism that hinder the human body in eradicating the *S. aureus* infection: Those evasion mechanisms include secretion of exoproteins that inhibits complement activation, resistance to phagocytosis by intracellular survival and resistance to lysozyme [112].

Typical infections of *S. aureus* represent localised skin infections, e.g. folliculitis [110]. Other typical entry portals into the human body – particularly in hospital-associated infections – include the lung, in which *S. aureus* can cause severe, necrotising pneumonia, or surgical and decubital wounds [110]. Those initially local infections can become systemic leading to bacteraemia [110]. *S. aureus* infections are a leading cause of sepsis, a severe inflammatory disease state associated with rapid organ dysfunction, particularly of the respiratory and cardiovascular system [113] caused – among other factors – by the released exoproteins which often act as toxins [110,114]. The international 'Surviving

Sepsis Campaign' identified rapid administration of empiric combination antimicrobial therapy *within one hour* after recognition of severe sepsis and septic shock as a key goal of therapy [115]. Thereby, the spectrum of the antibiotic regimen must cover the infective organism; inappropriate selection of this initial treatment is a significant risk factor for increased mortality [116]. As outlined in 1.2, the antibacterial spectrum of this initial regimen should – in addition to broad Gram-positive or Gram-negative coverage – also cover multi-drug resistant organisms. Due to an increasing burden of MRSA in overall >50% of hospital-associated infections [111], frequently LZD or VAN as ultima-ratio antibiotics with MRSA activity are added to the antibiotic regimens [105]. Yet, the burden of MRSA is geographically highly diverse and ranges from 0.7% in Sweden to 53.8% in Portugal in 2012 [117]. In Germany, 15.4% of the *S. aureus* isolates were MRSA [117]. Hence, in initial empiric therapy, even when staphylococcal infection is confirmed, the majority of patients would not require additional coverage by LZD or VAN in Germany, since even in high-risk settings, methicillin-susceptible *S. aureus* (MSSA) is dominant amongst staphylococcal infections. To avoid uncontrollable and undesired effects of the combination therapy, as outlined earlier (1.4.2), de-escalation to targeted therapy should be done as early as the infective organism is identified [115].

1.5 Objectives

Combinatory regimens of MER with either LZD or VAN are frequently employed for initial treatment of severe nosocomial infections. The combination of LZD with a carbapenem such as MER against MSSA has not been evaluated systematically, although LZD combined with MER vs. MSSA is a commonly utilised treatment option in patients with risk factors until MRSA is ruled out [105]. A published *in vitro* interaction study between the alternative antibiotic VAN and MER indicated no unfavourable interaction when subinhibitory concentrations of VAN were added to MER [118], but evidence about potential drug-drug interactions at higher concentrations of VAN is lacking.

The objective of the present thesis was to contribute to the understanding of the combination therapy between either LZD or VAN combined with MER against MSSA. As strategy, the single drug effects as well as the combinatory effects were to be explored by an integrated *in vitro-in silico* approach in which experimental data from various *in vitro* studies on the antibacterial effect were combined with PK/PD modelling to assess the observed drug effects in a translational framework. Thereby, the present work was motivated by both clinically-orientated (C), as well as methodologically-motivated (M) research questions.

In detail, the objectives of the present thesis ranging from experimental to *in silico* modelling and simulation studies were as follows:

Experimental:

- Development and validation of quantification assays for the study drugs LZD, MER and VAN in bacterial growth medium as well as for the bacterium methicillin-susceptible *S. aureus* to provide a sole basis of quantitative data for pharmacometric analysis (→ M).
- Elucidation of conventionally-used turbidity-based screening techniques for combinatory effects for antibiotic combinations ('conventional checkerboard') and comparison to techniques with a continuous effect measure ('dynamic checkerboard') (→ M).
- Experimental performance of time-kill curve studies with the LZD, MER and VAN alone, as well as double combinations of LZD/MER and VAN/MER against methicillin-susceptible *S. aureus* to explore the time-dependency of the (combined) antibiotic effects (→ C).
- Exploration of the impact of the growth-phase of the bacterial inoculum at drug exposure on the antibiotic effects, as a currently neglected possibly influential experimental factor (→ M).
- Investigation of the time course and magnitude of potential adaptive resistance development of methicillin-susceptible *S. aureus* under exposure to LZD, MER and VAN (→ C).

Modelling and Simulations:

- Elaboration and performance of a response-surface analysis for quantification and statistical assessment of drug interactions based on summary endpoint PD measures for checkerboard and time-kill curve data (→ CM).
- Characterisation of the entire time course of the antibacterial effect observed in the time-kill curve studies with a mathematical semi-mechanistic PD model (→ CM).
- Link of the semi-mechanistic PD model to published patient population PK models of LZD, MER and VAN to translate the observed single and combined antibacterial effects into the clinical setting (→ CM).
- Characterisation of the potential impact of patient covariates on the PD of the LZD, MER and VAN in a clinical trial simulation to evaluate established and alternative dosing regimens of the study drugs (→ C).

2 Materials and methods

2.1 Materials

2.1.1 Chemicals and consumables

5 mL tubes (sterile)	BD, Le Pont de Claix, Germany
48 well plates (transparent, flat bottom, sterile)	VWR, Darmstadt, Germany
96 well plates (transparent, conical bottom, non-sterile)	Nunclon, Thermo Fisher, Dreieich, Germany
Accucore® C-18 HPLC column (2.6 µm, 100 x 2.1 mm)	Thermo Fisher, Dreieich, Germany
Acetonitrile, super gradient-grade	VWR, Darmstadt, Germany
Bacterial storage equipment, Microbank®	Pro-Lab Diagnostics, Neston, UK
Calcium chloride dihydrate, LOT: 233199810	Carl Roth GmbH, Karlsruhe, Germany
Cannulas (disposable, various sizes)	B. Braun, Melsungen, Germany
Cell culture flasks (50 mL) with vented caps	BD, Le Pont de Claix, France
Columbia Agar, LOT: 433205700	Carl Roth GmbH, Karlsruhe, Germany
Disodium hydrogen phosphate, LOT: BCBK2569V	Sigma-Aldrich, Steinheim, Germany
Linezolid (free base), LOT: PF-00184033	Pfizer, Groton, CT, USA
Magnesium chloride hexahydrate, LOT: 293198927	Carl Roth GmbH, Karlsruhe, Germany
Meropenem trihydrate, LOT: 111202	Dainippon Sumitomo Pharma, obtained via Astra Zeneca Research Compound Program
Membrane filters, Whatman FP30/0.2 CA-S (0.2 µm) (various LOTs)	GE Healthcare Ltd., Little Chalfont, UK
Methanol, super gradient-grade	VWR, Darmstadt, Germany
Milli-Q® water, purified by Milli-Q Plus®	Millipore, Eschborn, Germany
Mueller-Hinton broth (unadjusted cation content), LOT: 1238500	Oxoid GmbH, Wesel, Germany

Mueller-Hinton broth II, (cation content adjusted by manufacturer to 20-25 mg/L Ca^{2+} and 10-12.5 mg/L Mg^{2+}), LOT: BCBG3391V	Sigma-Aldrich, Steinheim, Germany
Peptone (from Casein), LOT: 072175575	Carl Roth GmbH, Karlsruhe, Germany
Pipette tips (200 µL, 1000 µL, 5000 µL)	Eppendorf, Hamburg, Germany
Potassium dihydrogen phosphate, LOT: 081M00041V	Sigma-Aldrich, Steinheim, Germany
Rotilabo petri dishes	Carl Roth GMbH, Karlsruhe, Germany
Safe lock vials 1.5 mL	Eppendorf, Hamburg, Germany
Sodium chloride, LOT: 211096	ChemPur, Karlsruhe, Germany
Syringes (disposable, various volumes)	B. Braun, Melsungen, Germany
Triflouroacetic acid (99.9%)	Carl Roth GmbH, Karlsruhe, Germany
Vancomycin hydrochloride, LOT: SLBB4575V	Sigma-Aldrich, Steinheim, Germany

2.1.2 Devices and equipment

Autoclave Kronos B23	Newmed, Qattro Castella, Italy
Centrifuge 5417R	Eppendorf, Hamburg, Germany
Colony counter, Colony Quant ®	Schuett Biotec GmbH, Göttingen, Germany
Duran glass bottles (100 mL, 1000 mL)	Schott AG, Mainz, Germany
Fine balance, BP221S	Sarorius, Göttingen, Germany
HPLC System: Ultimate 3000 with binary pump, online solvent degasser, analytical autosampler, column oven and diode array detector	Thermo Fisher, Dreieich, Germany
Inoculation loop sterilizer, SteriMax	WLD-tec, Göttingen, Germany
Inoculation loops	Carl Roth, Karlsruhe, Germany
Laminar air flow hood LB-48-C	Haereus, Hanau, Germany
Magnetic stirrer	IKA, Staufen im Breisgau, Germany

Pipettes: Eppendorf Research (various volumes) Eppendorf, Hamburg, Germany

Shaking incubator, GFL3032 GFL Gesellschaft für Labortechnik, Burgwedel, Germany

Speed Vac Plus SC110A Savant, Farmingdale, USA

Turbiditiy standard for calibration of DensiCheck bioMérieux, Nuertingen, Germany

Turbidity meter, DensiCheck bioMérieux, Nuertingen, Germany

Vortexer REAX 2000 Heidolph, Schwabach, Germany

2.1.3 Bacterial strains

Staphylococcus aureus reference strain, ATCC 29213 American Type Culture Collection, Manassas, VA, USA

Staphylococcus aureus clinical isolate, MV13488, isolated from sputum, resistant to benzylpenicillin and ampicillin (MICs $\geq$ 0.5 mg/L) Institute for Microbiology and Hygiene, Charité University Hospital Berlin

Staphylococcus aureus clinical isolate, MV13391, isolated from tracheal secretion, no resistance to commonly tested antibiotics Institute for Microbiology and Hygiene, Charité University Hospital Berlin

2.1.4 Solutions

Cation-adjusted Mueller-Hinton broth (CaMHB). CaMHB was prepared as described in the manual of the manufacturer: 2.1 g Mueller-Hinton broth dry powder were dissolved in 100.0 mL of Milli-Q water in a 100 mL Duran® glass bottle. The suspended powder was dissolved on a heated magnet stirrer and the cation content was adjusted to 25 mg/L Ca^{2+} and 12.5 mg/L Mg^{2+} before sterilisation in an autoclave at 121° C for 15 min.

Phosphate-buffered saline with peptone (PBSP). Phosphate-buffered saline with peptone (pH 7.0) (PBSP) was prepared as gentle bacterial suspension medium as suggested by Koch [119]. 8.5 g NaCl, 0.3 g KH_2PO_4, 0.6 g Na_2HPO_4 and 1.0 g peptone were dissolved in 1.0 L Milli-Q water in a 1 L Duran® glass bottle. The solution was autoclaved for 15 min at 121° C.

Sodium chloride (NaCl) solution (0.9%). 0.9 g NaCl was dissolved in 100.0 mL Milli-Q water and subsequently autoclaved for 15 min at 121° C.

Antibiotic stock solutions. The primary antibiotic stock solutions with 1.0 mg/mL were prepared according to [12]: First, the potency of the antibiotic powder was calculated from the active fraction (as provided by the manufacturer) and corrected by the water content (e.g. MER powder is chemically meropenem trihydrate):

$$\text{potency} = \text{active fraction} \times (1\text{-water content})$$

Second, the required volume of diluent (Milli-Q water) was calculated from the potency and the actual weight of the powder:

$$\text{Volume of diluent [mL]} = \frac{\text{Weight [mg]} \times \text{Potency}}{\text{Desired concentration} \left[\frac{mg}{mL}\right]}$$

Finally, the prepared stock solutions were aliquoted into 1.5 mL Eppendorf cups in aliquots of 1.0 mL and stored at -80° C until required.

2.1.5 Software

Chromeleon® Version 7.2	Thermo Fisher, Dreieich, Germany
ColonyQuant® software Version 3.2	Schuett Biotec GmbH, Göttingen, Germany
Excel Version 2010	Microsoft, Redmond, USA
GraphClick Version 3.0	Arizona-software, Zurich, Switzerland
R Version 3.1.1	R Foundation for Statistical Computing, Vienna, Austria

2.2 Bioanalytical quantification of antibiotics in growth medium

In this chapter, the development of a bioanalytical high-performance liquid chromatography (HPLC) method for simultaneous quantification of the utilised antibiotics LZD, MER and VAN from the bacterial growth medium CaMHB is described. Therefore, a sample pre-treatment and HPLC instrument method had to be developed. Moreover, the method was to be validated according to the EMA guideline for bioanalytical method validation [120]. Finally, the method was used to quantify the drug concentrations during the *in vitro* time-kill curve experiments to ultimately assess potential degradation of the antibiotics under the experimental conditions of the *in vitro* infection model.

2.2.1 HPLC instrument setup

The HPLC system was a Dionex Ultimate 3000 HPLC+ system (Thermo Fisher, Dreieich, Germany), consisting of a WPS-3000 TPL RS Well Plate autosampler, a HPG-3200SD binary pump with online solvent degasser and a DAD-3000 diode array detector (DAD). An Accucore® C-18 HPLC column (2.6 µm, 100 x 2.1 mm, Thermo Fisher, Dreieich, Germany) was installed in the TCC-300SD column oven. The HPLC was controlled by the Chromeleon® software.

2.2.2 Development of the bioanalytical HPLC method

2.2.2.1 Sample treatment and recovery

As the samples originating from the time-kill curve experiments contained CaMHB as matrix, direct injection of the sample was not possible due to the considerable matrix content that might precipitate and then clog the HPLC column. Hence, matrix constituents were precipitated before injection into the HPLC system. Therefore, spiked samples of LZD, MER and VAN in CaMHB were prepared to study different sample preparation methods. The investigated treatment protocols included:

Precipitation with direct injection. 100 µL sample was precipitated with chilled methanol (MeOH) or acetonitrile (ACN) in various ratios (100 µL sample + 100 up to 400 µL solvent) in a 1.5 mL Eppendorf cup. The mixture was allowed to rest at 4° C for 10 min before centrifugation at 10000·g at 4° C for 10 min. 150 µL of the supernatant was removed, transferred into a 96 well plate and subsequently 2 µL were injected into the HPLC apparatus.

Precipitation with solvent evaporation. After precipitation and centrifugation as described above, 400 µL of the supernatant were removed from the precipitated pellet and transferred into a new Eppendorf cup. The solvent was evaporated using a vacuum concentrator (SpeedVac, Savant, Farmingdale, USA, dry rate: medium) for ca. 1 h until dryness. The obtained crystals were reconstituted in 100 µL Milli-Q water and 2 µL of the reconstituted sample was injected into the HPLC apparatus.

Recovery. The recoveries of the analytes from the matrices using both MeOH or ACN as precipitating agent was calculated based on the obtained analyte peak areas from processed samples in the matrix CaMHB compared to the peak area of an aqueous sample. Recovery experiments were carried out at a concentration of 10 mg/L for all antibiotics.

2.2.2.2 HPLC instrument method

The HPLC instrument method had (i) to sufficiently separate the analytes from the matrix constituents and (ii) to provide sufficient separation of the analytes LZD, MER and VAN itself. To fulfil both requirements, gradient elution (i.e. changing eluent composition over time) was chosen as it provided more flexibility than isocratic methods (i.e. constant eluent composition). Various mobile phases were

investigated and consisted of mixtures of water/ACN, water/MeOH with or without 0.1% trifluoroacetic acid (TFA). Gradient profiles were chosen to gradually increase the content of the organic solvent over time.

Detection wavelengths of the DAD were set to 251, 302 and 240 nm for LZD, MER and VAN, respectively. Injection volume was varied from 1 to 20 µL. Column oven temperature was evaluated between 20 and 40° C. Analyte peaks in the chromatograms were integrated and peak areas were calculated using the Chromeleon® software.

2.2.3 Validation of the bioanalytical HPLC method

The developed method was fully validated according to the EMA guideline for bioanalytical method validation [120].

Selectivity. The HPLC method was found selective if the peaks of LZD, MER and VAN in the chromatogram were separated and did not interfere with peaks originating from CaMHB as matrix components. Absence of interference was accepted if the response, i.e. the peak of the CaMHB constituents was <20% of the lower limit of quantification (LLOQ) of the analyte at the same retention time.

Carry-over. Analyte carry-over into a blank sample after injection of a sample with a high concentration should be <20% of the LLOQ of the analyte.

Lower limit of quantification (LLOQ). For determination of the LLOQ, drug solutions in CaMHB with concentrations ranging from 0.2 to 10 mg/L of LZD, MER and VAN were prepared and injected in to the HPLC system. The LLOQ was the lowest concentration of the analyte that could be quantified with acceptable accuracy and precision being described below.

Upper limit of quantification (ULOQ). The ULOQ was the highest concentration of the analyte that needed to be quantified with acceptable accuracy and precision being described below. It was determined by the highest concentrations studied in the *in vitro* infection model (see 2.3).

Calibration curve. Six calibration samples were prepared by spiking CaMHB (CaMHB content >90 %) with aqueous solutions of LZD, MER and VAN. Calibration concentration levels ranged from the LLOQ to the ULOQ and linearity was evaluated by (weighted) linear regression analysis. The calibration function was accepted for $R^2 \geq 0.98$ and if 75% (i.e. 4 of 6) of the calibration samples had back-calculated concentrations within ±15% of the nominal concentration or ±20% of the nominal concentration for the lowest calibration sample (= LLOQ), respectively.

Accuracy. Deviation of the analytically determined concentration from the nominal value was calculated as percentage of the nominal value (as a measure for inaccuracy of the assay) by analysing quality control (QC) samples. QC samples were prepared by spiking CaMHB (CaMHB content >90%) with analyte independently (i.e. using a different stock solution) from calibration samples.

For *within-run accuracy*, four QC concentration levels were prepared with five replicates per level. QC concentration levels were: the LLOQ (QC LLOQ), three times the LLOQ (QC L), ca. 50% of the calibration range (QC M) and ca. 80% of the calibration range (QC H). The mean accuracy at each QC level should be within 85-115%, except for the QC LLOQ were a range from 80-120% was acceptable.

For *between-run accuracy*, the QC samples from three analytically independent runs on three different days were evaluated according to the same acceptance criteria as for within-run accuracy.

Precision. Closeness of repeated individual measures of the analyte was calculated as coefficient of variation (%CV) as a measure for imprecision of the assay. For that, the same QC samples as described under 'Accuracy' were used.

For *within-run precision*, the analytical validation was accepted if the coefficient of variation (CV) was <15%, except for the QC LLOQ for which <20% were tolerated.

For *between-run precision*, the QC samples from three analytically independent runs on three different days were evaluated with the same acceptance criteria as for within-run precision.

Stability. For assessing the stability of the analytes under different conditions, five QC L and five QC H samples were prepared, exposed to various storage conditions and analysed against a fresh set of calibration and QC samples.

For *short-term stability*, unprocessed QC samples were stored at 25° C (room temperature) for 5 h to simulate benchtop conditions. The stored QC samples were analysed against a freshly prepared set of calibration samples and compared to freshly prepared QC samples.

For *autosampler stability*, the processed QC samples were analysed in the HPLC system and stored at 4° C in the autosampler. After 15 h, the QC samples were re-injected and evaluated.

For *freeze-thaw stability*, QC samples were frozen at -80° C and thawn at room temperature and re-frozen at -80° C on three consecutive days. Thereafter, the QC samples were analysed against a freshly prepared set of calibration samples and compared to freshly prepared QC samples.

For *long-term stability*, QC samples were frozen at -80° C and stored for 189 days (~ 6 months). Thereafter, the QC samples were analysed against a freshly prepared set of calibration samples and compared to freshly prepared QC samples.

2.2.4 Degradation of the antibiotics in the *in vitro* infection model

Potential degradation of the antibiotics was monitored in cell-culture flasks at a drug concentration of 10 mg/L under the same experimental conditions as in the actual time-kill curve studies (2.3.3). Samples of 200 µL were removed from the cell culture flaks at 0, 18 and 24 h and immediately frozen at -80° C until HPLC analysis (2.2.2.2). Degradation kinetics was monitored in n=3 per antibiotic. For all antibiotics, potential degradation was assumed as a first-order process, which was mathematically described by exponential decay:

$$C_t = C_{t=0} \times e^{-k_{deg} \times t}$$ (Eq. 1)

For estimating the first-order degradation rate constant k_{deg}, $C_{t=0}$ was set to the mean value of the drug concentration at t=0 and k_{deg} was estimated using ordinary least-squares regression (2.4.1.1). Degradation was considered significant if the 95% confidence interval (CI) of the estimate of k_{deg}, calculated from the relative standard error of the estimate of k_{deg}, was not including zero.

2.3 Microbiological experiments

This chapter starts with preliminary microbiological investigations, i.e. development and evaluation of a quantification method for *S. aureus* in bacterial growth medium, the determination of the MIC of the utilised antibiotics against the *S. aureus* strains and the characterisation of the growth properties of *S. aureus* in CaMHB. Thereafter, the methods for the determination of the antibiotic effect, i.e. the 'conventional' and 'dynamic checkerboard' as well as time-kill curve assays are presented. Finally, the developed method for elucidation of adaptive resistance of *S. aureus* to the investigated antibiotics is described.

2.3.1 Preliminary microbiological investigations

2.3.1.1 Droplet plate assay for quantification of *S. aureus*

2.3.1.1.1 Sample treatment

In order to quantify viable bacteria, a 'droplet-plate' assay [32] was adapted to the local environment at the Dept. of Clinical Pharmacy and Biochemistry for which in principle agar plates were spot-inoculated with the bacterial sample and the prepared plates were incubated to stimulate formation of CFUs. To allow for counting of single colonies, samples with bacteria had to be diluted prior to plating to obtain <50 CFU per spot. Therefore, a 100 µL sample containing bacteria was subjected to serial dilutions in PBSP.

For samples with (suspected) high bacterial concentrations ($>10^3$ CFU/mL), antibiotic carryover was avoided by direct dilution to subinhibitory concentrations: Serial ten-fold dilutions were performed using 100 µL sample + 900 µL PBSP in a 48 well-plate.

For samples with (suspected) low bacterial concentrations ($\leq 10^3$ CFU/mL) and/or samples with high antibiotic concentrations, a centrifugation/washing cycle was utilised to remove the antibiotic [31,121]: Briefly, the bacterial sample (100 µL) was diluted 1+9 in PBSP and centrifuged at 610 g for 10 min. Subsequently, the supernatant was removed (800 µL) and fresh PBSP (800 µL) was added. The mixture was vortexed and the cycle was repeated until sufficient dilution of the antibiotic was attained (<0.5x MIC).

For plating, Columbia agar plates were used, which were divided into four sectors. Each sector was spot-inoculated with the prepared dilutions (5× or 10×10 µL) according to Figure 4 and subsequently

incubated for 18-24 h at 37° C. CFU on agar plates were counted visually, documented with the Colony Quant® device, multiplied with the applied dilution factor and CFU/mL were calculated. 0 CFU/mL were set to 1 CFU/mL to allow log-transformation of CFU/mL to log10 CFU/mL.
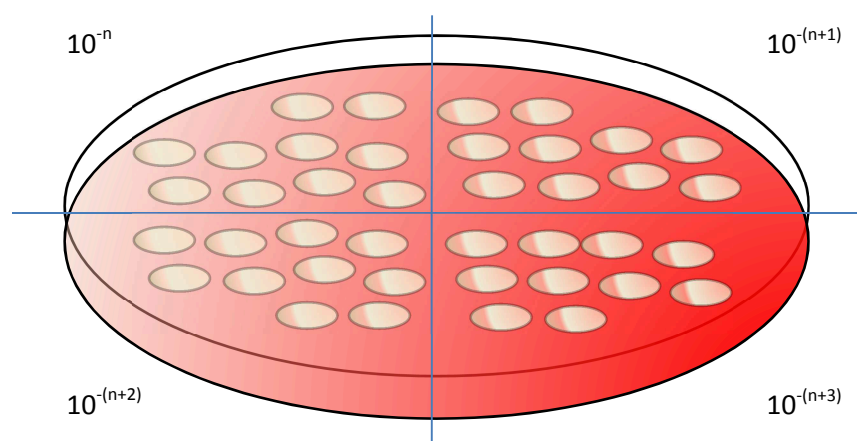
Figure 4: Spot inoculation scheme for preparing Columbia agar plates with 10×10 µL using the developed droplet-plate assay. Different dilutions of the bacterial sample were placed on the divided plate. In the graphical sketch, 'n' can be 0 to 4 depending on the anticipated CFU/mL in the *in vitro* infection model.

2.3.1.1.2 Evaluation of the bacterial quantification assay

As the described assay in 2.3.1.1.1 represents a down-scaled, resource-saving version of the previously established quantification assay by Scheerans [31] and Michael [122], which also used a different inoculation technique ('drigalski spreading' of one sample over an entire plate vs. 'droplet plate' inoculation using one plate for four samples), the assay performance was to be evaluated.

Accuracy and precision. An initial suspension of *S. aureus* adjusted to McFarland (McF) standard 0.5 (approx. $1 \cdot 10^8$ CFU/mL [31,121]) was used for the preparation of the standard solutions. Dilutions were performed to yield 20, 30, 40, 50 and 200, 300, 400, 500 colonies per 100 µL. Six replicates of each bacterial concentration level were processed as described in 2.3.1.1.1. Median counts, 5th and 95th percentile and preparation variability (expressed as %CV) were calculated to assess accuracy and precision, respectively.

Linearity between dilution vs. centrifugation/washing method. Three bacterial suspensions (10^3, 10^5, 10^7 CFU/mL) were processed by both direct dilution and centrifugation/washing (3 cycles), as described in 2.3.1.1.1. Agreement between both methods was evaluated based on a paired t-test.

Stability of the bacterial samples in diluents. Stability of *S. aureus* in the dilution media PBSP and 0.9% NaCl solution was investigated over a time period of 4 h to cover the processing time of an entire set of experiments. Bacteria were suspended in PBSB or 0.9% NaCl solution, stored at room temperature and bacteria were quantified according to 2.3.1.1.1 every 20 min over 4 h. Each diluent was tested in triplicate.

2.3.1.2 Storage of bacteria and bacterial stock suspension

All bacterial strains retrieved from the Dept. of Medical Microbiology and Hygiene of the Charité University Hospital were transferred into cryovials and stored at -80° C using the Microbank® storage system [123]. For recovery of a frozen bacterial strain, the cryovial was opened under aseptic conditions; a single cryobead was removed with a sterile forceps and subsequently spread on a Columbia agar plate. The inoculated agar plate was subsequently incubated overnight for 15-18 h at 37° C at ambient air. A freshly recovered bacterial culture from cryobeads was prepared every four weeks to prevent contamination of the bacterial strain.

For preparation of the bacterial stock solution used in the experiments, a fresh overnight subculture of the bacterial strain or the freshly recovered primary culture incubated overnight was utilised to ensure reproducible viability of the bacterial colonies being a prerequisite for using turbidity-based inoculum preparation [124]. The inoculum was prepared by direct colony suspension [124]: 2-4 colonies were picked from the incubated agar plate with a sterile inoculation loop, suspended into 3 mL of sterile 0.9% NaCl solution and turbidity was adjusted to 0.5 McF using a turbidity meter. With this procedure, a bacterial stock solution containing ca. $1 \cdot 10^8$ CFU/mL was obtained for *S. aureus* [31,121,124].

2.3.1.3 Determination of the minimal inhibitory concentration

The MIC of *S. aureus* ATCC 29213 and the two clinical isolates MV 13488 and MV 13391 was determined according to the 'Clinical Laboratory Standards Institute' (CLSI) guideline [12]. A bacterial stock suspension of *S. aureus* was prepared as described in 2.3.1.2. The bacterial stock suspension was diluted 1+1 with sterile 0.9% NaCl solution to yield a concentration of approx. $5 \cdot 10^7$ CFU/mL.

890 µL of CaMHB and 100 µL of appropriately diluted antibiotic solutions were dispensed into each well of a 48-well plate. The antibiotic concentrations were chosen as multiples and fractions of 1.0 mg/L in base 2 logarithmic steps. 10 µl of the diluted bacterial suspension containing $5 \cdot 10^7$ CFU/ml were added to yield a final inoculum size of $5 \cdot 10^5$ CFU/mL.

In addition, negative (containing no drug and no bacteria) and positive (containing no drug but bacteria) control samples were prepared. For the positive controls, 990 µl of CaMHB and 10 µl of the

freshly prepared $5 \cdot 10^7$ CFU/ml *S. aureus* dispersion were added into each well. For negative control, 1000 µl of CaMHB were dispensed into a well and no bacteria were added.

The well plate was incubated at 37° C at ambient air. The wells were read after ca. 20 hours of incubation, and the MIC was determined as the lowest concentration of the antibiotic allowing no visible growth indicated by turbidity.

2.3.1.4 Determination of the lag-time of *S. aureus*

The lag-time, i.e. time period to attain exponential growth was determined for *S. aureus* ATCC 29213 and the two clinical isolates MV 13488 and MV 13391. A bacterial stock suspension was prepared as described in 2.3.1.2. An inoculum of 100 µL of the freshly prepared bacterial stock suspension was added to the 50 mL-cell-culture flask filled with 9.9 mL sterile CaMHB. The inoculated flask was incubated at 37° C at ambient air for 4 h. A sample of 100 µL was taken at t=0 and every 20 min up to 240 min. Samples of 100 µL were taken from the culture flaks and bacteria were quantified as described in 2.3.1.1 using the direct dilution method. Log10 CFU/mL were plotted against time. The experiment was performed in triplicate with independent initial inocula for each culture flask. The lag-time was determined using an exponential biphasic growth model (Eq. 2) with the growth rates k_{growth} of k_{lag} and k_{log} for lag- and log-phase, respectively, and initial condition (IC) for the bacterial load N in log10 CFU/mL at t=0 and t_{lag} for the lag-time:

$$\frac{dN}{dt} = k_{growth} \times N \quad IC: N_{t=0} \text{ with } k_{growth} = k_{lag} \text{ for } t \leq t_{lag}$$

$$\text{and } k_{growth} = k_{log} \text{ for } t > t_{lag}$$

(Eq. 2)

Generation times, i.e. the time interval until doubling of the bacterial population of *S. aureus* in in lag- and log-phase were derived from the first-order growth rate constants ($\log(2)/k_{growth}$).

2.3.2 Checkerboard studies of linezolid with meropenem against *S. aureus*

The conventional checkerboard experiment was performed with *S. aureus* ATCC 29213 in a 48-well plate. 100 µL of appropriately diluted drug solutions of LZD and/or MER were added to 890 µL (single drug) or 790 µL (combinations) of CaMHB (Sigma-Aldrich, Steinheim, Germany) along the horizontal and vertical path of the well plate, respectively, in order to yield final drug concentrations covering both MICs and clinically relevant concentrations of both drugs [91,125]. Antibiotic concentrations ranged from 0.25 to 16 mg/L for LZD and 0.016 to 16 mg/L for MER. 10 µL of a bacterial stock suspension (2.3.1.2) were added to obtain an inoculum size of approx. 10^6 CFU/mL. The prepared checkerboard was incubated for 20 h at 37° C.

Conventional checkerboard with evaluation by turbidity. Conventionally, the checkerboard experiment is evaluated visually by turbidity [32,33]: Analogous to MIC determination, a turbid well indicated bacterial growth whilst a clear well indicated suppression of bacterial growth.

Dynamic checkerboard with quantification of bacteria. In addition, for the 'dynamic checkerboard', bacteria were quantified in each well with the developed droplet plate assay (2.3.1.1). A ≥3 log10-fold reduction of bacteria was defined as 'bactericidal', whilst smaller reductions were referred to as 'bacteriostatic' [126].

2.3.3   Time-kill curve studies in lag-phase in *in vitro* infection models

Time-kill curve studies in lag-phase were performed with the reference strain ATCC 29213 and the two clinical isolates MV 13488 and MV 13391 of *S. aureus*.

Linezolid, meropenem and vancomycin alone. Time-kill curve experiments were performed in 50 mL-cell-culture flasks. 1.0 mL of appropriately diluted drug solutions of LZD, VAN or MER was added to 8.9 mL of CaMHB to yield final drug concentrations ranging from 0.03-8 mg/L for MER, 0.5-32 mg/L for LZD and 0.25-16 mg/L for VAN. 100 µL of the bacterial stock suspension (2.3.1.2) were added to yield a final inoculum size of approximately $1 \cdot 10^6$ CFU/mL representing bacteria in their lag-phase of growth. The inoculated flasks were incubated for 24 h at 37° C while shaking at 1 Hz at ambient air. Samples of 100 µL for bacterial quantification were removed according to a rich sampling protocol (≥8 time points over 24 h) for *S. aureus* ATCC 29213 or at selected time points (0, 4, 8 and 24 h) for the confirmatory studies with the clinical isolates of *S. aureus*. Experiments were performed in n≥2. A ≥3 log10-fold reduction of bacteria was defined as 'bactericidal', whilst smaller reductions were referred to as 'bacteriostatic' [126].

Combinations of meropenem and linezolid. Time-kill curve experiments for combinations of MER and LZD were performed in 50 mL-cell culture flasks. 1.0 mL of appropriately diluted drug solutions of MER and LZD were added to 7.9 mL of CaMHB. Drug concentration covered both clinically relevant subinhitory (i.e. below the MIC) and inhibitory combinations (i.e. above the MIC) for both antibiotics ranging from 0.03-8 mg/L for MER and 1-32 mg/L for LZD. The inoculum, sampling schedule and evaluation were as described above.

Combinations of meropenem and vancomycin. Time-kill curve experiments for combinations of MER and VAN were performed in 50 mL-cell-culture flasks. 1.0 mL of appropriately diluted drug solutions of MER and VAN were added to 7.9 mL of CaMHB. Drug concentration covered both clinically relevant subinhitory and inhibitory combinations for both antibiotics and ranged from 0.015-

8 mg/L for MER and 0.06-16 mg/L for VAN. The inoculum, sampling schedule and evaluation were as described above.

2.3.4 Time-kill curve studies in log-phase in *in vitro* infection models

To explore the impact of the growth phase on the antibiotic effect, log-phase bacteria were also assessed in time-kill curve studies. Therefore, the reference strain *S. aureus* ATCC 29213 was utilised. **Linezolid, meropenem and vancomycin alone.** Time-kill curve experiments were performed in 50 mL-cell-culture flasks. 170 µL of the bacterial stock suspension (2.3.1.2) were diluted with 830 µL of sterile NaCl solution (0.9%), and 100 µL of the dilution were added to 8.9 mL of CaMHB resulting in an initial inoculum of approx. $2 \cdot 10^5$ CFU/mL [31,121]. Before adding 1.0 mL of diluted drug solutions of LZD, VAN or MER to the inoculated culture flasks, a pre-incubation step for 2 h at 37° C of the antibiotic-free culture flask was undertaken. This procedure generated exponentially replicating bacteria (log-phase) at drug exposure with an inoculum size of ca. $1 \cdot 10^6$ CFU/mL. Final drug concentrations ranged from 0.06-8 mg/L for MER, 1-32 mg/L for LZD and 0.25-16 mg/L for VAN. The inoculated flasks containing antibiotic(s) were incubated for 24 h at 37° C while shaking at 1 Hz at ambient air. Samples of 100 µL for bacterial quantification were removed according to a rich sampling protocol (≥8 time points). Experiments were performed in n≥2 and evaluated as described above.

Combinations of meropenem and linezolid. Time-kill curve experiments for combinations of MER and LZD were performed in 50 mL cell culture flasks. 1.0 mL of appropriately diluted drug solutions of MER and LZD were added to 7.9 mL of CaMHB for initial inoculum preparation. Selected drug concentrations were studied for both antibiotics. The inoculum, sampling schedule and evaluation were as described above.

Combinations of meropenem and vancomycin. Time-kill curve experiments for combinations of MER and VAN were performed in 50 mL cell culture flasks with vented caps. 1.0 mL of appropriately diluted drug solutions of MER and VAN were added to 7.9 mL of CaMHB for initial inoculum preparation. Selected drug concentrations were studied for both antibiotics. The inoculum, sampling schedule and evaluation were as described above.

2.3.5 Adaptive resistance studies of *S. aureus*

For time-kill curve scenarios displaying regrowth after initial killing, potential adaption of the bacteria to the antibiotic over time was evaluated as follows: A second time-kill curve study was performed, in which the inoculum consisted of *S. aureus* ATCC 29213 that was pre-exposed to an antibiotic

concentration in a first time-kill curve study in which regrowth after initial killing was observed. To exclude other influencing factors, the inoculum size was empirically (re-)adjusted to 10^6 CFU/mL for the second experiment using prior knowledge on the attained bacterial concentration at 24 h of the first experiment. Hence, depending on the bacterial concentration at the end of the first time-kill curve study, 10, 100 or 1000 µL were added as inoculum directly from the culture flask of the first time-kill curve experiment and added to 1 mL of the appropriately diluted drug solution and 8.99, 8.9 or 8 mL of CaMHB, respectively for the second time-kill curve study. Drug concentrations for the second experiment were chosen to be either equal or one log2-fold concentration level above or below the drug concentration of the first time-kill curve study to elucidate the magnitude of the adaption. CFU/mL were then quantified over another 24 h period using a dense sampling schedule (n≥8). Experiments were performed in n≥2.

2.4 Modelling and Simulations

The following chapter describes the methods used for analysing the quantitative data obtained in 2.2.4, 2.3.1.4, and 2.3.2-2.3.5. In the first part, 'Modelling', the mathematical background on maximum likelihood estimation, optimal experimental design and model evaluation techniques are introduced and/or derived followed by the section on PD modelling of the antibacterial effects of LZD, MER and VAN against *S. aureus*. The second part, 'Simulations', describes linking the developed semi-mechanistic PD models to literature-based population PK models to assess the observed drug (inter)actions in a translational framework.

All modelling and simulation tasks were performed in the software 'R' [127]. The 'R' package 'deSolve' was used for solving ordinary differential equations [128], 'MASS' [129] was utilised for handling of multivariate distributions and plots were generated using 'ggplot2' [130].

2.4.1 Modelling

2.4.1.1 Mathematical background for modelling in 'R'

2.4.1.1.1 Maximum likelihood estimation

In a nonlinear model, the mathematical solution of the model depends non-linearly on the model parameters. The observed variable y_i (e.g. log10 CFU/mL in the present work) is predicted by a function f of n independent variables $x_1, \dots, x_n$ (e.g. time or drug concentration) and a vector of model parameters θ. The differences between predicted and observed variable ε originate both from measurement uncertainty in CFU determination as well as model misspecification and are assumed to follow a normal distribution $\mathcal{N}$ with mean zero and variance σ^2.

$$y_i = f_i(x_1, \dots, x_n | \theta) + \varepsilon \quad \text{with} \quad \varepsilon \sim \mathcal{N}(0, \sigma^2) \tag{Eq. 3}$$

The utilised experimental measure of bacterial growth in this thesis, CFU/mL, is log-normally distributed as being the result of a multiplicative process – bacterial duplication [131]. Hence, log10 CFU/mL is (approximately) normally distributed the assumption for ε as additive residual variability component is justified.

Under the assumption of (Eq. 3), the maximum likelihood principle [132] was utilised which finds the (set of) model parameters θ describing the observed, experimental data y_i best. The maximum likelihood method selects the (set of) model parameters θ that maximise(s) the likelihood function. The likelihood function computes the likelihood to observe the experimental data y_i given the mathematical model $f_i(x_1, \ldots, x_n | \theta)$ with the independent variables $x_1, \ldots, x_n$ (i.e. drug concentrations and sampling time points in the present work) and the model parameters θ. Assuming the n samples being independent identically distributed (i.i.d.), with mean $f(x_1, \ldots, x_n | \theta)$ and variance σ^2, the likelihood function is the product of the so-called probability density functions:

$$f(x_1, \ldots, x_n | \theta, \sigma^2) = \prod_{i=1}^{n} f(x_i | \theta, \sigma^2) = \prod_{i=1}^{n} \left(\frac{1}{2\pi\sigma^2} \right)^{\frac{1}{2}} \exp\left(-\frac{(y_i - f(x_i|\theta))^2}{2\sigma^2} \right) \qquad \text{(Eq. 4)}$$

In order to maximise the likelihood function as function of θ, it is computationally easier to minimise the negative natural logarithm of the likelihood function, the minus log-likelihood function *LL*:

$$LL(x_1, \ldots, x_n | \theta, \sigma^2) = \frac{n}{2}\log(2\Pi) + \frac{n}{2}\log(\sigma^2) + \frac{1}{2\sigma^2} \sum_{i=1}^{n} (y_i - f(x_i|\theta))^2 \qquad \text{(Eq. 5)}$$

The first two terms and $\frac{1}{2\sigma^2}$ before the sum of the squared residuals between observed and predicted values in *LL* are constants for a purely additive residual variability. Hence, minimisation of *LL* w.r.t θ reduces *LL* to the ordinary least squares (*OLS*) estimator:

$$OLS(x_1, \ldots, x_n | \theta) = \sum_{i=1}^{n} (y_i - f(x_i|\theta))^2 \qquad \text{(Eq. 6)}$$

Because *f* is nonlinear, the minimization of the OLS w.r.t. θ is performed using numerical optimisation methods. The estimated parameter $\hat{\theta}$ is the maximum likelihood estimate.

The precision of the estimate $\hat{\theta}$ is derived from the second derivative of *LL* w.r.t. $\hat{\theta}$, which is also referred to as the 'Hessian' ∇ or the '<u>observed</u> Fisher information' of *LL* [133]. The first $\hat{\theta}$ derivative of *LL* is calculated by application of the "chain-rule" (inner times outer derivative):

$$LL'(x_1, \ldots, x_n|\hat{\theta}) = \frac{1}{2\sigma^2} \sum_{I=1}^{n} [2(y_i - f(x_i|\theta)) * f(x_i|\theta)'] \qquad \text{(Eq. 7)}$$

$$LL'(x_1, \ldots, x_n|\hat{\theta}) = \frac{1}{\sigma^2} \sum_{I=1}^{n} [(y_i - f(x_i|\theta)) * f(x_i|\theta)'] \qquad \text{(Eq. 8)}$$

The second θ derivative of LL is calculated by the application of the product- and chain-rule:

$$LL''(x_1, \ldots, x_n|\hat{\theta}) = \frac{1}{\sigma^2} \sum_{i=1}^{n} [(f(x_i|\theta)')^2 - (y_i - f(x_i|\theta)) * f(x_i|\theta)''] \qquad \text{(Eq. 9)}$$

For $\hat{\theta}$ of a multi-parameter model with $n > 1$ data points, the first and second $\hat{\theta}$-derivatives of the mathematical model $f_i(x_1, \ldots, x_n|\theta)$ are matrices. Hence, LL'' in matrix notation is expressed by the 'Jacobian' J and the 'Hessian' ∇ of $f_i(x_1, \ldots, x_n|\theta)$:

$$LL''(x_1, \ldots, x_n|\hat{\theta}) = \frac{1}{\sigma^2} \sum_{i=1}^{n} [J_i * J_i^T - (y_i - f(x_i|\theta)) * \nabla_i] \qquad \text{(Eq. 10)}$$

The inverse of the LL'' approximately yields the variance-covariance matrix Σ:

$$\Sigma(\hat{\theta}) \approx \frac{1}{LL''(x_1, \ldots, x_n|\hat{\theta})} \qquad \text{(Eq. 11)}$$

The diagonal elements of $\Sigma(\hat{\theta})$ represent the variances of each element of $\hat{\theta}$, which can be used to calculate the relative standard errors (RSE) of the model parameter estimates:

$$RSE(\hat{\theta}), \% = \frac{\sqrt{diag\left(\Sigma(\hat{\theta})\right)}}{\hat{\theta}} * 100 \qquad \text{(Eq. 12)}$$

With the parameter estimate $\hat{\theta}$ and its variance given by $diag\left(\Sigma(\hat{\theta})\right)$, the 95% CI of the model parameter was calculated as follows:

$$CI_{95\%}(\hat{\theta}) = \hat{\theta} \pm 1.96 * \sqrt{diag\left(\Sigma(\hat{\theta})\right)} \qquad \text{(Eq. 13)}$$

To assess possible correlation between model parameters, the variance-covariance matrix was transformed to the correlation matrix:

$$Corr(\hat{\theta}) = \sqrt{diag\left(\Sigma(\hat{\theta})\right)} * \Sigma(\hat{\theta}) * \sqrt{diag\left(\Sigma(\hat{\theta})\right)} \qquad \text{(Eq. 14)}$$

In $Corr(\hat{\theta})$, the diagonal elements are normalised to 1.0, whilst the off-diagonal elements are bound between -1.0 and 1.0 indicating negative or positive correlation, respectively. A value of 0.0 on an off-diagonal element indicated no correlation between those elements of $\hat{\theta}$.

2.4.1.1.2   Optimal design of experiments

An optimally designed experiment supports the parameters of a mathematical model (i.e. a model describing the underlying system) with informative data points [69]. Hence, model parameters of an optimally designed experiment are well identifiable, and can be estimated accurately with high precision, i.e. small RSE.

In optimal design, experimental data, i.e. y_i, is often not available when the study is planned. Hence, an underlying mathematical model $f(x_i|\theta)$ is assumed and the expectation (E) of LL'' is evaluated:

$$E\left(LL''(x_1, \dots, x_n|\hat{\theta})\right) = E\left(\frac{1}{\sigma^2} * \sum_{i=1}^{n}\{J_i * J_i^T - (y_i - f(x_i|\theta)) * \nabla_i\}\right) \qquad \text{(Eq. 15)}$$

As the expected value of $(y_i - f(x_i|\theta)) := 0$, i.e. in average, the mode of the observation distribution would be at the prediction, the 'expected Fisher information matrix' is:

$$E\left(LL''(x_1, \dots, x_n|\hat{\theta})\right) = \frac{1}{\sigma^2} * \sum_{i=1}^{n}\{J * J^T\} \qquad \text{(Eq. 16)}$$

Note, that the 'expected Fisher information matrix' is independent of experimental data and only dependent of the model with its parameters θ and the experimental design given by x_n (e.g. drug concentrations or sampling time points). For large *n* the standard errors obtained from the 'observed Fisher information matrix' will converge to the expected standard errors [132].

As mentioned above, optimal design of experiments requires knowledge about the underlying system in order to optimally design the experiment. Yet, this knowledge is most often not available before experimental conduct which limits the applicability of optimal design in experimental practice. To overcome those limits in the present work, an adaptive optimal design approach [71] was elaborated that went in parallel with experimental conduct. At the respective stage of experimental conduct, a mathematical model that described the experimental data was developed, and the 'expected Fisher information matrix' was used to evaluate the impact of upcoming experiments on parameter

identifiability and precision in an iterative cycle (Figure 7 in 2.4.1.3.3) until ideally all processes were uncovered and accurately described by the developed model.

2.4.1.2 Model development strategies and model evaluation techniques

Mathematical modelling was used in the present work to quantitatively understand the processes of bacterial growth and death under antibiotic exposure. Therefore, the developed mathematical models were evaluated and compared with model selection and evaluation techniques, which will be introduced in the following chapter. In order to select the mathematical model that described the experimental data best amongst different competing mathematical models, model selection techniques such as the likelihood ratio test and the Akaike's information criterion were used for statistical selection [42]. To evaluate the predictive performance, graphical tools such as goodness-of-fit plots and visual predictive checks were performed [134]. The generalisability of the mathematical model to predict time-kill curve data from antibiotic with a similar underlying mechanism of (inter)action was assessed by external evaluation.

Likelihood ratio test. The likelihood ratio test (LRT) [42] was used for statistical comparisons of two nested models of different complexity. Two models are nested if one model (reduced model, *r* parameters) emerges from a more complex model (full model, *f* parameters) by fixing (and not estimating) a subset of the parameter values. As an example, one can envision the sigmoidal maximum effect model with *H*=1, i.e. the ordinary maximum effect model as a reduced version of the sigmoidal maximum effect model with estimated *H* (2.4.1.3.1). The likelihood ratio test score is calculated from the ratio of the maximum likelihood function evaluated at the respective maximum likelihood estimates of reduced (LL_R) to the full model (LL_F). The test statistics can be approximated by the chi-squared distribution with *f-r* degrees of freedom, which - after applying the logarithmic rules - yields the test score *LRT*:

$$LRT = 2 \times (LL_f - LL_r) \tag{Eq. 17}$$

The decision for the more complex model was made based on the critical value of α=0.05. Hence, based on the chi-square distribution, for one degree of freedom, i.e. one more parameter in the full model, a difference of -3.84 in *-2LL* had to be observed to select for the full, i.e. more complex mathematical model.

Akaike's information criterion (AIC). The Akaike's information criterion was used for comparison of non-nested models. The test score *AIC* was derived by H. Akaike extending the maximum likelihood principle by an approximation of the Kullback-Leibler information measure [42,135], in which *-2LL* is two times the negative log likelihood at the objective function minimum and *k* the number of model parameters plus one, as σ² is intrinsically also estimated.

$$AIC = -2LL + 2k \qquad \text{(Eq. 18)}$$

For an additive residual variability model, as used in the present thesis, the log likelihood function (Eq. 5) and consequently *AIC* simplifies to:

$$AIC = n \times \log\left(\frac{\sum_{i=1}^{n}(y_i - f(x_i|\theta))^2}{n}\right) + 2k \qquad \text{(Eq. 19)}$$

with *n* being the number of data points.

According to Akaike's information criterion, the best model amongst a set of competing models has the lowest *AIC* score. As *AIC* was originally developed for large *n*, a corrected *AIC*, *AICc* was introduced [136] that corrects *AIC* with a second-order bias adjustment for small sample sizes with *n/p* < 40:

$$AICc = AIC + \frac{2k(k+1)}{n-k-1} \qquad \text{(Eq. 20)}$$

Goodness-of-fit analysis. For a graphical goodness-of-fit analysis, the observed variable y_i was plotted against the predicted variable $f(x_i|\theta)$. Furthermore, the residuals $(y_i - f(x_i|\theta))$ were plotted against the independent variables (i.e. time and log10 CFU/mL) to elucidate potential model misspecification indicated by systematic over- or underprediction or trends in the residuals [134].

Visual predictive check. The predictive performance of a model was evaluated by stochastic simulations stratified on every investigated experimental scenario. Both uncertainties of the model parameters θ, expressed in the estimated variance-covariance matrix, as well as the residual variability σ^2 were considered. The distributions of the simulated $f(x_i|\theta)$ were compared to the distributions of y_i for each investigated scenario [134].

External evaluation. If appropriate (or possible), the developed models were also externally evaluated by predicting scenarios from literature or other experiments that have not been provided for model parameter estimation. As this technique is rather difficult to generalise, it will be described in more detail at the respective mathematical model that was evaluated externally.

2.4.1.3 Modelling of the effects of linezolid, meropenem and vancomycin on *S. aureus*

2.4.1.3.1 Empiric modelling of individual drug effects

To provide a first insight at the different magnitudes of the antibacterial effects of LZD, MER and VAN and their potency to kill or inhibit growth of *S. aureus*, both checkerboard and time-kill curve studies were evaluated by sigmoidal maximum effect models, originally derived from Michaelis and Menten [47] and extended to describe sigmoidicity by Hill [137]:

$$E(C) = \frac{Emax \times C^H}{EC_{50}{}^H + C^H} \qquad \text{(Eq. 21)}$$

The sigmoidal maximum effect model (Eq. 21) described the drug effect stimulated by a defined concentration of an antibiotic *E(C)* and was parameterised by the maximum drug effect *Emax*, the drug concentration that stimulated the half-maximum effect *EC$_{50}$* and the Hill factor *H* accounting for the steepness at *EC$_{50}$* of the concentration-effect relationship: For *H*<1, hyperbolic concentration-effect curves were observed, whereas for *H*>1, the relationship became sigmoidal with increasing steepness (Figure 5). Summary PD measures (see below) were utilised for the empiric modelling.
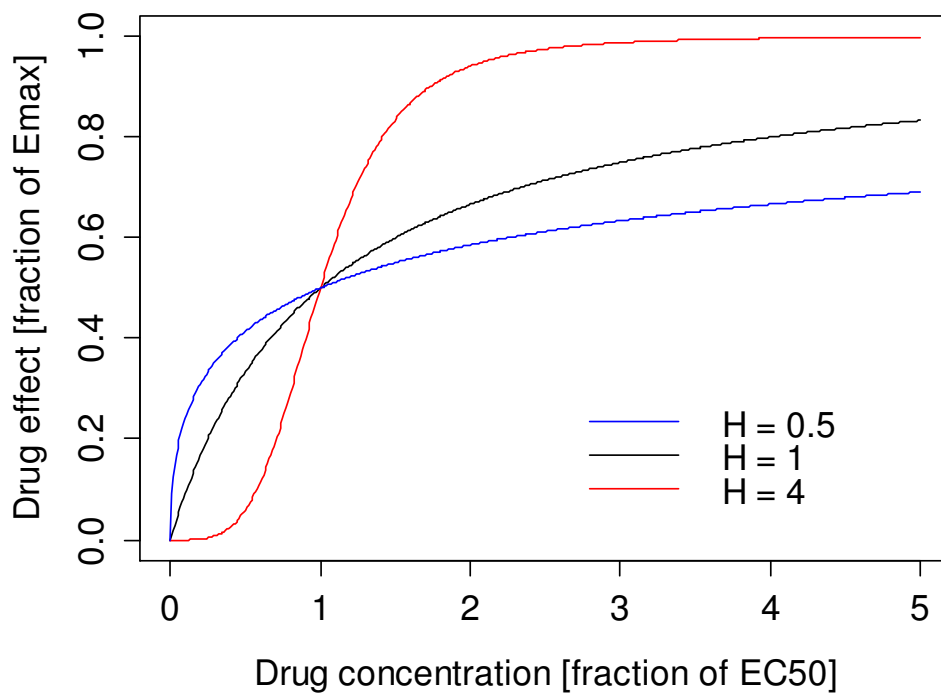
Figure 5: Simulated concentration-effect curves using the sigmoidal maximum effect model with Emax = 1, EC50 = 1 and three selected values for H.

Checkerboard studies. For the dynamic checkerboard, the mean bacterial concentration of log10 CFU/mL at the end of n=3 experiments was utilised as summary PD measure. The antibiotic was assumed to reduce the bacterial concentration using a sigmoidal maximum effect model (Eq. 21).

Time-kill curve studies. For the time-kill curve studies, the area between bacterial killing curve and growth control (GC) curve (intensity of the effect, *IE*), as described by Firsov and colleagues [48], was calculated as summary effect measure by the trapezoidal rule. Drug effects were also evaluated by a

sigmoidal maximum effect model (Eq. 21) and augmented the *IE* in a concentration-dependent manner.

Individual drug effects were estimated using ordinary least squares regression (Eq. 6) and precision of the estimates was computed from the variance-covariance matrix (Eq. 12).

2.4.1.3.2 Response surface analysis

Derivation of the expected additivity response surface. For quantification of the extent of the drug interactions between either LZD or VAN with MER, a response surface analysis described by Prichard and colleagues [138] using BI was used as a starting point. The expected additive effect $E_{comb,BI}$ was calculated based upon the two individual drug effects E_A and E_B using the final parameter estimates of the PD analyses of each drug alone (2.4.1.3.1):

$$E_{comb,BI} = E_A + E_B - E_A \times E_B \qquad \text{(Eq. 22)}$$

For antibiotics with a different maximum effect, the conventional BI equation was modified as follows: As BI was originally derived from probability theory [55], the maximum effect to be evaluated by BI is limited to 1.0. Hence to study antibiotics with different *Emax* values, the effect of the more effective drug (A), i.e. E_A was normalised to 1.0, whilst the effect of the individually less effective drug (B), i.e. E_B was set to a fraction of 1.0, i.e. *Emax*$_B$/*Emax*$_A$. The modified BI term was then scaled to the maximum effect *Emax*$_A$ of the more effective drug (A) to apply the elaborated equation to the experimental data on log10 CFU/mL-scale:

$$E_{comb,BI}(C_A, C_B) =$$

$$Emax_A \times \left(E_A(C_A) + \frac{Emax_B}{Emax_A} \times E_B(C_B) - E_A(C_A) \times \frac{Emax_B}{Emax_A} \times E_B(C_B) \right) \qquad \text{(Eq. 23)}$$

To quantify an interaction, the measured, i.e. observed, combined effect $E_{comb,obs}$ was compared to the predicted additive effect $E_{comb,BI}$. $E_{comb,obs} > E_{comb,BI}$ indicated synergy and vice versa antagonism. Deviations from additivity were reported either in log10 CFU/mL (checkerboard) or in changes in *IE* (time-kill curve studies).

Checkerboard studies. Bliss antagonism or Bliss synergy for the checkerboard dataset were tested for statistical significance using a t-test based on summarised data, in 'R' using the 'BSDA' package (V. 1.01). Therefore, both the point estimates of the calculated, expected combined additive effect $E_{comb,BI}(C_A, C_B)$, the experimentally observed combined effect $E_{comb,obs}(C_A, C_B)$ as well as the variability of both specimens were considered. For $E_{comb,obs}$, the variance of the experimental data was calculated whereas for $E_{comb,BI}$ the residual variance of the calculated additivity response surface was

used, generated with the delta-method [139] of the 'R' package 'msm' (V. 1.4). To correct for multiple testing (i.e. n statistical testing for each drug combination), the Bonferroni correction [140] was applied (alpha=0.05/n).

Time-kill curve studies. Calculation of the variance for the *IE* (i.e. area between growth and kill curve) is cumbersome, e.g. if not every time-kill curve had a corresponding GC curve. Therefore, 'range' as a conservative measure of dispersion was chosen as uncertainty measure for $E_{comb,obs}(C_A, C_B)$. For a 'significant' deviation from additivity, the range-bar of $E_{comb,obs}(C_A, C_B)$ should not overlap with the 95% confidence interval calculated from the variance of $E_{comb,BI}(C_A, C_B)$ (procedure similarly as described for the evaluation of the checkerboard studies).

2.4.1.3.3 Semi-mechanistic modelling of time-kill curve studies

The entire time courses of the antibacterial effects, alone and in combination, were to be modelled by a semi-mechanistic PD model as a prerequisite for time-continuous PK/PD modelling.

Model development. A simplified life-cycle model [141] was adapted as the core of the PD model which consisted of two bacterial growth states: Bacteria in the growing state ('GRO') transfer into the replicating state ('REP'). In 'REP' bacteria replicate ("doubling") and transfer back to 'GRO'. The first-order rate-constant k_{rep} was assumed to be rate-limiting and the actual bacterial replication process was assumed to be very fast (k_{doub} arbitrarily fixed to 100 h^{-1}). The life-cycle was extended to capture bacteria being not susceptible to antibiotic exposure and not replicating ('persisters'). Those bacteria were assumed to originate from initially replicating bacteria under drug exposure and were quantified in 'PER'. The differential equation system describing this extended life-cycle was initialised for 'GRO' with the bacterial concentration at t=0 (CFU$_0$) as initial condition (IC):

$$\frac{dGRO}{dt} = -k_{rep}(CFU) \times GRO + k_{doub} \times REP \times 2 \qquad \text{IC=CFU}_0 \qquad \text{(Eq. 24)}$$

$$\frac{dREP}{dt} = k_{rep}(CFU) \times GRO - k_{doub} \times REP - k_{per} \times REP \qquad \text{IC=0} \qquad \text{(Eq. 25)}$$

$$\frac{dPER}{dt} = k_{per} \times REP - k_{death,per} \times PER \qquad \text{IC=0} \qquad \text{(Eq. 26)}$$

k_{rep} was assumed to decrease if bacterial concentrations reached the capacity limit CFU$_{max}$:

$$k_{rep}(CFU) = k_{rep,0} \times \left(1 - \frac{GRO+REP+PER}{CFU_{max}}\right) \qquad \text{(Eq. 27)}$$

The extended life-cycle is visualised in a compartmental structure in Figure 6.
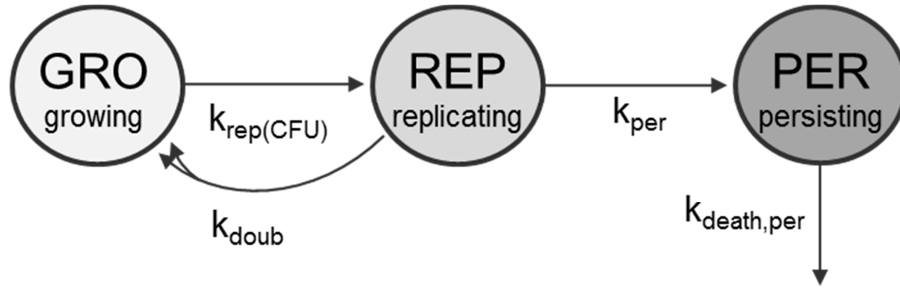
Figure 6: Compartmental representation of the extended life-cycle model with the three states 'GRO', 'REP' and 'PER' (see text for details).

Drug effects were implemented by sigmoidal maximum effect models (Eq. 21) on the respective turn-over rate constants in the simplified bacterial life-cycle. To assure parameter identifiability, *Emax* was generally fixed to 1.0 to allow for implementation of the drug effect model on the various turn-over rate constants. *Emax* was estimated (relative to 1.0) only if more than one drug altered the same rate constant and the magnitude of perturbation between those was (significantly) different.

Different implementations of the drug effects were assessed for LZD, VAN and MER including inhibition of replication, inhibition of successful doubling and stimulation of replication-dependent (perturbation of k_{doub}) and replication-independent (perturbation of k_{rep}) death of bacteria.

Potential adaptive resistance of the bacteria leading to regrowth after initial killing was implemented by an adaption submodel [142,143]: The degree of adaption was assumed to increase the EC_{50} over time as a function of drug exposure $C(t)$ and a second-order time-delay rate constant τ:

$$\frac{dAR_{off}}{dt} = -\tau \times C_{DRUG}(t) \times AR_{off} \qquad \text{IC=1} \qquad \text{(Eq. 28)}$$

$$\frac{dAR_{on}}{dt} = \tau \times C_{DRUG}(t) \times AR_{off} \qquad \text{IC=0} \qquad \text{(Eq. 29)}$$

The hypothetic amount transferred to AR_{on} was then multiplied with β to account for the magnitude of the adaption resulting in an adaption factor $\alpha(t)$, that ultimately scaled the EC_{50} over time [143]:

$$EC_{50}(t) = \alpha(t) \times EC_{50,t=0} \quad \text{with} \quad \alpha(t) = 1 + \beta \times AR_{on}(t) \qquad \text{(Eq. 30)}$$

Potential interactions on the adaption level, i.e. if drug A had an influence on the adaption of the bacteria to drug B, was explored by an inhibitory effect model (Emax model) of drug A on τ of drug B

and/or vice versa. The ODE system was numerically solved in 'R' using the 'lsoda' ODE solver of 'deSolve' [128].

Adaptive optimal design. The model development process (2.4.1.3.3) and the acquisition of the experimental time-kill curve data (2.3.3) were performed in parallel to support all parameters of the semi-mechanistic model with a firm base of experimental data. Based on the current data status, the base semi-mechanistic model was parameterised and model parameters were estimated. If estimation was impossible, e.g. due to missing information, hypotheses for experimental scenarios were simulated and the expected RSE values, as indicator for parameter identifiability, were calculated applying optimal design theory (2.4.1.1.2). The iterative process of performing experiments, specifying a mathematical model, prediction of subsequent informative experimental scenarios, performance of new experiments and repetition of this algorithm until 'learning experiments' became 'confirmatory' is illustrated in Figure 7.
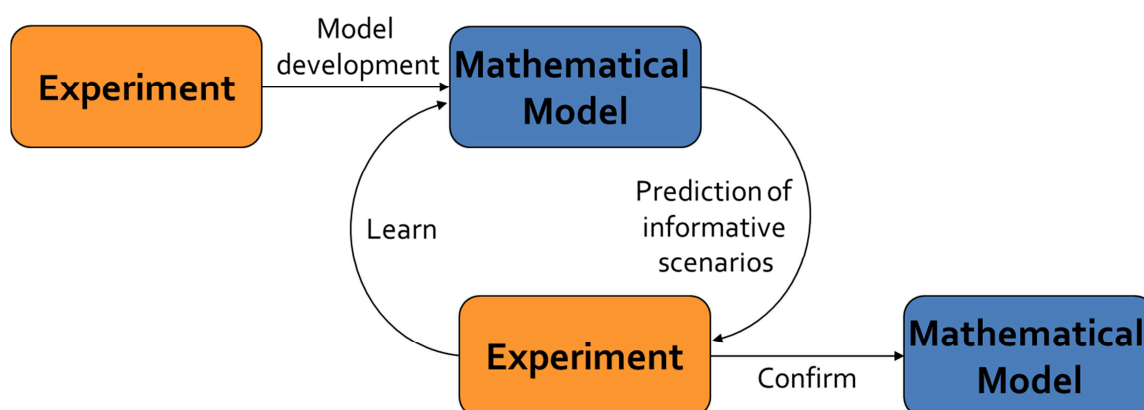
Figure 7: Flow chart of the sequential *in vitro* and *in silico* steps applied in this thesis.

Internal model evaluation

Graphical evaluation. The developed semi-mechanistic PD models were evaluated using goodness-of-fit plots and visual predictive checks (2.4.1.2) using n=1000 simulations.

Nonparametric bootstrap analysis. To evaluate the precision of the model parameter estimates, a non-parametric bootstrap analysis was performed [144,145]: Therefore, the final dataset of the time-kill curve study was bootstrapped by sampling from the dataset with replacement (n=1200). The parameters of the semi-mechanistic PD models were re-estimated for each of the 1200 bootstrap datasets. 95% confidence intervals were computed from the distributions of the bootstrap parameter estimates by calculating the 2.5^{th} and 97.5^{th} percentile.

External model evaluation

Evaluation of the adaption submodel. To externally evaluate the adaption sub-model (Eq. 30), the experimentally observed time-kill curves of the adapted bacteria (2.3.5) were not included in parameter estimation. The shape of those experimentally observed time-kill curves was compared to the model-predicted evolvement of the bacteria that were 'virtually' pre-exposed to an antibiotic. Therefore, initial conditions of the adaption submodel were set to simulated values at 24 h for the respective antibiotic concentrations and the inoculum was adjusted to the experimentally used inoculum, i.e. 10^6-10^7 CFU/mL (Eq. 24).

Evaluation of the generalisability of the semi-mechanistic PD model. To assess the generalisability of the developed semi-mechanistic PK/PD model to predict PD drug interactions, data from published time-kill curve studies was digitalised using the software GraphClick. The scenarios included combinations of cell-wall antibiotics and protein-synthesis inhibitors: vancomycin and linezolid vs. MRSA [146], penicillin and erythromycin vs. *Streptococcus pneumoniae* [147], and ampicillin and chloramphenicol vs. clinical isolates of group B Streptococci [148]. If estimation of an EC_{50} value was not possible due to exclusively inhibitory time-kill curve data in the respective study, EC_{50} was set to the respective minimal inhibitory concentration of the antibiotic and the Hill-factor was set to 4. Further, CFU_0, CFU_{max} and k_{rep} were adapted to the respective GC curves. The maximum drug effects were either a result of the growth-curve (for replication-dependent killing) or were adapted to drug effect that exhibited replication-independent killing. The persister development rate k_{per} was set to the final parameter estimate of MER if there was a lack of data to estimate it.

2.4.2 Simulations

To perform simulations, the developed 'final' semi-mechanistic PD model was linked to population PK models to explore the PK/PD relationships of LZD, MER and VAN in a quantitative fashion. In the first part of this chapter, the translational validity of the population PK/PD model was assessed in an *in silico* dose fractionation study [149] to calculate PK/PD indices and to derive PK/PD breakpoints for the study drugs. In the second part, clinically relevant dosing regimens were simulated and potential influences of patient covariates were elucidated.

2.4.2.1 Population pharmacokinetic models

Population PK investigates the PK of a drug in a population, very often using NLME [42]. NLME dissects the observed PK variability into interindividual and intraindividual variability. Patient covariates are investigated to potentially explain parts of the observed interindividual variability, thus reducing the unexplained interindividual variability. Population PK models from peer-reviewed publications were selected based on (i) heterogeneity of the patient population to ensure that covariates

could have been detected, (ii) parametric nature of the PK model to allow for facile implementation of the PK model in 'R' and (iii) quality of the PK model demonstrated by diagnostics in the publications. Suitable population PK models with their covariate relationships were encoded in 'R'. Interindividual variability that was not explained by the covariate relationships was mathematically described by assuming either an exponential or proportional variability model, as provided in the respective publications:

Exponential variability model: $P_{k,i} = \theta_k \times e^{\eta_{k,i}}$ (Eq. 31)

Proportional variability model: $P_{k,i} = \theta_k \times (1 + \eta_{k,i})$ (Eq. 32)

$P_{k,i}$ represented the estimated k'th PK parameter for the i'th individual calculated from the population PK parameter θ_k of the typical patient whilst $\eta_{k,i}$ represented the individual deviation from the typical PK parameter assuming the respective distribution. $\eta_{k,i}$ was sampled from a normal distribution with mean zero and variance ω^2. To avoid implausible negative individual PK parameters for the proportional variability model, sampling of $\eta_{k,i}$ was restricted to values of $\geq$-1. Residual intraindividual variability was not considered.

Linezolid. For LZD, a one-compartment disposition model with first-order processes [150] was implemented in 'R' assuming an exponential variability model for unexplained interindividual variability (Eq. 31). The published model contained creatinine clearance estimated by Cockcroft Gault in mL/min (CLCR) [151], severe liver cirrhosis (CIR) as dichotomous covariate (1: cirrhosis, Child Pugh grade C [152]; 0: no cirrhosis) and total body weight (WT) in kg as covariates. Plasma protein binding of LZD was assumed to be 13.4% [93].

Table 1: Population PK parameters for linezolid using a one-compartment disposition model with covariate relationships on the structural PK parameters clearance and volume of distribution used for simulation; interindividual variability is indicated as variance ω^2.

PK parameter	Published estimate
Clearance [L/h]	$2.85 \times (CLCR/60.9)^{0.618} \times 0.472^{CIR}$
ω_{CL}^2	0.124 (35.2 % CV)
Volume of distribution [L]	$33.6 \times WT/57.9$
ω_V^2	0.0949 (30.8 % CV)

Meropenem. For MER, a two-compartment disposition model with first-order processes [153] was implemented in 'R' assuming an exponential variability model for unexplained interindividual variability (Eq. 31). The published model contained creatinine clearance estimated by Cockcroft Gault in mL/min (CLCR) [151], age (AGE) in years and total body weight (WT) in kg as covariates. Plasma protein binding of MER was assumed to be 2 % [81].

Table 2: Population PK parameters for meropenem using a two-compartment disposition model with covariate relationships on the structural PK parameters clearance and central volume of distribution used for simulation; interindividual variability is indicated as variance ω^2.

PK parameter	Published estimate
Clearance [L/h]	$14.6 \times (CLCR/83)^{0.62} \times (AGE/35)^{-0.34}$
ω_{CL}^2	0.118 (34.4 % CV)
Central volume of distribution [L]	$10.8 \times (WT/70)^{0.99}$
ω_{V1}^2	0.143 (37.8 % CV)
Intercompartimental clearance [L/h]	18.6
ω_Q^2	0.290 (53.9 % CV)
Peripheral volume of distribution [L]	12.6
ω_{V2}^2	0.102 (31.9 % CV)

Vancomycin. For VAN, a two-compartment disposition model with first-order processes [154] was implemented in 'R' assuming a proportional variability model for unexplained interindividual variability (Eq. 32). The published model contained creatinine clearance estimated by Cockcroft Gault in mL/min (CLCR) [151] and total body weight (WT) in kg as covariates. Plasma protein binding of VAN was assumed to be 32.8% [155].

Table 3: Population PK parameters for vancomycin using a two-compartment disposition model with covariate relationships on the structural PK parameters clearance, central and peripheral volume of distribution, used for simulation. Residual interindividual variability is indicated as variance ω^2. For intercompartimental clearance, no interindividual variability was obtained. (n.a.: not applicable).

PK parameter	Published estimate
Clearance [L/h]	$0.034 \times CLCR + 0.015 \times WT$
ω_{CL}^2	0.0853 (29.2 % CV)
Central volume of distribution [L]	$0.414 \times WT$
ω_{V1}^2	0.133 (36.4 % CV)
Intercompartimental clearance [L/h]	7.48
ω_{Q}^2	n.a.
Peripheral volume of distribution [L]	$1.32 \times WT$
ω_{V2}^2	0.158 (39.8 % CV)

2.4.2.2 Prediction of PK/PD indices

The translational predictivity of the developed semi-mechanistic PD model was investigated by simulating a dose fractionation study [149]. For this purpose, the encoded population PK models described above (2.4.2.1) were linked to the developed semi-mechanistic PD model (2.4.1.3.3) to create a population PK/PD model. For this part, simulations were performed solely with the typical patient (i.e. no interindividual variability) and covariates of the population PK models were set to 35 years for age, 75.0 kg for total body weight, 120.0 mL/min for creatinine clearance and without liver cirrhosis. Six to ten dose levels were empirically chosen to cover concentrations around the MIC of methicillin-susceptible *S. aureus* and ranged from 80-1200 mg (LZD), 2.5-20 mg (MER) and 10-200 mg (VAN). These doses were virtually administered 1-12 (MER) and 1-6 times (LZD and VAN) over a simulation period of 24 h. PK/PD indices [156] were determined according to non-linear regression analysis and evaluated graphically and based on the coefficient of determination (R^2) and included:

- *%f*T$_{>MIC}$: The percentage of time that unbound drug concentrations exceed the MIC in a 24 h period.
- *f*C$_{max}$/MIC: The peak unbound drug concentration divided by the MIC.
- *f*AUC/MIC: The area under the unbound concentration-time profile divided by the MIC in a 24 h period.

The obtained model-predicted PK/PD indices were compared to the clinical PK/PD indices of MER [125], LZD [157] and VAN [96] and bacteriostatic and/or bactericidal PK/PD breakpoints were derived.

2.4.2.3 Clinical trial simulation

Virtual clinical trial with reference dosing regimens. In order to explore the antibiotic effects of LZD, MER and VAN, alone and in dual combinations, clinically utilised dosing regimens were used for simulations with the linked population PK/PD model. All drugs were virtually administered as intravenous infusions over 1 h to mimic a typical clinical situation. The exploratory scenarios were

- LZD 600 mg BID [90]
- MER 1000 mg TID [81]
- VAN 1000 mg BID [99]

alone and included double combinations of LZD/MER and VAN/MER. The exploratory simulations were performed with a virtual patient population of 1000 individuals. The covariates AGE, WT and serum creatinine (SCR) were sampled from log-normal distributions with geomean values of 75 kg, 35 yrs. and 1.0 mg/dL, respectively and a standard deviation of 10% CV for all covariates using the 'rlnorm' function in 'R'. SEX and CIR were simulated from binomial distributions with probabilities of 50% females and 5% liver cirrhosis. CLCR was subsequently calculated from those 'primary' patient covariates using the Cockcroft-Gault equation:

$$CLCR = \frac{(140 - AGE) \times WT}{72 \times SCR} (\times \, 0.85 \text{ if female})$$
(Eq. 33)

(Unexplained) interindividual variability on the population PK model and uncertainty of the parameters of the semi-mechanistic PD model was considered by using stochastic simulations in a Monte-Carlo approach [158] by sampling from the respective parameter distributions for each individual virtual patient: The unexplained interindividual PK variability between virtual patients with those covariates was included in the simulations as described in 2.4.2.1. Uncertainty of the PD model parameter estimates was considered by sampling the respective model parameter from a distribution generated by the final model parameter estimate as means and the obtained variance-covariance matrix (Eq. 11) as (co-)variances.

The PK/PD indices identified as being predictive in 2.4.2.2 were calculated and compared to the values obtained in the dose fractionation study.

Impact of covariates on the antibiotic effect. Potential impact of patient covariates was investigated by varying the covariate value in addition to the variability/uncertainty described above. Creatinine clearance was altered from 60-160 mL/min, total body weight was varied from 60-105 kg for all studied antibiotics. For LZD, the impact of liver cirrhosis was additionally explored. In order to provide an effect measure that is also frequently used in pre-clinical PK/PD studies for anti-infectives, log10 CFU/mL at 24 h was calculated in each scenario and used as an evaluation criterion. Probability of target attainment (PTA) to attain a bacteriostatic or bactericidal effect was calculated:

$$\text{PTA}=\frac{\text{No. of individuals attaining the PD target}}{\text{Total No. of individuals}} \tag{Eq. 34}$$

PTA >0.9 was considered as sufficient.

Exploratory simulations of alternative dosing regimens. If a covariate was found influential on the antibiotic effects, alternative dosing regimens (e.g. continuous infusion or dose intensification) were explored. If appropriate, also higher initial dosing was explored to reach the steady state earlier (PK-driven 'loading dose'), or to enhance initial drug effects (PD-driven 'front-loading').

2.5   General statistical techniques

In addition to the modelling-specific statistics for model comparison (2.4.1.2), some general descriptive and inductive statistical measures and tests were utilised in the present work. Calculations were performed in the software 'R' (version 3.1.1).

2.5.1   Descriptive statistics

The following measures of central tendency and dispersion were used to visualise and aggregate data.

2.5.1.1 Measures of central tendency

- Arithmetic mean $\quad \overline{x} = \frac{\sum_{i=1}^{n} x_i}{n}$

- Geometric mean $\quad \overline{x}_{geo} = \sqrt[n]{x_1 \cdot x_2 \cdot \ldots \cdot x_n}$

- Median $\quad \tilde{x} = \begin{cases} x_{\frac{n+1}{2}} & \text{for uneven n} \\ \frac{1}{2}\left(x_{\frac{n}{2}} + x_{\frac{n}{2}+1} \right) & \text{for even n} \end{cases}$

2.5.1.2 Measures of dispersion, accuracy and precision

- Variance $\quad \sigma^2 = \frac{\sum_{i=1}^{n}(x_i - \bar{x})^2}{n-1}$

- Standard deviation $\quad \sigma = \sqrt{\sigma^2}$

- Coefficient of variation $\quad CV, \% = \frac{\sigma}{\bar{x}} \cdot 100$

- Quantiles/percentiles $\quad \tilde{x}_p = \begin{cases} x_{n \cdot p} & \text{for uneven n·p} \\ \frac{1}{2}\left(x_{n \cdot p} + x_{n \cdot p+1} \right) & \text{for even n·p} \end{cases}$

- Relative error $\qquad RE, \% = \frac{x_{observed} - x_{nominal}}{x_{nominal}} \cdot 100$

- Accuracy $\qquad Accuracy, \% = \frac{x_{observed}}{x_{nominal}} \cdot 100$

2.5.2 Inductive statistics

In inductive statistics, statistical methods are utilised to analyse data in order to deduce properties of an underlying distribution.

2.5.2.1 Confidence intervals

The CI is an interval that provides information about the precision of a point estimate. CIs are characterised by their confidence level (often 95%), i.e. the probability that the determined CIs contain the underlying 'true' point estimate. In the present work, CIs were determined by parametric methods from the quantiles of a distribution, e.g. under assumption of a (log-) normal distribution using mean and variance, or by non-parametric methods such as the bootstrap (2.4.1.3.3) that does not assume an underlying distribution.

2.5.2.2 Hypothesis testing

For a parametric comparison of two groups from the same sample, the two sample t-test was used. For parametric comparison of two or more groups, the one-way analysis of variance (ANOVA) was applied. Statistical tests were performed with the 'stats'-package (version 3.1.1) of 'R'.

3 Results

3.1 Bioanalytical quantification of antibiotics in growth medium

In the present thesis, a bioanalytical HPLC assay for simultaneous quantification of LZD, MER and VAN from CaMHB was successfully developed and validated according to the EMA guideline for bioanalytical method validation [120].

3.1.1 Development of the bioanalytical HPLC method

3.1.1.1 Sample treatment and recovery

Precipitation of the sample with ACN or MeOH and subsequent direct injection into the HPLC apparatus resulted in 'diluted' samples. As the absorption intensity of VAN is rather low (compared to LZD or MER), the resulting LLOQ for VAN of 4-10 mg/L was considered too high and hence not suitable for the analytical needs.

Precipitation with subsequent solvent evaporation and reconstitution in Milli-Q water achieved highest recoveries using 400 µL MeOH + 100 µL sample: LZD was recovered to 72%, MER to 69% and to VAN 71%. ACN was not suitable as precipitating agent: Although recovery was high for LZD (76%), the resulting recoveries for MER (38%) and VAN (0.8%) were rather low if ACN + sample (4+1 v/v) was used. Hence, in the final method, MeOH + sample (4+1 v/v) was utilised as processing method. The coefficient of variation for this procedure was 7.5% for LZD, 6.6% for MER and 7.2% for VAN, as determined from processing four aliquots from a unique sample at a concentration of 10 mg/L.

3.1.1.2 HPLC instrument method

Of the investigated flow gradient elution modes, the following flow gradient program was found suitable (i) to sufficiently separate the analytes from the CaMHB matrix components and (ii) to provide sufficient separation of the analytes LZD, MER and VAN: Mobile phases were

(A) Milli-Q water with 0.1% TFA and

(B) ACN:Milli-Q water 40:60 (v/v) with 0.1% TFA.

The eluent flow rate was 0.4 mL/min during the entire gradient program. Mobile phase composition started with 10% B for 0.0 to 2.0 min. From 2.0 min to 12.0 min, solvent B increased to 62.5%. From 12.0 to 14.0 min, solvent B was reduced to 10% to re-equilibrate the HPLC column. The flow gradient is illustrated in Figure 8.
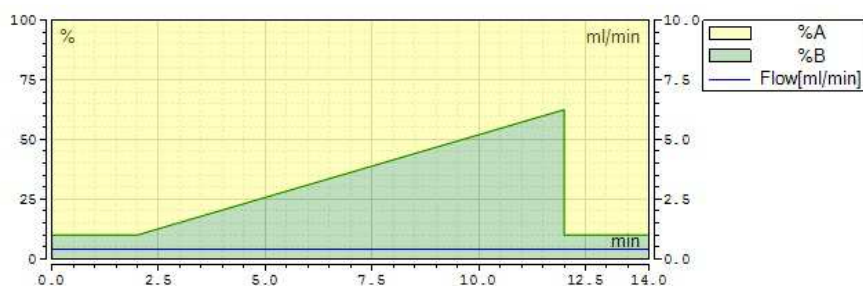
Figure 8: Flow gradient diagram of the final HPLC instrument method.

3.1.2 Validation of the bioanalytical HPLC method

Selectivity and carry-over. The developed HPLC instrument method was found selective and no carry-over was observed when a blank sample was injected after the highest quality control sample QC H. Typical chromatograms obtained at day 2 of the method validation are presented in Figure 9.
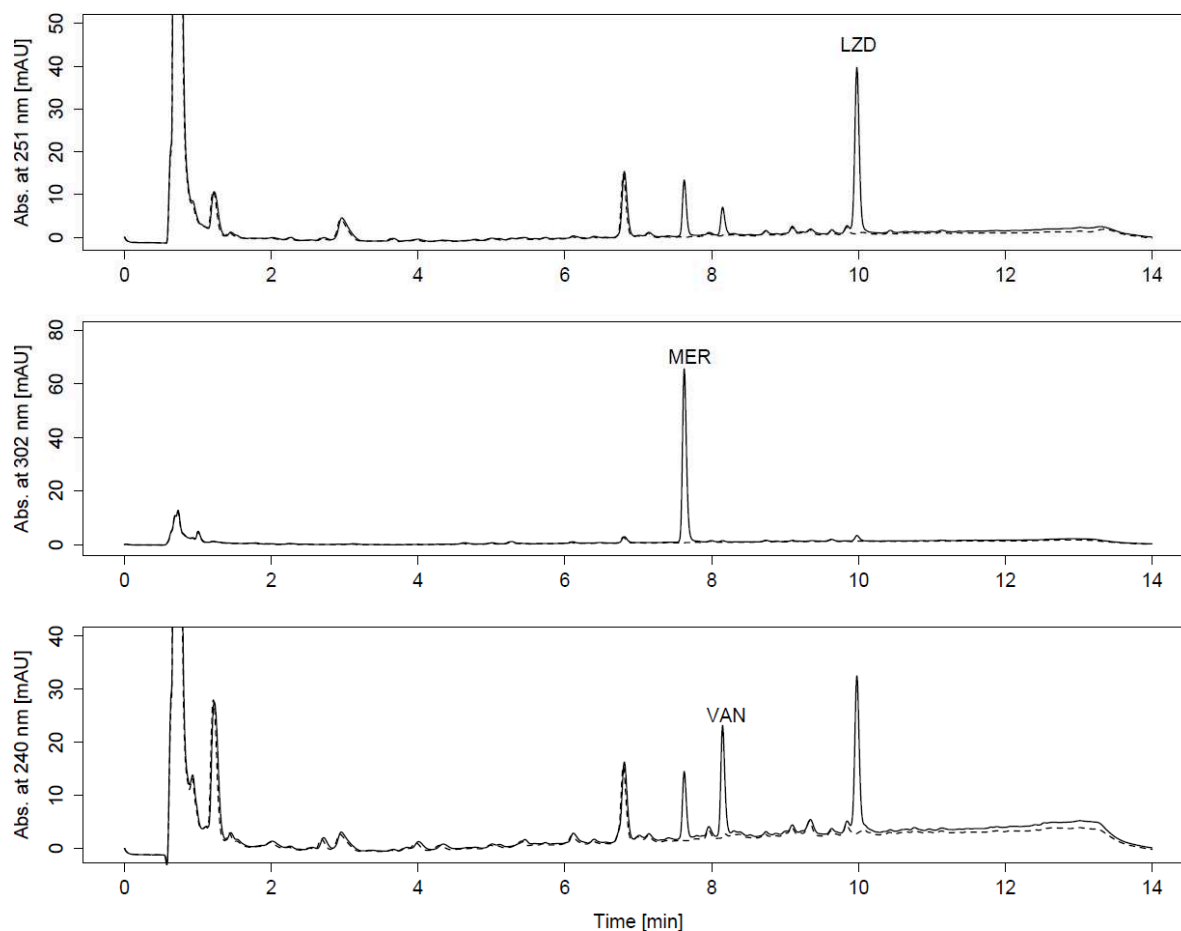
Figure 9: Chromatograms (solid line) at QC-level M for LZD at 251 nm (15 mg/L), MER at 302 nm (50 mg/L) and VAN at 240 nm (25 mg/L) along with matrix injection (dashed line) obtained during method validation.

Calibration curve. Peak area was plotted versus the concentration of the respective six calibration samples of the antibiotics and weighted ($1/x^2$) linear regression with intercept was performed in the

Results

Chromeleon® software. Calibration ranged from the LLOQ to the ULOQ, i.e. 0.5-25 mg/L for LZD, 0.5-100 mg/L for MER and 2-50 mg/L for VAN. Typical calibration functions (Figure 10) obtained on day 2 of method validation were:

- LZD: Area = 0.1451× C(LZD) - 0.0118   R² = 0.999
- MER: Area = 0.0701 × C(MER) - 0.0025   R² = 0.994
- VAN: Area = 0.0443 × C(VAN) - 0.0385   R² = 0.990

All calibration curves obtained during method validation were accepted as accuracy of the calibration samples based on back calculated concentrations ranged from 94.1-106.8 % for LZD, 88.4-109.2 % for MER and 85.5-108.8 % for VAN on the three validation days.
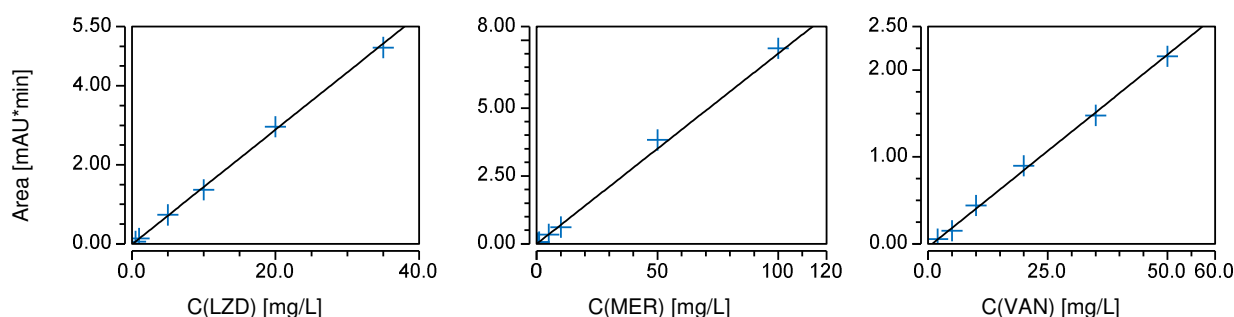
Figure 10: Typical calibration curves obtained at day 2 of method validation for LZD (left), MER (middle) and VAN (right).

Accuracy and precision. Intra- and interday accuracies and their precision determined by analysing (independent) QC samples against the respective calibration curves met the requirements of the EMA guideline [120], and are presented in Table 4. No statistical differences were observed between the three validation days for LZD (p=0.18), MER (p=0.07) and VAN (p=0.12) when analysing accuracy values with a one-way ANOVA (α=0.05).

Table 4: Intraday (n=5) and interday (n=15) accuracy and precision of the developed bioanalytical HPLC method for simultaneous quantification of LZD, MER and VAN from bacterial growth medium (CaMHB) determined from QC samples.

		Intraday						Interday	
		Day 1		Day 2		Day 3			
QC tier	c(LZD)	Accuracy	Precision	Accuracy	Precision	Accuracy	Precision	Accuracy	Precision
	[mg/L]	%	%CV	%	%CV	%	%CV	%	%CV
LLOQ	0.5	112.9	1.9	110.2	3.7	107.8	7.7	110.3	5.0
L	1.5	104.8	2.1	103.6	3.2	98.6	1.5	102.4	3.5
M	15	111.4	5.4	114.1	7.3	95.0	6.1	106.5	10.3
H	29	112.3	1.5	112.1	6.4	95.9	2.6	106.8	8.4

QC tier	c(MER) [mg/L]								
LLOQ	0.5	96.1	2.1	80.3	5.1	86.2	6.3	87.5	8.8
L	1.5	97.9	2.0	86.7	3.3	93.6	1.8	92.7	5.6
M	50	100.0	3.9	100.3	5.8	91.1	4.0	96.9	6.4
H	80	100.8	2.3	98.0	6.0	91.4	2.7	96.7	5.6
	c(VAN) [mg/L]								
LLOQ	2	106.4	2.6	97.2	2.4	101.5	10.8	101.7	7.2
L	6	104.1	3.6	87.5	3.2	102.6	1.9	98.1	8.4
M	25	105.5	5.6	105.3	7.4	96.3	5.9	102.2	7.4
H	40	105.7	1.6	102.5	6.6	96.5	3.2	101.6	5.6

Stability. The summary of the stability investigations related to the simultaneous bioanalysis of LZD, MER and VAN are presented in Table 5. As all concentrations were within ±15% of the nominal concentration of the respective QC sample, all antibiotics were considered stable according to the EMA guideline [120].

Table 5: Stability investigations for LZD, MER and VAN at various QC tiers; for autosampler stability, accuracy was calculated based on the concentration determined at t=0 h, for all other investigated stability tests, accuracy was calculated based on the nominal concentration; n=3 aliquots per QC tier and scenario.

QC tier	c(LZD) [mg/L]	Autosampler stability (15 h at 4° C) Accuracy %	Precision %CV	Short-term stability (5 h at 25° C) Accuracy %	Precision %CV	Freeze/thaw stability (3 cycles) Accuracy %	Precision %CV	Long term stability (~6 months at -80° C) Accuracy %	Precision %CV
LLOQ	0.5	100.7	2.2						
L	1.5	102.5	0.9	103.7	1.1	89.7	1.5	98.4	3.5
M	15	100.8	0.2	98.0	3.3			107.7	8.5
H	29	103.3	3.7			97.9	10.3		
	c(MER) [mg/L]								
LLOQ	0.5	96.7	2.2						
L	1.5	98.4	2.8	94.5	4.9	88.6	4.7	92.6	3.4
M	50	98.7	0.4	101.9	3.3			99.0	9.8
H	80	101.1	3.4			102.1	9.1		
	c(VAN) [mg/L]								
LLOQ	2	100.9	1.9						
L	6	100.3	1.0	97.6	1.7	100.7	5.2	106.5	3.6
M	25	94.3	0.6	91.3	3.3			104.6	9.0
H	40	101.7	3.6			105.7	12.1		

3.1.3 Degradation of the antibiotics in the *in vitro* infection model

First-order degradation rate constants are presented in Table 6 and visualised within 24 h along with the observed drug concentrations in time-kill curve studies (Figure 11).

Table 6: Estimates of first-order degradation rate constants for LZD, MER and VAN at 37° C in CaMHB.

Antibiotic	k_{deg} [h^{-1}]	[95% CI]
LZD	1.01e-04	[-1.27e-03; 1.47e-03]
MER	1.90e-02	[1.74e-02; 2.06e-02]
VAN	3.90e-03	[2.38e-03; 5.42e-03]
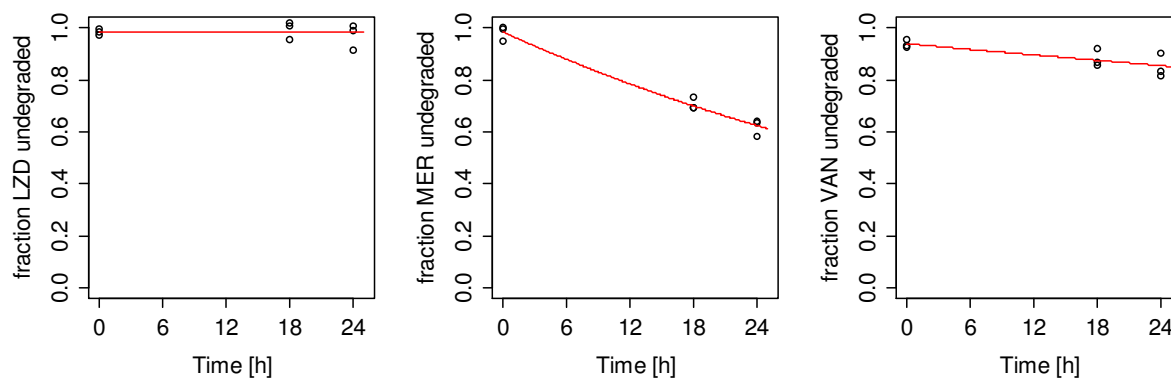
Figure 11: Experimentally observed drug concentrations normalised to nominal concentration at t=0 (points) and estimated first-order degradation kinetics (red lines) for LZD (left), MER (middle) and VAN (right), n=3 per drug.

For LZD, no significant degradation was observed during 24 h as indicated by the very low degradation rate constant of $1.01 \cdot 10^{-4}$ h^{-1} being not statistically different from zero. For MER, significant and substantial degradation was observed within 24 h and MER concentrations were reduced to 62.9% of MER at t=0. VAN also significantly degraded within 24 h and concentrations were reduced to 90.6% of VAN at t=0. Hence, degradation half-lives were $t_{1/2}$(MER) = 36.5 h and $t_{1/2}$(VAN) = 177.8 h.

3.2   Microbiological experiments

3.2.1   Preliminary microbiological investigations

3.2.1.1 Droplet plate assay for quantification of *S. aureus*

Accuracy and precision of the developed sample treatment and quantification method (2.3.1.1) for *S. aureus* are presented in Table 7. The assay range was investigated from 20-500 CFU/sector. For practical reasons, an ULOQ of 300 seemed reasonable. Accuracy was within 90.0-110.0% and precision ranged from 30.1% at 20 CFU/sector to 1.7% at 500 CFU/sector.

Table 7: Accuracy and preparation variability of the developed droplet plate assay (n=6).

Nominal CFU/sector	Median CFU/sector	Accuracy [%]	Precision [%CV]
500	484	96.7	1.7
400	404	100.9	2.8
300	306	101.8	5.8
200	203	101.5	9.5
50	55	110.0	11.6
40	41	102.5	12.0
30	29	96.7	17.0
20	18	90.0	30.1

The developed droplet plate assay was found linear (Figure 12 left). The established processing methods 'centrifugation/washing' and 'direct dilution' were statistically different as indicated by a paired, two-sided, two sample t-test (p=0.00658) when log10 CFU/mL of both method were compared (Figure 12 right). However, the mean bias of the centrifugation method (-0.065 log10 CFU/mL) was not relevant for experimental practice and both method were considered equivalent.
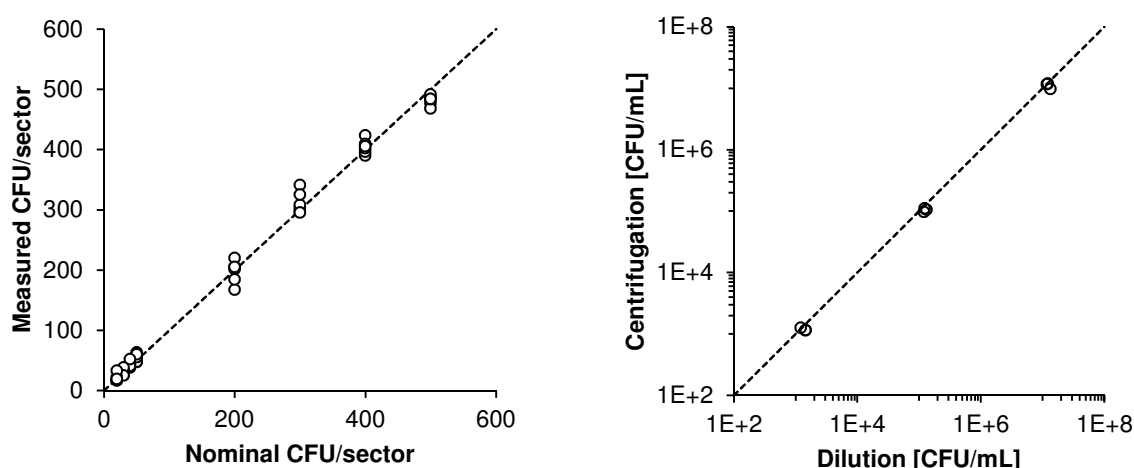
Figure 12: Measured vs. nominal CFU per sector of the incubated agar plate in n=6 per concentration level (left). Comparison between the centrifugation/washing and the direct dilution processing method in n=3 per concentration level (right). Points represent experimental data and dashed lines represent the 'line of identity'.

Stability in dilution media 0.9% NaCl solution and PBSP was investigated over 4 h. First order degradation rate constants were determined by the same mathematical model used for determination of drug degradation (2.2.4). Parameter estimates are presented in Table 8. In 0.9% NaCl solution survival of *S. aureus* at t=4 h was reduced to 69.5% of t=0 (Figure 13). In PBSP, median bacterial counts increased to 111% of t=0 after t=4 h which was also indicated by the negative degradation rate constant. Hence, PBSP was chosen as the more gentle dilution medium for *S. aureus*.

Table 8: Estimates of first-order degradation rate constants for *S. aureus* in the dilution media 0.9% NaCl solution and PBSP at 25° C.

Dilution medium	k_{deg} [h^{-1}]	[95% CI]
0.9% NaCl	9.09e-02	[6.62e-02; 1.16e-01]
PBSP	-2.57e-02	[-4.38e-03; -4.71e-02]
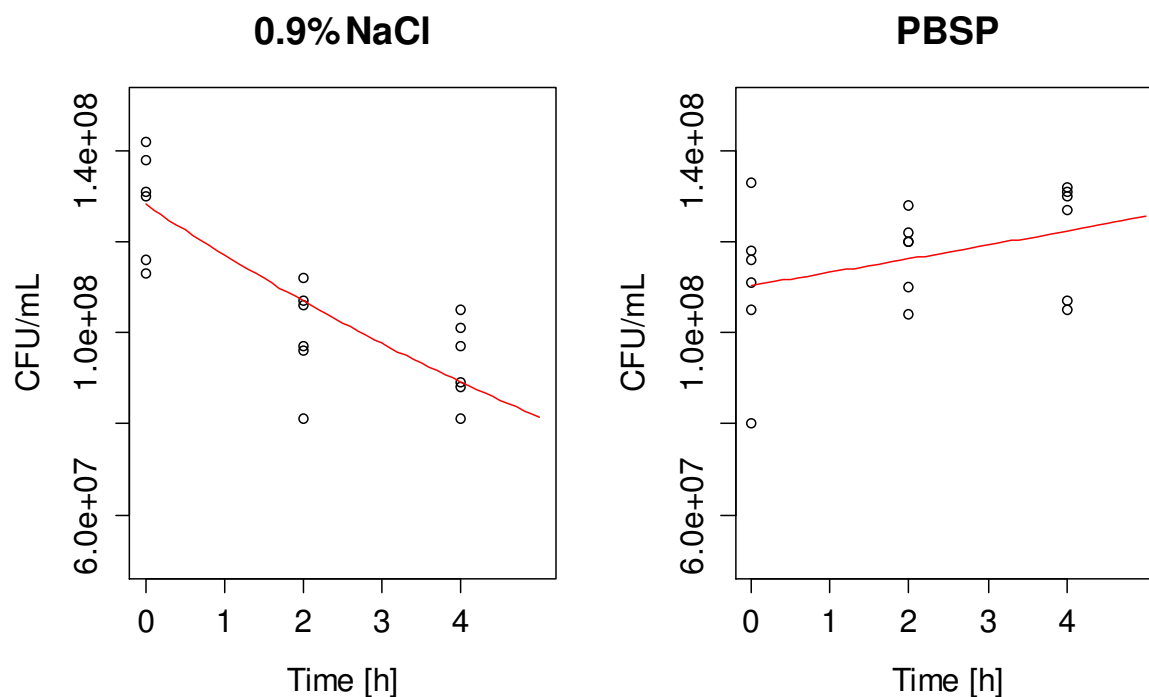
Figure 13: Survival of *S. aureus* in 0.9% NaCl solution (blue triangles) and PBSP (red squares). Symbols represent median values and bars represent range of the experimental data (n=6). Large dashed line represents mean CFU/mL at t=0 of both methods and small dashed lines represent median ± 15%.

3.2.1.2 Determination of the minimal inhibitory concentrations

The MIC values for LZD, MER and VAN were read visually and were indicated as the lowest concentration that did not stimulate visual turbidity (Figure 14).

Figure 14: Example of visual determination of the MIC of LZD vs. *S. aureus* clinical isolate MV 13488. The lowest concentration that prevented turbid growth was 2 mg/L. Numbers: Concentration of LZD in mg/L; GC: growth control; NC: negative control; (n=3 replicates).

MIC values for all investigated antibiotics and bacterial strains are presented in Table 9. Notably, the MIC displayed the same individual value for all replicates within the individual *S. aureus* strains. Also, the MIC values were consistent between the strains for LZD and VAN, except for MER for which the clinical isolate MV 13488 displayed an MIC value of one tier below the other strains.

Table 9: MIC values of LZD, MER and VAN vs. the utilised three strains of *S. aureus*. (Median of n=3).

S. aureus strain	MIC of Antibiotic [mg/L]		
	LZD	MER	VAN
ATCC 29213	2.0	0.125	1.0
MV 13488	2.0	0.0625	1.0
MV 13391	2.0	0.125	1.0

3.2.1.3 Determination of the lag-time of *S. aureus*

The experimental data for lag-time determination of all three strains is presented in Figure 15 and visual inspection of the semi-logarithmic plots suggested two log-linear slopes with an intercept between 80 and 120 min. The estimated lag-time using the biphasic exponential growth model was between 86 and 102 min for all *S. aureus* strains (Table 10). Hence, the utilised pre-incubation time of 2 h was sufficient for the time-kill curve studies to obtain exponentially growing *S. aureus* at drug exposure (2.3.4). Growth rate constants were very similar between the different strains with overlapping 95% CI in the lag-and log-phase (Table 10).

The resulting generation times in lag-phase *S. aureus* were 79 min, 96 min and 57 min for ATCC 29213, MV 13488 and MV13391, respectively. In log-phase *S. aureus*, the generation times were 24 min, 30 min and 25 min for ATCC 29213, MV 13488 and MV13391, respectively.

ATCC 29213

MV13488

MV13391
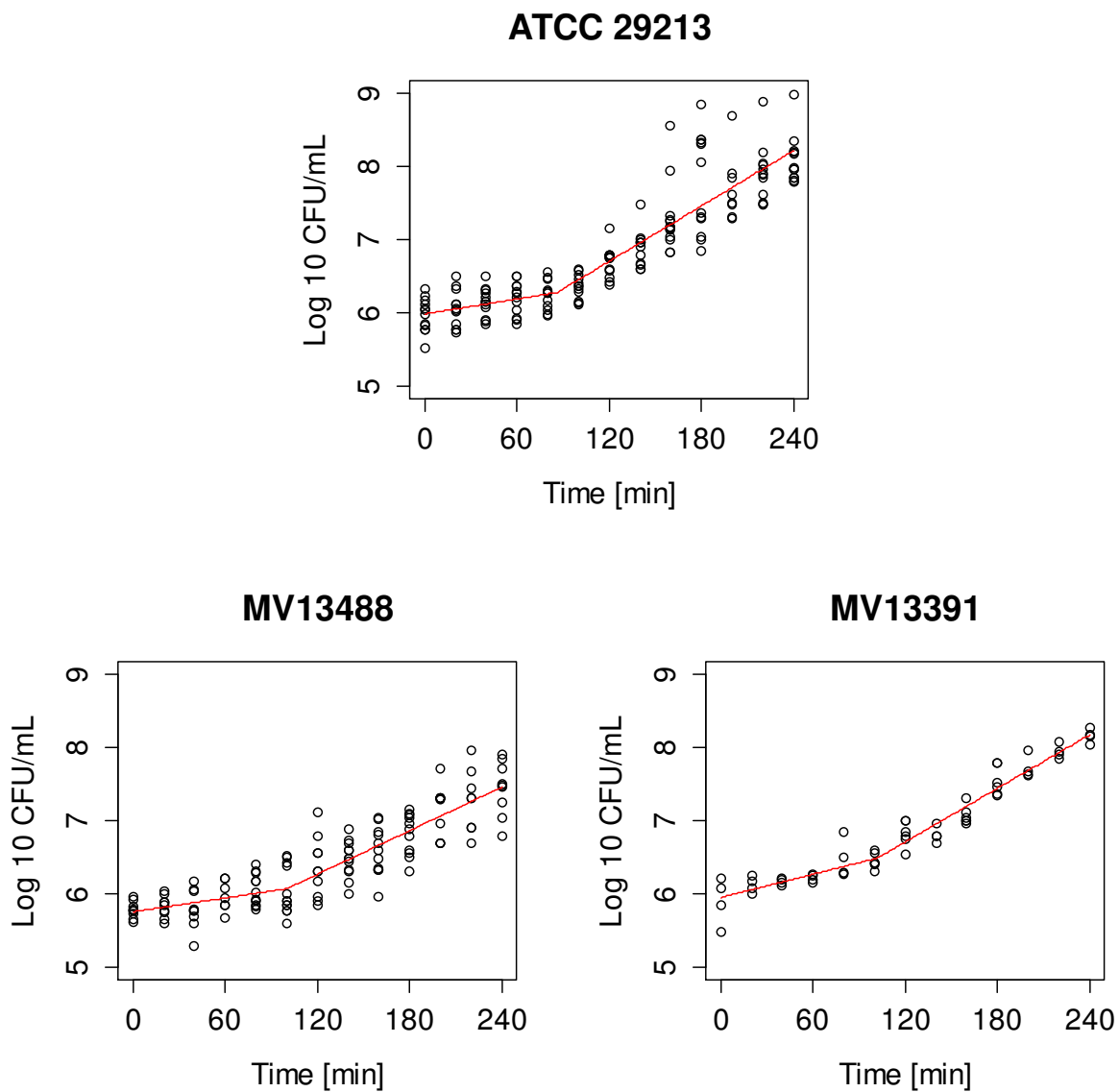
Figure 15: Determination of the lag-times of the utilised three strains of *S. aureus*. Points represent raw experimental data (n=3-6), red line represents predicted growth curve from the utilised biphasic growth model (2.3.1.4).

Table 10: Estimated growth parameters of the utilised three strains of *S. aureus*.

S. aureus strain	Growth parameter		
	Lag-time [min] ($CI_{95\%}$)	Growth rate constant [min^{-1}]	
		lag-phase ($CI_{95\%}$)	log-phase ($CI_{95\%}$)
ATCC 29213	86 (67-105)	0.00782 (0.00201-0.0136)	0.0289 (0.0255-0.0323)
MV 13488	100 (95-105)	0.00723 (0.00306-0.0114)	0.0227 (0.0199-0.0257)
MV 13391	102 (90-114)	0.0121 (0.00832-0.0159)	0.0280 (0.0253-0.0307)

3.2.2 Checkerboard studies of linezolid and meropenem against *S. aureus*

Evaluation of the checkerboard by turbidity ('conventional checkerboard') revealed that both agents did not alter the antibacterial effect as indicated by turbid (bacterial growth) and clear (inhibition of bacterial growth) wells of the 48-well plate. Hence, no interaction between LZD and MER was found with the conventional checkerboard study (Figure 16, upper panel). Notably, the MIC (indicated by [+] in Figure 16) for MER was 0.06 mg/L in the utilised CaMHB (Sigma-Aldrich) in comparison to the CaMHB (Oxoid) used for susceptibility testing and performance of the time-kill curve studies in which the MIC was 0.13 mg/L (3.2.1.2).

The results of the 'dynamic checkerboard' study when bacteria were additionally quantified are presented in the lower panel of Figure 16. MER alone (≥ 0.25 mg/L) reduced the bacteria by >3 log10 CFU/mL. LZD alone reduced the bacteria at maximum by ca. 1.5 log10 CFU/mL. In combination, if drug concentrations exceeded the MIC, the bactericidal effect of MER was antagonised and the combinatory effect corresponded to the bacteriostatic effect of LZD alone.
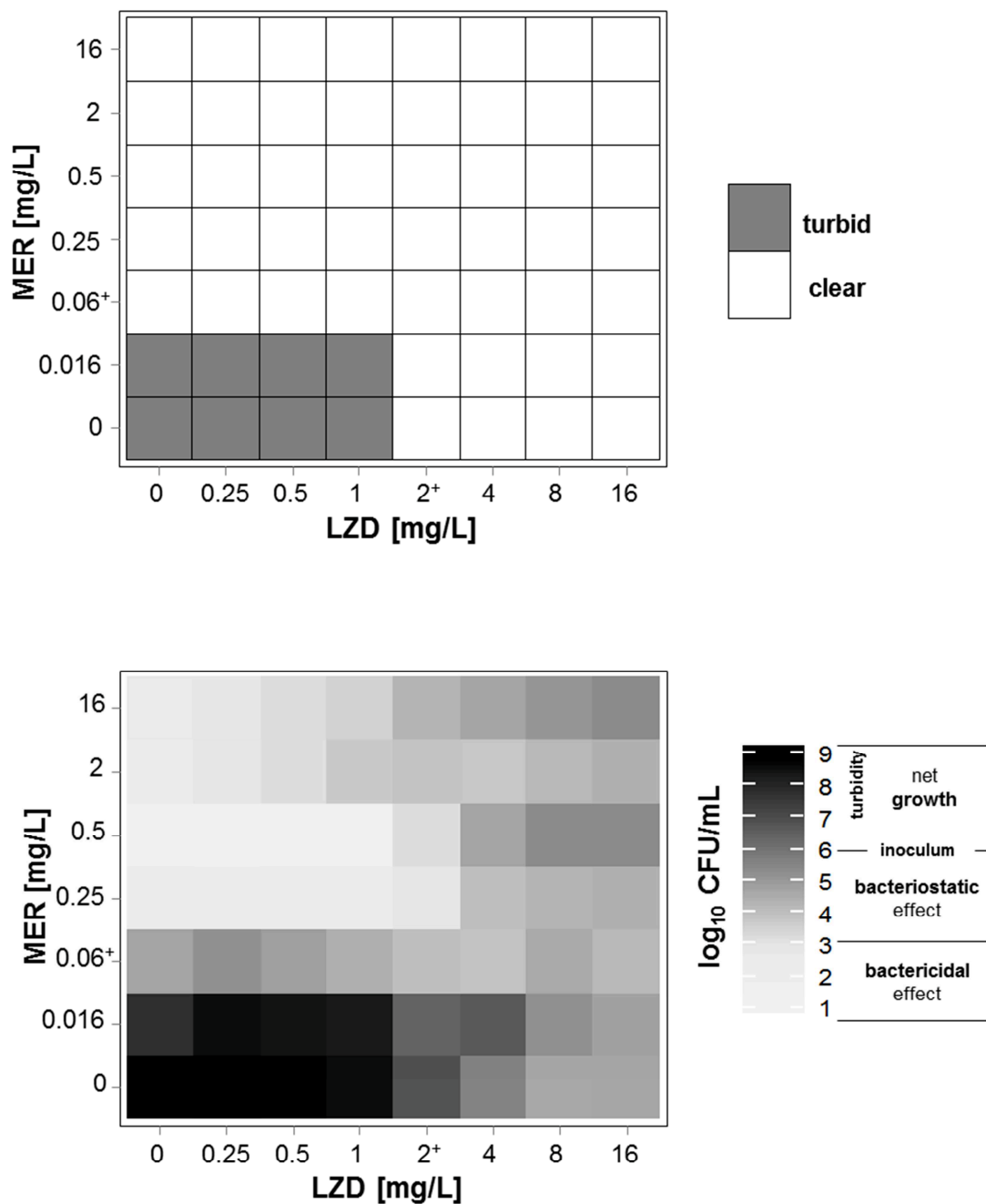
Figure 16: Checkerboard study between LZD and MER. Upper panel: Conventional checkerboard evaluated by turbidity; turbid cavities of the well plate indicated bacterial growth; clear cavities indicated inhibition of bacterial growth. Lower panel: Dynamic checkerboard evaluated by quantification of bacteria; Gradient indicates concentration of bacteria in log10 CFU/mL; Inoculum, bacteriostatic and bactericidal effect thresholds are indicated next to the gradient. [+] indicates the MIC values (n=3).

3.2.3 Time-kill curve studies in lag-phase in *in vitro* infection models

The time-kill curve studies provided a continuous measure of the individual and combined antibacterial effects of LZD, MER and VAN. First, the results for the reference strain *S. aureus* ATCC 29213 are presented, subsequently those of the two clinical isolates.

For lag-phase bacteria, in all GC experiments, a lag time of ca. 90-100 minutes was observed until exponential growth was observed. After 6-8 h, bacteria reached the stationary phase of growth with ca. $1 \cdot 10^{10}$ CFU/mL.

For LZD (Figure 17), concentrations up to 2 mg/L protracted growth of *S. aureus* and moderate killing was observed between 4 and 32 mg/L. Bacterial killing was only marginally increased between 8 and 32 mg/L indicating that the maximum effect of LZD against lag-phase *S. aureus* was reached at 32 mg/L. LZD reduced *S. aureus* by ca. 1 log10 CFU/mL and hence displayed a bacteriostatic effect after 24 h.

Figure 17: Time-kill curve study of LZD versus *S. aureus* ATCC 29213 in lag-phase at drug exposure. Points represent median concentration of bacteria in log10 CFU/mL and bars represent range of 2-6 determinations of n=2-3 independent experiments. Inhibitory concentrations, i.e. concentrations ≥1×MIC (filled symbols), subinhibitory concentrations (open symbols).

For MER (Figure 18), concentrations up to 0.0625 mg/L protracted growth of *S. aureus* ATCC 29213 and resulted in a decreased bacterial load at 24 h compared to the GC curves (1×10^8 CFU/mL vs. 1×10^{10} CFU/mL). For MER at 0.125 mg/L (=MIC), bactericidal killing was observed at 6-8 h, but was followed by regrowth up to ca. 5×10^7 CFU/mL at 24 h. For MER at 0.25 mg/L, the effect of MER was most pronounced and a bactericidal effect was attained at 6-8 h, which was stable until 24 h. For MER at higher concentrations (≥2 mg/L), a paradoxically reduced initial effect of MER was observed. Yet, a bactericidal effect was attained at 24 h for MER ≥2 mg/L.

Figure 18: Time-kill curve study of MER versus *S. aureus* ATCC 29213 in lag-phase at drug exposure. Points represent median concentration of bacteria in log10 CFU/mL and bars represent range of 2-6 determinations of n=2-3 independent experiments. Inhibitory concentrations (filled symbols), subinhibitory concentrations (open symbols). Dotted lines highlight concentrations that displayed a paradoxically reduced initial effect of MER.

For VAN (Figure 19), concentrations up to 0.5 mg/L did not have an antibacterial effect compared to the GC curve. For VAN at 0.75-1.0 mg/L, initial killing to 10^4-10^5 CFU/mL until 12 h was observed, which was followed by regrowth to ca. 10^9 CFU/mL. For VAN $\geq$1.5 mg/L, persistent killing without regrowth was observed and a bactericidal effect was obtained for VAN $\geq$2 mg/L at 24 h.
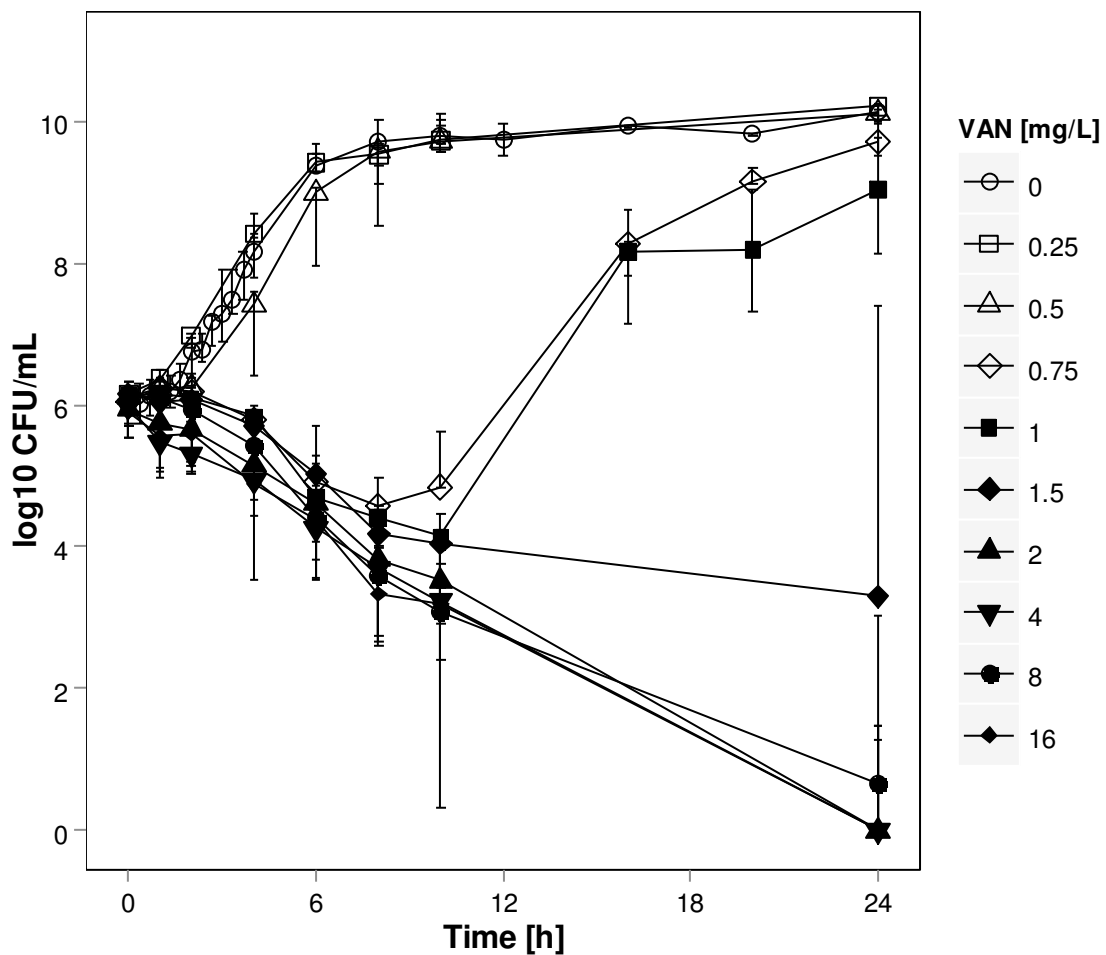
Figure 19: Time-kill curve study of VAN versus *S. aureus* ATCC 29213 in lag-phase at drug exposure. Points represent median concentration of bacteria in log10 CFU/mL and bars represent range of 2-6 determinations of n=2-3 independent experiments. Inhibitory concentrations (filled symbols), subinhibitory concentrations (open symbols).

In subinhibitory combination, LZD at 1 mg/L and MER at 0.03125 mg/L protracted growth of *S. aureus* ATCC 29213, but resulted in net-growth up to ca. 10^9 CFU/mL at 24 h (Figure 20). For inhibitory concentrations of LZD and MER, the combined effect corresponded to the effect of LZD alone (Figure 17) and the bactericidal effect of MER (Figure 18) was antagonised to bacteriostasis.

Figure 20: Time-kill curve study of combinations of LZD and MER versus *S. aureus* ATCC 29213 in lag-phase at drug exposure. Points represent median concentration of bacteria in log10 CFU/mL and bar represents range of 2-6 determinations of n=2-3 independent experiments. Inhibitory concentrations (filled symbols), subinhibitory concentrations (open symbols). Dotted line represents killing curve of MER at the maximum effect for comparison.

Subinhibitory combinations of VAN and MER substantially inhibited growth of *S. aureus* and displayed an increased antibacterial effect compared to the effect of each agent alone (Figure 21). For instance, MER alone at 0.06 mg/L displayed modest killing with regrowth and resulted in 10^8-10^9 CFU/mL at 24 h (Figure 18). VAN alone at 0.75 mg/L displayed initial killing with regrowth and resulted in >10^9 CFU/mL at 24 h (Figure 19). In combination, *S. aureus* was reduced to ca. $5 \cdot 10^3$ CFU/mL. Addition of subinhibitory VAN at 0.25 mg/L, which displayed no effect alone (Figure 19), to MER at 0.125 mg/L substantially reduced regrowth of the *S. aureus* that was observed with MER at 0.125 mg/L alone. For VAN at 0.5 mg/L and MER at 0.13 mg/L a bactericidal effect was observed. Hence, a favourable interaction between VAN and MER was observed, but their nature (additivity, synergy) is yet unclear from raw time-kill curve data.
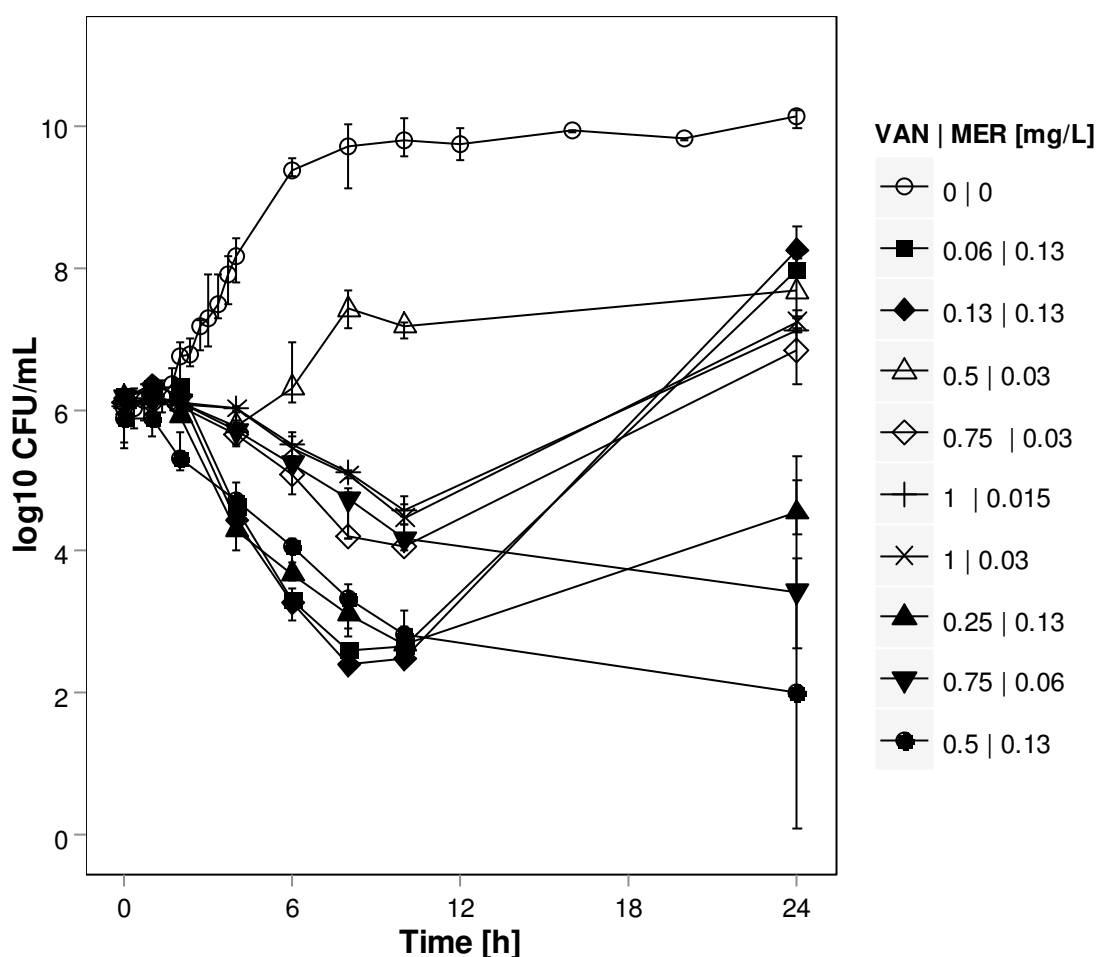
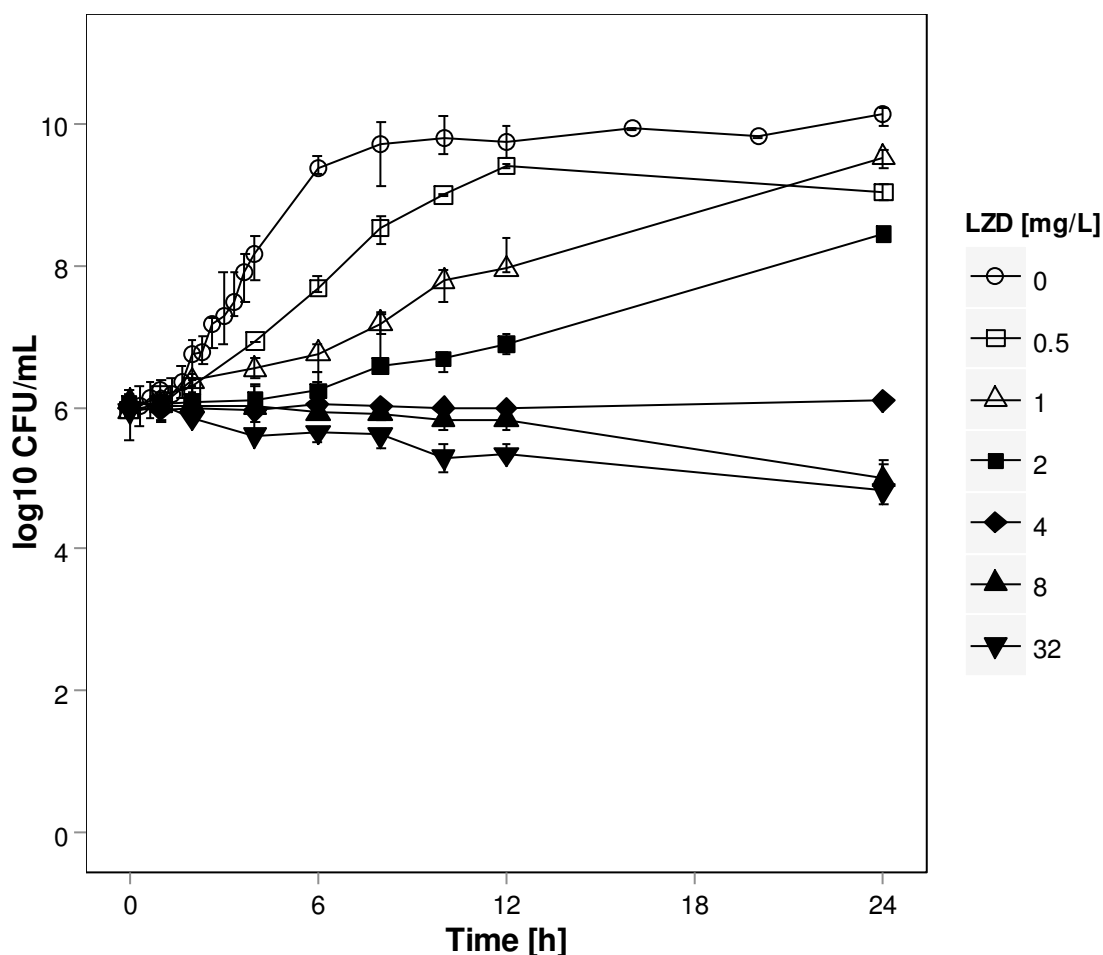**Figure 21:** Time-kill curve study of subinhibitory combinations of VAN and MER versus *S. aureus* ATCC 29213 in lag-phase at drug exposure. Points represent median concentration of bacteria in log10 CFU/mL and bars represent range of 2-6 determinations of n=2-3 independent experiments. Legend symbols were aligned with appearance in the plot at 12-24 h.

For inhibitory combinations of VAN and MER (Figure 22), the combined effect corresponded to the effect of VAN alone, which was marginally less than the effect of MER alone at maximally effective concentrations (0.25 and 0.5 mg/L), but similar compared to higher concentrations of MER (2-8 mg/L) (Figure 18). Overall, the combination of VAN and MER was bactericidal at 24 h if concentrations were ≥2 mg/L for VAN and ≥0.5 mg/L for MER.

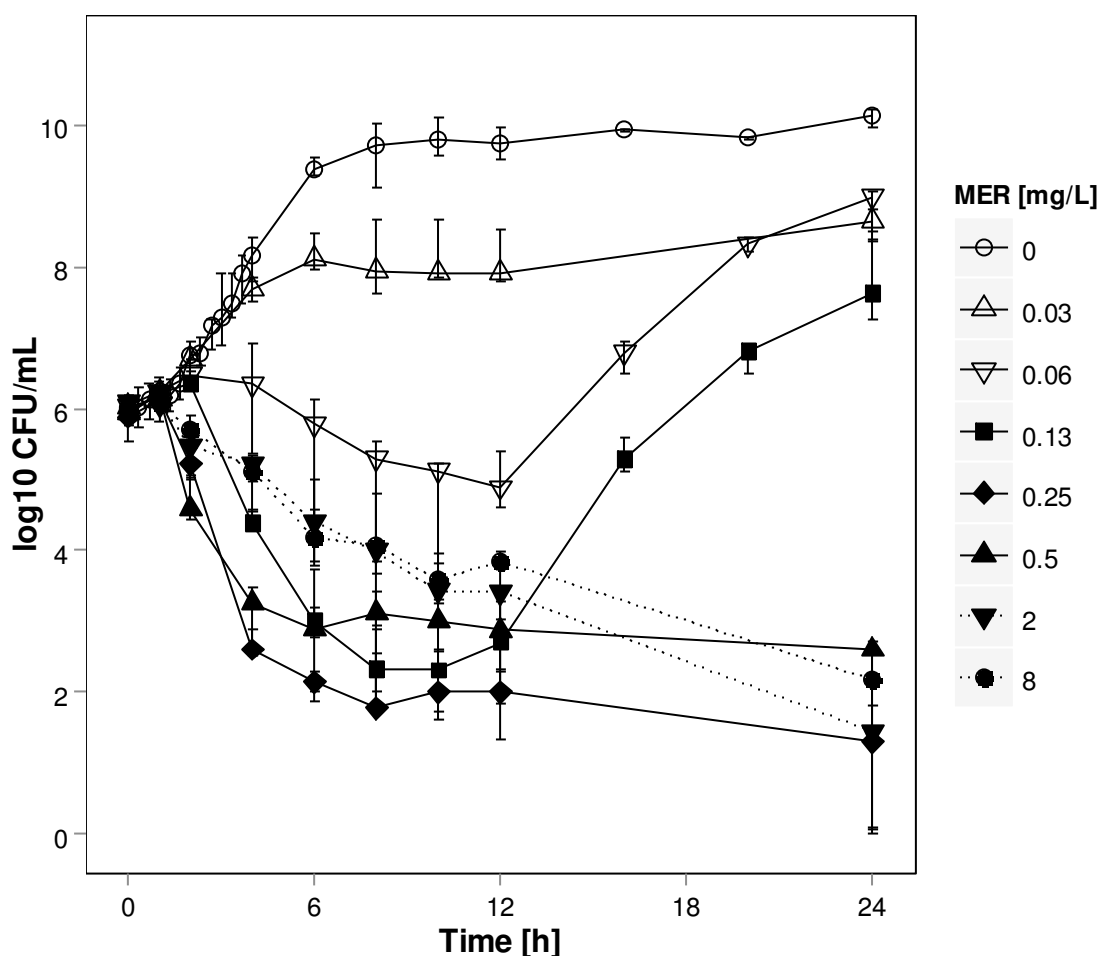**Figure 22:** Time-kill curve study of inhibitory combinations of VAN and MER versus *S. aureus* ATCC 29213 in lag-phase at drug exposure. Points represent median concentration of bacteria in log10 CFU/mL and bars represent range of 2-6 determinations of n=2-3 independent experiments. Dotted line represents killing curve of MER at the maximum effect for comparison.

The studies with the clinical isolates MV 13391 and MV 13488 of *S. aureus* also confirmed an antagonistic interaction between LZD and MER (Figure 23). The combined effect for combinations of VAN and MER also corresponded to the effect of VAN (Figure 24) as observed with the reference of *S. aureus* strain (ATCC 29213). Notably, MV 13488 did not exhibit a paradoxically reduced effect at higher concentrations of MER (Figure 23).

Figure 23: Time-kill curve study of selected combinations of LZD and MER versus *S. aureus* clinical isolates in lag-phase at drug exposure. Points represent median concentration of bacteria in log10 CFU/mL and bar represents range of 2-4 determinations of n=2 independent experiments.
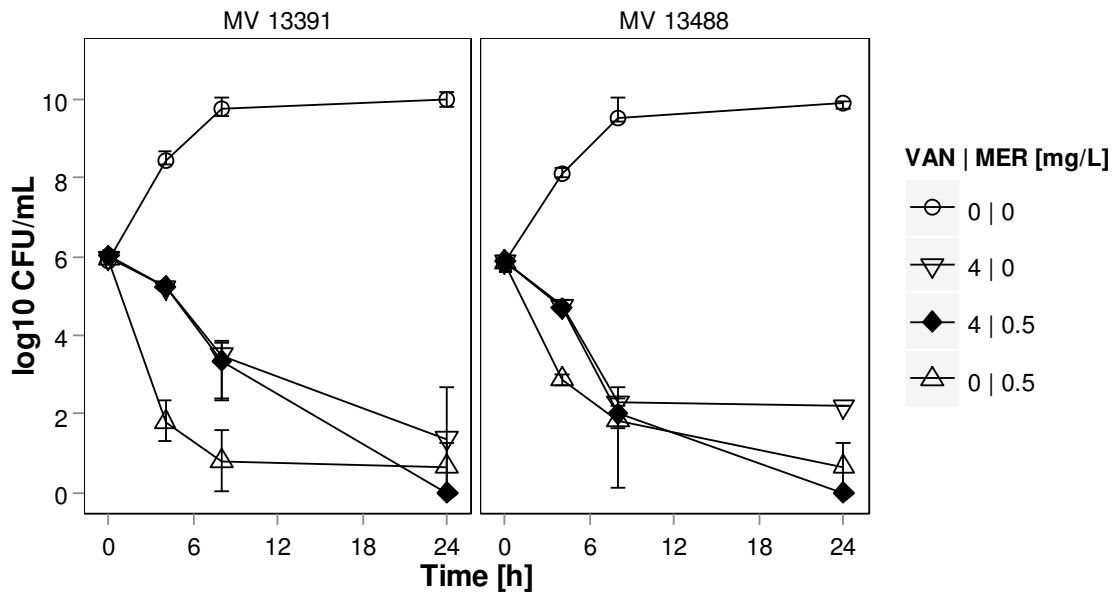
Figure 24: Time-kill curve study of selected combinations of VAN and MER versus *S. aureus* clinical isolates in lag-phase at drug exposure. Points represent median concentration of bacteria in log10 CFU/mL and bar represents range of 2-4 determinations of n=2 independent experiments.

3.2.4 Time-kill curve studies in log-phase in *in vitro* infection models

To assess a potential impact of the growth state at drug exposure, for the following experiments, *S. aureus* ATCC 29213 was pre-incubated for 2 h at 37° C which assured exponential growth at drug exposue (3.2.1.3). Hence, in contrast to time-kill curves in the lag-phase at drug exposure, only a single initial slope was observed in the GC curves with log-phase *S. aureus*. Maximum growth was similar as in lag-phase *S. aureus* and a ca. $1 \cdot 10^{10}$ CFU/mL were reached after 24 h.

The effect of LZD against log-phase *S. aureus* ATCC 29213 is illustrated in Figure 25: LZD at concentrations up to 2 mg/L protracted growth compared to the GC curve and for LZD at 4 mg/L the bacterial load remained constant at ca. 10^6 CFU/mL for the entire experiment until 24 h. For higher concentrations of LZD, two phases of killing were observed: After initial considerably intense killing up to 4-6 h a persisting phase with much slower killing was observed. LZD at 32 mg/L exhibited a bactericidal effect against *S. aureus* ATCC 29213.
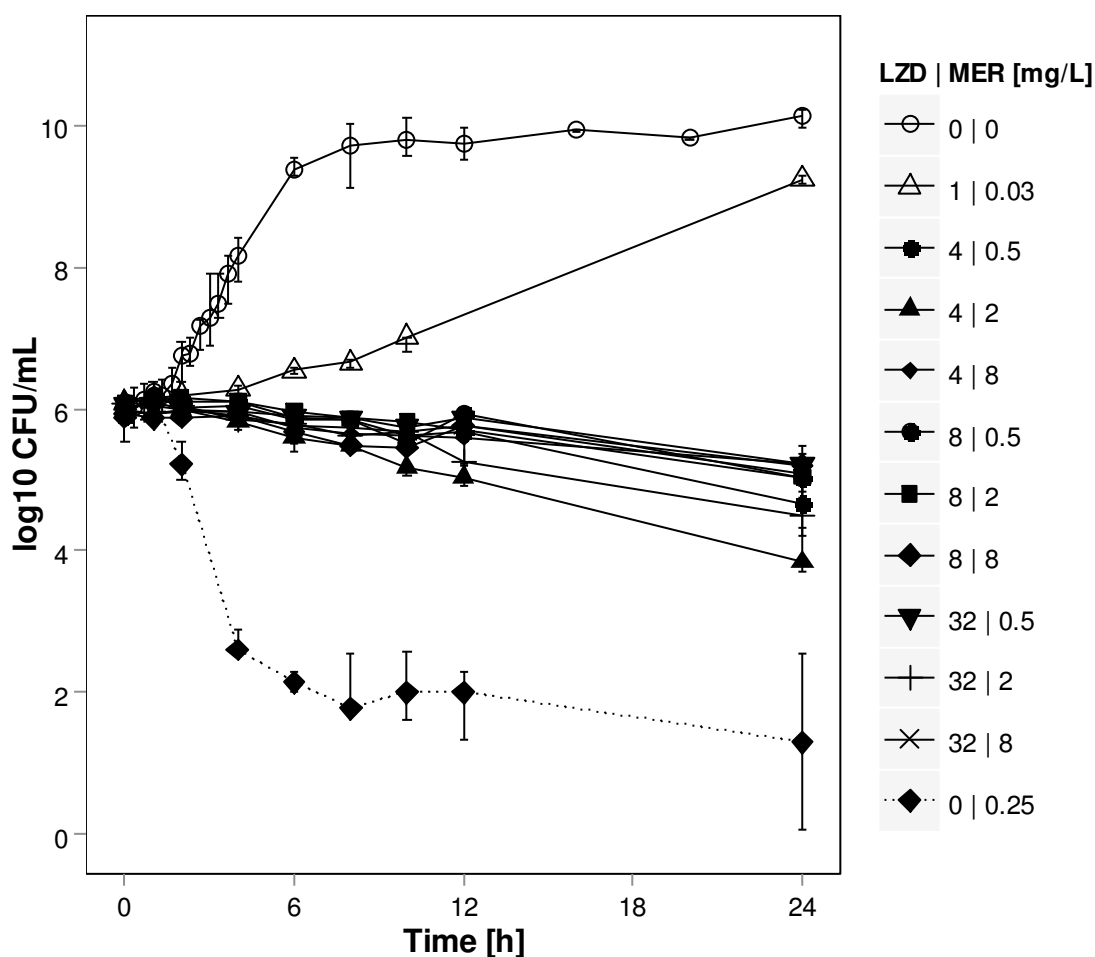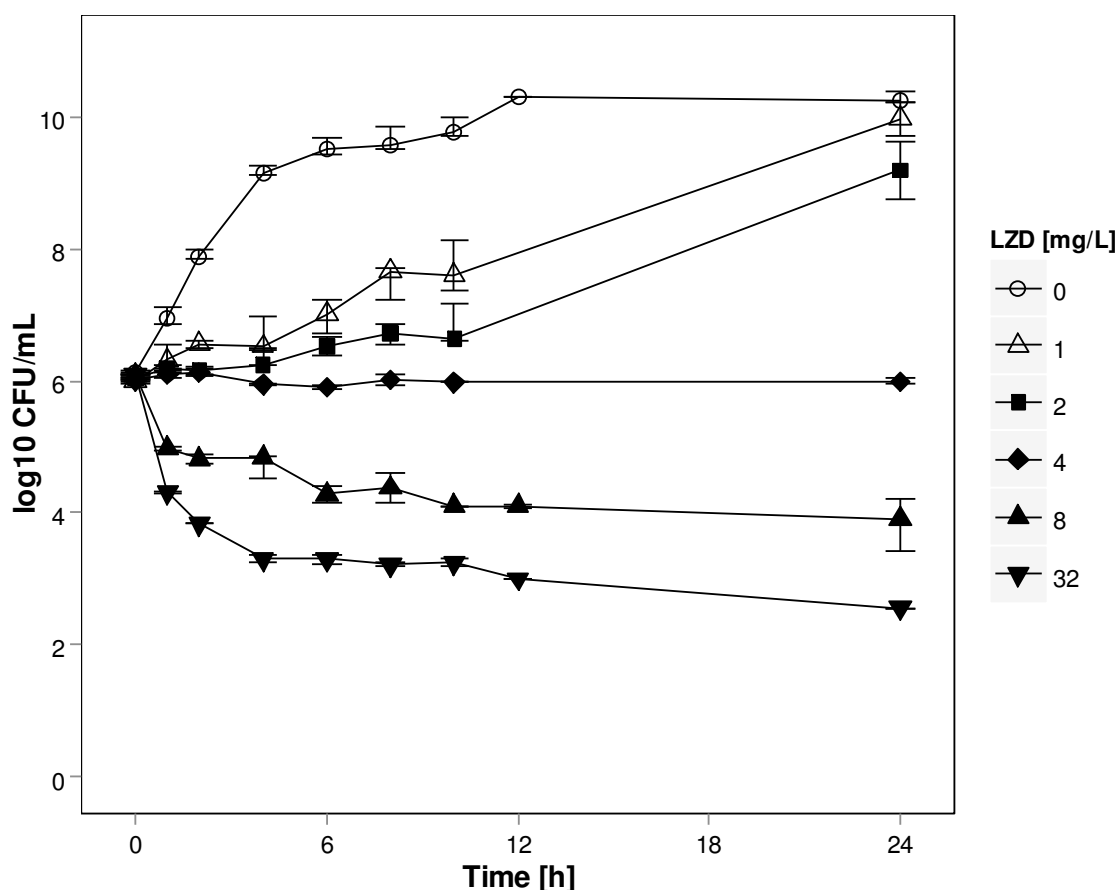

Figure 25: Time-kill curve study of LZD versus *S. aureus* ATCC 29213 in log-phase at drug exposure. Points represent median concentration of bacteria in log10 CFU/mL and bars represent range of 2-4 determinations of n=2 independent experiments. Inhibitory concentrations (filled symbols), subinhibitory concentrations (open symbols).

For MER (Figure 26), concentrations up to 0.125 mg/L protracted growth or provided killing up to maximal ca. 10^4 CFU/mL at 6 h, followed by regrowth which yielded $>10^8$ CFU/mL at 24 h. For MER 0.25 and 0.5 mg/L, a rapid bactericidal effect was observed after 4 h, which was stable until 24 h. Higher concentrations of MER (2 and 8 mg/L) were initially slightly less effective being bactericidal after 6 h.
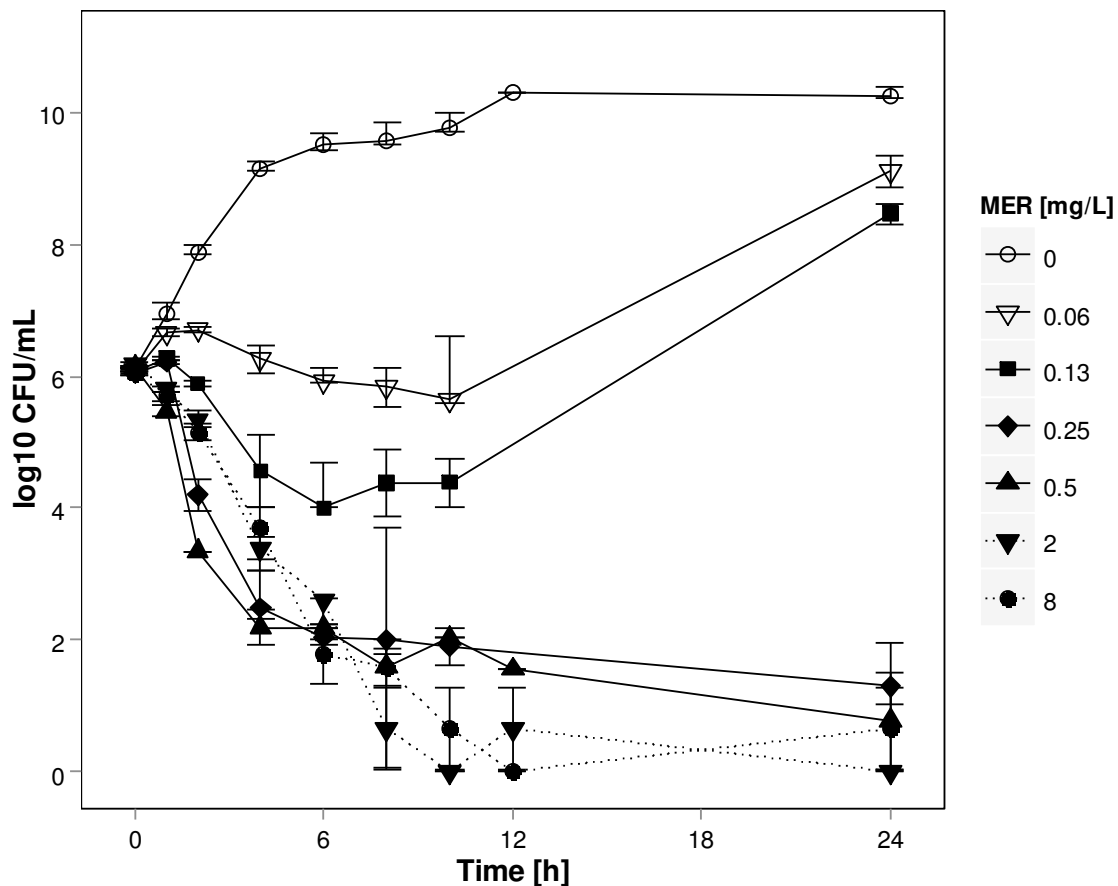
Figure 26: Time-kill curve study of MER versus *S. aureus* ATCC 29213 in log-phase at drug exposure. Points represent median concentration of bacteria in log10 CFU/mL and bars represent range of 2-4 determinations of n=2 independent experiments. Inhibitory concentrations (filled symbols), subinhibitory concentrations (open symbols). Dotted lines highlight concentrations that displayed a paradoxically reduced initial effect of MER.

For VAN (Figure 27), concentrations up to 0.5 mg/L did not have a substantial antibacterial effect compared to the GC curve. Initial killing with net regrowth was observed up to 4 mg/L. For VAN at 8 and 16 mg/L, marked killing to $<10^4$ CFU/mL was observed at 10 h, but bacterial load re-increased to ca. 10^5 CFU/mL and only a bacteriostatic effect was obtained at 24 h.
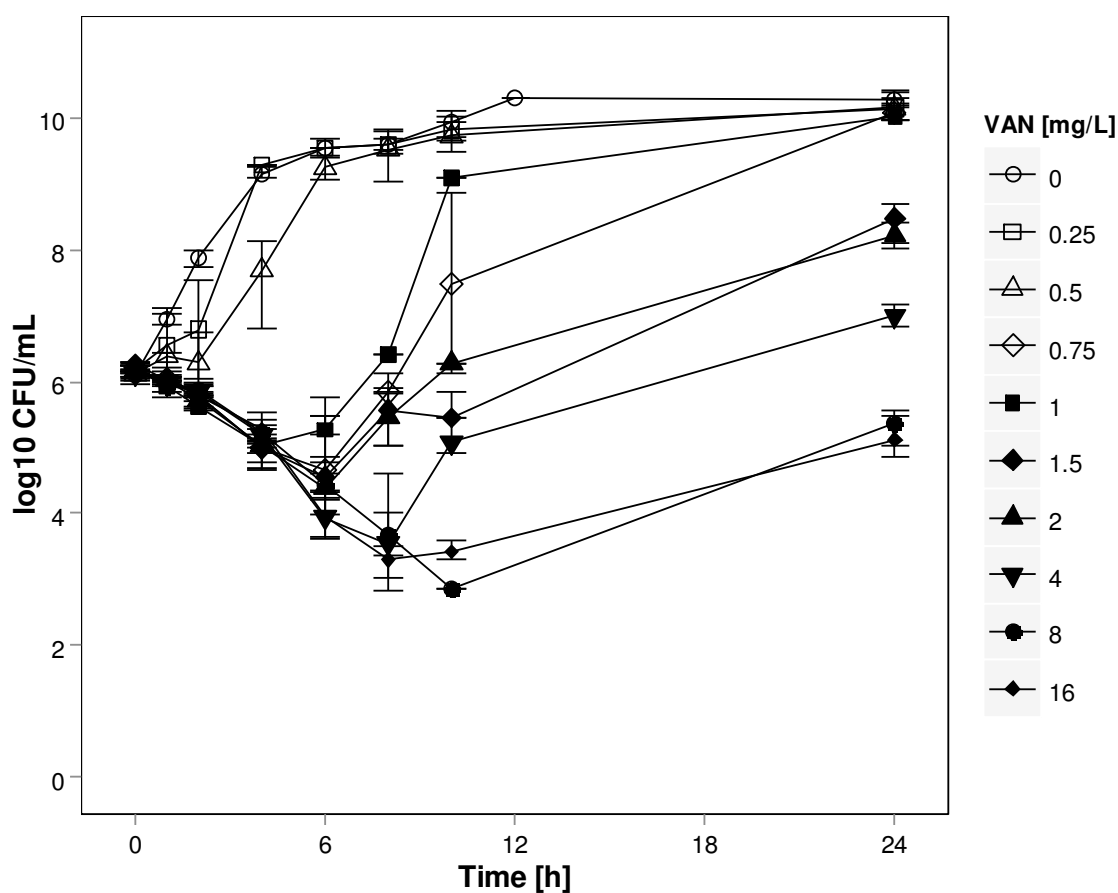
Figure 27: Time-kill curve study of VAN versus *S. aureus* ATCC 29213 in log-phase at drug exposure. Points represent median concentration of bacteria in log10 CFU/mL and bars represent range of 2-4 determinations of n=2 independent experiments. Inhibitory concentrations (filled symbols), subinhibitory concentrations (open symbols).

For the investigated combinations of LZD and MER, the combined effect was inferior compared to the maximum effect of both LZD and MER at their respective maximally effective concentrations (Figure 28) and a bacteriostatic effect was obtained at 24 h.
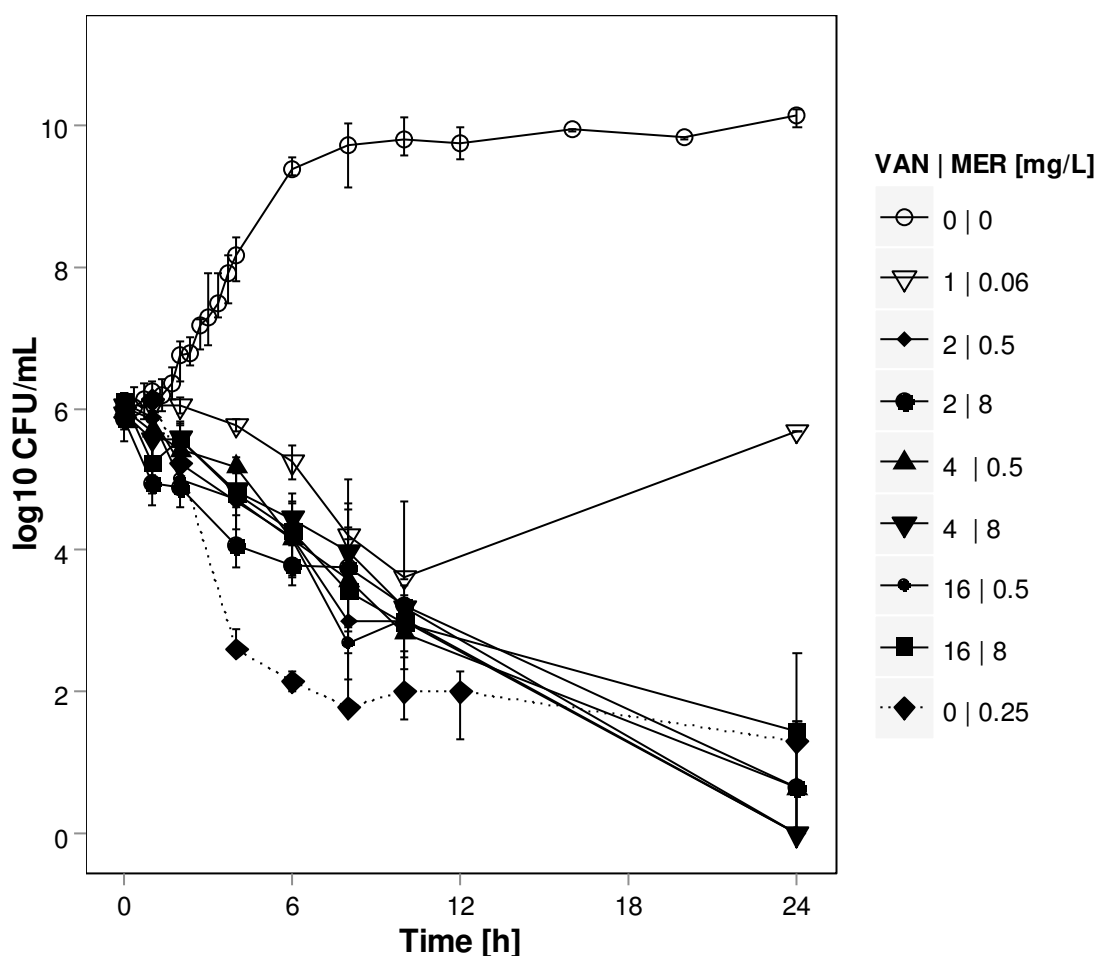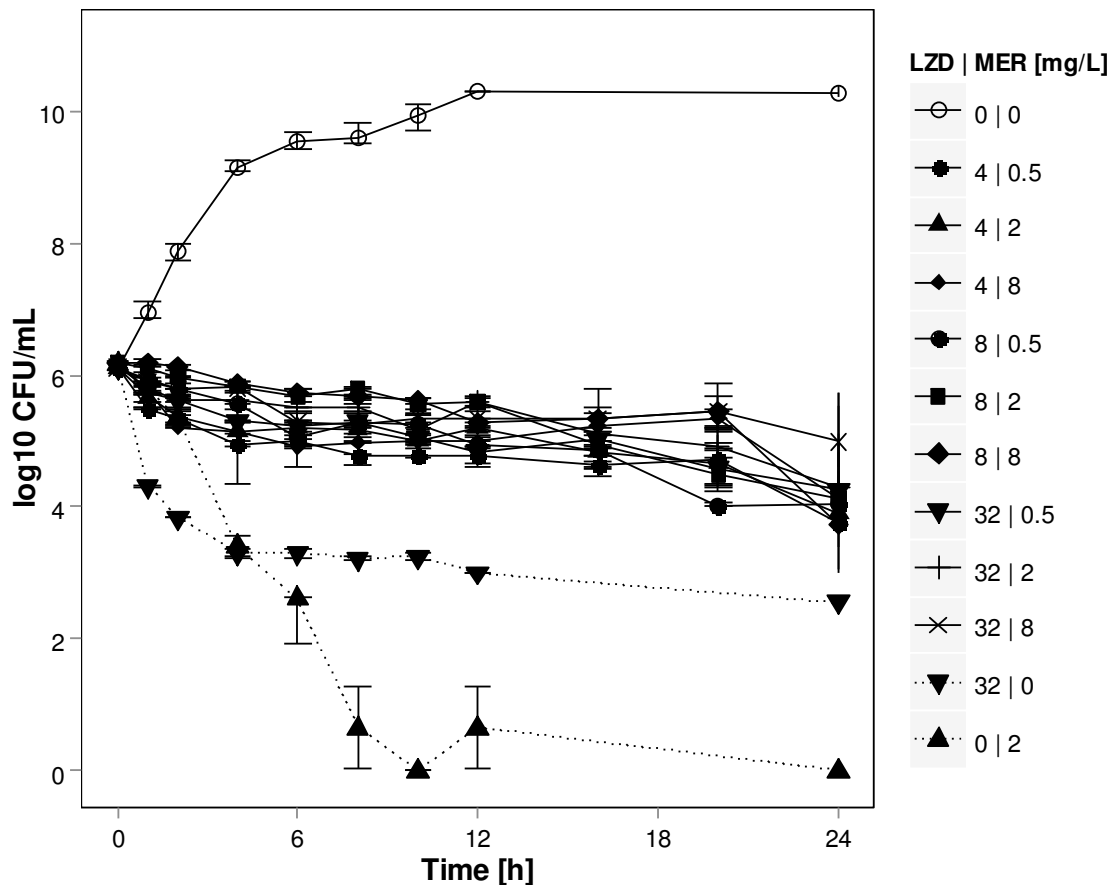

Figure 28: Time-kill curve study of combinations of LZD and MER versus *S. aureus* ATCC 29213 in log-phase at drug exposure. Points represent median concentration of bacteria in log10 CFU/mL and bar represents range of 2-6 determinations of n=2-3 independent experiments. Dotted line represents killing curve of LZD and MER at their maximum effects for comparison.

For the combinations of VAN and MER (Figure 29), the combined effect corresponded to the initial effect of VAN until 10 h, and was inferior to the effect of MER alone (Figure 26). However, at 24 h a bactericidal effect was observed for all investigated combinations and no regrowth was stimulated as observed for VAN alone at 2 and 4 mg/L (Figure 27).
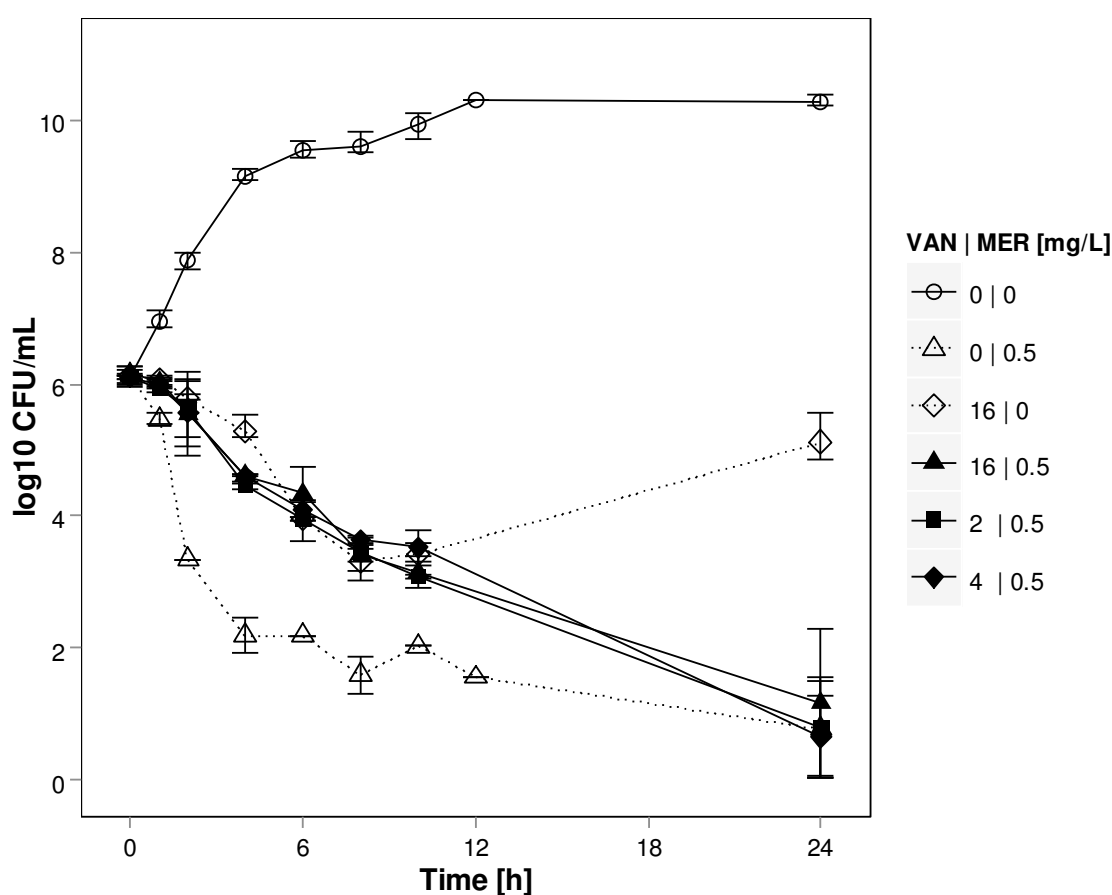
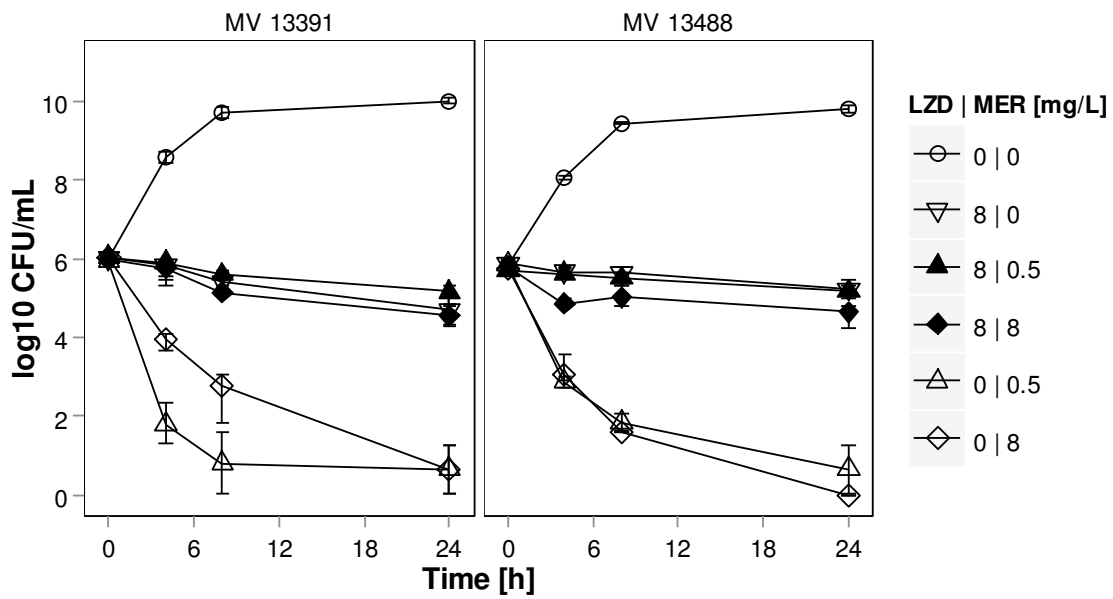**Figure 29:** Time-kill curve study of combinations of VAN and MER versus *S. aureus* ATCC 29213 in log-phase at drug exposure. Points represent median concentration of bacteria in log10 CFU/mL and bar represents range of 2-4 determinations of n=2 independent experiments. Dotted line represents killing curve of VAN and MER at their individual effects alone for comparison.

3.2.5 Adaptive resistance studies

Regrowth after initial killing was observed for both MER up to 0.125 mg/L (Figure 18) and VAN up to 1 mg/L in lag-phase *S. aureus* (Figure 19). Hence, those concentrations were used for pre-exposure of *S. aureus* for 24 h, and concentrations of this level and one higher and/or lower log2 level were investigated to assess the magnitude of adaption of the bacteria to the antibiotics.

For MER, pre-exposure to concentrations up to 0.125 mg/L (= 1x MIC; M1) rendered the second exposure to MER less effective (e.g. M1-M1) or even ineffective (e.g. M0.5-M0.5) indicating adaption of *S. aureus* to MER. Regrowth was observed for up to 0.25 mg/L (= 2x MIC; M2) indicating a decrease in susceptibility by at least one MIC level over 24 h.

For VAN, pre-exposure to concentrations up to 1 mg/L (= 1x MIC; V1) rendered the second exposure to VAN less effective (e.g. V1-V2) or ineffective (e.g. V0.75-V0.75). Hence, *S. aureus* also adapted to VAN and susceptibility to VAN decreased by one MIC level over 24 h.
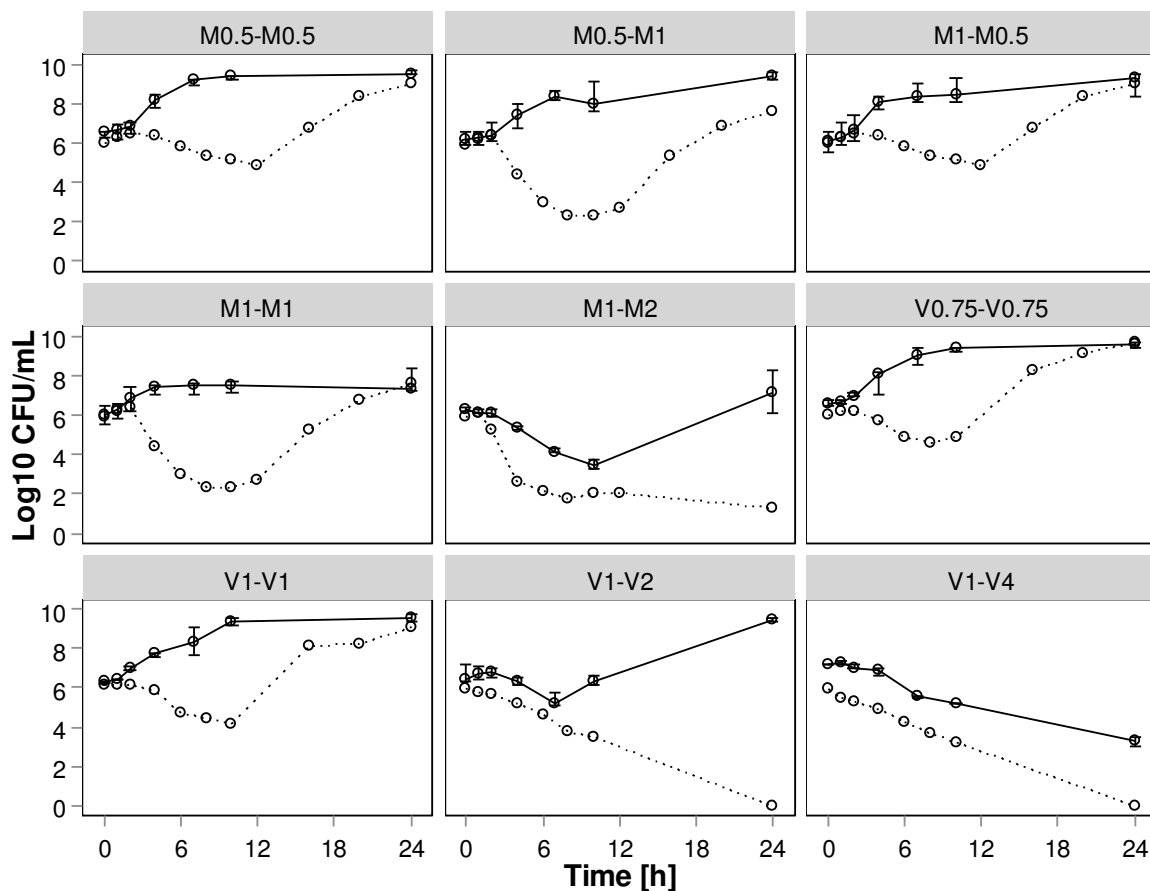
Figure 30: Adaptive resistance investigations with MER (M) and VAN (V) against *S. aureus* at concentrations around their MIC value (number indicates multiple/fraction of MIC). Dotted lines represent the obtained time-kill curve of 'native' *S. aureus* as described in 3.2.3 at a concentration indicated by the first part of the label; solid lines represent the obtained time-kill curves from the bacteria that have been pre-exposed to a concentration of the first label and exposed to the concentration indicated in the second label for another 24 h time period (n=2-3).

3.3 Modelling and Simulations

The obtained experimental PD data of LZD, VAN and MER described in the previous chapters was first analysed by empiric modelling using summary PD measures. By using the individual effects of the antibiotics against *S. aureus*, the observed interactions between LZD or VAN and MER were quantified in the newly elaborated response surface analysis. Finally, a semi-mechanistic PK/PD model was developed to assess individual and combined use of the antibiotics and to translate the obtained results into a clinical setting. The developed mathematical models were built upon experimental data with *S. aureus* ATCC 29213. For all Modelling and Simulation tasks, 'R' scripts were developed (7.3).

3.3.1 Modelling

3.3.1.1 Empiric modelling of individual drug effects

Checkerboard. For the dynamic checkerboard study, the bacterial load in log10 CFU/mL was utilised as summary PD effect measure. The estimated parameters of the developed inhibitory sigmoidal maximum effect model reliably described the experimental data (Figure 31).
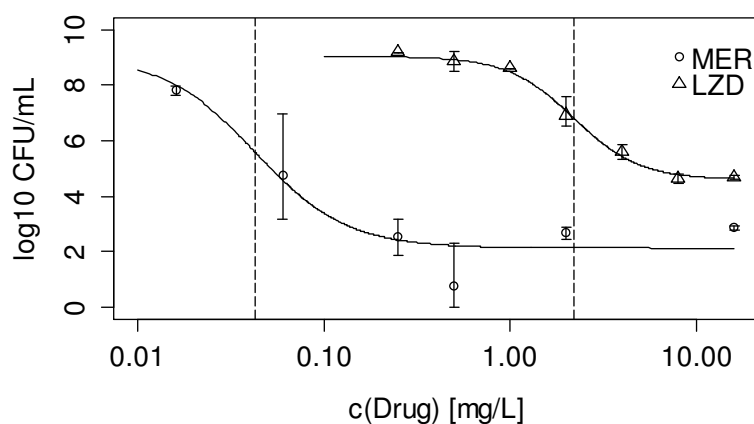
Figure 31: Individual concentration-effect relationships for LZD and MER against *S. aureus* ATCC 29213 observed in the checkerboard studies. Mean experimental data (points) and range (bar) are presented along with predictions of the sigmoidal maximum effect model (solide line). EC_{50} values for LZD and MER are indicated as vertical dashed lines.

The parameter estimates of the utilised sigmoidal maximum effect model for *S. aureus* ATCC 29213 are summarised in Table 11 for the checkerboard. For simple comparison of the antibacterial effects, the symbol 'E' was used for both inhibitory as well as excitatory sigmoidal maximum effect models throughout the present work.

Table 11: PD parameter estimates of the utilised sigmoidal maximum effect model (relative standard error, %), [95% CI] from the PD analysis of the individual antibacterial effects of LZD, MER and VAN in the checkerboard studies with *S. aureus* ATCC 29213. (n.d. = not determined).

PD parameter	MER	LZD	VAN
Emax [log10 CFU/mL]	6.88 (5.2)	4.42 (2.6)	n.d.
	[5.89; 7.88]	[4.12; 4.72]	
EC_{50} [mg/L]	0.043 (22.7)	2.19 (5.1)	n.d.
	[0.016; 0.070]	[1.91; 2.48]	
H [-]	1.77 (29.7)	2.45 (9.8)	n.d.
	[0.31; 3.23]	[1.83; 3.07]	

In the checkerboard study, MER displayed a higher maximum effect than LZD at a drastically lower EC_{50}. MER was hence more potent than LZD, as both drugs have similar molecular weights (MER: 383 g/mol [159], LZD: 337 g/mol [160]). The parameter estimates were overall precise, except for EC_{50} and H of MER for which imprecision was to some extent higher with RSEs >20%.

Time-kill curve studies. For the time-kill curve studies, the *IE* representing the area between growth and time-kill curve served as summary PD effect measure. Similarly to the checkerboard, the fitted sigmoidal maximum effect model described the experimental data well for both lag- (Figure 32) and log-phase *S. aureus* ATCC 29213 (Figure 33).
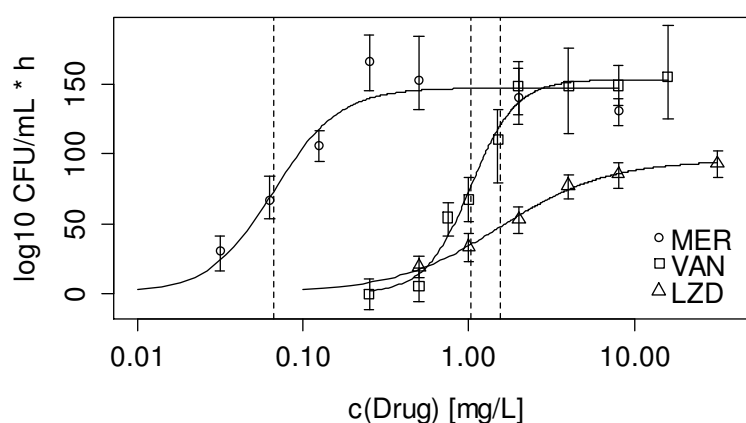
Figure 32: Individual concentration-effect relationships for LZD, MER and VAN against lag-phase *S. aureus* ATCC 29213 observed in time-kill curve studies. Mean experimental data (points) and range (bar) are presented along with predictions of the sigmoidal maximum effect model (solid line). EC_{50} values for LZD, MER and VAN are indicated as vertical dashed lines.
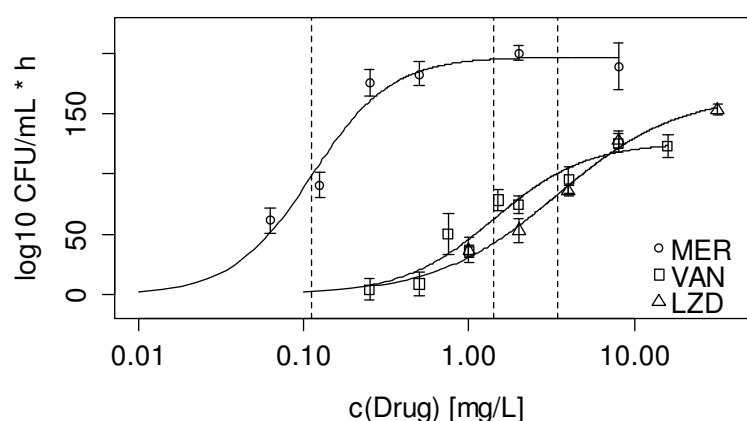
Figure 33: Individual concentration-effect relationships for LZD, MER and VAN against log-phase *S. aureus* ATCC 29213 observed in time-kill curve studies. Mean experimental data (points) and range (bars) are presented along with predictions of the sigmoidal maximum effect model (solide line). EC_{50} values for LZD, MER and VAN are indicated as vertical dashed lines.

Table 12: PD parameter estimates of the utilised sigmoidal maximum effect model (relative standard error, %), [95% CI] from the PD analysis of the individual antibacterial effects of LZD, MER and VAN in the time-kill curve studies in lag- and log-phase *S. aureus* ATCC 29213. Non-overlapping confidence intervals between estimates in lag- and log-phase of the respective antibiotics are italicised.

PD parameter	MER	LZD	VAN
	lag-phase		
Emax [(log10 CFU/mL) · h]	*148 (4.6)*	*96 (1.9)*	154 (2.8)
	[130; 164]	*[91; 101]*	[144; 164]
EC_{50} [mg/L]	0.067 (13.4)	*1.55 (4.8)*	1.02 (4.6)
	[0.044; 0.089]	*[1.35; 1.77]*	[0.92; 1.14]
H [-]	2.21 (21.9)	1.33 (5.7)	3.17 (11.5)
	[0.96; 3.45]	[1.12; 1.55]	[2.31; 4.04]
	log-phase		
Emax [(log10 CFU/mL) · h]	*196 (3.5)*	*166 (4.5)*	126 (7.6)
	[178; 216]	*[142; 189]*	[103; 148]
EC_{50} [mg/L]	0.111 (9.8)	*3.44 (10.7)*	1.42 (16.9)
	[0.081; 0.142]	*[2.27; 4.61]*	[0.85; 1.99]
H [-]	1.82 (17.1)	1.19 (10.7)	1.55 (20.9)
	[0.96; 2.68]	[0.78; 1.59]	[0.79; 2.33]

The parameter estimates for the time-kill curve studies in lag- and log-phase are presented in Table 12. Precision of the estimates was overall high and RSE were <21.9%. Similarly to the checkerboard, MER was the most potent antibiotic, followed by VAN (molecular weight: 1449 g/mol [161]) and LZD.

Significant differences in the parameter estimates of the sigmoidal maximum effect model between both growth phases were indicated by non-overlapping 95% CIs: The maximum effect of MER and LZD was higher against log-phase *S. aureus*. Conversely, for VAN, the maximum effect was lower in log-phase *S. aureus*, but the CIs were slightly overlapping. For LZD, also the EC_{50} values of lag- and log-phase bacteria were significantly different with higher EC_{50} for log-phase bacteria. EC_{50} values were also higher for MER and VAN against log-phase *S. aureus*, but CIs were overlapping. For the Hill factor, moderate steepness (*H*: 1-2) was observed for all antibiotics, except for VAN against lag-phase *S. aureus*, for which the steepness was comparably high (*H*=3.17).

3.3.1.2 Response surface analysis

The estimates of the individual antibacterial effects (3.3.1.1) were employed for calculation of the expected additive effects of the investigated antibiotic combinations using the elaborated BI equation (Eq. 23). Results were then compared to the observed experimental data and tested for significant deviation from additivity.

Dynamic checkerboard studies. The expected additive effects of LZD and MER were bactericidal for MER ≥0.25 mg/L (Figure 34, upper panel). The observed combined effects resulted in significant Bliss antagonism if LZD concentrations exceeded concentrations around the MIC (Figure 34, lower panel).
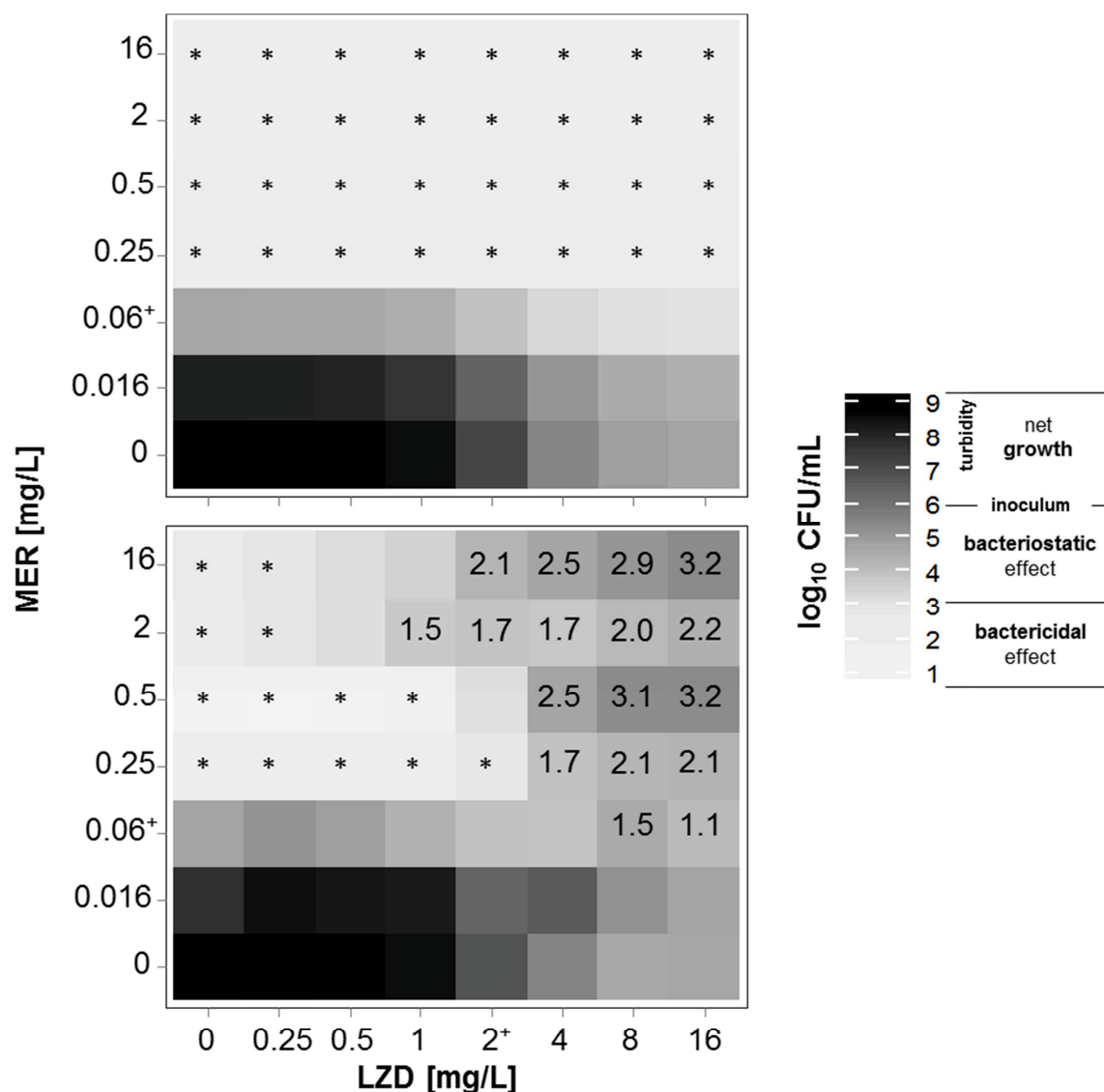
Figure 34: Heat map of calculated additive response surface based on BI (upper panel) and the observed, experimental data of the dynamic checkerboard (lower panel) for each investigated combination of LZD and MER: Gradient represents bacterial counts after 18 h of incubation (mean of log10 CFU/mL, n=3); (*) indicates bactericidal effect, ($^+$) indicates the MIC. Significant Bliss antagonism is given as Δ log10 CFU/mL directly in the heat map; no Bliss synergy was observed.

Time-kill curve studies in lag-phase. The response surface analysis for time-kill curve studies with *S. aureus* ATCC 29213 in the lag-phase is illustrated in Figure 35. For the investigated combination of subinhibitory LZD and MER, an additive interaction was observed. If concentrations for LZD ≥4 mg/L (=2x MIC), significant Bliss antagonism was observed for all studied concentrations of MER (0.5-8 mg/L). A trend towards Bliss synergy was observed at subinhibitory combinations of VAN and MER. For inhibitory combinations of VAN and MER, the interaction was Bliss additive.
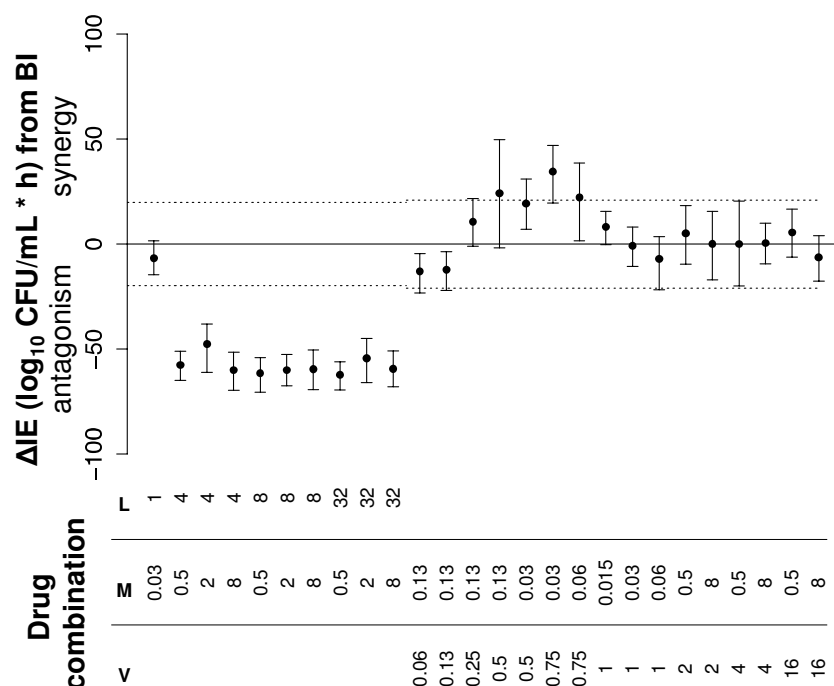
Figure 35: Deviation of intensity of effect (*IE*) from expected additivity calculated by BI ± range for the scenarios studied in the time-kill curve studies with lag-phase *S. aureus* ATCC 29213 (L / M / V = concentration of linezolid, meropenem and vancomycin, respectively, in mg/L). 'Significant' negative or positive deviation from Bliss independence (non-overlap of range with 95% confidence interval of residual variability of expected additivity response surfaces represented by dashed lines) indicated Bliss antagonism or synergy, respectively.

Time-kill curve studies in log-phase. The response surface analysis for log-phase *S. aureus* ATCC 29213 is presented in Figure 36. Bliss antagonism between LZD and MER was more pronounced against log-phase *S. aureus* than against lag-phase *S. aureus* (Figure 35). The investigated combinations of VAN and MER were Bliss additive with a trend towards Bliss synergy.
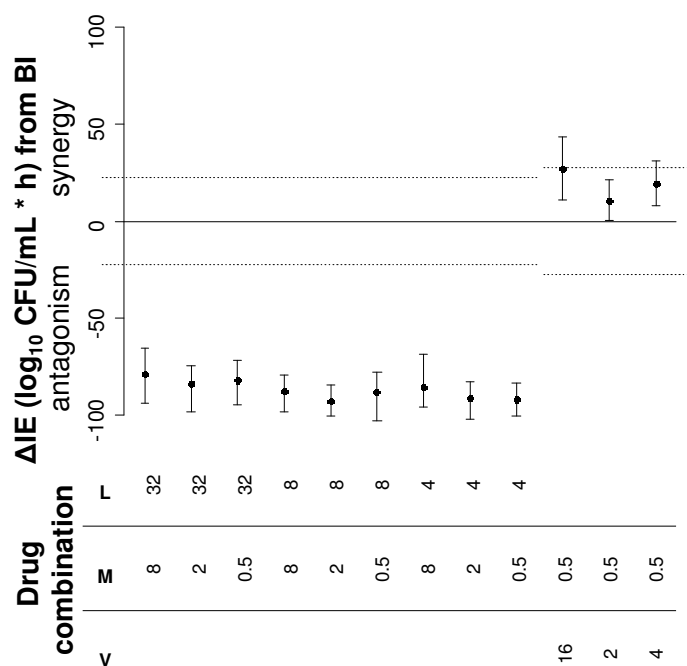
Figure 36: Deviation of intensity of effect (*IE*) from expected additivity calculated by BI ± range for the scenarios studied in the time-kill curve studies with log-phase *S. aureus* ATCC 29213 (L / M / V = concentration of linezolid, meropenem and vancomycin, respectively, in mg/L). 'Significant' negative or positive deviation from BI (non-overlap of range with 95% confidence interval of residual variability of expected additivity response surfaces represented by dashed lines) indicated Bliss antagonism or synergy, respectively.

3.3.1.3 Semi-mechanistic modelling of time-kill curve studies

The empiric modelling of the individual and combined effects provided quantitative insight into the individual (3.3.1.1) and combined effects (3.3.1.2) of LZD, MER and VAN. However, the mathematical model of the drug effect used (sigmoidal maximum effect model) was time-independent. For continuous prediction of antibacterial effects as a prerequisite for linking a population PK model to PD, a semi-mechanistic PD model was developed that described the time-dependency of the antibiotic effects and considered their mechanisms of action. Due to their different nature, two semi-mechanistic PD models were developed for lag- and log-phase *S. aureus*, respectively. As a basis for modelling of both growth states, a life cycle-model [141] and an adaption submodel [142,143] was utilised (2.4.1.3.3).

3.3.1.3.1 *S. aureus* in lag-phase at drug exposure

Development of the PD model was a continuous process which was performed in parallel to data acquisition using *S. aureus* ATCC 29213 over a time period of ca. 2.5 years utilising the 'learning and confirming' approach outlined in 'adaptive optimal design' (2.4.1.3.3). An example of one intermediate step in this circular algorithm is presented under 3.3.1.3.1.2.

3.3.1.3.1.1 Model development

The milestones of model development and experimental dataset generation are presented in Table 13.

Table 13: Summary of milestones in development of the semi-mechanistic PD model along with dataset generation (final dataset of lag-phase *S. aureus*, cf. 3.2.3), GC: growth control, Lx/Mx/Vx: concentration of LZD, MER and VAN as multiples/fraction of MIC.

Milestone	Dataset	Effect implementation	Parameters
	Parameterisation of the life-cycle model for LZD and MER with prior knowledge		
I	GC	Biphasic growth model (2.3.1.4)	3.2.1.3
	L2-L16	LZD: Inhibition of replication k_{rep} Induction of $k_{death,LZD}$ (replication-indep.)	*Emax, EC$_{50}$* of checkerboard (3.3.1.1), graphical
	M4	MER: Inhibition of k_{doub} (replication-dependent) Stimulation of persiters in REP ($k_{per,MER}$)	
	L2M4, L4M4, L16M4	Combined effect limited to effect of LZD alone, as effect of MER was precluded due to growth-arrest by LZD.	
	Addition of subinhibitory concentrations of LZD and MER allowing for parameter estimation		
II	GC	Biphasic growth model (2.3.1.4)	Estimated
	I + L0.25-L1	as I	
	I + M0.25-M2	as I	
	Implementation of the Eagle-effect of MER		
III	II + M16, M64	MER: Paradoxically reduced effect of MER at higher concentrations implemented as self-inhibitory effect on MER effect on k_{doub}	Estimated
	L2M16, L4M16, L16M16, L2M64, L4M64 L16M64	as I	
	Implementation of the single and combined effects of VAN with MER		
IV	III + V0.25-16	VAN: Inhibition of k_{doub} (replication-dependent) Stimulation of persiters in 'REP' ($k_{per,VAN}$)	Estimated
	V2M4, V2M64, V4M4, V4M64, V16M4, V16M64	Combined effect limited to effect of VAN: Inhibitory effect of VAN on effect of MER on k_{doub}	
	Estimation of adaption of the bacteria to the effects of MER and VAN		
V	IV	Consideration of adaption by bacteria using a concentration and time-dependent increase of EC_{50} of MER and VAN	Estimated
	Characterisation of the interaction of VAN and MER on the level of adaptive resistance		
VI	V + various subinh. combinations of M/V (Figure 21)	Subinhibitory VAN delayed adaption of *S. aureus* to MER	Estimated

The basic idea of parameterising the simplified bacterial life-cycle with a replication-dependent effect of MER as inhibitory effect on k_{doub}, and an inhibitory effect of LZD on k_{rep}, using sigmoidal maximum effect models was already realised in milestone I (Table 13) with a rather small dataset: As solely inhibitory concentrations were investigated at this stage, parameter values such as EC_{50} or H could not be estimated and were thus obtained using prior knowledge from e.g. checkerboard studies (3.2.2) or graphical determination (for $k_{death.LZD}$ and $k_{per,MER}$). With this model, the replication-dependent effect and persister development by MER, as well as the replication-independent effect of LZD which lead to growth-arrest associated with replication-independent killing ($k_{death,LZD}$) was implemented. As a result, even the observed antagonistic interaction between LZD and MER was already predicted without any further modification of the life-cycle. Subinhibitory concentration of LZD and MER became available in milestone II and eventually allowed for estimation of the model parameters for the drug effects.

With milestone III, higher concentrations of MER were available to cover the entire clinically relevant concentration range of MER. The observed paradoxically reduced effect of MER at higher concentrations (Figure 18) was implemented by a self-inhibitory effect of MER on k_{doub} with a second inhibitory sigmoidal maximum effect model: $k_{doub} \cdot [1 - E_{MER} \cdot (1 - E_{MER,Eagle})]$.

Studies with VAN alone and in combination with MER were generated in milestone IV: The effect of VAN was also implemented as a replication-dependent, inhibitory effect on k_{doub}. VAN was less active than MER and did not fully inhibit successful doubling of bacteria. Hence, a maximum inhibitory effect of VAN had to be estimated. In combination, the effect corresponded to the effect of VAN alone: $k_{doub} \cdot [1 - E_{MER} \cdot (1 - E_{MER,Eagle}) \cdot (1 - E_{VAN})] \cdot (1 - E_{VAN})$. VAN also stimulated persister development ($k_{per,VAN}$).

In milestone V, the observed regrowth after initial killing for MER (e.g. 0.0625 or 0.125 mg/L in Figure 18) and VAN (e.g. 0.75 or 1 mg/L in Figure 19) was mathematically described using separate adaption submodels for MER (Eq. 43) and VAN (Eq. 40).

In milestone VI, the observed interaction of VAN and MER on the adaption level was implemented. Subinhibitory VAN was ineffective alone, but suppressed or delayed regrowth of *S. aureus* when combined with MER (Figure 37). This observation was implemented into the model by an inhibitory maximum effect model of VAN on the second-order time-delay rate constant τ (Eq. 43). A detailed description of the final model is given after the adaptive optimal design at 3.3.1.3.1.3.

3.3.1.3.1.2   Adaptive optimal design

Adaptive optimal design for planning experimental scenarios was performed in parallel throughout the entire period of experimental dataset generation according to the 'learning and confirming' algorithm described in 2.4.1.3.3. An example for this adaptive process was e.g. progress from milestone V to VI (final experimental design) in Table 13 and will be discussed more detailed for illustration purposes.

At the stage of milestone V, the scenarios of subinhibitory concentrations between VAN and MER had partly not yet been performed and the interaction between subinhibitory VAN and MER at the adaption level not yet been fully exploited. However, the experimental data from V0.5M1 indicated that VAN at 0.5x MIC being not at all effective alone suppressed regrowth observed with MER alone at 1x MIC (Figure 37).
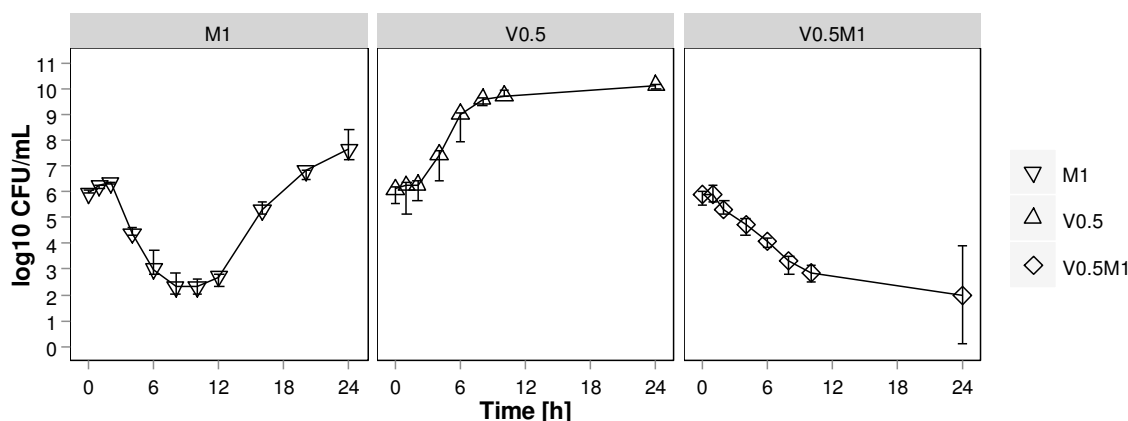
Figure 37: VAN at 0.5x MIC, being ineffective itself, supressed the regrowth observed with MER at 1x MIC.

Implementation of a maximum effect model of VAN on the adaption process of MER $[(1 - E_{VAN,ARI}) \times \tau_{MER}]$ (Eq. 43) at the stage of milestone V did not result in an estimable value for $EC50_{VAN,ARI}$. Hence, the knowledge-gain of performing above mentioned subinhibitory scenarios (i.e. V0.06M1, V0.125M1, V0.25M1, V0.5M0.25, V0.75M0.25, V0.75M0.5, V1M0.125, V1M0.25 and V1M0.5) was assessed by computing the expected Fisher information matrix of the experimental design to obtain the expected RSE (2.4.1.1.2) *before* performing those experiments. A value of 0.2 mg/L for $EC50_{VAN,ARI}$ was assumed at that stage based on graphical examination. The other model parameters were set to their estimate at the stage of milestone V (First column in Table 14). The expected RSE for $EC50_{VAN,ARI}$ was unacceptably high (87.1%) indicating that the interaction between VAN and MER on the level of the adaption submodel could not be identified using the reduced dataset of milestone V. The expected RSE for the final design including the subinhibitory combinations between VAN and MER resulted in an expected RSE of 3.1% for $EC50_{VAN,ARI,}$ supporting the performance of the experiments. After that, the final parameter estimates with the final design (fourth column in Table 14) were partly different from the ones obtained at milestone V (Table 14), e.g. the drug-related parameters of MER and VAN originating from the estimated $EC50_{VAN,ARI}$ of 0.39 mg/L being different from the previously assumed 0.20 mg/L. Yet, the expected and observed RSE were in reasonable agreement for the final design.

Table 14: Illustration of adaptive optimal design at transition from milestone V to the experimental design for obtaining the dataset of milestone VI (= final design): Parameter estimates at milestone V were utilised to compute expected RSE of designs of milestone V and the final design (left) and compared to the parameter estimates from the final design and the observed RSE (right). *: assumed. Bold values: RSE of example mentioned in the text. For explanation of the parameters see Table 15.

Parameter	Estimate (milest. V)	Exp. RSE (milest. V)	Exp. RSE (final design)	Estimate (final design)	Obs. RSE (final design)
Parameters of the bacterial life-cycle					
CFU_0 [log10 CFU/mL]	6.00	0.4	0.4	6.07	0.4
CFU_{max} [log10 CFU/mL]	9.64	0.7	0.6	9.43	0.6
k_{lag} [h^{-1}]	1.69	43.8	40.8	0.88	16.0
k_{rep} [h^{-1}]	1.38	4.5	4.2	1.56	7.2
$k_{death, per}$ [h^{-1}]	0.16	34.8	30.6	0.23	9.3
Drug-related parameters					
$EC_{50,LZD}$ [mg/L]	0.71	9.5	9.4	0.68	9.1
H_{LZD} [-]	1.48	7.7	7.6	1.55	7.5
$k_{death, LZD}$ [h^{-1}]	0.093	9.0	8.9	0.10	7.5
$EC_{50,MER,t=0}$ [mg/L]	0.030	4.0	2.4	0.022	2.8
H_{MER} [-]	3.06	10.4	9.0	3.23	11.7
$Emax_{MER,Eagle}$, %	0.30	6.3	6.2	0.33	5.9
$EC_{50,MER,Eagle}$ [mg/L]	1.07	13.4	13.4	1.35	8.9
β_{MER} [-]	7.38	9.6	9.4	9.53	4.2
τ_{MER} [L/(mg·h)]	0.35	16.6	14.2	0.47	5.8
$k_{per,MER}$ [h^{-1}]	0.034	78.8	68.1	0.11	32.6
$Emax_{VAN}$, %	0.76	1.6	1.5	0.74	1.9
$EC_{50,VAN,t=0}$ [mg/L]	0.49	2.3	2.1	0.46	1.8
$EC50_{VAN,ARI}$ [mg/L]	0.20*	**87.1**	**3.1**	0.39	**5.0**
β_{VAN} [-]	3.30	6.3	5.9	3.60	6.7
τ_{VAN} [L/(mg·h)]	0.034	22.6	20.7	0.034	11.2
$k_{per,VAN}$ [h^{-1}]	0.0037	31.7	28.7	0.017	50.9

3.3.1.3.1.3   Final model

The final semi-mechanistic PD model that simultaneously described the single and combined effects of LZD, MER and VAN against lag-phase *S. aureus* ATCC 29213 with the final experimentally obtained dataset of milestone VI is illustrated in Figure 38.
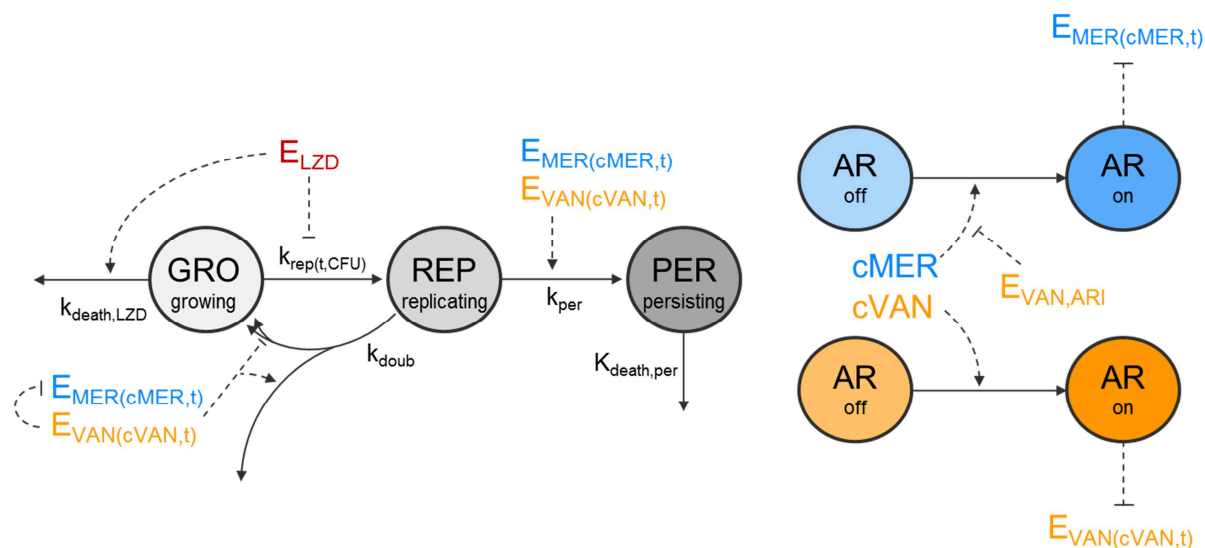
Figure 38: Graphical sketch of the semi-mechanistic PD model (left) and adaption submodel of VAN and MER (right) for lag-phase *S. aureus*; Solid arrows: Mass transfer between compartments; dashed arrows: stimulatory effects; ----|: inhibitory effects; abbreviations see text.

The system of ODEs (Eq. 35)-(Eq. 37) characterising the bacterial life cycle comprised stages of growing ('GRO'), replicating ('REP') and persisting bacteria ('PER'). Initial conditions (IC) are presented next to the respective ODE. Drug effects that perturbed the bacterial life cycle were implemented with sigmoidal maximum effect models (E_{DRUG}) with *Emax*=1 as the magnitude of perturbation was quantified by the respective rate constants *k*. A different parameterisation with an estimated value of *Emax* potentially <1 was only required for effects on k_{doub}, as (i) k_{doub} represented the rate constant for doubling and drug effects could potentially only inhibit a fraction of successful doublings, and (ii) the combination of effects of MER and VAN on k_{doub} required more flexibility to cover the observed interactions between MER and VAN and the paradoxical effect of MER. In particular, the drug effects were implemented as follows: LZD was assumed to growth-arrest the bacteria in 'GRO' leading to a replication-independent death quantified by $k_{death,LZD}$. The effects of VAN and MER were implemented by a modified BI term $(1-E_{MER}) \times (1-E_{VAN})$, accounting for the self-inhibitory Eagle effect of MER and the observation that the maximum joint effect of MER and VAN was limited to the effect of VAN (Eq. 35) as outlined in 3.3.1.3.1.1. The biphasic killing, i.e. persister development after initial killing for MER and VAN was described by the rate constants $k_{per,MER}$ and

$k_{per,VAN}$, which were stimulated by the respective antibiotics during replication (Eq. 36) and quantified in 'PER' (Eq. 37).

$$\frac{dGRO}{dt} = -k_{death,LZD} \times E_{LZD} \times GRO$$
$$- k_{rep}(t, CFU) \times (1 - E_{LZD}) \times GRO$$
$$+ k_{doub} \times \left[1 - E_{MER,t} \times \left(1 - Emax_{MER,Eagle} \times E_{MER,Eagle} \right) \right.$$
$$\left. \times \left(1 - E_{VAN,t} \right) \right] \times \left(1 - Emax_{VAN} \times E_{VAN,t} \right) \times REP \times 2$$

$$\text{(Eq. 35)}$$

$$\text{IC: } CFU_0$$

$$\frac{dREP}{dt} = k_{rep}(t, CFU) \times (1 - E_{LZD}) \times GRO$$
$$- k_{doub} \times REP - k_{per,MER} \times E_{MER,t} \times REP - k_{per,VAN} \times E_{VAN,t} \times REP \quad \text{(Eq. 36)}$$

$$\text{IC: } 0$$

$$\frac{dPER}{dt} = k_{per,MER} \times E_{MER,t} \times REP + k_{per,VAN} \times E_{VAN,t} \times REP$$
$$- k_{death,PER} \times PER$$

$$\text{(Eq. 37)}$$

$$\text{IC: } 0$$

k_{rep} was assumed to decrease if bacterial concentrations reached the capacity limit CFU_{max}. The lag-phase to attain exponential growth was estimated by a first-order delay rate constant k_{lag}. Both aspects were considered as follows:

$$k_{rep}(t, CFU) = k_{rep} \times \left(1 - e^{-k_{lag}t} \right) \times \left(1 - \frac{GRO + REP + PER}{CFU_{max}} \right) \qquad \text{(Eq. 38)}$$

The adaption of *S. aureus* to MER and VAN was implemented as an increasing EC_{50} over time (cf. 2.4.1.3.3 for notation) for VAN (Eq. 41) and MER (Eq. 44) and stimulated by exposure to VAN (Eq. 40) and MER (Eq. 43). As subinhibitory VAN delayed the adaption of *S. aureus* to MER, an inhibitory effect quantifying the adaptive resistance interaction between VAN and MER, $E_{VAN,ARI}$, was implemented (Eq. 43).

$$\frac{dAR_{off,VAN}}{dt} = -\tau \times C_{VAN}(t) \times AR_{off} \qquad \text{IC=1} \qquad \text{(Eq. 39)}$$

$$\frac{dAR_{on,VAN}}{dt} = \tau \times C_{VAN}(t) \times AR_{off} \qquad\qquad \text{IC=0} \qquad\qquad \text{(Eq. 40)}$$

$$EC_{50,VAN}(t) = \alpha_{VAN}(t) \times EC_{50,VAN,t=0}$$

$$\text{with } \alpha_{VAN}(t) = 1 + \beta_{VAN} \times AR_{on,VAN}(t) \qquad\qquad \text{(Eq. 41)}$$

$$\frac{dAR_{off,MER}}{dt} = -(1 - E_{VAN,ARI}) \times \tau_{MER} \times C_{MER}(t) \times AR_{off,MER} \quad \text{IC=1} \qquad \text{(Eq. 42)}$$

$$\frac{dAR_{on,MER}}{dt} = (1 - E_{VAN,ARI}) \times \tau_{MER} \times C_{MER}(t) \times AR_{off,MER} \qquad \text{IC=0} \qquad \text{(Eq. 43)}$$

$$EC_{50,MER}(t) = \alpha_{MER}(t) \times EC_{50,MER,t=0}$$

$$\text{with } \alpha_{MER}(t) = 1 + \beta_{MER} \times AR_{on,MER}(t) \qquad\qquad \text{(Eq. 44)}$$

The ODE system was numerically solved using 'lsoda' (automatic detection of stiff- and non-stiff ODE system) of 'deSolve' in 'R' [128] with a relative error tolerance set to 1e-10. Parameters were estimated in a sequential manner: (i) log-transformed parameters were used to avoid convergence to implausible negative parameter values and to indirectly harmonise the parameter step-size for the estimation algorithm. The robust derivative-free Nelder-Mead algorithm [162] (implemented in 'optim' of R Core [127]) was used for this first step. For step (ii), parameters were back-transformed to normal scale and the parameter estimates of stage (i) were used as initial estimates for the more sensitive gradient-based 'BFGS' algorithm [163] ('optim' of R Core [127]). The final parameter estimates from stage (ii) were used to compute the observed Fisher information matrix to obtain the standard errors of the estimates.

The final parameter estimates of the semi-mechanistic PD model for lag-phase *S. aureus* are presented in Table 15 and are divided in parameters of the bacterial life-cycle and drug-specific parameters. The parameter values of the bacterial life-cycle, i.e. CFU_0, CFU_{max} was in well agreement with those that one would determine by visual inspection (e.g. from Figure 17). k_{rep} was very close to the value obtained in the log-phase with the biphasic growth model (1.73 h^{-1} in 3.2.1.3); overlapping CIs indicated that the various drug-effects of LZD, MER and VAN did not perturb the parameter estimates of drug-free growth. For LZD, the drug effects were constant over time and EC_{50} and *H* were in range of the parameter estimates from the empiric model (3.3.1.1). When interpreting the plain parameter values of the drugs MER and VAN, it has to be noted that comparison of single parameter values provides only limited insight, e.g. due to the interplay of EC_{50} with the adaption parameters β and τ. A combined interpretation of the adaption processes is given in the discussion (4.3.3).

Table 15: Parameter estimates of the final semi-mechanistic PD model for lag-phase *S. aureus*, relative standard errors (RSE) in % obtained from the variance-covariance matrix, 95% confidence intervals determined by a non-parametric bootstrap analysis (n=1198) and short explanation of the model parameters.

Parameter [Unit]	Estimate	RSE % [CI$_{95\%}$]	Explanation
Parameters of the bacterial life-cycle			
CFU$_0$ [log10 CFU/mL]	6.06	0.4 [6.02; 6.09]	Initial colony forming units (CFU)/mL at beginning of the experiment
CFU$_{max}$ [log10 CFU/mL]	9.43	0.6 [9.26; 9.68]	Maximum attainable bacterial growth
k$_{lag}$ [h^{-1}]	0.88	16.0 [0.662; 2.28]	First-order time delay rate constant to attain log-phase
k$_{rep}$ [h^{-1}]	1.56	7.2 [1.25; 1.90]	Transit rate constant from growing to replicating state; rate-limiting step for growth
k$_{doub}$ [h^{-1}]	100	FIX [-]	Rate constant of doubling; represents actual replication (fixed to high rate constant as not rate-limiting); MER and VAN impaired successful replication
k$_{death, per}$ [h^{-1}]	0.23	9.3 [0.189; 0.307]	Basal death rate constant of persistent bacteria
Drug-related parameters			
EC$_{50,LZD}$ [mg/L]	0.68	9.1 [0.563; 0.802]	C$_{LZD}$ leading to half-maximum drug effect of LZD on k$_{rep}$ (growth arrest) and stimulation of k$_{death,LZD}$
H$_{LZD}$ [-]	1.55	7.5 [1.35; 1.63]	Hill factor LZD (steepness of the concentration-effect relationship)
k$_{death, LZD}$ [h^{-1}]	0.10	7.5 [0.092; 0.114]	Basal death rate constant of growth-arrested bacteria, induced by LZD
EC$_{50,MER,t=0}$ [mg/L]	0.022	2.8 [0.0189; 0.0262]	C$_{MER}$ leading to half-maximum drug effect of MER on k$_{doub}$ and k$_{per,MER}$ at t=0
H$_{MER}$ [-]	3.23	11.7 [2.27; 5.48]	Hill factor MER (steepness of the concentration-effect relationship)
Emax$_{MER,Eagle}$,%	32.8	5.9 [26.2; 35.6]	Percentage by which the effect of MER at higher concentration decreased from maximum (67.2 % impaired doublings remained)
EC$_{50,MER,Eagle}$ [mg/L]	1.35	8.9 [0.856; 1.41]	C$_{MER}$ leading to half-maximum paradoxical effect of MER on k$_{doub}$
H$_{MER, Eagle}$ [-]	4	FIX [-]	Hill factor MER (steepness of the concentration-Eagle-effect relationship)

β_{MER} [-]	9.53	4.2 [7.61; 22.0]	Factor that calculates maximum possible adapted EC_{50} of bacteria by $[(1+\beta_{MER})\times EC_{50,MER,t=0}]$
τ_{MER} [L/(mg·h)]	0.47	5.8 [0.154; 0.653]	Second-order delay rate constant for adaption with respect to time and C_{MER}
$k_{per,MER}$ [h^{-1}]	0.11	32.6 [0.0545; 0.263]	Persister development rate for MER during replication
$k_{deg,MER}$ [h^{-1}]	0.019	FIX [-]	First-order degradation rate constant of C_{MER}; drug degradation determined by HPLC (3.1.3), hence fixed during estimation
$Emax_{VAN}$, %	74.3	1.9 [70.8; 78.5]	Percentage by which VAN decreased successful doubling at maximum
$EC_{50,VAN,t=0}$ [mg/L]	0.46	1.8 [0.430; 0.482]	C_{VAN} leading to half-maximum drug effect of VAN on k_{doub} and $k_{per,VAN}$ at t=0
H_{VAN} [-]	20	FIX [-]	Hill factor VAN (steepness of the concentration-effect relationship); fixed as estimation was not possible and very steep (on/off) initial concentration-effect relationship was observed in time-kill curves
$EC50_{VAN,ARI}$ [mg/L]	0.39	5.0 [0.293; 0.515]	C_{VAN} leading to half-maximum suppression of adaption of *S. aureus* to MER
$H_{,VAN,ARI}$ [-]	1.0	FIX [-]	Hill factor VAN for suppression of adaption of *S. aureus* to MER
β_{VAN} [-]	3.59	6.7 [2.60; 4.81]	Factor that calculates maximum possible adapted EC_{50} of bacteria by $[(1+\beta_{VAN})\times EC_{50,VAN,t=0}]$
τ_{VAN} [L/(mg·h)]	0.034	11.2 [0.0197; 0.0638]	Second-order delay rate constant for adaption with respect to time and C_{VAN}
$k_{per,VAN}$ [h^{-1}]	0.017	50.9 [0.00722; 0.0561]	Persister development rate constant for VAN during replication
$k_{deg,VAN}$ [h^{-1}]	3.9e-03	FIX [-]	First-order degradation rate constant of C_{VAN}; drug degradation determined by HPLC (3.1.3), as an independent variable, was fixed during estimation
σ [log10CFU/mL]	0.63	-	Residual additive variability, no RSE reported as calculated from final objective function value

The superiority of the final model over other key models was assessed by calculation of model selection criteria (Appendix Table 19). As the number of data points to parameters (n/p) was >73.5 even for the most complex model tested, AIC and not AICc was used (if appropriate):

- Both inclusion of the persister development rates $k_{per,MER}$ (Δ-2LL: -64.89) and $k_{per,VAN}$ (Δ-2LL: -47.80) were statistically significant as indicated by the LRT and hence remained in the final model.

- The inclusion of the paradoxically reduced (Eagle-) effect [164] for MER substantially improved the model (ΔAIC: -104.64).

- Inclusion of $Emax_{VAN}$ significantly improved the model compared to a model with a maximum effect determined solely by the replication rate constant (Δ-2LL: -58.34).

- Considering the interaction on the adaption submodel (i.e. that subinhibitory VAN delayed the adaption of *S. aureus* to VAN) was highly significant (Δ-2LL: -663.20). Conversely, if a potential interaction on the adaption level between MER influencing the adaption of *S. aureus* to VAN was evaluated, the more complex model with both adaption processes resulted in a worse model fit than the final model and also the LRT favoured the final model (Δ-2LL: -18.32).

- A biphasic growth model with a separate growth rate for lag- and log-phase (2.3.1.4) was superior to the single growth rate with first-order delay (Eq. 38) (ΔAIC: +18.01). However, the parameter estimates were highly imprecise for k_{lag} (RSE: 77.4 %) leading to model instabilities during estimation. In addition, the biphasic growth model only slightly improved the fit of the GC curve with its very dense sampling, but none of the time-kill curves with antibiotic. Hence, it was not considered as the final model.

3.3.1.3.1.4 Final model evaluation

Internal evaluation. The precision of the parameter estimates (RSE% in Table 15) was assessed by evaluating the relative standard errors computed from the variance-covariance matrix at the objective function minimum. Except for $k_{per,VAN}$, the parameters were estimated with adequate or high precision. $k_{per,VAN}$ remained in the final model as its inclusion improved the model (as outlines above) and the 95% CI of the bootstrap analysis for this parameter did not include zero.

Correlation between the structural parameters of the semi-mechanistic PD model was assessed by inspecting the correlation matrix (Eq. 14) which was graphically illustrated in Figure 73 in the Appendix using the 'corrplot' package in 'R' based on [165]: High positive correlation ($\geq$0.8) was observed for $k_{per,MER}$ with $k_{death,PER}$ (0.82) and H_{MER} with $Emax_{VAN}$ (0.83). High negative correlation ($\leq$-0.8) was observed for H_{MER} with k_{rep} (-0.85), $Emax_{VAN}$ with k_{rep} (-0.88), β_{VAN} with τ_{VAN} (-0.91) and k_{lag} with k_{rep} (-0.86). For computation of 95% CIs (CI$_{95\%}$ in Table 15), a non-parametric bootstrap analysis was performed to consider potentially asymmetric intervals and non-normally distributed parameter estimates. As a single bootstrap run required ca. 4 h of single thread CPU time, the performed 1200 bootstrap runs were split into 12 parallel tasks and required ca. 20 days to finish. 1198 of 1200 runs

converged, two runs failed due to parameter values leading to instabilities of the ODE solver. Assessment of the frequency distribution of the obtained 1198 bootstrap parameter sets revealed very few implausible negative estimates (48 out of 25158 estimates; 0.19%) originating from the unconstrained estimation in stage (ii) (Figure 74 in Appendix). Overall, the 95% CIs reflected the RSE which were obtained from the variance-covariance matrix at the final parameter estimates. None of the 95% CIs included zero.

Goodness-of-fit plots (Figure 75) and residual analyses (Figure 76 in appendix) indicated good agreement of the predicted and the observed log10 CFU/mL. As all experimental raw data was included in the analysis, cluster formation could be observed in the goodness-of-fit plots originating from multiple observations per predicted observation.

A visual predictive check was performed simulating 1000 time-kill curves stratified for the different experimental scenarios and considering both the variability of the parameters (using the variance-covariance matrix) and the residual variability σ^2. Those simulated time-kill curves were in very good agreement with the experimentally observed data, indicating good predictive performance of the developed semi-mechanistic PD model (Figure 39).
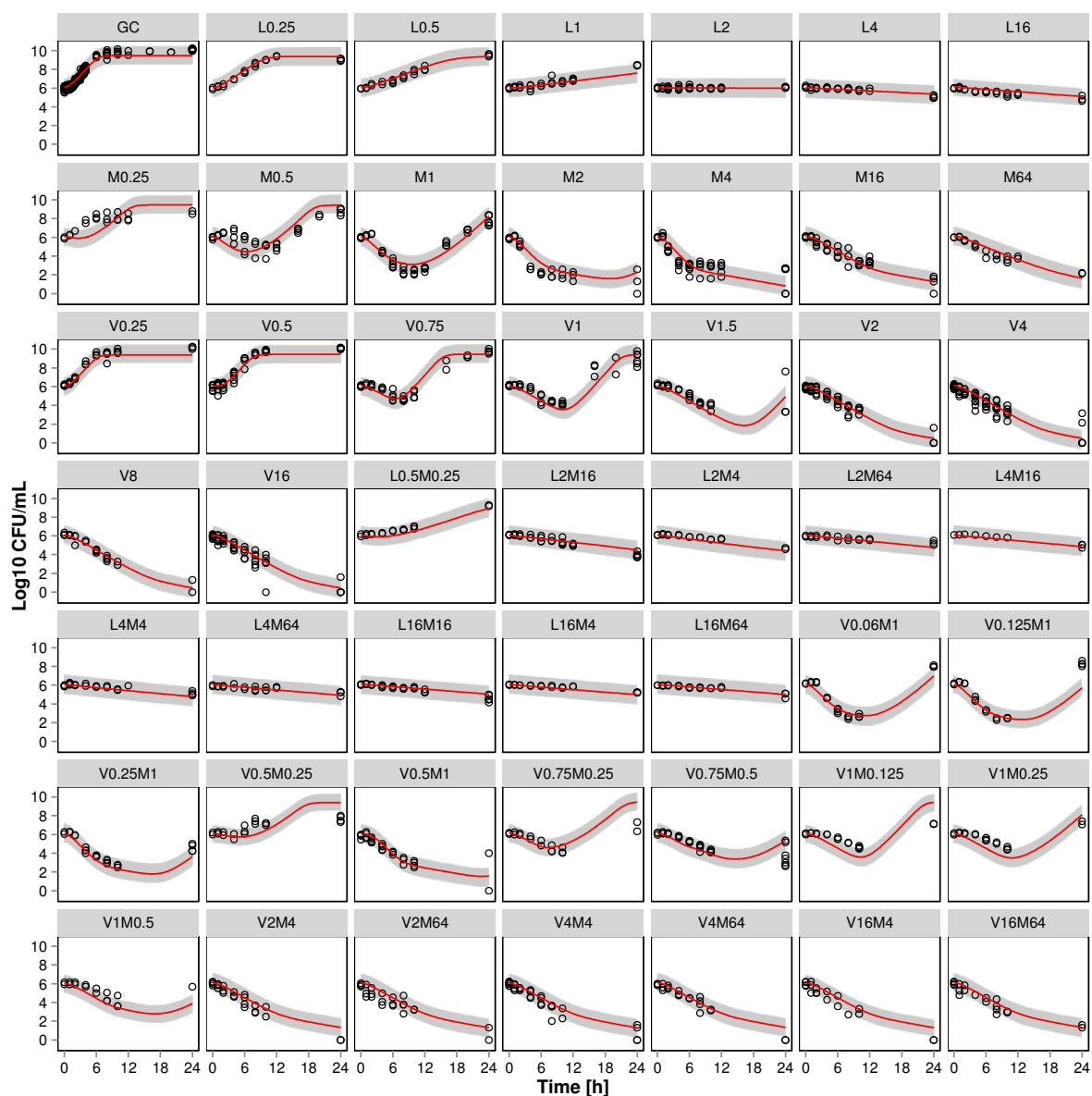
Figure 39: Visual predictive check plots for the final semi-mechanistic PD model for lag-phase *S. aureus*. Points represent experimental data; red line indicates median prediction and grey shaded area represents the 90% prediction intervals (PI) based on 1000 stochastic simulations for each scenario. Lx / Mx / Vx = multiples/fractions of the MIC of linezolid, meropenem and vancomycin, respectively.

External evaluation. The experimental data from the adaptive resistance studies (3.2.5) being not part of the model development process was used to externally evaluate the adaption submodel of the final semi-mechanistic PD model for lag-phase *S. aureus*. The effect of the second exposure period to the antibiotic was evaluated based upon experimentally pre-exposed bacteria (points in Figure 40) and compared to the model prediction (red lines in Figure 40). Figure 40 overall displays very good agreement of the experimentally observed and the predicted time-kill curves. A trend to underprediction of the adaptive resistance towards VAN (scenario V1-V2) was observed, but the

91

overall trend (regrowth) was well predicted. This indicated that the utilised adaption submodel [142,143] was suitable to describe the adaption of *S. aureus* by an increasing EC_{50} over time for MER and VAN.
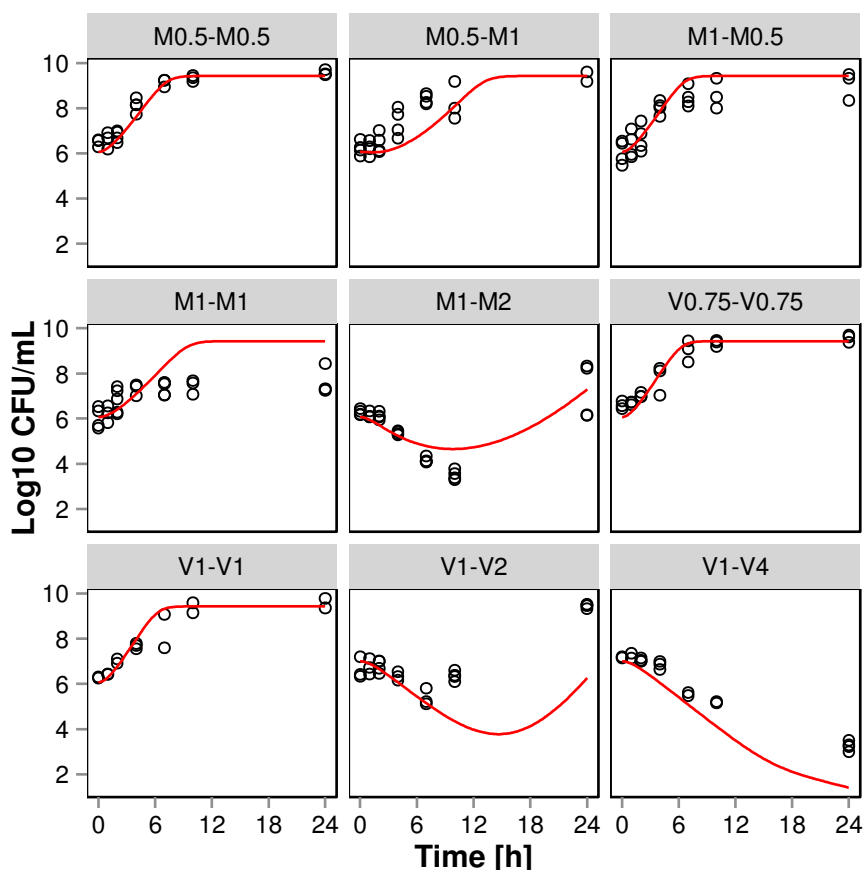
Figure 40: Prediction (red lines) of adaptive resistance investigations with MER (M) and VAN (V) at concentrations around their MIC value (number indicates multiple/fraction of MIC). First part of the label indicates concentration tier of first (pre-)exposure period, second part of the label the concentration tier of the second exposure that is displayed in the plot. Points represent experimental data from 3.2.5.

The developed semi-mechanistic PD model was challenged with prediction of other assumed antagonistic antibiotic combinations between cell-wall antibiotics and protein-synthesis inhibitors and was found to successfully predict antagonism between VAN and LZD against five MRSA strains [146] (Appendix Figure 77), penicillin and erythromycin against three strains of streptococcus pneumoniae [147] (Appendix Figure 78) and ampicillin and chloramphenicol against a meningeal isolate of group B streptococci [148] (Appendix Figure 79). In all scenarios, the EC_{50} of the drug effects could not be estimated (exclusively inhibitory concentrations studied) and hence were set to the respective MIC value reported in the publications. The values of CFU_o, CFU_{max}, k_{rep}, the value of the killing rate constant of the protein-synthesis inhibitors (analogous to $k_{death,LZD}$) and persister

92

development rate constants k_{per} were estimated separately for each strain. Figure 41 illustrates reliable prediction of all external scenarios.
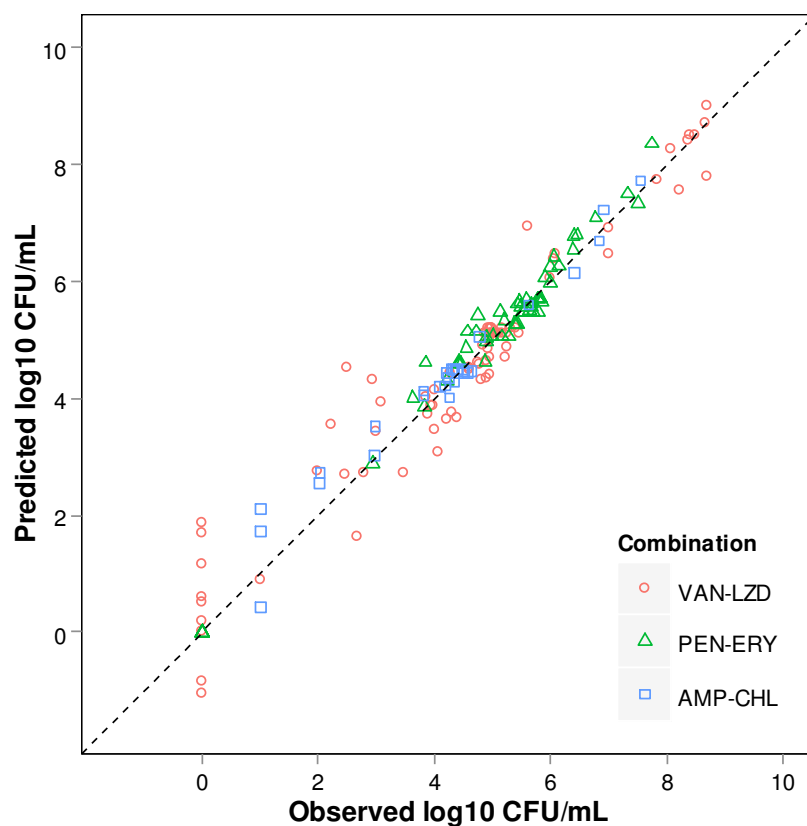
Figure 41: Observed vs. predicted log10 CFU/mL for the external evaluation of the semi-mechanistic PD model. VAN and LZD against MRSA, penicillin (PEN) and erythromycin (ERY) against *S. pneumoniae* and ampicillin (AMP) and chloramphenicol (CHL) against group B streptococci.

3.3.1.3.2   *S. aureus* in log-phase at drug exposure

3.3.1.3.2.1   Model development

In addition to the lag-phase dataset, experimental data on the effect of LZD, MER and VAN against log-phase *S. aureus* ATCC 29213 was generated the present thesis when the impact of the growth-state at drug exposure was assessed. As a starting point, the developed semi-mechanistic PD model from lag-phase (3.3.1.3.1) was also applied to the log-phase dataset. As the log-phase time-kill curve studies contained few combinatory experiments, and particularly no subinhibitory combinations, solely the single drug effects were subject to modelling tasks.

The final semi-mechanistic PD model for lag-phase *S. aureus* (3.3.1.3.1.3) was modified such as to capture the PD of LZD, MER and VAN against log-phase *S. aureus*. Key models generated during model development are summarised in Table 20 in the Appendix. The superiority of the final model

over other key models was assessed by calculation of model selection criteria (Appendix Table 19). As the number of data points to parameters (n/p) was 29.6 and hence <40, AICc was used (if appropriate). For LZD, the time-kill curves for log-phase *S. aureus* had a very similar shape for concentration up to 4 mg/L compared to lag-phase bacteria. This effect was implemented by a growth-arresting effect of LZD, similarly to the lag-phase model. However, for higher concentrations of LZD, an additional killing effect was observed up to 4 h and mathematically considered by an additional time-dependent killing rate on 'GRO'. This approach was superior to not considering this killing effect at higher concentrations (ΔAICc: -97.24) or to implementing an initial replication dependent effect of LZD (ΔAICc:-65.47).

For MER, the paradoxically reduced effect at higher concentrations (Eagle effect [164]) was much less pronounced in log-phase compared to lag-phase *S. aureus*. Mathematical implementation of an Eagle-effect did not improve the model fit and a simpler model with a single replication-dependent effect for MER was superior (AICc: -4.42).

Estimation of a persister development rate for MER was imprecise; still $k_{per,MER}$ was implemented and fixed to its final estimate to increase model stability which improved the model with very high significance (Δ-2LL: -249.33).

For VAN, the model structure was similar compared to the final PD model for lag-phase *S. aureus*. The initial maximum killing effect was also inferior to the maximum initial effect of MER in the log-phase scenario. Considering $Emax_{VAN}$ significantly improved the model compared to a simpler model that had the maximum effect of VAN solely determined by the replication rate (Δ-2LL: -41.13). The persister development rate $k_{per,VAN}$ significantly improved the model (Δ-2LL: -156.75).

Implementation of a basal death rate for persisting bacteria ($k_{death,per}$) did not improve the model (ΔAIC: -0.15) as its estimate was close to zero and the 95% CI included zero. Yet, it is likely that for longer observation periods it can be assumed that persisting bacteria would eventually decline, but this was not observed within the studied time period of 24 h.

3.3.1.3.2.2 Final model

The final model that simultaneously described the single effects of MER, LZD and VAN against log-phase *S. aureus* is illustrated in Figure 42.
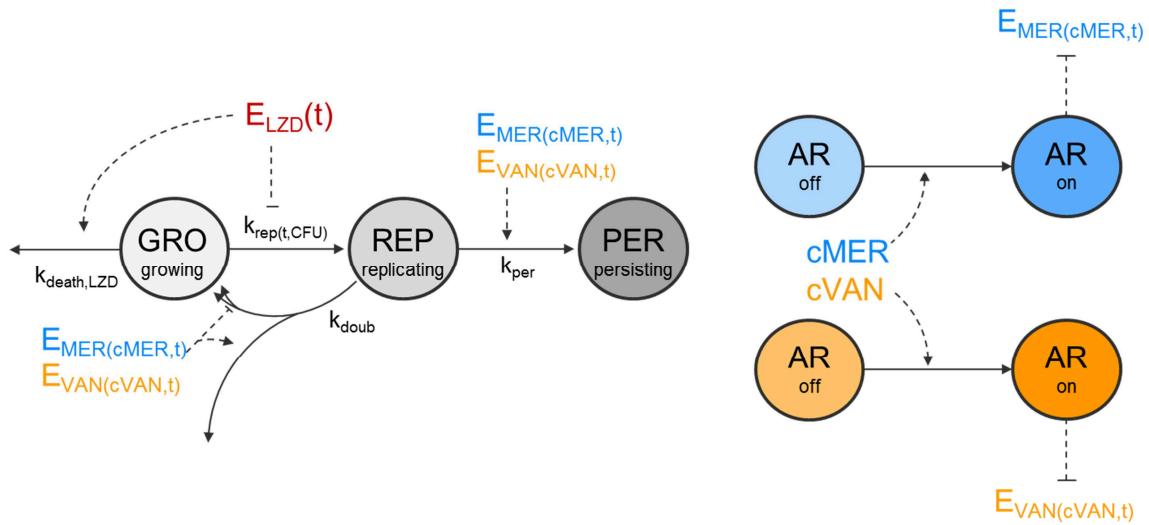
Figure 42: Graphical sketch of the semi-mechanistic PD model (left) and adaption submodel of VAN and MER (right) for log-phase *S. aureus*; solid arrows: Mass transfer between compartments; dashed arrows: stimulatory effects; dashed ----|: inhibitory effects.

The bacterial life-cycle was parameterised taking into account the differences observed in time-kill curve studies between the lag- and log-phase *S. aureus* as elaborated in 3.3.1.3.2.1. The ODE system for growing bacteria 'GRO', replicating bacteria 'REP' and persisting bacteria 'PER' was as follows:

$$\frac{dGRO}{dt} = -k_{death,LZD} \times E_{LZD} \times GRO$$

$$-k_{death,LZD,log} \times E_{LZD,log} \times GRO \times (e^{-k_{LZD,log}t})$$

$$- k_{rep}(t, CFU) \times (1 - E_{LZD}) \times GRO \quad \text{(Eq. 45)}$$

$$+k_{doub} \times \left(1 - E_{MER,t}\right) \times \left(1 - Emax_{VAN} \times E_{VAN,t}\right) \times REP \times 2$$

$$\text{IC: } CFU_0$$

$$\frac{dREP}{dt} = k_{rep}(t, CFU) \times (1 - E_{LZD}) \times GRO$$

$$-k_{doub} \times REP - k_{per,MER} \times E_{MER,t} \times REP - k_{per,VAN} \times E_{VAN,t} \times REP \quad \text{(Eq. 46)}$$

$$\text{IC: } 0$$

$$\frac{dPER}{dt} = k_{per,MER} \times E_{MER,t} \times REP + k_{per,VAN} \times E_{VAN,t} \times REP$$

$$\text{(Eq. 47)}$$

$$\text{IC: } 0$$

As for the lag-phase model, k_{rep} was assumed to decrease if bacterial concentrations reached the capacity limit *CFU_{max}*. Conversely, no lag-time to attain exponential growth was required as bacteria had already reached exponential growth at drug exposure:

$$k_{rep}(t, CFU) = k_{rep} \times \left(1 - \frac{GRO + REP + PER}{CFU_{max}}\right) \qquad \text{(Eq. 48)}$$

The adaption of *S. aureus* to MER and VAN was implemented as an increasing *EC50* over time for MER and VAN stimulated by exposure to MER and VAN analogous to the lag-phase model. However, no interaction between VAN and MER was implemented as only single drug effects were assessed for log-phase *S. aureus*.

$$\frac{dAR_{off,MER}}{dt} = \tau_{MER} \times c(t) \times AR_{off,MER} \quad IC=1 \qquad \text{(Eq. 49)}$$

$$\frac{dAR_{on,MER}}{dt} = \tau_{MER} \times c(t) \times AR_{off,MER} \quad IC=0 \qquad \text{(Eq. 50)}$$

$$EC_{50,MER}(t) = \alpha_{MER}(t) \times EC_{50,MER,t=0}$$
$$\text{with } \alpha_{MER}(t) = 1 + \beta_{MER} \times AR_{on,MER}(t) \qquad \text{(Eq. 51)}$$

$$\frac{dAR_{off,VAN}}{dt} = -\tau \times c(t) \times AR_{off} \qquad\qquad IC=1 \qquad \text{(Eq. 52)}$$

$$\frac{dAR_{on,VAN}}{dt} = \tau \times c(t) \times AR_{off} \qquad\qquad IC=0 \qquad \text{(Eq. 53)}$$

$$EC_{50,VAN}(t) = \alpha_{VAN}(t) \times EC_{50,VAN,t=0}$$
$$\text{with } \alpha_{VAN}(t) = 1 + \beta_{VAN} \times AR_{on,VAN}(t) \qquad \text{(Eq. 54)}$$

The final parameter estimates of the semi-mechanistic PD model for log-phase *S. aureus* are presented in Table 16 and presented in a similar fashion as the estimates of the lag-phase model (Table 15). The parameter values of the bacterial life-cycle, i.e. *CFU_{0}*, *CFU_{max}* were in well agreement with those that one would determine by visual inspection (e.g. from Figure 17). k_{rep} of 1.64 h^{-1} was very close to the value obtained in the log-phase with the biphasic growth model (1.73 h^{-1} in 3.2.1.3); as for the lag-phase model, overlapping CIs indicated that the various drug-effects of LZD, MER and VAN did not perturb the parameter estimates of drug-free growth. For LZD, the drug effects were separated into a time-dependent effect at higher concentrations (EC$_{50,LZD,log}$: 6.34 mg/L) that decreased with a first-order time-delay rate constant $k_{LZD,log}$ and a time-invariant effect with an *EC_{50}* of 0.41 mg/L. As for the lag-phase model, the plain parameter values of the drugs MER and VAN are difficult to interpret and a combined interpretation of the adaption processes is given in the discussion (4.3.3).

Table 16: Parameter estimates of the final semi-mechanistic PD model for log-phase *S. aureus*, relative standard errors (RSE) in % obtained from the variance-covariance matrix, 95% confidence intervals determined by a non-parametric bootstrap analysis (n=1190) and short explanation of the model parameters.

Parameter [Unit]	Estimate	RSE % [CI$_{95\%}$]	Explanation
Parameters of the bacterial life-cycle			
CFU$_0$ [log10 CFU/mL]	6.23	0.8 [6.04; 6.29]	Initial colony forming units (CFU)/mL at beginning of the experiment
CFU$_{max}$ [log10 CFU/mL]	9.76	0.8 [9.59; 9.94]	Maximum attainable bacterial growth
k$_{rep}$ [h^{-1}]	1.64	3.8 [1.45; 2.00]	Transit rate constant from growing to replicating state; used to calculate observed, rate-limiting step for bacterial growth
k$_{doub}$ [h^{-1}]	100	FIX [-]	Rate constant of doubling; represents actual replication (fixed to high rate constant as not rate-limiting); MER and VAN impaired successful replication
Drug-related parameters			
EC$_{50,LZD}$ [mg/L]	0.41	26.8 [0.200; 0.737]	C$_{LZD}$ leading to half-maximum drug effect of LZD on k$_{rep}$ (growth arrest) and stimulation of k$_{death,LZD}$
H$_{LZD}$ [-]	0.82	29.1 [0.427; 1.58]	Hill factor LZD (steepness of the concentration-effect relationship for growth arrest)
k$_{death, LZD}$ [h^{-1}]	0.20	51.3 [0.0656; 0.345]	Basal death rate constant of growth-arrested bacteria, induced by LZD
EC$_{50,LZD,log}$ [mg/L]	6.34	11.5 [4.37; 20.7]	C$_{LZD}$ leading to half-maximum drug effect of LZD of initial killing against log-phase bacteria
H$_{LZD,log}$ [-]	3.39	29.6 [1.25; 13.2]	Hill factor LZD (steepness of the concentration-effect relationship for initial log-phase killing)
k$_{death, LZD, log}$ [h^{-1}]	6.80	32.5 [2.89; 18.0]	Initial log-phase LZD killing rate constant
k$_{LZD, log}$ [h^{-1}]	1.18	38.1 [0.321; 1.29]	First-order time delay rate constant for decreasing initial log-phase killing by LZD
EC$_{50,MER,t=0}$ [mg/L]	0.040	9.5 [0.0315; 0.0525]	C$_{MER}$ leading to half-maximum drug effect of MER on k$_{doub}$ and k$_{per,MER}$ at t=0
H$_{MER}$ [-]	2.26	8.6 [1.54; 2.94]	Hill factor MER (steepness of the concentration-effect relationship)
β$_{MER}$ [-]	4.10	10.4 [2.81; 9.51]	[(1+β$_{MER}$)× EC$_{50,MER,t=0}$] calculates maximum possible adapted EC$_{50}$ of bacteria

τ_{MER} [L/(mg·h)]	0.55	23.0 [0.122; 0.822]	Second-order delay rate constant for adaption with respect to time and C_{MER}
$k_{per,MER}$ [h^{-1}]	2.65e-04	FIX [-]	Persister development rate for MER during replication
$k_{deg,MER}$ [h^{-1}]	0.019	FIX [-]	First-order degradation rate constant of C_{MER}; drug degradation determined by HPLC (3.1.3), hence fixed during estimation
$Emax_{VAN}$ [%]	73.7	2.8 [67.9; 79.8]	Percentage by which VAN decreased successful doubling at maximum
$EC_{50,VAN,t=0}$ [mg/L]	0.43	3.3 [0.354; 0.493]	C_{VAN} leading to half-maximum drug effect of VAN on k_{doub} and $k_{per,VAN}$ at t=0
H_{VAN} [-]	20	FIX [-]	Hill factor for replication dependent effect of VAN; fixed as estimation was imprecise
β_{VAN} [-]	11.5	7.3 [9.19; 38.8]	$[(1+\beta_{VAN})\times EC_{50,VAN,t=0}]$ calculates maximum possible adapted EC_{50} of bacteria
τ_{VAN} [L/(mg·h)]	0.019	17.5 [0.00296; 0.0381]	Second-order delay rate constant for adaption with respect to time and C_{VAN}
$k_{per,VAN}$ [h^{-1}]	0.66	33.0 [0.237; 1.86]	Persister development rate for VAN during replication
$k_{deg,VAN}$ [h^{-1}]	3.9e-03	FIX [-]	First-order degradation rate constant of C_{VAN}; drug degradation determined by HPLC (3.1.3), as an independent variable, was fixed during estimation
σ [log10CFU/mL]	0.58	-	Residual additive variability, no RSE reported as calculated from final objective function value

3.3.1.3.2.3 Final model evaluation

The precision of the parameter estimates (RSE% in Table 16) was assessed by evaluating the relative standard errors computed from the variance-covariance matrix at the objective function minimum. Apart from $k_{death,\,LZD}$, the parameters were estimated with adequate or high precision.

Correlation between the structural parameters of the semi-mechanistic PD model was assessed by inspecting the correlation matrix (Eq. 14) which was graphically illustrated in Figure 80 (Appendix) using the 'corrplot' package in 'R' based on [165]: High positive correlation ($\geq$0.8) was observed for $k_{death,LZD}$ with $k_{death,LZD,log}$ (0.95). High negative correlation ($\leq$-0.8) was observed for β_{VAN} with τ_{VAN} (-0.9) and $k_{death,LZD}$ with H_{LZD} (-0.83).

For computation of 95% CIs (CI$_{95\%}$ in Table 15), a non-parametric bootstrap analysis was performed to consider potentially asymmetric intervals and non-normally distributed parameter estimates. A

single bootstrap run required ca. 0.5 h of single thread CPU time. 1190 of 1200 runs converged, 10 runs failed due to parameter values leading to instabilities of the ODE solver. Assessment of the frequency distribution of the obtained 19 bootstrap parameter sets revealed very few implausible negative estimates (130 out of 22762 estimates; 0.57%) originating from the unconstrained estimation in stage (ii) (Appendix Figure 81). For the parameters related to the initial log-phase effect of LZD, bimodal parameter distributions were observed, potentially originating from the comparably sparse data situation (scenarios 8 and 32 mg/L) leading to a higher chance that no data point from one or the other scenario was sampled. For the other parameters, single mode distributions were observed.

Goodness-of-fit plots (Appendix Figure 82) and residual analyses (Appendix Figure 83) indicated good agreement of the predicted with the observed log10 CFU/mL.

A visual predictive check was performed simulating 1000 time-kill curves stratified for each experimental scenario considering both the variability of the parameters (using the variance-covariance matrix) and the residual variability σ^2. Those simulated time-kill curves were in decent agreement with the experimentally observed data indicating good predictivity of the developed semi-mechanistic PD model (Figure 43).
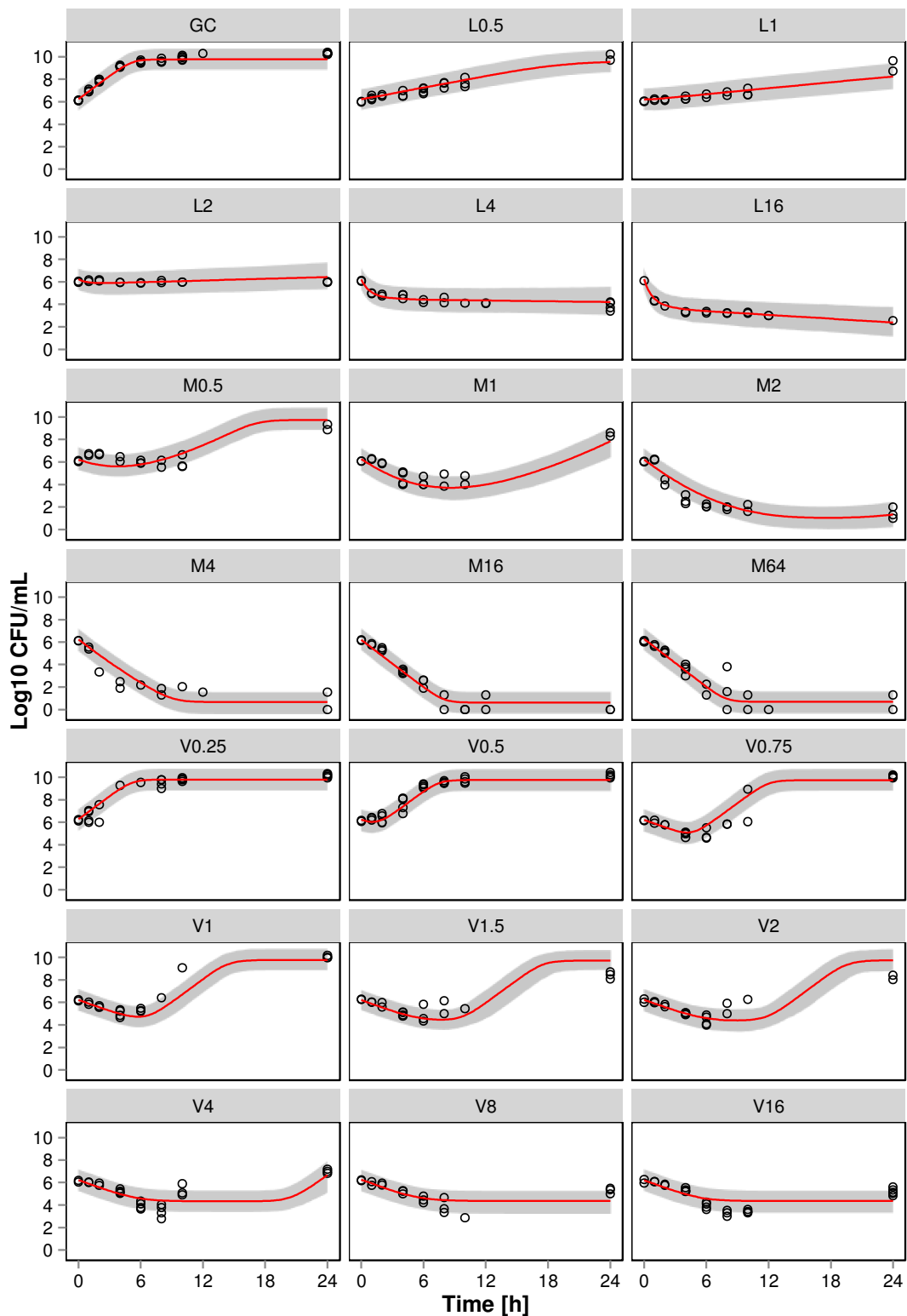
Figure 43: Visual predictive check plots for the final semi-mechanistic PD model for log-phase *S. aureus*. Points represent experimental data; Red line indicates median prediction and grey shaded area represents 90% PIs based on 1000 stochastic simulations for each scenario. Lx / Mx / Vx = multiples/fractions of the MIC of linezolid, meropenem and vancomycin, respectively.

3.3.2 Simulations

3.3.2.1 Prediction of PK/PD indices

Published population PK models for MER, LZD and VAN (2.4.2.1) were utilised to calculate unbound concentration time profiles which were linked to the final semi-mechanistic PD models for both lag- (3.3.1.3.1) and log-phase *S. aureus* (3.3.1.3.2). Typical PK profiles for MER, LZD and VAN are presented in Figure 84 in the Appendix. With the resulting population PK/PD model, an *in silico* dose fractionation study was performed and the PK/PD indices $f\mathrm{C}_{max}/\mathrm{MIC}$, $f\mathrm{AUC}/\mathrm{MIC}$ and $\%f\mathrm{T}_{>\mathrm{MIC}}$ were calculated and correlated with the obtained bacterial load in log10 CFU/mL at 24 h for both lag- and log-phase *S. aureus* (Figure 44 and Figure 45) to identify the PK/PD indices that best correlate with the effect. In addition, the obtained PK/PD-index - effect relationship was used to calculate bacteriostatic (i.e. no growth or killing compared to the inoculum) and/or bactericidal (i.e. log3-fold bacterial killing compared to the inoculum) PK/PD breakpoints.
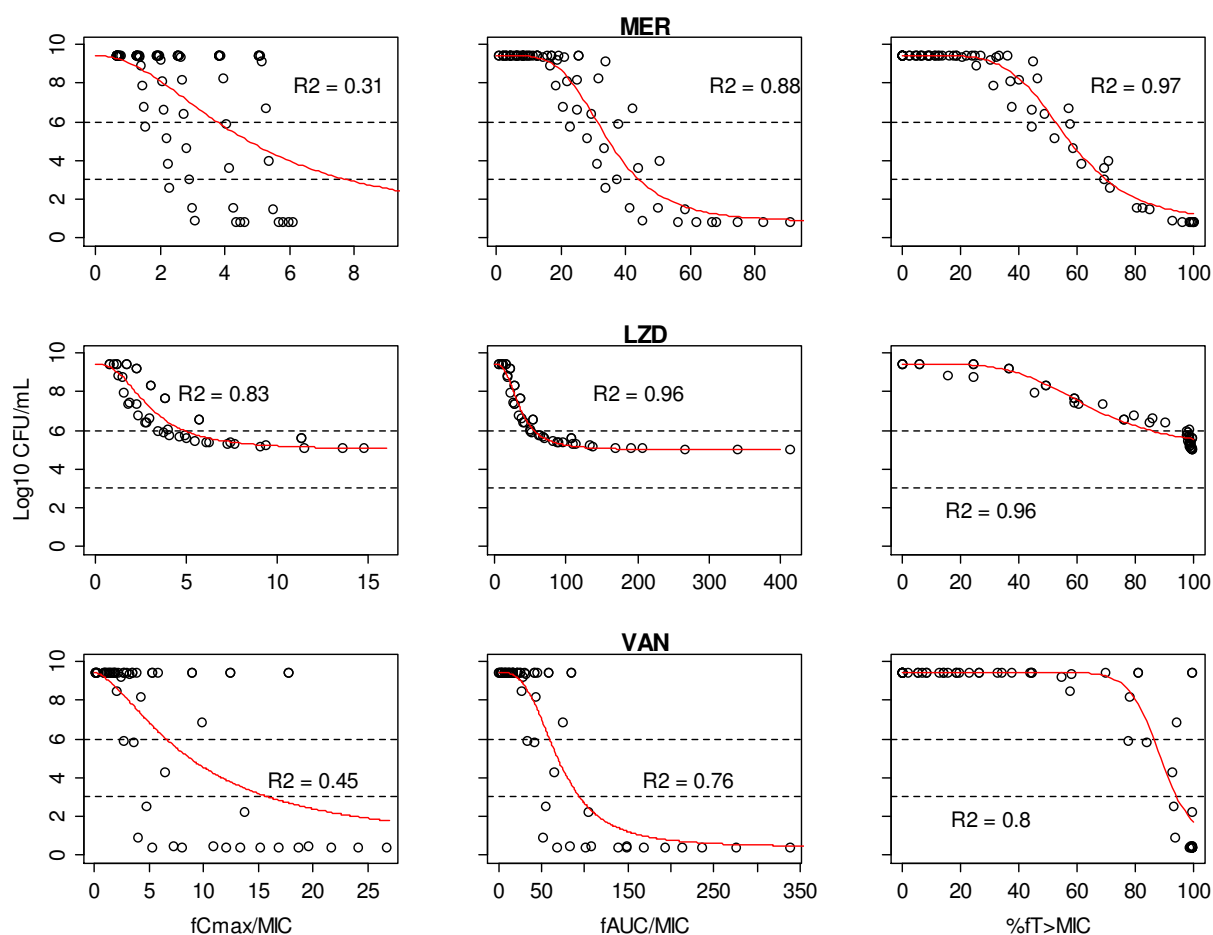
Figure 44: Prediction of PK/PD indices $f\mathrm{C}_{max}/\mathrm{MIC}$, $f\mathrm{AUC}/\mathrm{MIC}$ and $\%f\mathrm{T}_{>\mathrm{MIC}}$ for MER, LZD and VAN against lag-phase *S. aureus*. Points represent simulated log10 CFU/mL at 24 h using the linked population PK/PD model, dashed horizontal lines at 6 log10 CFU/mL represent inoculum and bacteriostatic effect, dashed horizontal line at 3 log10 CFU/mL represents bactericidal effect, red lines represent prediction of an inhibitory sigmoidal maximum effect model (2.4.1.3.1) fitted to the simulated data, R²: coefficient of determination.
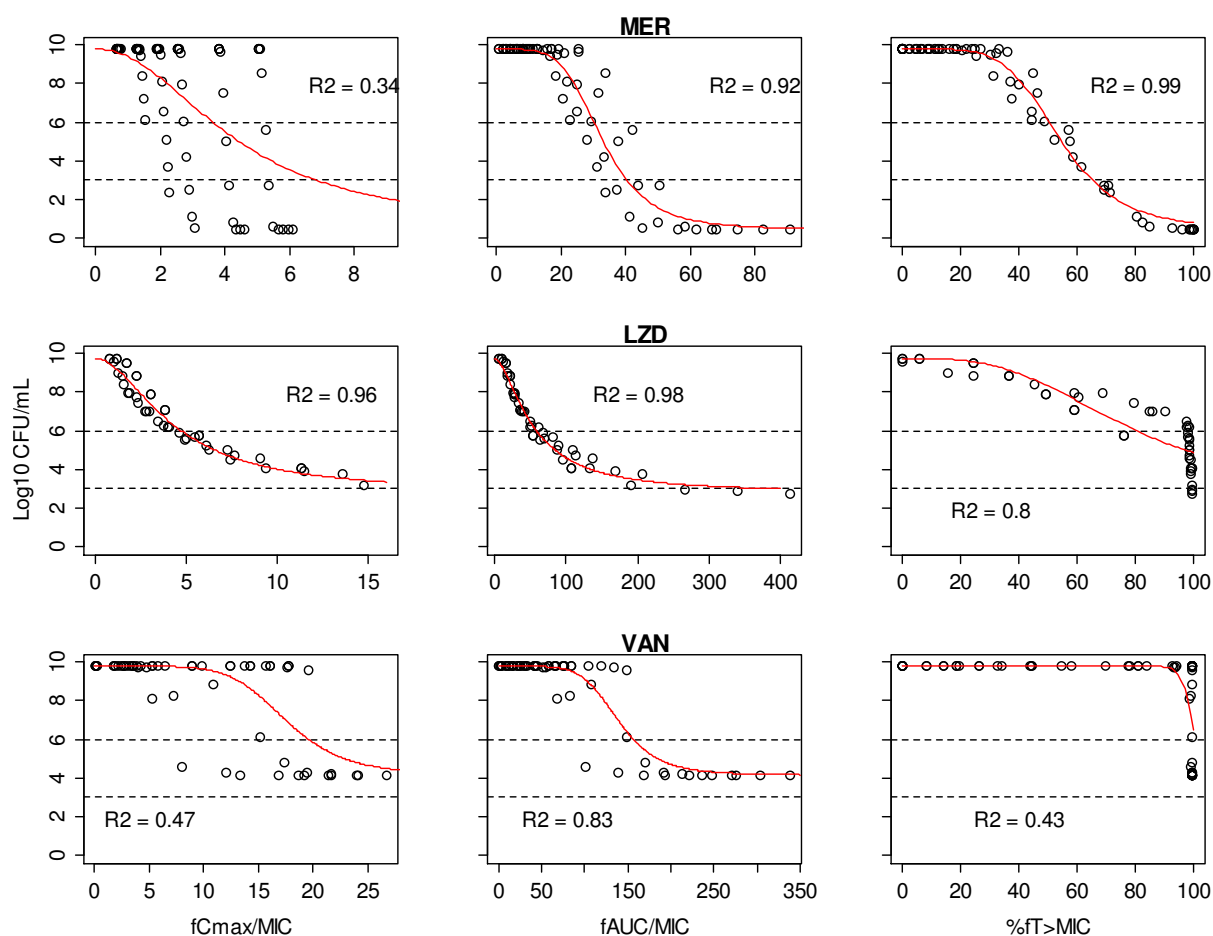
Figure 45: Prediction of PK/PD indices fC$_{max}$/MIC, fAUC/MIC and $\%f$T$_{>MIC}$ for MER, LZD and VAN against log-phase *S. aureus*. Points represent simulated log10 CFU/mL at 24 h using the linked population PK/PD model, dashed horizontal lines at 6 log10 CFU/mL represent inoculum and bacteriostatic effect, dashed horizontal line at 3 log10 CFU/mL represents bactericidal effect, red lines represent prediction of an inhibitory sigmoidal maximum effect model (2.4.1.3.1) fitted to the simulated data, R²: coefficient of determination.

For lag-phase *S. aureus*, $\%f$T$_{>MIC}$ correlated best with the effect of MER at 24 h as indicated by the highest R² in Figure 44. For LZD, all PK/PD indices displayed good correlation. For VAN, best correlation was observed for $\%f$T$_{>MIC}$, but correlation overall was <0.80 and a clear distinction for identifying the 'best' PK/PD index was rather difficult.

For log-phase *S. aureus*, the overall correlation pattern was similar compared to lag-phase *S. aureus*. However, for LZD a higher maximum effect (ca. 2 log10-fold vs. 1 log10-fold reduction of inoculum) was obtained if fAUC/MIC was >100 compared to lag-phase *S. aureus*. Correlation for $\%f$T$_{>MIC}$ was worse due to the formation of a cluster at 100% originating from further increase of the effect above 100%. In addition, log-phase *S. aureus* was much less susceptible towards the effect of VAN as indicated by overall substantially higher PK/PD breakpoints. No bactericidal effect was obtained for VAN against log-phase *S. aureus*. Similar to LZD, cluster-formation was observed at fT$_{>MIC}$ of 100%

indicating that in some scenarios even 100% fT$_{>MIC}$ was insufficient to decrease bacteria compared to the inoculum.

Bacteriostatic and bactericidal PK/PD breakpoints were determined by the intercept between the fitted inhibitory sigmoidal maximum effect model (red lines in e.g. Figure 45) and the thresholds for a bacteriostatic and bactericidal effect (dashed horizontal lines in e.g. Figure 45). Table 17 summarises the obtained PK/PD breakpoints for a bacteriostatic and bactericidal antibiotic effect at 24 h for both lag- and log-phase *S. aureus*. For MER in lag-phase *S.aureus*, a bacteriostatic or bactericidal effect was observed when fT$_{>MIC}$ exceeded 50% or 65%, respectively. For MER in log-phase *S.aureus*, a bacteriostatic or bactericidal effect was observed when fT$_{>MIC}$ exceeded 52% or 70%, respectively. For LZD, solely a bacteriostatic effect was attained at fAUC/MIC 56 or 59 for lag- and log-phase *S. aureus*. For VAN in lag-phase *S. aureus* fT$_{>MIC}$ correlated best and a bacteriostatic or bactericidal effect was observed for fT$_{>MIC}$ of 86% or 94%, respectively. For VAN in log-phase *S. aureus* fAUC/MIC correlated best and solely a bacteriostatic effect was achieved if fAUC/MIC exceeded 160.

Table 17: PK/PD breakpoints calculated from the *in silico* dose fractionation study for a bacteriostatic and bactericidal antibiotic effect for MER, LZD and VAN against both lag- and log-phase *S. aureus;* n.r. = not reached; bold: highest R².

	PK/PD breakpoint
	\multicolumn{2}{c}{fC$_{max}$/MIC [-]}		\multicolumn{2}{c}{fAUC/MIC [-]}		\multicolumn{2}{c}{%fT$_{>MIC}$}
	bacteriostatic effect
Drug	lag	log	lag	log	lag	log
MER	3.8	3.6	31	30	**52**	**50**
LZD	4.8	4.7	**56**	**59**	85	80
VAN	6.6	20	59	**160**	**86**	100
	bactericidal effect
Drug	lag	log	lag	log	lag	log
MER	7.8	6.9	44	40	**70**	**65**
LZD	n.r.	n.r.	n.r.	n.r.	n.r.	n.r.
VAN	16	n.r.	94	n.r.	**94**	n.r.

3.3.2.2 Clinical trial simulation

The elaborated population PK/PD models for LZD, MER and VAN for both lag- and log-phase *S. aureus* were also used to evaluate clinically relevant dosing regimens. In a first step, a clinical trial was simulated with 1000 virtual patients that received standard dosing regimens for LZD, MER and VAN. In a second step, the impact of patient covariates for drug disposition (total body weight) and

drug elimination (total body weight, liver function, and creatinine clearance) was investigated and alternative dosing regimens were investigated if appropriate.

3.3.2.2.1 Virtual clinical trial with reference dosing regimens.

The clinical trial was simulated with 1000 patients receiving the standard dosing regimens MER, VAN and LZD, alone and in combination. The characteristics, i.e. PK covariates of the virtual patient population were overall in range of the covariates of the real patient populations on which the population PK models were built (Table 18) to avoid extrapolation. In contrast to the literature [150,153,154] that reported covariate ranges, the 2.5th-97.5th percentiles of the covariates was reported for the virtual population of the present study due to the larger population (Table 18). The virtual patients were in median 35 years old and were with 74.7 kg of normal total body weight. The renal function as indicated by CLCR was normal and mild renal impairment <80 mL/min was observed in only 8.2% of the virtual patients. 5.2% of the virtual patients were assumed to suffer from liver cirrhosis (Child Pugh grade C).

Table 18: Characteristics of the simulated virtual population of the present study (median, 2.5th-97.5th percentile) in comparison to the 'real' patient populations underlying the population PK models from literature used for simulation of the PK of MER, LZD and VAN (median, range); n.r.: not reported.

Covariate	Present study n=1000	MER [153] n=79	LZD [150] n=50	VAN [154] n=50
WT [kg]	74.7 (60.6-91.7)	70.0 (40.6-137)	57.3 (38.4-100)	60.6 (40-130)
AGE [yrs.]	35 (28-43)	35 (18-93)	69.1 (32-92)	60 (18-81)
SCR [mg/dL]	1.00 (0.81-1.23)	1.00 (0.4-6.9)	1.10 (0.2-4.24)	n.r.
CLCR [mL/min]	100.8 (71.6-139.7)	n.r.	74.0 (9.43-330)	76.3 (16.3-120)
SEX [% female]	48.1%	22.8%	28.0%	44.0%
CIR [% liver cirrhosis]	5.2%	n.r.	4.0%	n.r.

The clinical trial simulation exhibited PK variability of MER of 1000 mg TID in the virtual patient population and unbound C_{max} was in median (5th-95th percentile) 32.6 mg/L (22.2-46.1 mg/L) and unbound C_{min} was 0.51 mg/L (0.022-2.94 mg/L) after the first dose (Figure 46, upper panel). With

respect to the PD consequences of this PK variability, the regimen was effective against both lag- and log-phase *S. aureus* and, in median a bactericidal effect was obtained after 24 h (Figure 46, lower panel). The median effect was close to the maximum possible effect as indicated by the narrow spread between the 5th and 50th percentile. For lag-phase *S. aureus*, in 91 % of the virtual patients, a bactericidal effect was attained at 24 h. Against log-phase *S. aureus*, MER was more rapidly bactericidal within 10 h for 96% of the simulated patients.

The PK/PD breakpoint $\%fT_{>MIC}$ was 72% or 86% for lag-phase *S. aureus* for a bacteriostatic or bactericidal effect, respectively, and thus higher than the values derived from the dose fractionation study (Table 17). For log-phase *S. aureus*, the PK/PD index of $\%fT_{>MIC}$ was 56% or 62% for a bacteriostatic or bactericidal effect, respectively, and thus comparable to the previously determined value from the dose fractionation study.
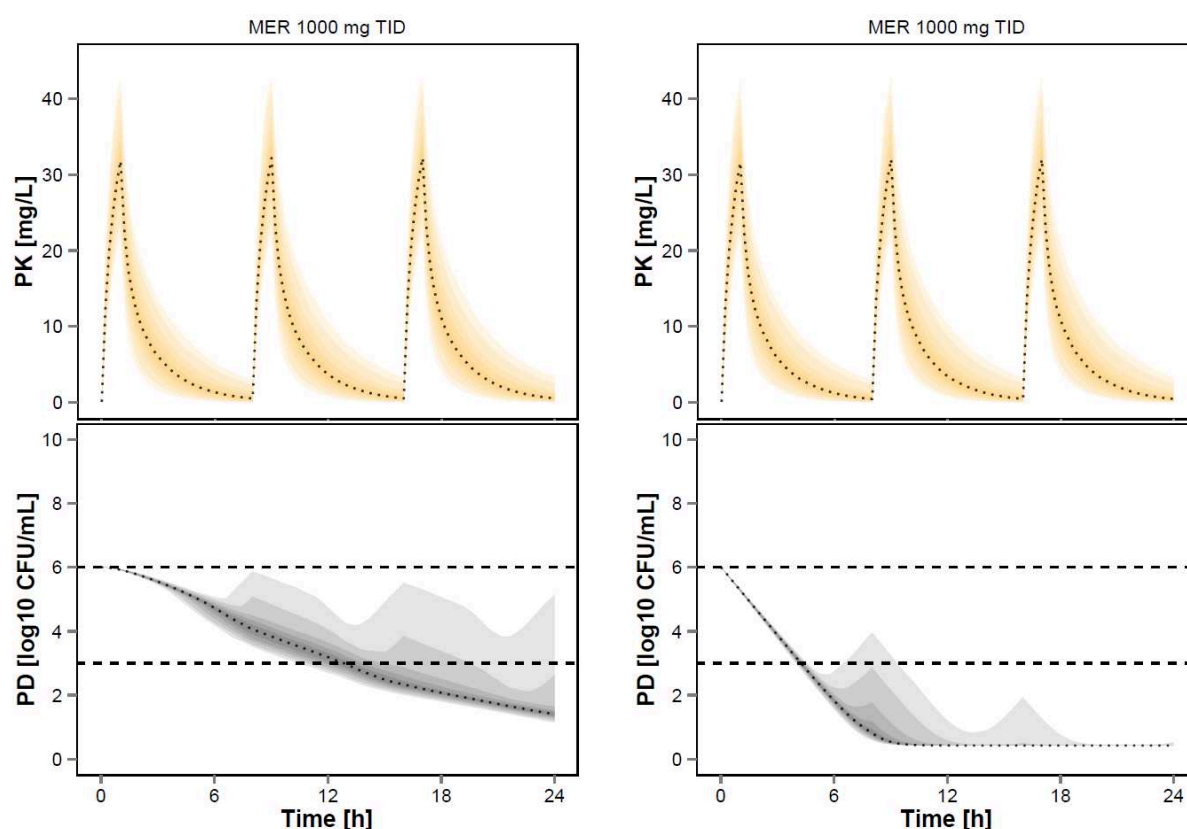
Figure 46: PK/PD for lag- (left) and log-phase (right) *S. aureus* against MER 1000 mg TID; median prediction (dotted lines) of unbound drug concentrations (PK; upper panel) and drug effect as log10 CFU/mL over time (PD; lower panel), variability (shaded area) ranging from the 5th to the 95th percentile ($20^{th}, 40^{th}, 60^{th}, 80^{th}$ and 90th PIs), dashed horizontal line at 6 log10 CFU/mL represents inoculum and bacteriostatic effect, dashed horizontal line at 3 log10 CFU/mL represents bactericidal effect.

Figure 47: PK/PD index *%f*T$_{>MIC}$ for MER in lag- (left) and log-phase *S. aureus* (right) derived from the clinical trial simulation with MER 1000 mg TID, red lines represent prediction of an inhibitory sigmoidal maximum effect model (2.4.1.3.1) fitted to the simulated data, dashed horizontal line at 6 log10 CFU/mL represents inoculum and bacteriostatic effect, dashed horizontal line at 3 log10 CFU/mL represents bactericidal effect.

With the standard dosing regimen of 600 mg LZD BID, unbound C_{max} was in median (5th-95th percentile) 11.6 mg/L (6.7-19.2 mg/L) and unbound C_{min} was 4.22 mg/L (1.70-7.60 mg/L) after the first dose. This PK exposure stimulated a bacteriostatic effect for both lag- and log-phase *S. aureus* (Figure 48). For lag-phase *S. aureus*, only marginal median killing to 5.4 log10 CFU/mL with a narrow effect spread (90% PI: 5.1-6.1 log10 CFU/mL) was observed after 24 h, indicating the for most virtual patients the maximum effect was attained. For log-phase *S. aureus*, LZD 600 mg BID reduced the bacterial load to 4.7 log10 CFU/mL at 24 h (90% PI: 3.5 and 6.1 log10 CFU/mL). In log-phase, the spread in the PD curve was less narrow than for lag-phase *S. aureus* originating from variability in the beginning of the PK profile that determines the initial effect of LZD against log-phase bacteria.

The PK/PD breakpoint *f*AUC/MIC determined in the clinical trial simulation (Figure 49) for a bacteriostatic effect were 64 in lag- and 53 in log-phase and thus comparable to the previously determined values of the dose fractionation study (Table 17). In log-phase, a bactericidal effect was predicted for *f*AUC/MIC of 224. In summary, due to the considerable variability around the predicted relationship, higher *f*AUC/MIC > 100-150 is required to assure reliable reduction in the bacterial load for all virtual patients.
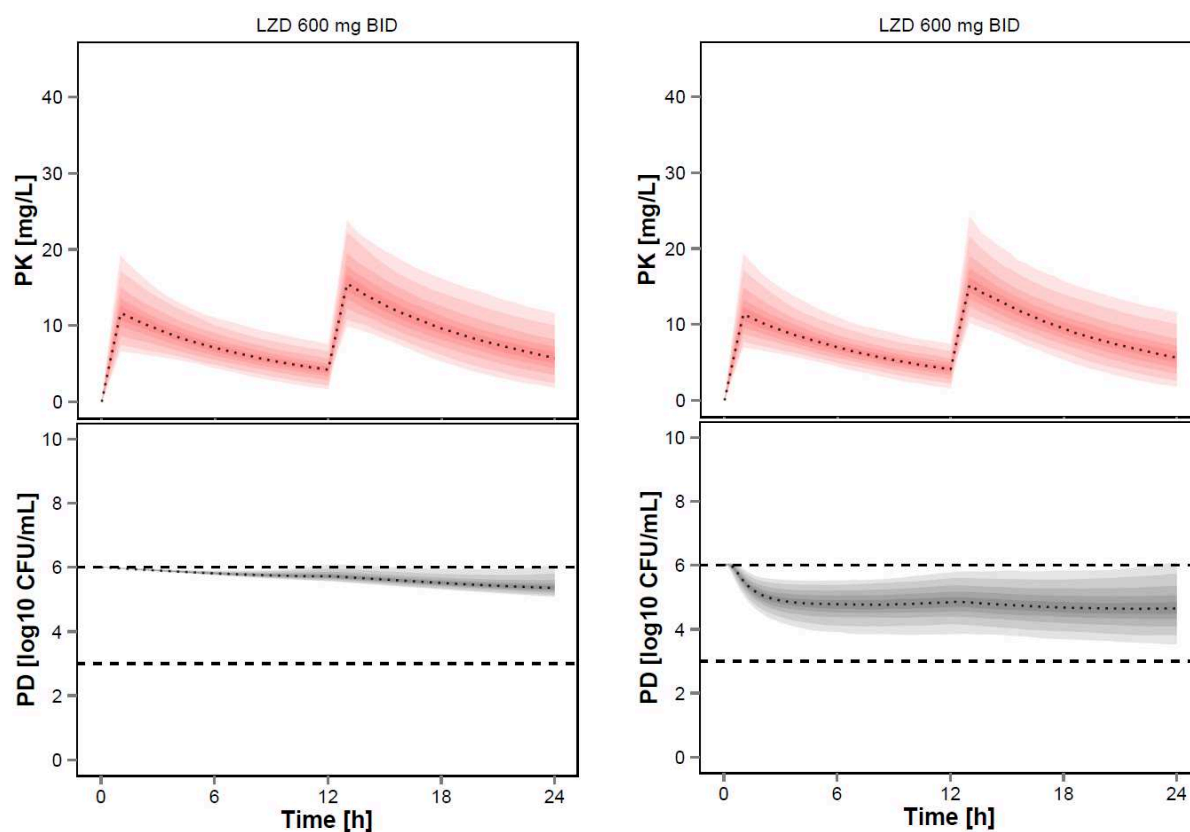
Figure 48: PK/PD for lag- (left) and log-phase (right) *S. aureus* against LZD 600 mg BID; for further details refer to caption of Figure 46.
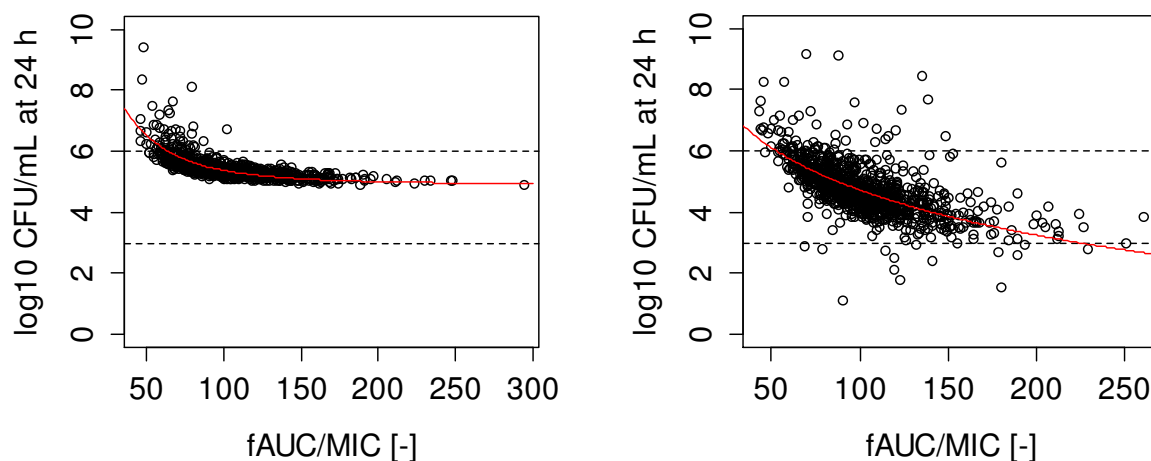
Figure 49: PK/PD index *f*AUC/MIC for LZD in lag- (left) and log-phase *S. aureus* (right) derived from the clinical trial simulation with LZD 600 mg BID.

For lag-phase *S. aureus*, VAN 1000 mg BID was a bactericidal regimen after 12 h for 62% of the virtual patients (Figure 50). At 24 h, 95 % of the virtual patients had a bacterial load lower than

4.5 log10 CFU/mL. For log-phase *S. aureus*, VAN 1000 mg BID did not stimulate net-killing (i.e. a reduction of bacteria compared to the inoculum) in median and net-growth to 8.2 log10 CFU/mL was observed (90% PI: 4.1-9.8 log10 CFU/mL). For 31% of the patients, net-killing was observed.

In contrast to LZD and MER, the variability in the relationship between the PK/PD index *f*AUC/MIC and the bacterial load at 24 h was substantial and thus it was not meaningful to describe it with a mathematical model to derive PK/PD breakpoints. The maximum effect for all virtual patients was achieved for *f*AUC/MIC between 200 and 250 in both growth phases.
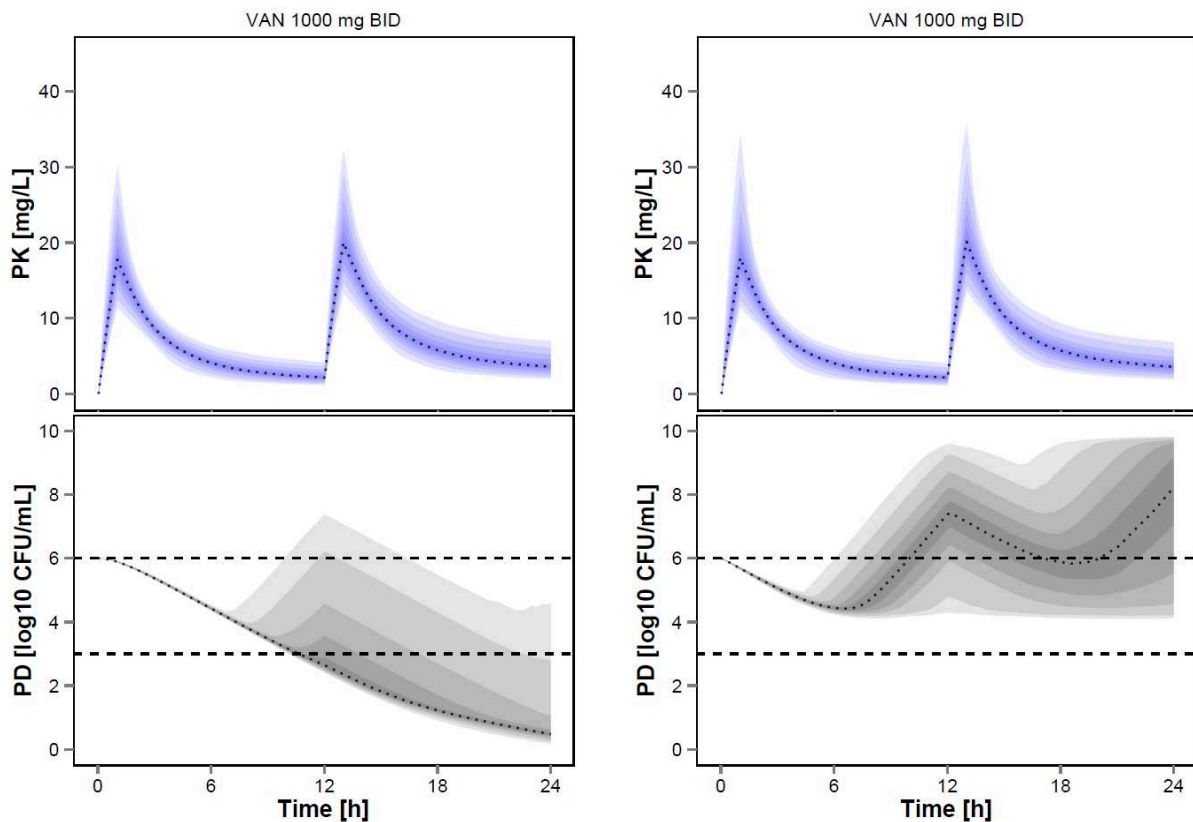
Figure 50: PK/PD for lag- (left) and log-phase (right) *S. aureus* against VAN 1000 mg BID; for further details refer to caption of Figure 46.
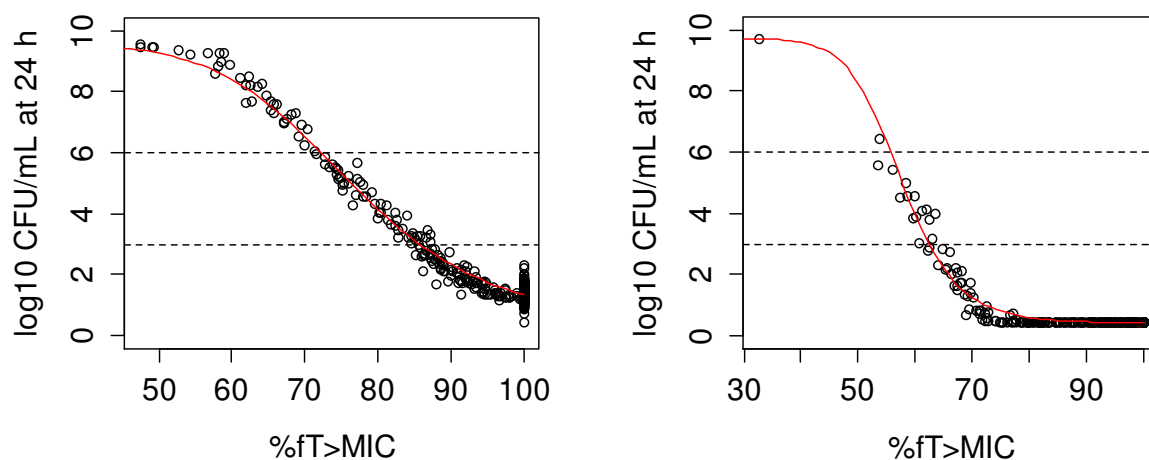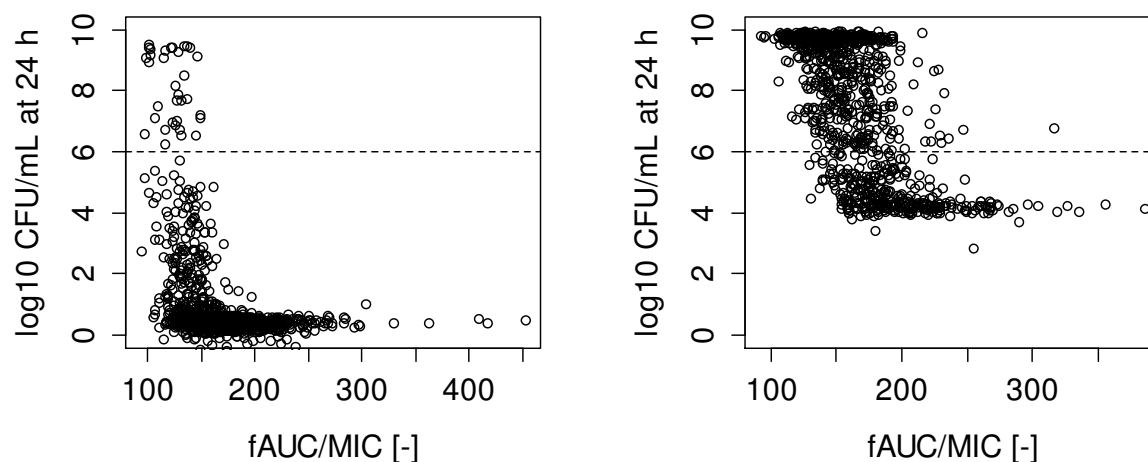
Figure 51: PK/PD index *f*AUC/MIC for VAN in lag- (left) and log-phase *S. aureus* (right) derived from the clinical trial simulation with VAN 1000 mg BID.

For combinations of standard dosing regimens of LZD and MER or VAN and MER, solely the lag-phase scenarios were evaluated (Figure 52) as the semi-mechanistic PD model for log-phase *S. aureus* was not built upon combinatory regimens.

The combination of LZD 600 mg BID with MER 1000 mg TID stimulated a bacteriostatic effect to a median bacterial load of 4.8 log10 CFU/mL after 24 h (90% PI: 4.6-5.0 log10 CFU/mL), being inferior to the effect of MER 1000 mg TID alone after 24 h (median: 1.4 log10 CFU/mL; 90% PI: 1.1-5.2 log10 CFU/mL), but slightly superior compared to LZD 600 mg BID alone after 24 h (median 5.4 log10 CFU/mL, 90% PI: 5.1-6.1 log10 CFU/mL).

The combination of VAN 1000 mg BID with MER 1000 mg TID resulted in a bactericidal effect at 24 h, as observed with both antibiotics individually. However, the combinatory regimen reduced the observed inter-individual variability of the antibacterial effects observed with the single antibiotic regimens (Figure 46 and Figure 50) and a bacterial load of 1.2 log10 CFU/mL (90% PI: 1.1-1.5 log10 CFU/mL) was attained at 24 h. Due to the BID / TID administration, the PD variability was considerably low in both scenarios as drug concentrations of either combination partner exceeded its EC_{50}.
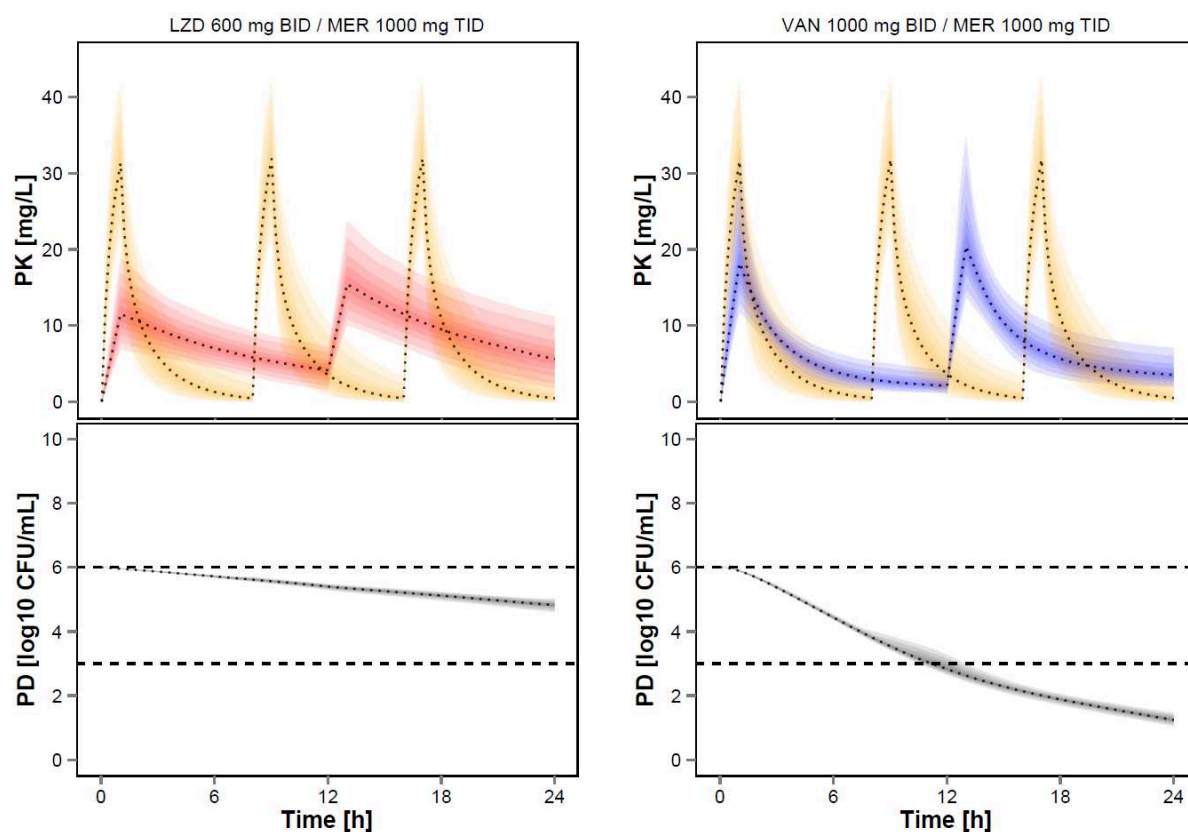
Figure 52: PK/PD for lag-phase *S. aureus* against a combination of LZD 600 mg BID (red) with MER 1000 mg TID (yellow) (left) and VAN 1000 mg BID (blue) with MER 1000 mg TID (right); for further details refer to caption of Figure 46.

3.3.2.2.2   Impact of covariates on the antibiotic effect.

For assessment of the PD influence of the PK covariates, the covariate of interest was varied while the other covariates were set to their 'standard' value of 75 kg for WT, 120 mL/min for CLCR and no liver cirrhosis. The impact of the covariates on the antibiotic effect is presented as log10 CFU/mL at 24 h vs. the value of the respective covariate, e.g. CLCR in Figure 53. The distribution of the effect is presented in percentiles, i.e. shaded areas e.g. in Figure 53 and the PTA to attain a bacteriostatic of bactericidal effect is given as number within the plot.

Meropenem. The impact of CLCR on the effect of the standard dosing regimen 1000 mg TID and also the low-dose standard regimen of 500 mg TID for MER is presented in Figure 53.
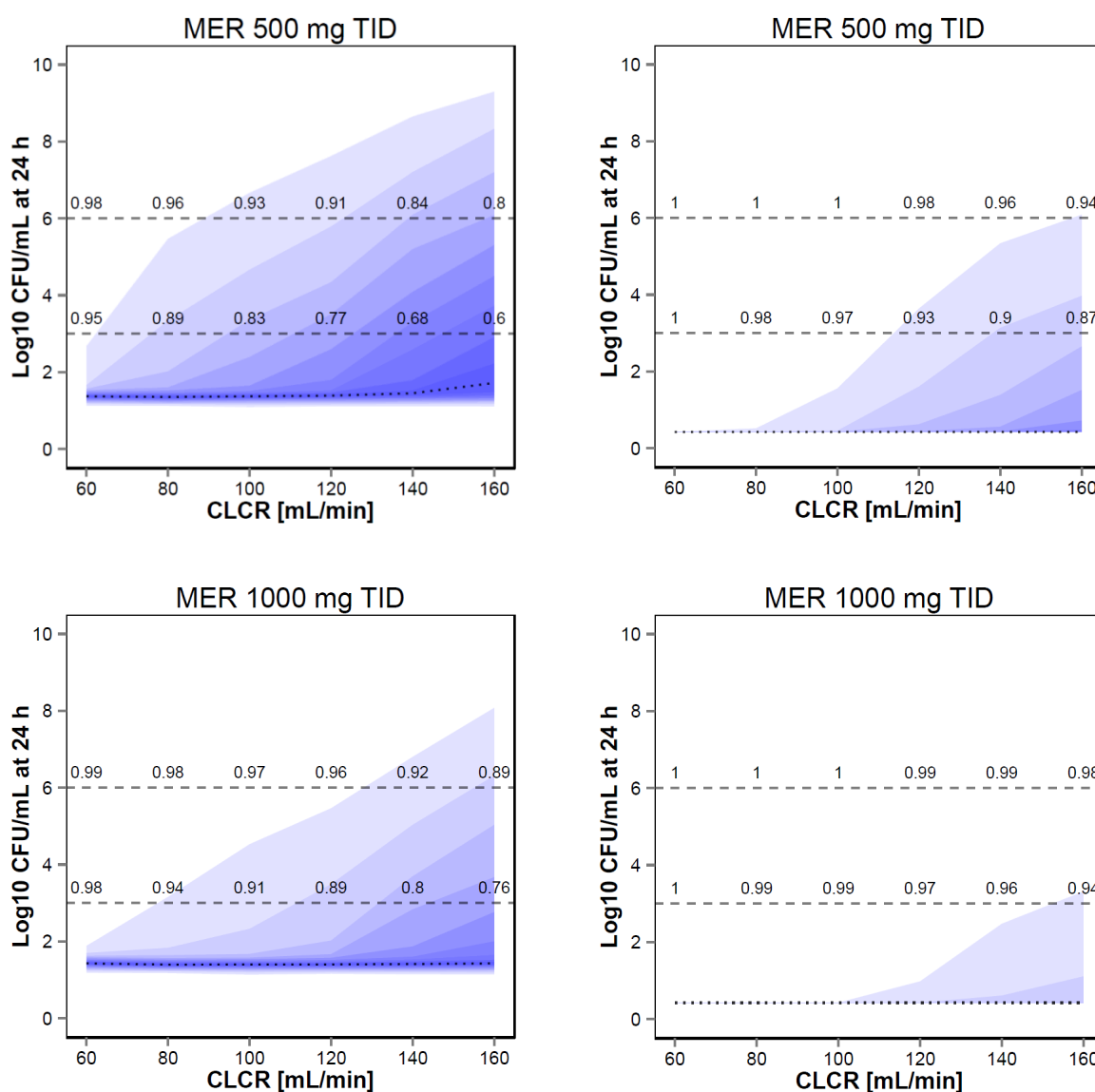
Figure 53: Impact of CLCR on the effect of the standard regimens MER 500 mg TID (upper panel) and MER 1000 mg TID (lower panel) for lag- (left) and log-phase *S. aureus* (right), dashed horizontal lines at 6 log10 CFU/mL represent inoculum and bacteriostatic effect, dashed horizontal line at 3 log10 CFU/mL represents bacteriostatic effect, number indicates PTA to attain the bacteriostatic of bactericidal effect, median prediction is given by the dotted line and variability is illustrated by shaded areas as 5th to 95th percentile in 5-percentile steps.

In lag-phase *S. aureus*, for MER 500 TID, the bacteriostatic target was reliably achieved for CLCR ≤120 mL/min. For supraphysiological, higher CLCR up to 160 mL/min, the bacteriostatic PTA decreased to 80%. A reliable bactericidal effect was achieved for CLCR <80 mL/min. MER 1000 mg TID shifted the sufficiently high PTA to higher CLCR and a bacteriostatic effect was achieved for CLCR ≤140 mL/min and a bactericidal effect was achieved for CLCR ≤100 mL/min. As MER was more active against log-phase *S. aureus*, a high bactericidal PTA of 87% was achieved up to CLCR of

160 mL/min. For WT from 60 to 105 kg (Figure 54), a trend to lower PTA was seen for lower WT for MER 500 mg TID, which originates from lower MER peak exposure at higher WT and thus slower adaption of *S. aureus* to the effect of MER. Yet, overall PTA varied only marginally within ca. 10% absolute difference and was hence not further explored.

Figure 54: Impact of WT on the effect of the standard regimen MER 500 mg TID for lag- (left) and log-phase *S. aureus* (right). Refer to Figure 53 for explanation of the illustration.

The alternative regimen of continuous infusion of 1500 mg MER over 24 h (Figure 55) was superior over the regimens with short-term infusion and provided sufficient PTA up to CLCR of 160 mL/min.

Figure 55: Impact of CLCR on the effect of the alternative regimen MER 1500 mg as continuous infusion over one day for lag- (left) and log-phase *S. aureus* (right). Refer to Figure 53 for explanation of the illustration.

Linezolid. The bacteriostatic PTA was sufficient for LZD 600 mg BID for CLCR ≤120 mL/min for both lag- and log-phase *S. aureus* when no liver cirrhosis was assumed (upper panel Figure 56). For higher values of CLCR up to 160 mL/min, PTA was still high (79% for lag- and 86% for log-phase *S. aureus*). In presence of liver cirrhosis, the baceriostatic PTA was higher and ≥96%, even for CLCR of 160 mL/min (lower panel Figure 56). The standard dosing regimen did not stimulate an appreciable bactericidal effect in any of the scenarios (bactericidal PTA ≤5%).

Higher WT was corellated with slightly lower bacteriostatic PTA for log-phase *S. aureus*, but even for a subpopulation with 105 kg, a high PTA of 85% was observed.
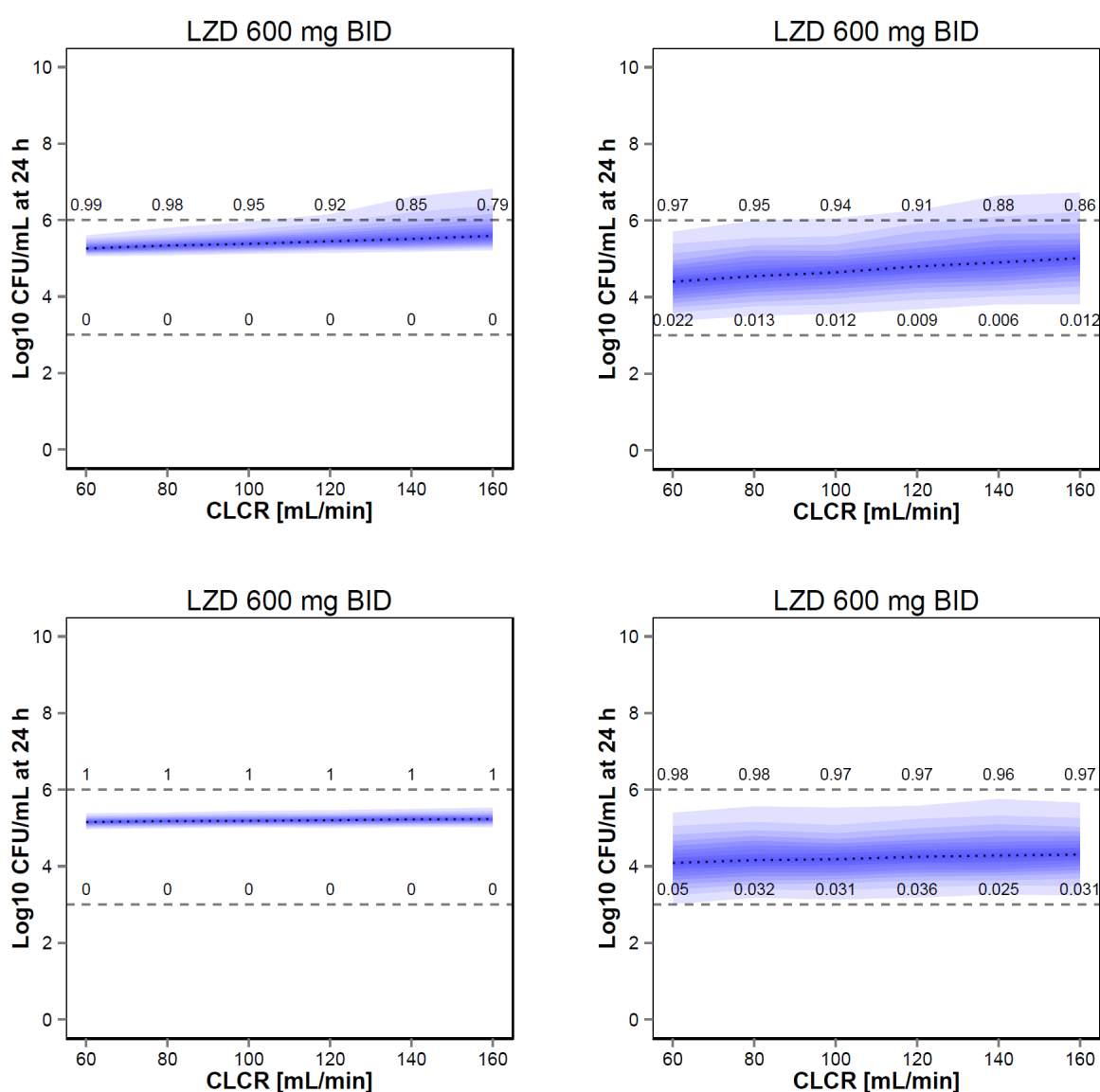
Figure 56: Impact of CLCR on the effect of the standard regimen LZD 600 mg BID for a patient population without (upper panel) and with liver cirrhosis (lower panel) for lag- (left) and log-phase *S. aureus* (right). Refer to Figure 53 for explanation of the illustration.
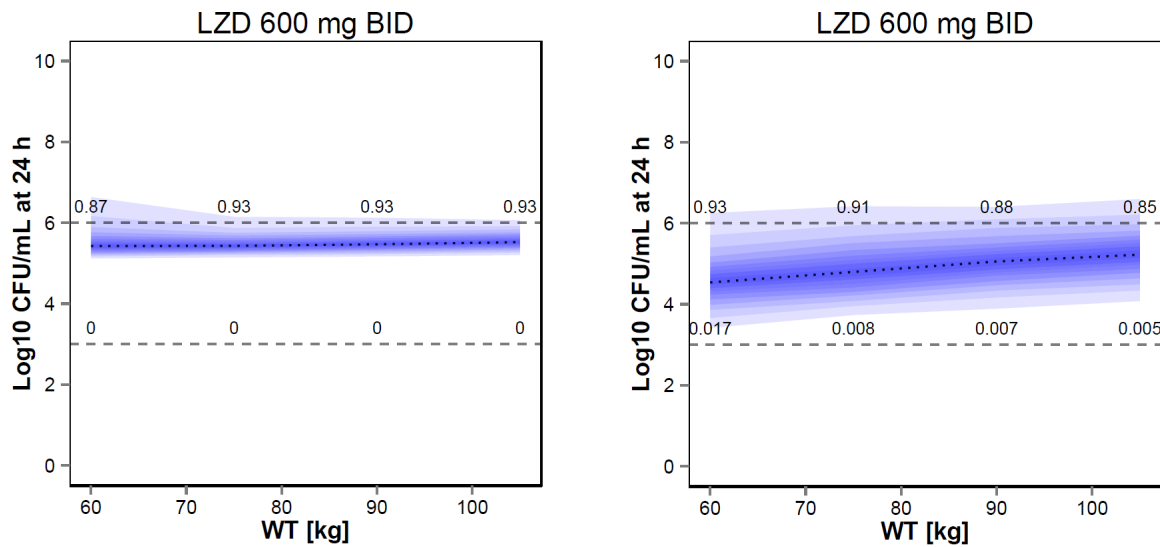
Figure 57: Impact of WT on the effect of the standard regimen LZD 600 mg BID for a patient population without liver cirrhosis for lag- (left) and log-phase *S. aureus* (right). Refer to Figure 53 for explanation of the illustration.

For the alternative dosing regimens, solely the impact of CLCR is presented as the simulations with WT provided qualitatively similar results. The alternative dosing regimen of 1200 mg LZD applied as continuous infusion over 24 h was inferior compared to the standard regimen (Figure 58): The bacteriostatic PTA ranged from 62% to 83% in lag- and from 13% to 29% in log-phase *S. aureus,* respectively.
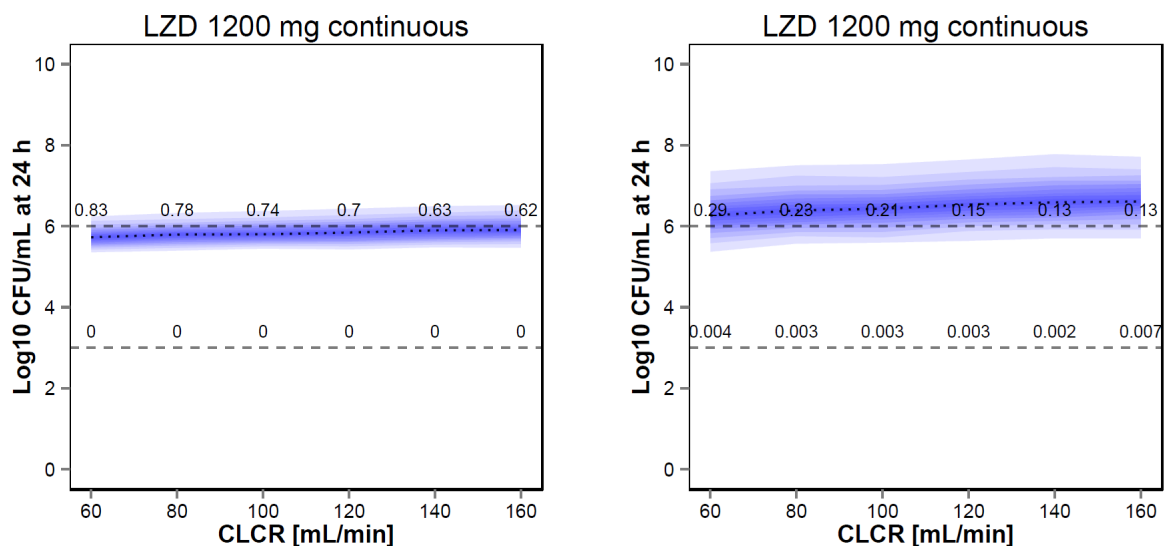
Figure 58: Impact of CLCR on the effect of the alternative regimen LZD 1200 mg as continuous infusion over 24 h for a patient population without liver cirrhosis for lag- (left) and log-phase *S. aureus* (right). Refer to Figure 53 for explanation of the illustration.

Two alternative LZD regimens with intensified dosing, LZD 600 mg TID as 1 h infusion and 'front-loaded' LZD 1200 mg followed by 600 mg q 12 h, are all presented in Figure 59. Whilst both intensified regimens increased the bacteriostatic PTA, the 'front-loading' regimen overall reduced the bacterial load to a higher extent than LZD 600 mg TID which even resulted in a bactericidal effect for a minor portion of the virtual patients for log-phase *S. aureus*.
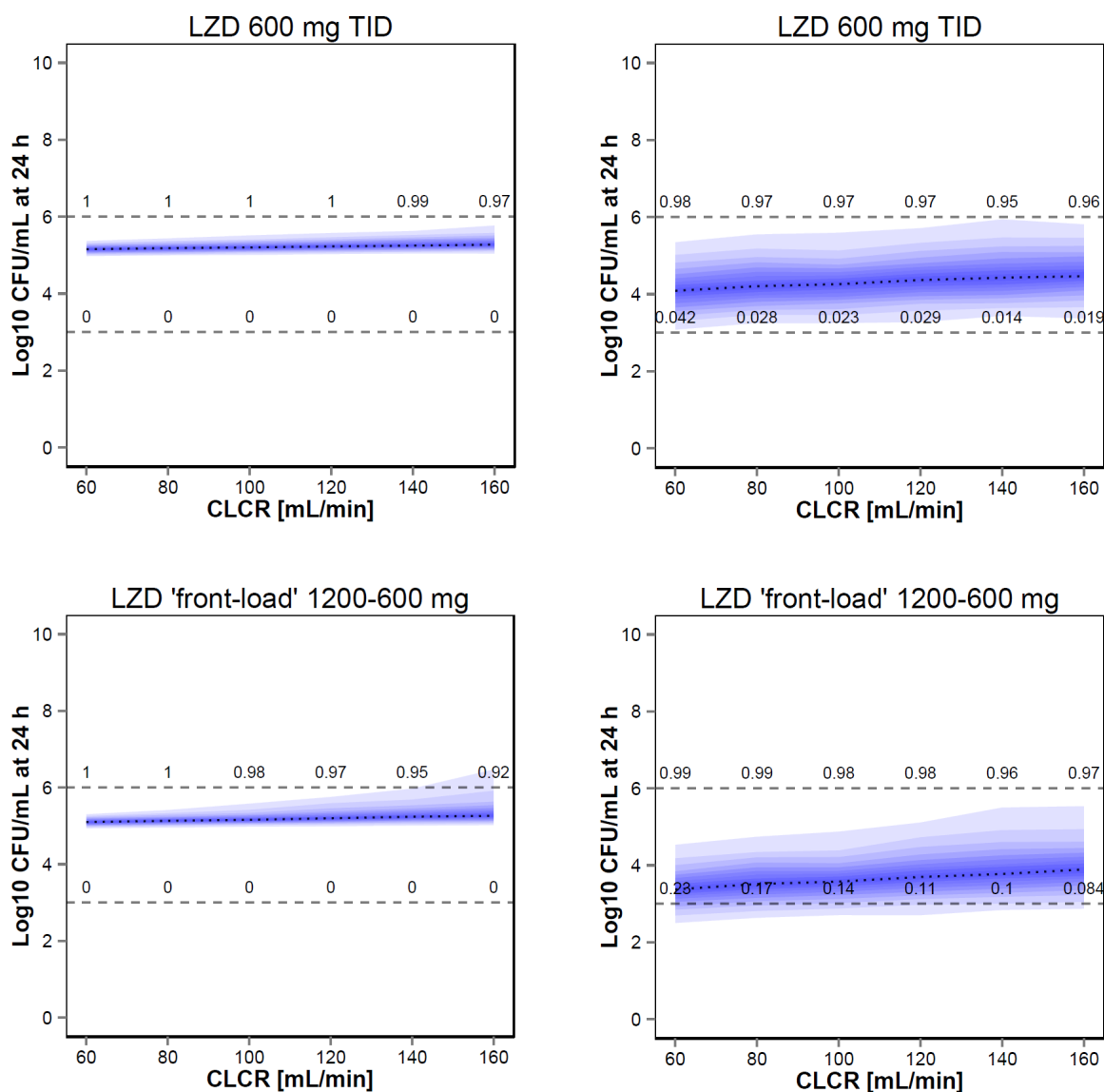
Figure 59: Impact of CLCR on the effect of the alternative regimens LZD 600 mg TID (upper panel) and 'front-loaded' LZD 1200 followed by 600 mg q 12 h (lower panel) for a patient population without liver cirrhosis for lag- (left) and log-phase *S. aureus* (right). Refer to Figure 53 for explanation of the illustration.

Vancomycin. Extensive differences between lag- and log-phase *S. aureus* were observed for the standard dosing regimen VAN 1000 mg BID (Figure 60). For lag-phase *S. aureus*, a sufficient bacteriostatic or bactericidal PTA was observed for CLCR ≤120 or ≤100 mL/min, respectively. Conversely, for log-phase *S. aureus*, no sufficient bacteriostatic PTA was attained even for the lowest CLCR of 60 mL/min (PTA: 81%).
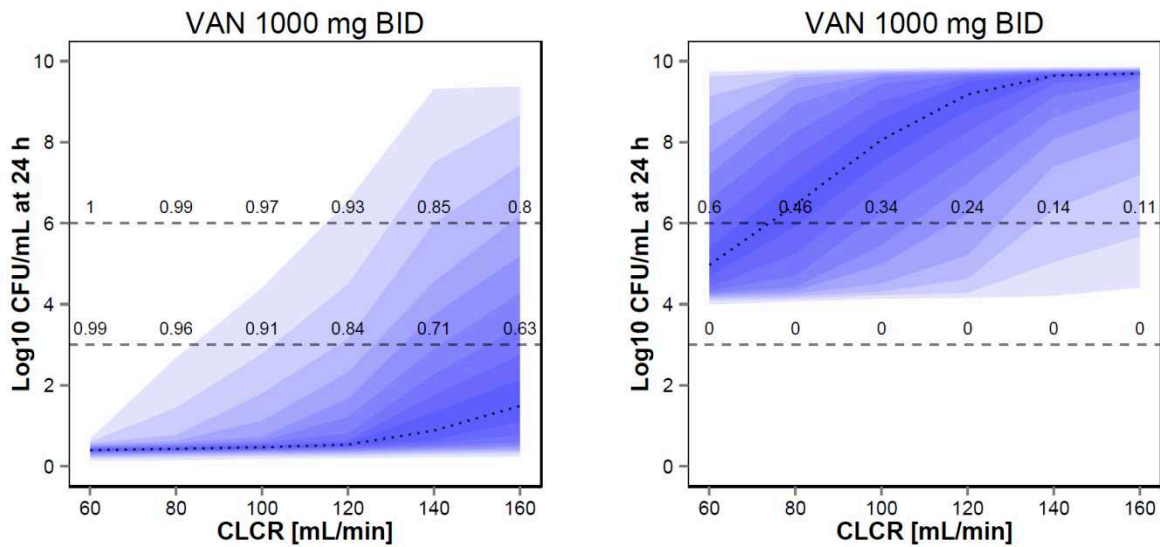
Figure 60: Impact of CLCR on the effect of the standard regimen VAN 1000 mg BID for lag- (left) and log-phase *S. aureus* (right). Refer to Figure 53 for explanation of the illustration.

PTA decreased with increasing WT for both lag- and log-phase *S. aureus*, being less influential than CLCR (Figure 61).
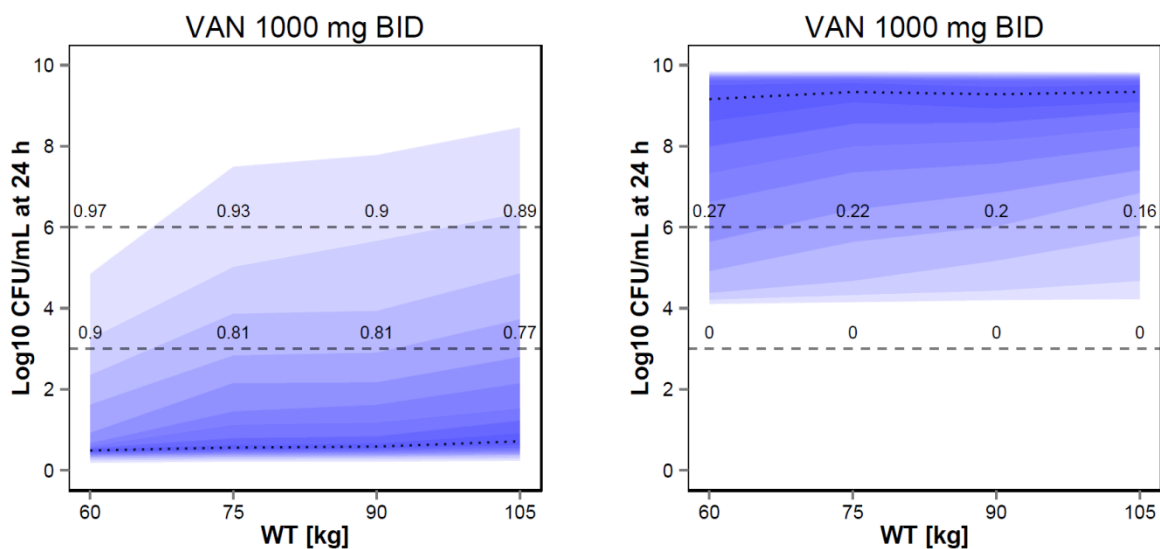
Figure 61: Impact of WT on the effect of the standard regimen VAN 1000 mg BID for lag- (left) and log-phase *S. aureus* (right). Refer to Figure 53 for explanation of the illustration.

The alternative regimens with similar total daily doses, but decreased dosing interval, i.e. VAN 500 mg four times daily (QID) or continuous infusion (VAN 2000 mg over 24 h) are presented in Figure 62 and Figure 63: For lag-phase *S. aureus*, VAN 500 mg QID resulted in overall higher PTAs being sufficient for a bactericidal effect up to a CLCR of 140 mL/min. For log-phase *S. aureus*, a sufficient bacteriostatic PTA was attained up to CLCR of ca. 80 mL/min. No bactericidal effect was attained for log-phase *S. aureus*. WT did not influence 500 mg QID dosing of VAN.

Continuous infusion of 2000 mg VAN over 24 h resulted in a sufficient bactericidal effect for lag-phase and a sufficient bacteriostatic effect for log-phase *S. aureus* for CLCR up to 160 mL/min. WT did not influence continuous infusion of VAN 2000 mg.
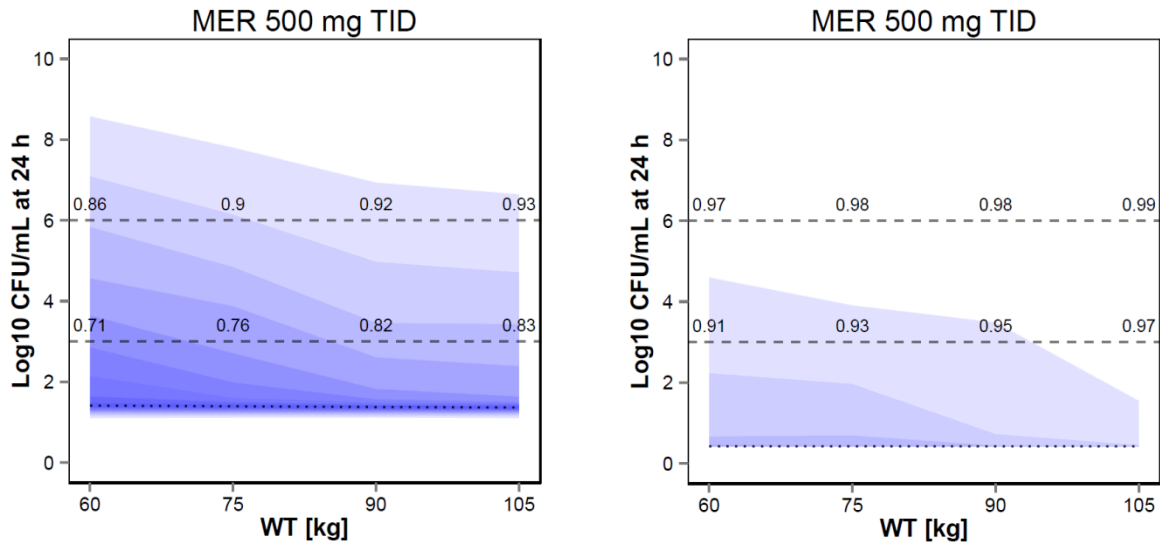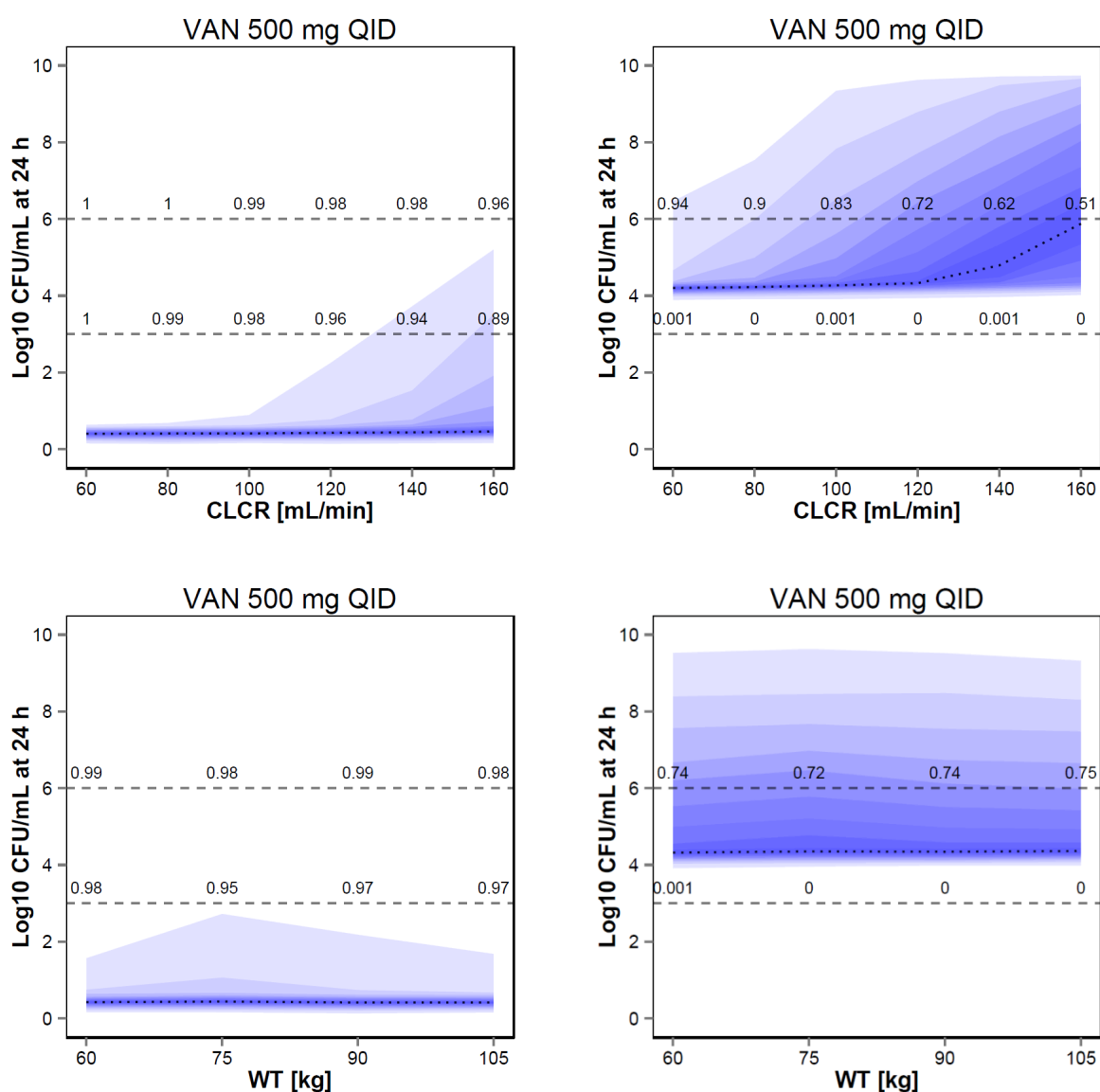
Figure 62: Impact of CLCR and WT on the effect of the alternative regimens VAN 500 mg QID for lag- (left) and log-phase *S. aureus* (right). Refer to Figure 53 for explanation of the illustration.
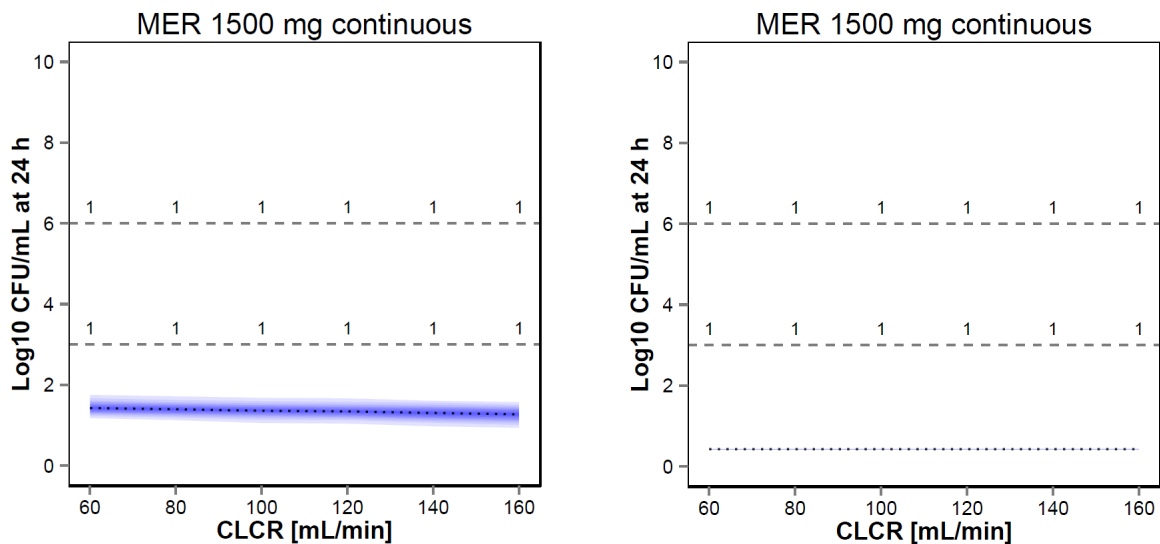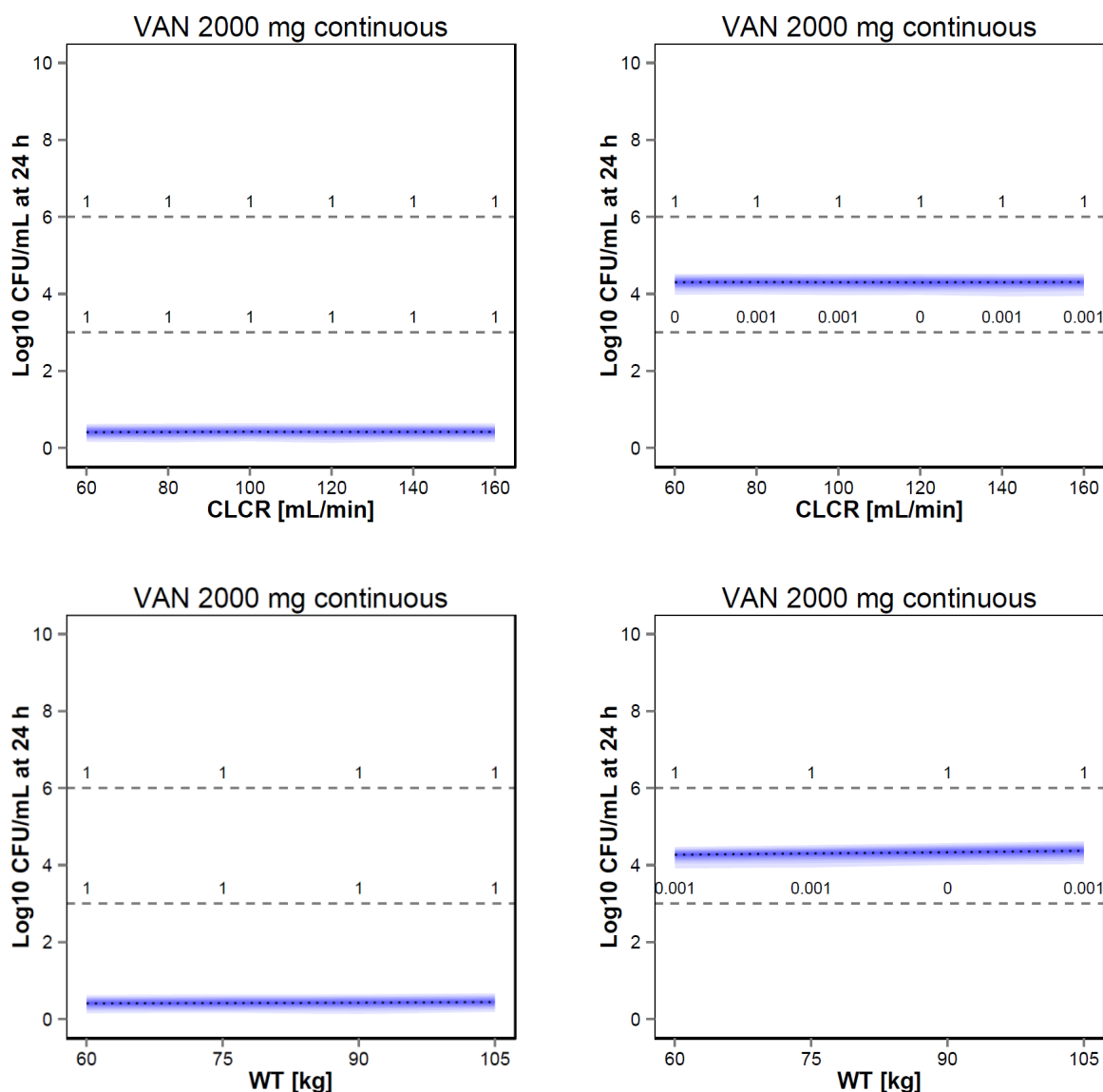
Figure 63: Impact of CLCR and WT on the effect of the alternative regimens VAN 2000 mg as continuous infusion over 24 h for lag- (left) and log-phase *S. aureus* (right). Refer to Figure 53 for explanation of the illustration.

WT-adjusted dosing for VAN (15 mg/kg BID) inverted the observed influence of WT on the effect of VAN (Figure 64), and for lag-phase *S. aureus*, a sufficient bactericidal PTA was observed for WT ≥75 kg and for CLCR ≤120 mL/min. This inversion, i.e. a higher PTA for higher WT originates from WT-driven increase of the peripheral volume of distribution, which outbeats the WT-driven increase of the central volume of distribution leading to a more shallow decline of the PK profile with higher WT. For log-phase *S. aureus*, no sufficient PTA for any WT and CLR was observed (Figure 65).
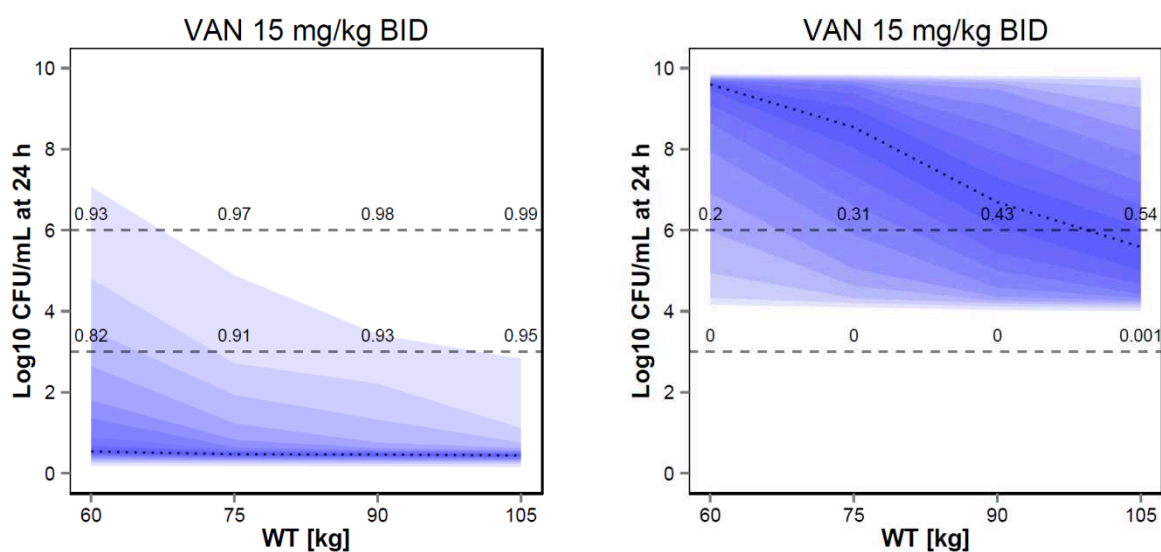
Figure 64: Impact of WT on the effect of the body weight adjusted dosing regimen VAN 15 mg/kg BID for lag- (left) and log-phase *S. aureus* (right). Refer to Figure 53 for explanation of the illustration.
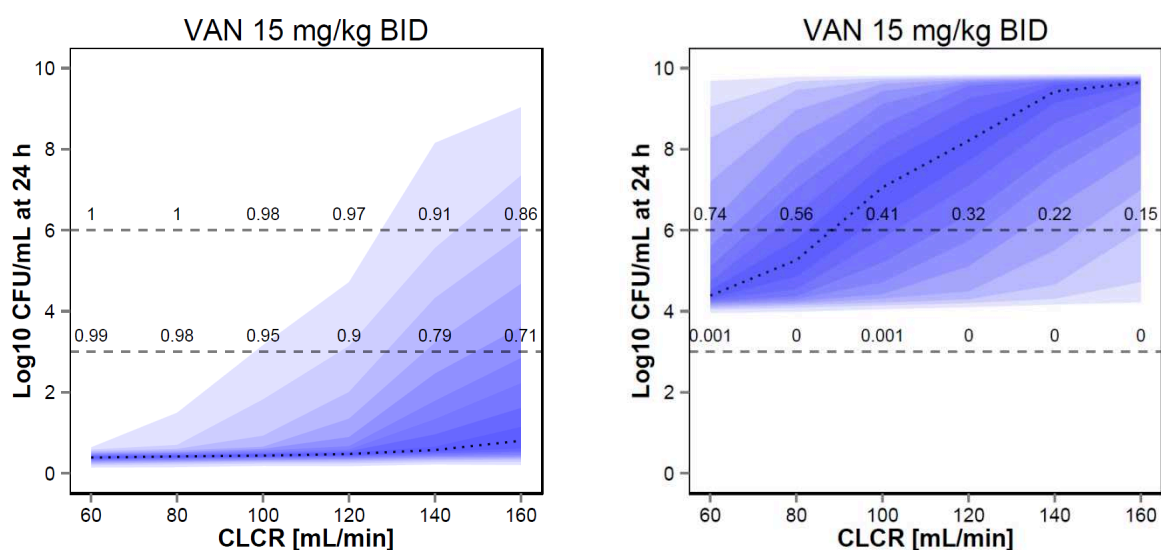
Figure 65: Impact of CLCR on the effect of the body weight adjusted dosing regimen VAN 15 mg/kg BID for lag- (left) and log-phase *S. aureus* (right). Refer to Figure 53 for explanation of the illustration.

WT-adjusted dosing for VAN with a loading dose (25 - 15 mg/kg) led to a sufficient bactericidal PTA for lag-phase *S. aureus* for all investigated WT's and for CLCR ≤160 mL/min. Insufficient PTA for any WT was observed for log-phase *S. aureus* and the higher dose did only result in a sufficient bacteriostatic PTA for CLCR ≤60 mL/min (Figure 66 and Figure 67).
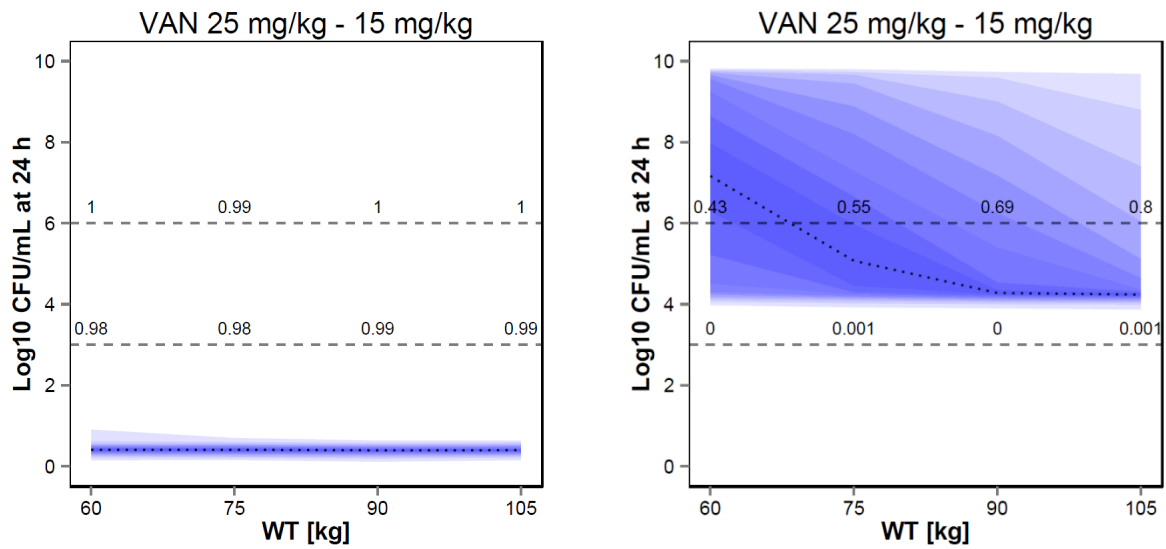
Figure 66: Impact of WT on the effect of the body weight adjusted dosing regimen with a loading dose of VAN 25 mg/kg followed by VAN 15 mg/kg for lag- (left) and log-phase *S. aureus* (right). Refer to Figure 53 for explanation of the illustration.
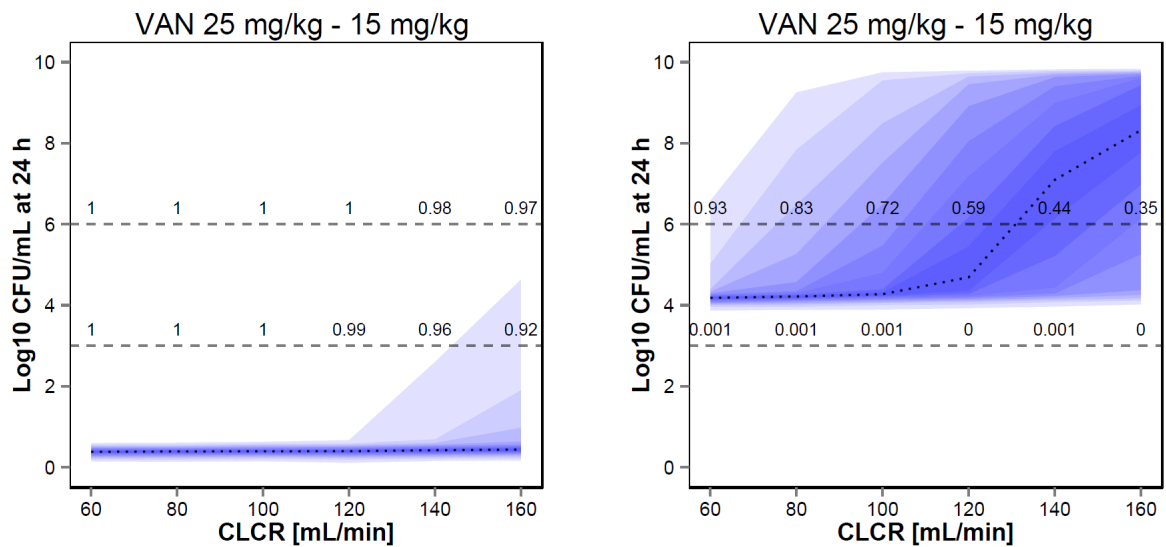
Figure 67: Impact of CLCR on the effect of the body weight adjusted dosing regimen with a loading dose of VAN 25 mg/kg followed by VAN 15 mg/kg for lag- (left) and log-phase *S. aureus* (right). Refer to Figure 53 for explanation of the illustration.

WT-adjusted dosing for VAN with a higher loading dose (30 - 15 mg/kg) led to a sufficient bactericidal PTA for lag-phase *S. aureus* for all investigated WT's and for CLCR ≤160 mL/min (Figure 68 and Figure 69). For log-phase *S. aureus,* no sufficient PTA for any WT was observed, but

PTA was considerably higher (0.55-0.85) than for VAN 15 mg/kg BID without a loading dose (0.2-0.54). The higher loading dose did result in a sufficient bacteriostatic PTA for CLCR ≤80 mL/min.
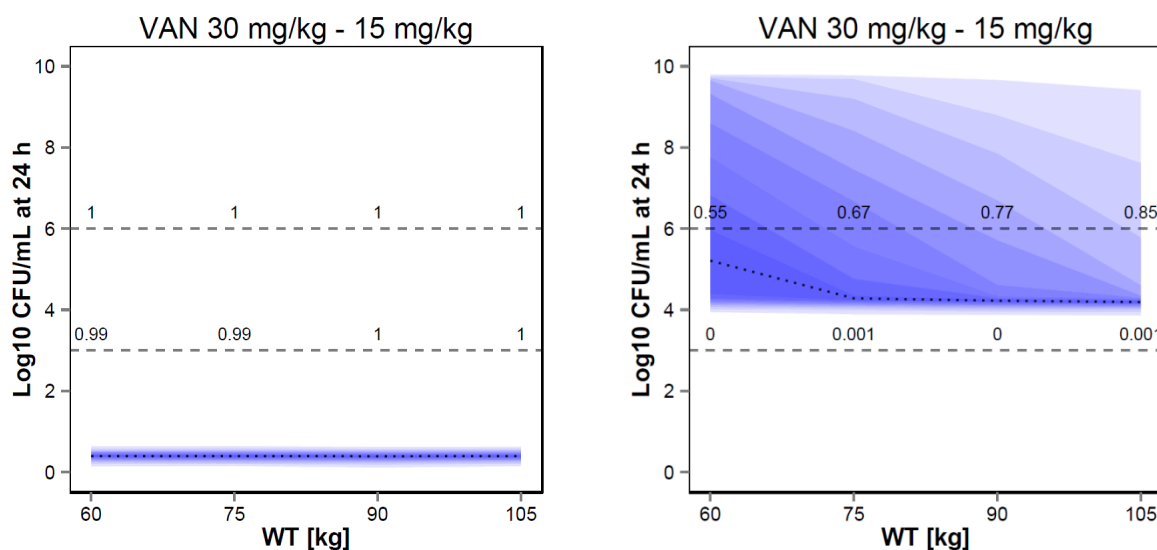
Figure 68: Impact of WT on the effect of WT adjusted dosing regimen with a loading dose of VAN 30 mg/kg followed by VAN 15 mg/kg for lag- (left) and log-phase *S. aureus* (right). Refer to Figure 53 for explanation of the illustration.
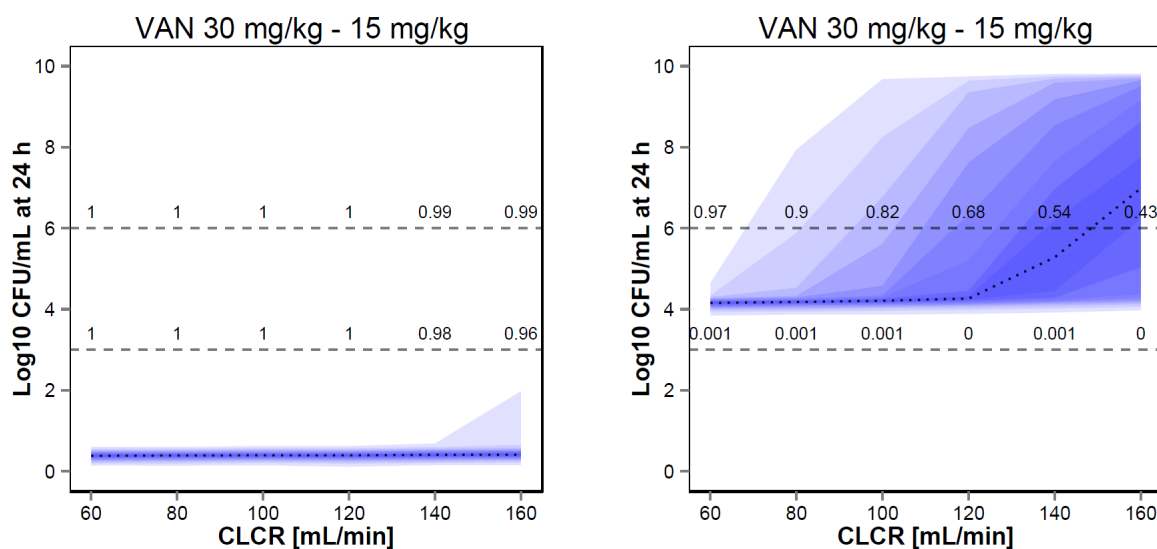
Figure 69: Impact of CLCR on the effect of the body weight adjusted dosing regimen with a loading dose of VAN 30 mg/kg followed by VAN 15 mg/kg for lag- (left) and log-phase *S. aureus* (right). Refer to Figure 53 for explanation of the illustration.

4 Discussion

In the following section, the utilised and developed methods, as well as the generated results are critically discussed and compared to current knowledge from scientific literature.

4.1 Bioanalytical quantification of antibiotics in growth medium

In the present thesis, a bioanalytical HPLC assay was developed and validated (3.1) according to the EMA guideline for bioanalytical method development [120] that allows for reliable, simultaneous quantification of LZD, MER and VAN in the bacterial growth medium CaMHB. The assay was developed mainly for two purposes: (i) quality control of the antibiotics concentration in the *in vitro* infection model, and (ii) assessment of the potential degradation profile of the utilised antibiotics. To the author's knowledge, the present work describes the first HPLC assay that provides simultaneous quantification of the three utilised antibiotics in bacterial growth medium.

Sample treatment. The developed sample treatment method using sample+MeOH (1+4) with subsequent solvent evaporation and reconstitution in water reliably precipitated the matrix constituents in CaMHB and prevented column clogging as indicated by no increase of pump pressure over time. The obtained recoveries by this processing method were reproducible and ranged from 69% to 72%, which is close to the maximum possible value of 80% in this case due to the 1+4 dilution of the sample and removal of the supernatant. Hence, 'dilution-corrected' recovery values were 86-90% for all analytes.

For MER, recovery was higher if MeOH was used for protein precipitation instead of ACN (69% vs. 38%), which was also found by Kipper and colleagues who precipitated plasma samples with MeOH (1+1) [166]. Yet, precipitation with ACN has been used for MER in published HPLC assays for simultaneous quantification of beta-lactam antibiotics, but their resulting assay was ten times less sensitive with LLOQ values of 5 mg/L [167,168] than the assay of the present work (MER LLOQ of 0.5 mg/L). Solid phase extraction as alternative for separation of proteins and other matrix residues has been proposed for MER by Ohmori et al [169], which resulted in a slightly lower LLOQ of 0.1 mg/L compared to the present work, but might also have been the result of the utilised tandem mass spectrometry detection.

For LZD, both protein precipitation with ACN and MeOH provided reasonable recoveries during sample treatment. The obtained result of 76% ('dilution-corrected': 95%) for ACN + sample (4+1) is in line with previous findings for MHB described by Scheerans (96.6%) [31]. Ba et al used an online extraction method for MHB that generated slightly lower recoveries (88.0% - 93.3%) [170]. Higher analytical recoveries have been observed for other matrices such as plasma and microdialysate (108.9%) [93], which might have contributed to their slightly lower LLOQ of 0.2 mg/L for LZD compared to 0.5 mg/L in the present work.

For VAN, recovery was 71% for precipitation with MeOH and only 0.8% when using ACN. Contrarily, Hagihara et al found high recoveries of VAN from mouse serum, ranging from 85.1% - 90.8% also for ACN [171], but their method had a lower ACN content (200 µL sample + 50 µL internal standard + 500 µL ACN). As the developed gradient method increased the organic ACN content to a considerable amount (up to 37.5% v/v) and also contained 0.1% TFA, a higher organic content of 4+1 was chosen for sample treatment to avoid potential protein precipitation during elution on the HPLC column. The LLOQ for VAN was set to 2 mg/L to provide reliable quantification [120] in presence of some baseline noise from matrix residues. Hence, the LLOQ of the present work was higher compared to published methods for the matrices human plasma (1 mg/L [171,172]) or brochoalveolar lavage fluid (0.1 mg/L [171]).

In total, for simultaneous determination of LZD, MER and VAN in CaMHB, sample preparation was best if 4 aliquots of MeOH were used as precipitating agent for one aliquot of sample.

HPLC instrument method. Isocratic elution methods for LZD [93,170,173] were used as starting point for development of a potential isocratic method for simultaneous quantification of LZD, MER and VAN. Addition of 0.1% TFA was assessed to acidify the mobile phase to provide reproducible retention of MER on a C-18 column [166–169]. The resulting isocratic mobile phases were highly sensitive to changes of the organic content in the mobile phase with respect to retention time of MER and not further elaborated. Instead, the developed gradient was highly reproducible and provided simultaneous determination of MER, LZD and VAN in a reasonable time of 15 min. The utilised Accucore® C-18 HPLC column allowed for the use of considerably low injection volumes of 2 µL, which minimised the required sample volume from the *in vitro* infection model and permitted several injections of the sample. Published assays for MER, LZD and VAN required an order of magnitude higher injection volumes of 20 µL [167–169,174], 40 µL [166] or even 50 µL [172,173].

Degradation of the antibiotics in the *in vitro* infection model. The application of the developed HPLC assay to monitoring drug concentrations over time revealed markedly different stability profiles for the investigated antibiotics MER, LZD and VAN. LZD displayed a favourable stability profile and did not degrade under the experimental conditions of the *in vitro* infection model. This is in agreement with previous results for MHB from Scheerans [31,121] and Schmidt [30] or under yet more stressed conditions (LZD in aqueous solution at 70° C for 48 h) described by Raju and co-workers [175] who also found no significant degradation of LZD.

For VAN, minor degradation to 90.6% of the initial concentration was observed within 24 h which is still considered stable by the EMA guideline [120]. However, due to the accurate and precise HPLC assay with intraday precision between 1.9% and 7.4% CV in the relevant concentration range for VAN, degradation was found significant as indicated by the non-zero-overlapping CI of the first-order degradation rate constant estimated for VAN. Stratton and Weeks used a less sensitive bioassay and

reported VAN to be within ±10% of the initial value in CaMHB and human serum at 37° C after 24 h [176]. Hence, albeit minor, degradation of VAN was considered in the semi-mechanistic PD model.

For MER, significant and substantial degradation to 62.9% of the initial concentration was observed within 24 h at 37° C in CaMHB. There is evidence in the literature that degradation might be even more pronounced at higher concentrations of MER than those used in the present work: Lemaire and colleagues found degradation to 50% of the initial concentration of 50 mg/L at 37° C in broth after 24 h [177]. Viane and co-workers assessed the stability of MER in concentrated solutions for intravenous infusion and monitored a decrease by up to 70% from an initial concentration of 64 g/L at 37° C within 24 h[178]. Hence, the observed substantial degradation of MER in CaMHB was in the magnitude of one MIC tier and could potentially drive a regrowth pattern after initial killing in time-kill curve studies. Notably, this knowledge was not considered when the regrowth pattern of *P. aeruginosa* under static MER exposure was described with mathematical PK/PD modelling by Tam and colleagues [143]. Katsube and co-workers also neglected degradation of MER when modelling the PK/PD relationship of MER in a dynamic *in vitro* infection model, although they claimed that deviation of predicted and actually observed mimicked PK profiles was within 20% without providing evidence for that [179]. In summary, the developed, validated HPLC assay of the present thesis was useful to reliably determine the actual concentrations of the antibiotic over time in the present *in vitro* experiments, which might be of high value also for studies in dynamic *in vitro* infection models [22] to measure if the anticipated PK profiles were in fact obtained.

4.2   Microbiological experiments

4.2.1   Preliminary microbiological experiments

Droplet plate assay for quantification of *S. aureus*. To provide a quantitative basis for the pharmacodynamic evaluation of single and combined drug effects, a quantification assay for *S. aureus* was established (3.2.1.1) based on the 'droplet plate' technique [32] that was adapted to the local requirements and environment. Evaluation showed that the assay was accurate and had a precision ranging from 30.1% CV for 20 CFU/sector to 1.7% for 500 CFU/sector. The developed assay was resource saving compared to a previously established quantification method at the Department of Clinical Pharmacy and Biochemistry for both *S. aureus* [31] and *E. faecium* [122]: Whilst previously a 100 µL bacterial sample was spread over the surface of an entire agar plate with a 'Drigalski' plate spreader, the agar plate was divided into four sectors for spot inoculation with the newly developed droplet plate assay reducing the consumption of agar plates to 25%. Moreover, biohazard waste was reduced by 90% using a downscaled dilution procedure in 48 well plates (1 mL vs. 10 mL per dilution step [31,122]). The measure CFU was chosen as a surrogate for the number of viable bacteria. It has to be noted that one CFU does not necessarily originate from a unique bacterium. In particular, *S. aureus*

tends to form bunches similar to grapes that might eventually form a CFU [110]. Nonetheless, CFU assays are the most frequently used method for quantification of viable bacteria [22]. Other methods to quantify viable bacteria include measuring phosphatase activity with a fluorescence-based assay [23], intracellular ATP measured by a bioluminescence assay [24] or polymerase chain reaction (PCR)-based RNA profiling [180,181]. Of those, one method used calibration functions to approximate CFU/mL [23]. Some of those methods have been solely used to monitor growth kinetics [23,180], but not for monitoring bacterial viability under antibiotic exposure, as performed in the present work. Hence their usefulness for this purpose needs to be investigated in further studies. Another very common method to count bacteria utilises the 'Thoma cell counting chamber' that requires manual, visual cell counting in a defined volume through a microscope [25]: However, the correlation of bacterial cells/mL with CFU/mL was not convincing for bacterial killing, as shown by Hanberger and co-workers who assessed the post-antibiotic effect of imipenem against *E. coli* with different counting techniques [24]. In studies from our laboratory, Goebgen investigated the use of a coulter counter to count bacteria as particles in particle-free bacterial growth media [182]: Whilst the correlation between CFU/mL and counts/mL could be established for resting and growing cultures, quantification of a killing culture did not succeed, possibly due to the contribution of dead cells or cell debris to the count measure. Hence, because of no convincing alternative the established droplet plate assay belonging to the family of CFU assays represents a robust and comparable measurement method for viable bacteria, but at cost of being more labour-intense than other methods [23,24,180,182].

Minimal inhibitory concentration. The MIC values for the investigated study drugs (3.2.1.2) were determined according to the CLSI guideline [12]. As the utilised *S. aureus* ATCC 29213 strain is a widely used reference strain, the determined MIC values could be compared to reference values published by the CLSI for quality control [18]: The determined MIC values in the CaMHB from Oxoid® of 0.125 mg/L for MER (reference 0.03-0.125 mg/L), 2 mg/L for LZD (reference: 1-4 mg/L) and 1 mg/L for VAN (reference: 0.5-2 mg/L) all laid within the acceptable ranges proposed by the CLSI. The MIC values for the two clinical isolates of *S. aureus* were in the typical range for MSSA for MER [79] and were found susceptible to both LZD [183] and VAN [184]. Regarding the quality control criteria of the CLSI [18], there is a considerable acceptance range of distribution mode - 50%/+100% (± 1 MIC tier). This large uncertainty of the MIC originates from several factors influencing the determined MIC value: (i) The MIC is determined visually; it is certainly subjective to the experimentalist to identify turbidity. (ii) Bacterial growth and killing is inherently continuous in both time and magnitude e.g. as seen in any time-kill curve generated within this thesis. The MIC neglects this time-dependency, as it is allowed to be read within 16 to 20 h [12]. Yet, the MIC only snapshots this time span once and the choice of the precise time point of this snapshot might influence the result. (iii) The incubation temperature is allowed to vary between 35±2° C, which might influence the growth rate and hence also the antibacterial effect of replication-dependent antibiotics. (iv) The

choice of the growth medium might also have an influence: As seen in the present work, the MIC of MER read in the checkerboard experiment using a CaMHB from Sigma-Aldrich® was 0.0625 mg/L whilst the MIC was 0.125 mg/L for the CaMHB from Oxoid®.

Moreover, the MIC converts the continuous antibacterial effect into a binary variable, i.e. turbidity indicates growth whilst clear growth medium indicates inhibition of growth. To explore the effect beyond the turbidity threshold of ca. 10^7 CFU/mL, the minimum bactericidal concentration (MBC) is sometimes assessed [185], but this concept neither considers the concentration-dependency of the effect between MIC and MBC, nor does it provide a continuous effect measure itself. Despite these shortcomings, the MIC has been found useful as 'scaling factor' for assessing the attainment of predefined PK/PD targets that have been found predictive for antibacterial growth suppression or killing in clinical practice, but does not contain enough information for quantitative research as continuous effect description or for mechanistic PK/PD modelling [19].

Determination of the lag-time of *S. aureus*. The lag-times (3.2.1.3), i.e. the time period to attain exponential growth ranged between 86 and 102 min for the three investigated *S. aureus* strains. This indicated, that – under the present conditions – a pre-incubation period of 2 h is sufficient to ensure that *S. aureus* was growing exponentially, i.e. was in the 'log-phase' of bacterial growth. Yet, the lag-time may depend on several factors. For instance, it can be speculated that the growth medium composition of the agar plates from which the colonies are harvested, the incubation time of the plate-culture, but also the liquid growth medium and the precise incubation temperature can affect the lag-time. Therefore, determination of the lag-time under the local experimental environment is crucial to ascertain exponential growth, if this is warranted in the specific experimental setting.

4.2.2 Checkerboard studies

To investigate the effect of antibiotics in combination, the concept of the MIC was extended in 'checkerboard' experiments: The commonly used two-dimensional checkerboard array is constructed using the antibiotics in two-fold dilutions centred on their individual MIC. The 'outer' rows, i.e. left and bottom of that array represent the respective single drug MIC experiments whilst the 'inner' area of this array contains the drug combinations [33]. A positive or negative interaction between the antibiotics is conventionally indicated if the combined MIC is lower or higher than the single drug MIC values. These combined MIC values are then used to calculate FIC indices (1.3.1.3) [33] for decision-making using the concept of Loewe additivity [54]. This conventional checkerboard approach shares the limitation of assessing the effect as binary and imprecise measure with the MIC: Turbidity-based checkerboard studies have been criticised regarding their reproducibility [35], which led to stricter FIC thresholds for antagonism or synergy to prevent 'fine-scale' decisions using the conventional checkerboard [34]. To further complicate matters, the FIC calculation is not standardised leading to qualitatively different results depending on the chosen method as described by Bonapace

and colleagues [33]. Ultimately, the FIC approach assumes a monotonic interaction, i.e. only one single type of interaction and only concentrations around the MIC and not in the entire clinically relevant concentration range is assessed.

The checkerboard experiments in the present work (3.2.2) underline the limitations of the 'conventional' checkerboard method when only turbidity was used as evaluation criterion. The turbidity threshold ($>10^7$ CFU/mL) was insensitive to detect the antagonistic interaction between LZD and MER at inhibitory concentrations, possibly a reason why the interaction had not been detected in a large study applying this technique [186]. It has to be acknowledged that calculation of a precise FIC index for LZD and MER was not possible with the present checkerboard data as the aim was to elucidate the entire clinically relevant concentration range of the study drugs and not solely concentrations around the MIC, which led to partly larger than two-fold increments in the concentration tiers.

In contrast to the conventional turbidity-based checkerboard, the 'dynamic checkerboard' with quantification of bacteria provided a continuous effect measure and allowed for a more detailed exploration of the interaction between MER and LZD. Although the dynamic checkerboard was exploited in detail using modelling and simulation techniques which will be discussed later, the antagonism between LZD and MER was apparent already from the raw, unprocessed dataset: The antagonistic effect of LZD seemed to be present if LZD concentrations exceeded its MIC as indicated by the darker shading in the colour gradient in the upper right part in Figure 16, but did not stimulate a bacterial load that is visible as turbidity. Hence, the bactericidal effect of MER was antagonised at inhibitory LZD, but at subinhibitory concentrations no obvious interaction could be detected from the raw data. Hence, the 'dynamic' checkerboard with quantification of bacteria in combination with modelling and simulation techniques, as applied in the present work, was a powerful tool for screening and hypotheses generation with a reasonable compromise between workload and knowledge gain. Yet, despite all its limitation, the conventional turbidity-based checkerboard is still much more frequently used than the dynamic technique with quantification of bacteria: Surprisingly 10/59 publications related to the search term "synergy" in the renowned Journal of Antimicrobial Chemotherapy in 2013[1] *solely* relied on turbidity-based checkerboard methods for decision making [187–196].

4.2.3   Time-kill curve studies of single antibiotics

The time and magnitude domain of the antibacterial effects of MER, LZD and VAN were elucidated by time-kill curve studies (3.2.3 and 3.2.4). Firstly, the single drug effects of the investigated antibiotics in both investigated growth phases will be discussed.

---

[1] Search keyword: „synergy", year: 2013, http://jac.oxfordjournals.org/search, accessed at 26.3.2015.

Discussion

Meropenem. For MER, a persistent bactericidal effect was obtained for the scenarios with 0.25 mg/L for both lag- and log-phase *S. aureus*. Regrowth after initial killing was observed up to MER at 0.125 mg/L for both investigated growth phases. The effect of MER was slightly more rapid against log-phase bacteria, i.e. immediate killing was observed for MER ≥0.5 mg/L, whilst for lag-phase *S. aureus*, minor growth was observed within the first hour of exposure even at the highest studied concentration of 8 mg/L. A possible explanation for this observation might be the mechanism of action of MER: As a beta-lactam antibiotic, MER interferes with cross-linking of peptidoglycan chains by inhibition of transpeptidase enzymes, leading to instabilities in the bacterial cell wall [77]. Potentially a combination of this weakened cell wall and stimulation of autolysins by the beta-lactam cause lysis of the bacterium [77]. As those processes require active metabolism and replication [197,198], MER-mediated killing of lag-phase bacteria might start once they enter the log-phase after 1.5 h. Moreover, the observed paradoxically reduced effect of MER at 'higher' concentrations (≥2 mg/L) was much more pronounced for lag-phase *S. aureus* (Figure 70 left). This paradoxical effect was in general first described for penicillin by Eagle and Musselman already in 1948 [164], and later also for cephalosporins [199] and carbapenems [198] against Gram-positive bacteria. It has been speculated that high concentrations of the antibiotic inhibit protein synthesis to a degree that the replication-dependent effect is decreased leading to the 'Eagle-effect' [21,200]. Fontana and co-workers found a decreased level of one autolysin in *E. faecalis* when exposed to higher concentrations of penicillin [201]. Yet, the pharmacological origin of the 'Eagle-effect' remains to be elucidated. The author is not aware of a study that showed differences in this paradoxical effect depending on the growth phase of the bacterium at drug exposure. One study that investigated both lag- and log-phase for MER did not include high enough concentrations and hence did not observe this phenomenon [202].

Linezolid. For LZD, the shape of the time-kill curves was similar between both growth phases up to concentrations of 4 mg/L and a bacteriostatic effect was obtained. For lag-phase *S. aureus*, the antibacterial effect only slightly increased with higher concentrations and remained bacteriostatic whilst for log-phase *S. aureus*, a bactericidal effect was observed after 24 h at 32 mg/L (Figure 70 middle). Moreover, biphasic killing was observed for log-phase *S. aureus*: After an initially intense killing phase up to 4 h, slower killing comparable to the lag-phase scenario was observed for the scenarios with 8 and 32 mg/L. Apparently, log-phase bacteria were much more susceptible to LZD at higher concentrations. A speculative explanation for this can be given in LZDs mechanism of action: In the log-phase, more bacteria are replicating; LZD acts as protein-synthesis inhibitor and inhibits the formation of the initiation complex of the ribosomal subunits [85]. If this vital metabolic component is fully inhibited (at higher concentrations) at crucial steps during replication, this might lead to cell death and only bacteria that are in a growth phase, in which all vital proteins for replication have already been synthesised, survive. The surviving bacteria manage to substantially decrease their metabolic activity, leading to a growth-arrested *S. aureus* that is much less susceptible towards the

128

effect of LZD. As lag-phase *S. aureus* has a much slower initial replication rate, LZD does not 'hit' a large number of bacteria at critical, vital stages of the replication cycle and *S. aureus* has more 'time' to enter the growth-arrested state, leading to considerably slow killing. Published studies on the effect of LZD on *S. aureus* ATCC 29213 [28,31,87,203] and other MSSA [29] or MRSA strains [29,30] cluster depending on the pre-incubation time (and thus the resulting growth phase) before addition of LZD into the culture flask. Investigators that either did not pre-incubate [27], pre-incubated for 30 min [28] or 1 h [29] found a bacteriostatic effect with a reduction of ca. 1 log10 CFU/mL at maximum, whilst investigators that pre-incubated for 2 h [30,31] or explicitly used log-phase *S. aureus* [203,204] determined a maximum reduction of 1.9-3.8 log10 CFU/mL depending on the concentration studied. Maximum LZD concentrations of the cited articles were covered by the present experiments and inocula were similar to our study, providing evidence for the validity of this comparison. Interestingly, none of the investigators mentions the contradictory maximum effects in their works.

Vancomycin. For VAN, the most striking and counter-intuitive findings were observed between both growth-phases of *S. aureus*. For lag-phase *S. aureus*, 5 log-fold bactericidal killing was observed for VAN ≥2 mg/L at 24 h. Conversely, for log-phase *S. aureus*, no bactericidal effect was observed at all and even at the highest VAN concentration of 16 mg/L, a tendency for regrowth was observed (Figure 70 right). The observation is counter-intuitive as (i) it is often observed that antibiotics kill replicating bacteria more intensely [77] and (ii) VAN in particular has its target in the cell wall, exerting a replication-dependent effect [26]. Although the initial slopes of the time-kill curves of VAN were similar in both growth-phases, it seemed that log-phase *S. aureus* had more efficient mechanisms to efficiently evade from the effect of VAN. Experimental reasons can be ruled out as the result was obtained in several replicates on different days with similar precision comparable to the other studies. Yet, in case of VAN, it was more difficult to 'externally evaluate' the present results than for the other investigated drugs: Several investigators [97,176,205,206] reported to have examined the effect of VAN on log-phase cultures of *S. aureus*. Yet, three of the four cited results rather follow the killing pattern of the present lag-phase experiments [176,205,206]. Löwdin prepared the inoculum for the time-kill curve study by pre-incubating *S. aureus* for 6 h with subsequent dilution to $5 \cdot 10^5$ CFU/mL [205]. Lim followed a similar procedure and reported a pre-incubation period of 4-6 h [206]. In two papers, no details on the preparation of the log-phase inocula are reported [97,176]. Hence, at least for Löwdin's and Lim's experiments, it can be concluded that their inoculum might represent late log-phase or already early stationary phase cultures compared to the (early) log-phase culture in the present study. Solely the results from Small and Chambers [97] are similar to the present study, but they only investigated VAN at four times the MIC, used clinical isolates of *S. aureus* and utilised a higher inoculum of 10^7 CFU/mL, making a direct comparison difficult. Hence, to the author's knowledge, the drastically reduced effect of VAN in (early) log-phase generated by a pre-incubation period of 2 h compared to lag-phase *S. aureus* is not known yet.
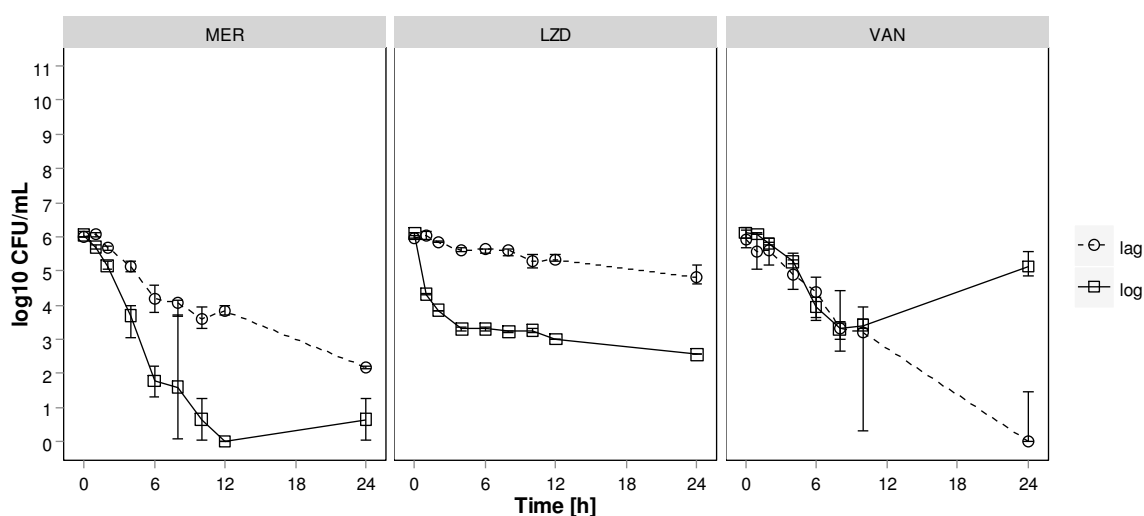
Figure 70: Time-kill curves at the highest concentration studied for MER at 8 mg/L (left), LZD at 32 mg/L (middle) and VAN at 16 mg/L (right) in lag- and log-phase *S. aureus*.

4.2.4 Time-kill curve studies of dual combinations

Linezolid and Meropenem. For the combination of LZD and MER, the time-kill curve studies in lag-phase *S. aureus* displayed that the effect of MER in combination with inhibitory concentrations of LZD was antagonised and corresponded to the maximum effect of LZD over the entire interval of 24 h. This is in agreement with the dynamic checkerboard studies of the present work, but adds insight about the kinetics of the interaction. For lag-phase *S. aureus*, the antagonism was also found in the confirmatory studies with the two clinical isolates of *S. aureus*. MER, as a cell-wall antibiotic, exerts its effect against actively replicating bacteria. As a protein-synthesis inhibitor, LZD might growth-arrest the bacteria and thus could preclude the effect of MER. This mechanism of interaction has been described for several other antibiotics of the respective drug classes [146–148], but, to the author's knowledge, this is the first time for LZD in combination with a beta-lactam against MSSA. Moreover, MSSA does *not at all* exhibit the same interaction pattern as MRSA, for which synergy between the carbapenem antibiotics imipenem and ertapenem combined with LZD was described both *in vitro* and in animal models [37,38]. The latter is, of course, an interesting, but rather unrepresentative finding for the majority of *S. aureus* isolates in Germany and the EU, which are MSSA [117]. Also, with other antibiotics and pathogens, antagonism was prevalent for combinations with LZD: It has been observed that LZD attenuated the effect of penicillin in time-kill curve studies against two clinical isolates of *S. pyogenes* within the first 8 h [207]; however, the interaction after 24 h was much less significant than against *S. aureus* in the present experiments. Furthermore, LZD, although inactive against Gram-negative bacteria, even attenuated the effects of aztreonam and ceftazidime against *E. coli* [208]. The authors hypothesised that LZD was able to permeate through the Gram-negative cell wall due to the cell-wall disrupting effect of the beta-lactam, leading to growth-arrest which in turn attenuated the

beta-lactam effect [208]. For the studies with log-phase *S. aureus*, the combined effect of LZD and MER was even inferior to the effect of LZD alone, which was indicative for a reciprocal suppressive antagonistic effect [209] between LZD and MER. Certainly, more research is crucial to elucidate the precise molecular mechanism of this suppressive effect of the combination.

Vancomycin and Meropenem. For the combination of VAN and MER, detailed time-kill curve studies with different inhibitory concentrations of VAN and MER in lag-phase *S. aureus* revealed that the combinations were bactericidal after 24 h as were both individual agents alone. However, the killing kinetics was 'dominated' by the effect of VAN, as the early bactericidal effect (4-6 h) of MER alone at 'optimal', maximally effective concentrations (e.g. 0.25 mg/L) was antagonised and the combined effect corresponded to the effect of VAN. For lag-phase *S. aureus*, this killing pattern with a combined effect corresponding to the effect of VAN was also found in the confirmatory studies with the two clinical isolates of MSSA. MER acts at a later stage in cell-wall synthesis than VAN, which might explain how VAN could have precluded the effect of MER: VAN interrupts cell-wall synthesis by complex formation with the peptidoglycan precursors. Hence, the effect of MER that is inhibition of the enzyme transpeptidase that attaches the newly synthesised peptidoglycan to the existing cell wall, could have been precluded, as the substrate of this enzyme was complexated by VAN [76]. The slower killing rate of the combination might also result from inhibition of the autolytic system of *S. aureus* by VAN [210]. Yet, as the killing kinetics of MER at higher concentrations was similar to VAN due to the 'Eagle-effect', no difference was seen for those scenarios and the clinical relevance of this 'antagonism' is potentially questionable. For studies with subinhibitory concentrations, the combinatory effect was frequently superior to the effect of both agents alone, but sound distinction between additivity and synergy is difficult from unprocessed time-kill curve data and interpretation and discussion will be given later (4.3.2). For log-phase *S. aureus*, the combined effect was also limited to the effect of VAN alone. However, MER suppressed the substantial regrowth of *S. aureus* under VAN exposure in the combinatory scenarios.

4.2.5   Impact of the growth phase at drug exposure on the antibacterial effect

The differences between the obtained time-kill curves depending on the growth phase at drug exposure had already been mentioned above. Yet, some further general statements on this aspect of the present thesis have to be made. It is well known that the size of the inoculum negatively correlates with the *in vitro* antibacterial effect of many antibiotics – a phenomenon referred to as the 'inoculum effect' [21]. The present work goes beyond the inoculum size and points to the importance of considering the growth phase of this inoculum: The growth phase was highly influential on the obtained time-kill curves for LZD, MER and VAN, even though the inoculum size was standardised to 10^6 CFU/mL in the present work. As discussed above, time-kill curve studies are not (yet) standardised with respect to the growth phase at drug exposure as indicated by the variety of methods for inoculum preparation

found in the cited literature above. The present results also challenge the suggested inoculum preparation methods of the respective CLSI guideline for susceptibility testing that can be used interchangeably for many organisms [12]: The guideline describes two methods which are (i) the "Direct colony suspension method" and (ii) the "Growth method". Method (i) is very similar to the procedure of preparing the lag-phase inoculum in the present work. For method (ii), some colonies of the bacterium are picked from an agar plate and incubated for 2-6 h, until a turbidity equivalent to McF 0.5 is attained, and then diluted to the relevant inoculum size. Depending on the medium, bacteria might then be in (late) log-phase or early stationary phase. It has to be acknowledged that the guideline was mainly developed for MIC testing which might be less susceptible to the effect of the growth state, but researchers should be wary when adopting this guideline to perform time-kill curve studies. Ultimately, it has to be noted that the lag-phase does not represent a surrogate for the stationary phase. For instance, for MER [202,211] or VAN [212], a diluted stationary culture was used to study the respective drug effects explicitly in the *stationary phase* of growth. However, this diluted stationary culture rather represents a lag-phase culture, as bacteria can re-enter log-phase. In 'true' stationary phase at higher bacterial loads, e.g. for MER, bacteria replicate much slower and much less rapid killing is observed [213] than in the diluted stationary cultures [202,211].

4.2.6   Adaptive resistance studies

Adaptive resistance studies (3.2.5) were performed in lag-phase *S. aureus*. For MER and VAN, regrowth after initial killing was observed up to 1x MIC, i.e. at 0.125 mg/L and 1.0 mg/L, respectively. Both VAN and MER lost effectiveness over 24 h: Adapted *S. aureus* showed direct growth at re-exposure to 1x MIC of MER and only modest killing with substantial regrowth at 2x MIC. For VAN, also 2x MIC was ineffective against adapted *S. aureus* and VAN at 4x MIC was required for killing without regrowth. Often, only, and if at all, the MIC is tested after adaption; in the present work, a 'second' time-kill curve study was performed with the adapted bacteria. Hence, the obtained results provided an excellent basis for external evaluation of the adaption submodel of the developed semi-mechanistic PD model, which will be discussed later (4.3.3). Future studies should focus on the impact of the growth phase at drug exposure on the adaption process, which might be particularly interesting for VAN. Moreover, quantification of subpopulations with different susceptibility to the antibiotic could be performed by the use of agar-plates containing antibiotic [122,214]. This could provide insight into the time course of the development of resistant subpopulations, but was not the focus of the present work. In addition, future studies could aim at the quantification of bacterial subpopulations based on their phenotypical colony properties, e.g. colony size, colour and time to appearance on the agar plate, as observed with small colony variants [31,215]. This could contribute to the understanding of the processes that bacteria undergo when exposed to antibiotics.

4.3 Modelling

4.3.1 Empiric modelling of individual drug effects

In empiric modelling, summary PD measures from the dynamic checkerboard and time-kill curve studies were used for deriving concentrations-effect relationships for the individual antibiotics (2.4.1.3.1). The single drug experiments from the dynamic checkerboard study were directly suitable for empiric analysis as they represent a single effect measure per drug concentration. For empiric modelling of the antibacterial effects observed in time-kill curves studies, a summary PD measures had to be utilised as effect measure to characterise the concentration-effect relationships of the antibiotics by a sigmoidal maximum effect model. In the present thesis, the area between growth and time-kill curve, the 'intensity of the antibacterial effect' *IE* as introduced by Firsov and colleagues [48] was used. As this area reflects the entire effect-time course, it was considered superior to other summary effect measures as e.g. the initial slope of the time-kill curve [49], the time until nadir bacterial load [50] or simply the bacterial load at the end of the time-kill curve [51,52].

The empiric modelling approach provided easy interpretable parameters for efficacy (*Emax*), potency (*EC$_{50}$*) and steepness of the concentration-effect relationship (*H*) for LZD, MER and VAN in both the checkerboard and time-kill curve studies. Moreover, it allowed for facile comparison of the different effects in the studied growth phases.

At first, the result from the checkerboard shall be related to the lag-phase time-kill curve studies with *S. aureus* due to the similar growth state of the inoculum: When comparing the *EC$_{50}$* values, it has to be noted that the *EC$_{50}$* values of the checkerboard depended on the chosen time point (20 h in present thesis), while the area-based summary PD measure in time-kill curve studies captured the entire time course. For instance, a higher *EC$_{50}$* value of 2.19 mg/L was observed in the checkerboard for LZD compared to 1.55 mg/L for the lag-phase time-kill curve study. Subinhibitory LZD had an effect on *S. aureus* by substantially delaying the exponential growth and hence was considered in the *IE*. Yet, as the time-kill curves of such scenarios had already adapted to the GC curve at 20 h and those early effects of LZD were not detectable in the checkerboard, higher *EC$_{50}$* value were obtained in the checkerboard. Due to their different nature, the values for *Emax* cannot be directly related.

When comparing the parameters of lag- and log-phase experiments for the time-kill curve studies, a significantly higher *EC$_{50}$* value for LZD was observed for log-phase *S. aureus.* This can be attributed to the similarities in the killing kinetics between both scenarios up to LZD of 4 mg/L and the fact that for LZD ≥8 mg/L killing could be enhanced for log- but not for lag-phase *S. aureus*. A trend towards higher log-phase *EC$_{50}$* values was also seen for MER and VAN, but the 95% confidence intervals were overlapping. *Emax* values in the log-phase for MER (196 vs. 148 log10 CFU/mL·h) and LZD (166 vs. 96 log10 CFU/mL·h) provided a quantitative measure for the already qualitatively discussed higher effect of both antibiotics against log-phase *S. aureus*. It has to be noted that the area-based effect

measure and hence also *Emax* itself is difficult to interpret, e.g. due to the log-transformation of the bacterial load. Moreover, the *IE* is not informative about the slope of the time-kill curve. Various time-kill curve profiles can lead to very similar area values for the *IE*. Yet, a scenario with a monotonously decreasing time-kill curve might be more favourable compared to a profile with rapid killing followed by rapid bacterial regrowth, if both profiles had the same *IE*. This is also reflected in the analysis of VAN. The value for *Emax* was lower in log-phase *S. aureus* (126 vs. 154 log10 CFU/mL·h). However, the drastically different killing pattern for VAN with regrowth up to 1 mg/L in lag-phase and up to 16 mg/L in log-phase *S. aureus*, which can be considered much less favourable, cannot be expressed in this summary measure. Furthermore, no mechanistic aspects that might lead to deviations from the sigmoidal concentration-effect course [47] is included in this basic analysis. Hence, although it might not be suitable to draw direct clinical conclusions from the parameters obtained from the area-based approach *IE*, it still represents a single measurement quantifying the entire antibiotic effect. This measurement can be useful to compare the magnitude of the antibiotic effect and allows for performing a response surface analysis to quantify the nature of potential drug interactions.

4.3.2   Response surface analysis

To elucidate the nature of the drug interactions, the previously discussed single drug concentration-effect relationships based on checkerboard or summary PD measures for the time-kill curve studies were utilised to compute the anticipated combined additive antibacterial effects (3.3.1.2). As combinations of two antibiotics were studied in the present thesis, the resulting additive response surface resulted in a three dimensional 'heat-map' with the drug concentrations of both antibiotics on the x- and y-axis and the effect measure on the z-axis. The difference between the anticipated additive and the observed response was calculated to assess deviation from additivity: Positive deviation (i.e. an effect greater than anticipated additive effect in reducing CFU/mL) indicated synergy whilst negative deviation (i.e. a smaller effect than anticipated additive effect) indicated antagonism [138]. A response surface approach is not necessarily limited to combinations of two antibiotics as demonstrated by Prichard and co-workers, who have also applied this method to triple drug combinations [216]. The two commonly utilised additivity criteria are 'Loewe Additivity' [54] and 'Bliss Independence' [55] which will be briefly discussed:

Loewe additivity. For 'Loewe Additivity', it is assumed that two agents exert their effect on the same target (or different indistinguishable targets) and display same maximum effects, but different potencies [54,217,218]. Hence, at a certain effect X, a fraction of the concentration of drug A could be replaced by drug B to obtain the exact same effect X. The 'Loewe Additivity' criterion is given by:

$$\frac{C_{A(B),Effect\,X}}{C_{A,Effect\,X}} + \frac{C_{B(A),Effect\,X}}{C_{B,Effect\,X}} = 1 \qquad\qquad\qquad \text{(Eq. 55)}$$

C_A and C_B are the concentrations of drug A or B that individually stimulate an 'Effect X' and $C_{A(B)}$ and $C_{B(A)}$ represent the concentrations of drug A and B that produce the same 'Effect X' in presence of the respective other drug. If the criterion is not set to 1.0 (for additivity), but the calculated combination index is >1, this indicates antagonism or vice versa synergy [217]. If the 'Effect X' is the MIC, the relation of 'Loewe Additivity' to the previously discussed FIC index calculation (4.2) becomes evident. If the effect measure is continuous and follows a sigmoidal maximum effect model, the 'Loewe Additivity' criterion can be formulated as follows [219]:

$$1 = \frac{C_A}{EC50_A \times (\frac{E}{Emax_A - E})^{1/H_A}} + \frac{C_B}{EC50_B \times (\frac{E}{Emax_B - E})^{1/H_B}} \qquad \text{(Eq. 56)}$$

A graphical illustration of the Loewe criterion is given in Figure 71. For additivity, the isoboles for an 'Effect X' of 50%, i.e. lines of same effects with different combinations are linear whereas for synergy and antagonism the isoboles are curved (Figure 71).
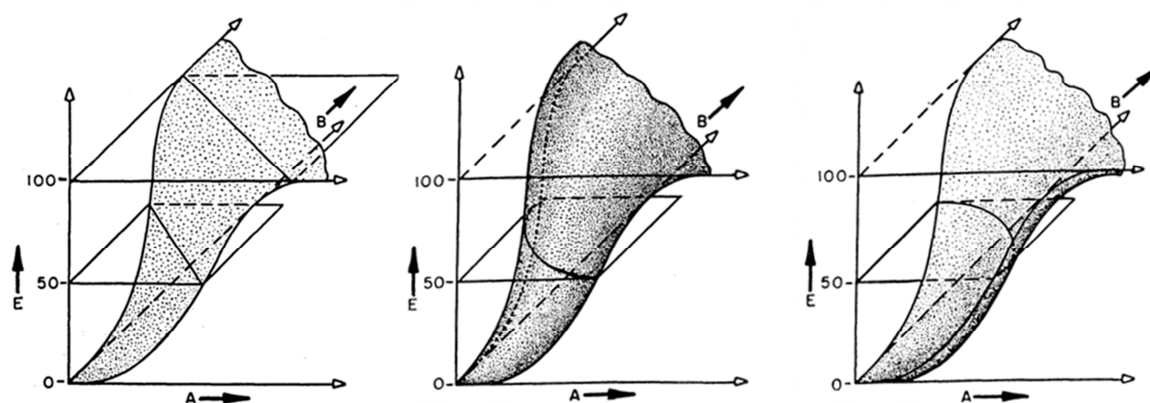
Figure 71: (Joint) effect(s) E of drugs A and B with an additive (left), synergistic (middle) and antagonistic (right) interaction; isoboles, i.e. lines of similar effects are drawn for the half-maximum effect. Extracted from the original work of Loewe [54].

Bliss Independence. The underlying assumption for BI is opposite to the 'Loewe Additivity' criterion: Here, the two agents are assumed to exert their effects simultaneously and mutually nonexclusively by distinct mechanisms of action [55,217,218]. BI uses the concept of effect multiplication (Eq. 22 in 2.4.1.3.2) that was originally derived from probability theory [55]. Translated to the context of the present work, this concept can be understood as one bacterium that has been killed by one antibiotic cannot be killed by the other antibiotic, if combined. The concept of BI seemed slightly more suitable for the present experiments, e.g. since all studied antibiotics exhibit differing mechanisms of action. Still, it was initially planned to analyse the data from the present thesis with both additivity criteria, e.g. as performed by Drusano and colleagues [220], to satisfy the adherents and detractors of both additivity concepts.

Discussion

Application of Bliss Independence in the present response surface analysis. However, direct application of the two criteria was not possible as both 'Loewe Additivity' and BI assume the same maximum attainable effect for both combination partners [54,55,217,218]. Since the maximum effects between the antibiotics were different for both combinations (LZD-MER and VAN-MER), it was attempted to modify the criteria to apply them to the present experimental data with different individual maximum effects, but a mutual maximum possible effect given by the more active antibiotic. When using the 'Loewe Additivity' criterion with different maximum effects, e.g. $Emax_A >$ $Emax_B$ and an 'Effect X' between both $Emax$ values, the 'Loewe Additivity' criterion is not defined as the summand with the lower $Emax_B$ will become negative and for $H>1$ a root of a negative value is not defined (Eq. 56). Jonker also gave a graphical illustration of this property [221]: In our example with $Emax_A > Emax_B$, the isoboles, cannot intersect with both concentration axes as the value of $C_{B,Effect\ X}$ cannot exist as drug B cannot stimulate an effect higher than its individual $Emax_B$.

Hence, the BI criterion had to be used and was modified to compute an additivity response surface to investigate drug combinations with different individual maximum effects, but a mutual maximum possible effect. For that purpose, e.g. for $Emax_A > Emax_B$, the antibacterial effects were first normalised to 1.0 by the maximum effect of the individually more effective drug while the effect of the individually less effective drug was set to a fraction of $Emax_A/Emax_B$ (Eq. 23). The properties of this newly derived BI equation can be illustrated if the combined effect is evaluated at the EC_{50} values of both drugs. For the conventional BI with the same $Emax$ value (i.e. 1.0) for both drugs (Eq. 22), the combined effect would result in 75% of $Emax$ (0.5+0.5-(0.5×0.5)). If the maximum effect of drug B was 50% of that of drug A, according to the modified BI equation (Eq. 23) the combined effect would result in 62.5% of $Emax_A$ due to the minor contribution of drug B to the combined effect [1.0×(0.5+0.25-(0.5×0.25))]. At concentrations of $Emax$ of both drugs, the effect will eventually reach $Emax_A$, the maximum effect of the more effective drug [1.0×(1.0+0.5-(1.0×0.5))].

Moreover, also the uncertainty of the expected additivity response surface was considered for decision-making by taking into account the residual variability of the additivity surface. This uncertainty is frequently neglected and hence the present analysis goes also methodologically beyond previous work that solely considered the uncertainty of the experimental data [51,216,220,222]. The author is not aware of any previous work that has adopted the BI criterion in this way.

The presented response surface approach allows for an individual quantitative analysis of every investigated scenario. No assumption is made on a constant interaction type over the entire drug concentration range as other approaches do, such as the isobole-based FIC index [33] or the parametric approach by Greco that computes a single interaction parameter α for interpretation [222,223]. The present checkerboard and time-kill curve data for LZD and MER emphasise that drug interactions are not necessarily monotonic in nature and hence difficult to be captured within a single estimate: Whilst the interaction between LZD and MER was additive for subinhibitory concentrations in both the

136

dynamic checkerboard and time-kill curve studies, an antagonistic interaction was observed for inhibitory concentrations of both drugs. Hence, the conclusion regarding the nature of a drug interaction (favourable or harmful) can be a function of the investigated drug concentration(s). This also stresses the importance of covering the full concentration range observed at the effect site in the humans if the researcher wants to draw clinically relevant conclusions from PD drug interaction studies. Whereas PK drug-drug interaction studies typically investigate the clinically relevant drug concentration range, this has rarely been exploited for PD drug-drug interactions. Very often, PD interactions are only assessed with subinhibitory concentrations of the antibiotic [106], potentially leading to incorrect clinical conclusions regarding the nature of PD interactions.

The presented response surface approach was useful to provide measures for the scenarios in which the interaction was not obvious, e.g. to discriminate between additivity and synergy. This was particularly useful for drug concentrations below the respective individual maximum effects. For instance, the time-kill curves with lag-phase *S. aureus* exposed to a combination of VAN at 0.5 mg/L and MER at 0.13 mg/L displayed a bactericidal effect whilst the antibiotics alone showed very limited effect (VAN) or killing followed by extensive regrowth (MER). Yet, although the response surface analysis indicated a trend towards synergy for this scenario, the interaction was statistically not significantly different from additive.

The response surface analysis in the present thesis has some limitations which have to be acknowledged: There is some considerable debate which of the additivity criteria – Loewe or Bliss – is reflecting the situation best and appropriate definition of additivity still remains a controversial issue [53]. Boucher and Tam criticised that BI is generally limited to a mutual maximum effect [52]. Although this was actually the case in the present work, i.e. no combinatory effect exceeded the effect of the more active single drug experiment, it can be assumed that a certain drug combination of other drug classes might stimulate a combined effect exceeding the maximum effect of one of the single drug experiments. Such an observation would prevent application of BI in that case. Finally, BI, but also 'Loewe Additivity' are 'black-box' approaches that do not take into account the mechanism of (inter)action of the investigated antibiotics. Particularly, no kinetic information about the PD could be retrieved from the present interaction analysis preventing coupling to pharmacokinetic data, which was the motivation for the development of the semi-mechanistic PD model.

4.3.3 Semi-mechanistic modelling of time-kill curve studies

Modelling approach. The basic principle of modelling the time course of growth and killing of the cell count *N* over time was originally developed for anticancer cells by Jusko [57]:

$$\frac{dN}{dt} = k_{growth} \times N - k_{death} \times N \qquad \text{(Eq. 57)}$$

Discussion

As it is difficult to distinguish between growth and natural death in GC experiments when measuring viable bacteria, very often only k_{growth} is estimated and k_{death} is assumed to be zero in absence of the antibiotic. Hence, in such an approach, k_{growth} represents the net growth rate [224]. As exponential growth is limited for bacteria with increasing N, k_{growth} decreases with N using a logistic function $k_{growth}=k_{growth0}\times(1-N/N_{max})$ [224]. Michaelis-Menten models have also been utilised to describe the dependency of the growth rate on the total number of bacteria [225].

Antibacterial effects are typically implemented in the Jusko model [57] as inhibition of the growth rate k_{growth} or enhancement of the death rate k_{death}. Although, this modelling concept and its extensions to account for time-delays of the effect [226] and/or changes in bacterial susceptibility [30,58,225,227–229] are most frequently used [56], it was found not to be suitable to simultaneously describe the single and combined effects of LZD, MER and VAN against *S. aureus* observed in the present work. Particularly, the parallel implementation of replication-dependent and -independent drug effects and the resulting interactions was not possible to describe with that mathematical model (Eq. 57).

Parameterisation of the bacterial life-cycle. For this purpose, the bacterial life cycle model from Bulitta [141] was used in the present work as a starting point for model development (3.3.1.3). The life cycle model assumes two bacterial compartments ('states'): The first state represents the bacteria after successful doubling (termed 'growing' state 'GRO' in the present thesis) and the second state is attained immediately before doubling ('replicating' state, 'REP'). The transition between 'GRO' and 'REP' is rate-limiting in the cell-cycle whilst the actual doubling, i.e. formation of two cells after leaving state 'REP' and transition to 'GRO' was assumed to be very fast and not estimated. Bulitta has envisioned this model to describe the inoculum effect of *Pseudomonas aeruginosa* exposed to ceftazidime [141] in which hypothetical signal molecules produced by the bacteria in dependence of CFU_0 inhibited the transition rate from 'GRO' to 'REP' leading to a reduced replication-dependent effect of ceftazidime. Other applications of this model included the evaluation of the PK/PD relationship of fusidic acid against *S. aureus* and *S. pyogenes* [230] or the evaluation of front-loaded LZD against enterococci [231].

Implementation of the drug effects. The life-cycle model was a useful core to implement the single and combined drug effects of LZD, MER and VAN in a mechanistic fashion. As cell wall-active antibiotics, MER and VAN were assumed to exert a replication-dependent effect (i.e. perturbation of successful doubling), whilst LZD, as a protein-synthesis inhibitor inhibited the transition rate into the replicating state. By doing so, the antagonism between LZD and MER was already intrinsically implemented in the lag-phase model in a mechanistic fashion as the effect of LZD mathematically growth-arrested the life-cycle and thus precluded the effect of MER. The performed external evaluation demonstrated the ability of this modelling concept to generalise into other antagonistic combinations comprising a cell-wall antibiotic and a protein-synthesis inhibitor [146–148].

The combined effects of VAN and MER in the lag-phase model were implemented as an inhibitory replication-dependent effect, reducing the percentage of successful doublings according to a modified BI term [55,217]. The core of this term, $(1-E_{MER})\times(1-E_{VAN})$ was extended to account for the observed deviations from conventional BI: (i) The maximum effect regarding inhibition of 'successful' doubling of VAN was inferior (lag-phase: 74.3%, log-phase: 73.7%) to the effect of MER (100% in both phases). (ii) The effect of MER in lag-phase was described by two sigmoidal maximum effect models, of which one effect model was inhibitory on the other one to account for the paradoxically reduced 'Eagle-effect' [164] at higher concentrations observed for MER. A more mechanistic implementation of the 'Eagle-effect' (and its quasi-absence in log-phase *S. aureus*) would require more knowledge on the pharmacological basis of this phenomenon. Yet, the current knowledge, as discussed in 4.2, was not considered a reliable basis to support a more mechanistic implementation of the 'Eagle-effect' and the developed semi-mechanistic PD model could reliably describe this phenomenon. (iii) The combined effect of VAN and MER was limited to the effect of VAN, which was achieved by an inhibitory effect of VAN on the effect of MER. More detailed measurements of the processes occurring in the cell-wall during replication under perturbation of MER and VAN could support more mechanistic implementation of the drug effects of MER and VAN. At this stage, the present implementation provided reliable prediction of the observed effects alone and in combination.

Adaptive resistance. Until now, solely the initial effects of the antibiotics were discussed; the effects of the studied antibiotics partially changed over time, which will be discussed in the following section: Apart from LZD in lag-phase *S. aureus*, the antibiotic effects were time-dependent and not monotonic in nature. Two phenomena were encountered in the present work: Persistence of bacteria displaying no replication under antibiotic exposure after initial killing and (adaptive) resistance development manifested as regrowth after initial killing by the antibiotic. Bacterial persistence was mathematically implemented in the semi-mechanistic PD model by either growth-arrest (for LZD) or selection of a drug-unsusceptible, non-replicating subpopulation during replication (for MER and VAN). The mathematical approach of selecting a drug-unsusceptible subpopulation under antibiotic exposure has been previously used in the literature [30,58,229]. Other investigators have employed modelling approaches assuming pre-existing subpopulations that dominate the time-kill curve pattern after killing of the susceptible population [225,227,228]. The first approach (i.e. growth-arrest and selection of persister cells) was chosen as subpopulations were not quantified in the present work and hence fewer assumptions were made. Persistent subpopulations could be quantified in future studies by e.g. microfluidic devices that allow for tracking down the growth history of a single bacterial cell and their dependants [232].

The adaptive resistance of MER and VAN leading to regrowth after initial killing was modelled as an increase in EC_{50} over time [142,143]. Due to the incorporation of drug degradation, measured by HPLC, into the mathematical model, the observed regrowth was dissected into regrowth due to decay

of the antibiotic and adaption of the bacteria. Interestingly, Tam and co-workers who introduced the utilised adaption model with an increasing EC_{50} did not consider drug degradation when modelling the PD of MER against *P. aeruginosa* [143], although substantial and relevant degradation to 62.9% was found in the present work under similar experimental conditions (i.e. use of CaMHB and a similar temperature of 35° C). Yano and colleagues also did not measure drug degradation to support their modelling activities, but estimated a first-order rate constant K_d to mathematically reduce the 'active' drug concentration over time to describe the regrowth of various strains exposed to MER and other beta-lactam antibiotics [229]. Yet, the authors acknowledge in their publication that the 'active' fraction could be reduced by both degradation and adaption of the bacteria. Also for other considerably instable beta-lactam antibiotics such as ceftazidime [233], drug degradation was not measured and hence not separated from adaption when performing mathematical modelling of time-kill curve data [141,228]. This should be considered when interpreting their modelling results, as adaption-related parameters might overestimate the 'true' adaption of the bacteria. Other concepts of modelling adaptive resistance included a declining *Emax* [234] or an increasing growth rate over time [228]: A decreasing *Emax* could originate from target site alteration [224] whilst the mechanistic basis for an increasing growth rate seems rather unclear. Since higher concentrations of the antibiotic overrode the adaption, a decrease in *Emax* over time seemed not suitable for modelling the present time-kill curves of MER and VAN and the approach with the increasing EC_{50} [143] stimulated by exposure to the antibiotic over time was chosen. An increasing growth rate was also deemed not suitable, as in the life-cycle model in the present work, this would increase the growth rate proportionally with the replication-dependent killing rate of the antibiotic, leading to yet faster killing. Figure 72 illustrates the time course of the 'effective' EC_{50} values for MER and VAN in both studied growth phases from the present work. Whilst both time course and magnitude of the adaption were similar for MER in the investigated growth phases (e.g. maximum possible 'effective' EC_{50}: 0.23 mg/L in lag- and 0.20 mg/L in log-phase), the maximum possible adaption of VAN was substantially higher in log-phase *S. aureus* ('effective' EC_{50} of 5.36 mg/L in log- and 2.12 mg/L in lag-phase). As a function of drug concentration, the time to reach the maximum-possible EC_{50} was variable (Figure 72).
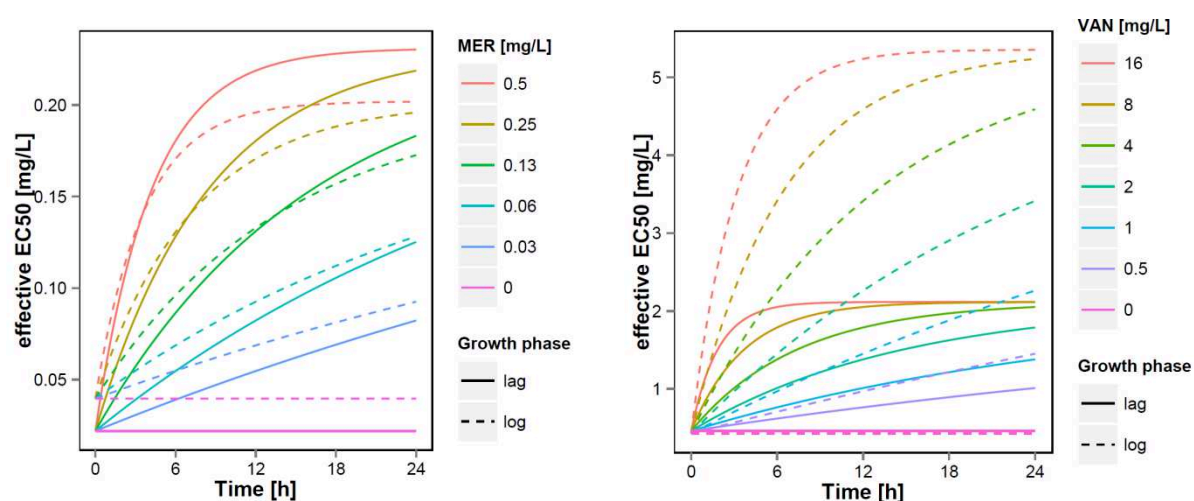
Figure 72: Time course of the 'effective' EC_{50} for MER (left) and VAN (right) in both lag- and log-phase *S. aureus* predicted from the utilised adaption submodel [143] of the semi-mechanistic PD model. The $EC_{50,t=0}$ is represented by the scenarios with no drugs.

The estimation of the adaption parameters β and τ is mainly driven by the (few) scenarios that displayed regrowth and one can assume that several combinations of β and τ can lead to similar adaption profiles for those scenarios. This causal correlation between β and τ is also apparent in the correlation matrices of lag- (Figure 73) and log-phase *S. aureus* (Figure 80) and in the considerably broad confidence intervals of those parameters obtained from the bootstrap analysis (Table 15 and Table 16). However, the present work provides experimental evidence from the adaptive resistance studies to support the adaption submodel and its parameter values for adaptive resistance of *S. aureus* to MER and VAN (3.2.5): Remarkably, the magnitude of the adaption process was well predicted in the external model evaluation with adapted bacteria (3.2.5 and 3.3.1.3.1.4).

The adaption submodel with an increasing EC_{50} was not implemented as an analytical solution as proposed in the original publication by Tam et al [143], but as part of the ODE system, following a similar approach as Mohamed and colleagues [142]. The ODE implementation has two advantages over the analytical solution: (i) it is applicable changing drug concentrations including drug degradation and (ii) it allows for implementation of interactions on the adaption level, as observed in the present thesis, to quantify the interaction between 'inactive' subinhibitory VAN suppressing regrowth of MER at up to 0.125 mg/L.

Limitations and perspectives. Some limitations of the developed semi-mechanistic PD model have to be acknowledged. Some processes such as the adaptive resistance as well as the persister development are implemented unidirectional, i.e. the acquired resistance is modelled as an irreversible process. One can imagine that both persistence and resistance could be reversible over time when a bacterial population survived an antibiotic treatment. The experimental data in the present work did

not support an implementation of this reversion which adds uncertainty if extrapolation beyond the studied 'experimental range' is performed. Nielsen et al and Schmidt et al formally included return from the persister state to the susceptible state, but fixed the respective rate constant to zero for similar reasons as in the present work [30,58]. Yano et al could estimate the reversion from the persisting state since no death rate constant of the persisting population was implemented in their model [229]. Time-kill curve data obtained in dynamic *in vitro* infection models [22] could help to inform such potentially reversible processes in future studies. The present experimental data did not support the implementation of separate death rate constants for bacteria persisting under exposure to MER or VAN. If those differences were observed in other experiments, the present semi-mechanistic PD model would have to be modified to quantify the bacteria persisting under exposure to several antibiotics in separate compartments. Overall, the developed semi-mechanistic PD model described the experimental data of the lag- and log-phase scenarios very well and considered mechanistic aspects of the drug effects. In future studies, also the combined effects in log-phase should be further explored and integrated into the model.

4.3.4 Adaptive optimal design

The adaptive optimal design approach (3.3.1.3.1.2) enabled performance of informative experiments and, thus, characterisation of the single and particularly the combined effects observed in lag-phase *S. aureus* by a considerably complex mathematical model that captured even details in the time-kill curve profiles. This represents an application of the "learning and confirming" approach introduced into clinical drug development by Sheiner in 1997 [70] and extends this concept to pre-clinical "learning and confirming" when planning and analysing experimental data. Moreover, it could be demonstrated that mathematical optimal design techniques could be valuable to assess the impact of experimental information on the precision of model parameters, i.e. if an experiments does or does not add information to support estimation of this particular model parameter. A next step of optimisation would go beyond evaluation of designs to prediction of 'fully optimised' optimal designs. Whilst it has been recently shown, that e.g. D-optimal design [69] could reduce the number of required sampling time points [235] or concentration tiers [236] in time-kill curve studies, the practical value of such 'fully optimised' experimental designs is questionable as prediction of the D-optimal design requires a priori knowledge on both the model structure as well as the model parameter values. This knowledge either supersedes the performance of the experiments or is not available before performance of the study. Hence, the parallel performance of experiments, modelling activities and iterative design evaluation as utilised in the present work seems a reasonable compromise to translate the value of optimal design into an experimental setting.

In summary, the developed semi-mechanistic PD model reliably described the observed time-kill curve data and the performed internal and external model evaluation provided evidence for the

robustness of the developed model. Hence, the developed semi-mechanistic PD model provided a reliable basis for performance of simulations, will be discussed in the next chapter.

4.4 Simulations

4.4.1 Drug concentrations in the biophase

A prerequisite to answer clinically relevant questions with the developed population PK/PD models was to study clinically relevant drug concentrations to inform the semi-mechanistic PD model. For MER, the studied concentrations up to 16 mg/L in the present work particularly matched concentrations observed at the target site, e.g. in the lung: steady state concentrations up to 11.4±10.9 mg/L were measured in the interstitial fluid of the lung tissue applying microdialysis after 1 g MER every 8 hours administered via a short-term infusion [82]. Another study reported similar concentrations up to 7.7±3.1 mg/L in epithelial lining fluid of the lung obtained via bronchoalveolar lavage using the same dosing regimen [237]. Maximum plasma concentrations after administration of 1 g MER exceeded the investigated concentrations of the present work with C_{max} values of 53.5±19.7 mg/L [237]. Due to the short half-life of 1.3 h, however, MER concentrations in plasma are covered by the studied concentration range of the present work (up to 16 mg/L) for the major portion of the dosing interval. For LZD, steady state concentrations in epithelial lining fluid ranged from 2.6±1.7 to 14.4±5.6 mg/L after 600 mg intravenous LZD infusion twice daily [94] which matched the concomitant plasma concentrations (2.43±2.15 to 17.8±6.03 mg/L) [238]. Also for VAN, the investigated drug concentrations matched the clinically observed concentrations at the target site: VAN concentrations in epithelial lining fluid of the lung ranged from 0.4 to 8.1 mg/L after C_{min}-adjusted multiple dosing [239]. Plasma concentrations were reported to be higher ranging from 7.9 to 65.7 mg/L [98]. Hence, the investigated concentrations used in the present thesis reflected the concentrations at the target site *in vivo*, which are partly lower for MER and VAN than plasma concentrations. Yet, the fact that the C_{max} concentrations in plasma were not fully covered by the present experiments was not that relevant as the maximum effects for MER and VAN were well established below those C_{max} concentrations and a further increase of the effect at C_{max} seemed unlikely.

4.4.2 Prediction of PK/PD indices

The developed semi-mechanistic PD model from the present work was linked to published population plasma PK models of LZD [150], MER [153] and VAN [154], which were also corrected for plasma protein binding to predict unbound (active) drug concentrations over time (3.3.2.2). The experimental results were thereby exploited in a quantitative and translational fashion and allowed for performing clinical trial simulation. Beforehand, the validity of the population PK/PD model was assessed by

performing an *in silico* dose fractionation study to predict commonly utilised PK/PD indices, which are in the following related to literature data.

Meropenem. For MER, the *in silico* dose fractionation study revealed that the PK/PD index $fT_{>MIC}$ correlated best with the effect, i.e. reduction of log10 CFU/mL at 24 h in both lag- and log-phase *S. aureus*. For $fAUC/MIC$ and fC_{max}/MIC, the correlation was (substantially) inferior. This first qualitative result is in line with knowledge gained from seminal animal studies by Eagle [60] that were the initial stepping stone of the later development of PK/PD indices by Craig and co-workers [59]: The effect of beta-lactams was found to be time-dependent. Three different mechanisms drive this PK/PD relationship: Firstly, higher concentrations above the MIC do not further increase the antibacterial effect, i.e. the maximum effect is established. Secondly, beta-lactams display only a modest post-antibiotic effect (i.e. persistent effects after removal of the antibiotic) of e.g. 0.7-1.7 h for MER against *S. aureus* [240]. Lastly, beta-lactam antibiotics typically display considerably short *in vivo* elimination half-lives of ~ 1 h [59] which reveals this time-dependency of the effect also in the clinical setting. The quantitative PK/PD breakpoint $fT_{>MIC}$ for MER determined in the present work was similar against lag- and log-phase *S. aureus.* PK/PD breakpoints for $fT_{>MIC}$ were determined by non-linear regression analysis and were 52% for lag- and 50% for log-phase *S. aureus* for a bacteriostatic effect and 65% for lag- and 70% for log-phase *S. aureus* for a bactericidal effect. Notably, the PK/PD index $\%fT_{>MIC}$ for a bacteriostatic effect in lag-phase *S. aureus* was higher in the clinical trial simulation (3.3.2.2.1), i.e. ca. 70%, compared to the *in silico* dose fractionation study (3.3.2.1). This phenomenon might originate from the use of higher doses in the simulated clinical trial leading to higher concentrations of MER and in turn faster and more intense adaption of *S. aureus* to MER. Yet, overall the determined PK/PD index is in reasonable agreement with the clinical breakpoint for microbiological response of 54% determined in patients with lower respiratory tract infections, in which *S. aureus* was the second-most abundant pathogen [241]. A bacteriostatic effect or log2 killing was also observed if $fT_{>MIC}$ exceeded 45% or 75%, respectively, in animal studies evaluating the effect of MER on Gram-negative bacteria using a mouse thigh model [78]. Yet, also lower values for a bacteriostatic $fT_{>MIC}$ of 23% for the Gram-negative bacterium *Pseudomonas aeruginosa* was reported [242]. Worthy to discuss is the EUCAST rationale document that reports lower values for $fT_{>MIC}$ of 10-30% or 15-40% for a bacteriostatic or log-2 killing effect, respectively, also for *S. aureus* [79]. In the EUCAST document, the PK/PD relationship of carbapenems is presented as a 'class effect' as long as unbound drug concentrations are compared. While this might in fact be true, this assumption heavily relies on correct determination of unbound concentrations. A substantial part of the EUCAST PK/PD summary is originating from PK/PD studies with the highly protein-bound antibiotic ertapenem [78,243,244]. An unbound fraction of 4.5% was determined once by Xuan et al [244], which was used in Xuan's [244] and several later studies [78,243] for calculation of $fT_{>MIC}$. Yet, work from our department and collaborators could recently show that the ultrafiltration process, also used by Xuan

[244], is highly dependent of temperature, pH and centrifugal force [155,245,246]. Particularly, ertapenem is susceptible to those experimental parameters [245]. In the ultrafiltration protocol of Xuan [244], pH of the plasma sample was not controlled by buffering which might have led to alkalotic pH values due to evaporation of carbon dioxide at 37° C: When pH was controlled and buffered to 7.4, the unbound fraction of ertapenem was significantly higher than that determined by Xuan, and was ca. 20% in healthy volunteers and between 30.9% and 53.6% in ICU patients [245]. Hence, the 'true' $f\mathrm{T}_{>\mathrm{MIC}}$ to attain the PK/PD breakpoints with respect to the unbound concentrations might be substantially higher than those proposed by the EUCAST [79].

Linezolid. For LZD, the *in silico* dose fractionation study revealed that the PK/PD indices $f\mathrm{AUC}/\mathrm{MIC}$ correlated best with the effect, i.e. reduction of log10 CFU/mL at 24 h in both lag- and log-phase *S. aureus*. For $f\mathrm{T}_{>\mathrm{MIC}}$ and $f\mathrm{C}_{\max}/\mathrm{MIC}$, the correlation was inferior, but this inferiority was much less pronounced than for MER. This is in accordance with animal studies from Andes et al [247], in which a clear distinction between these three PK/PD indices was also difficult. As no bactericidal effect was attained for LZD, no bactericidal PK/PD breakpoint could be calculated. The bacteriostatic $f\mathrm{AUC}/\mathrm{MIC}$ was 56 in lag- and 59 in log-phase *S. aureus*. Andes and colleagues also could not find a bactericidal effect and determined a bacteriostatic (total, not unbound) AUC/MIC of 83 in animal studies using the mouse thigh model [247]. This result is well in the range of the present study, if protein binding is considered. Yet, also for LZD there is some uncertainty about the precise value of the unbound fraction and results range from 86.6% [93] to 69% [90]. The impact of the precise value is, however, certainly less drastic than for highly protein-bound drugs. Rayner and colleagues investigated the clinical PK/PD relationship of LZD in seriously ill patients in a compassionate use program [157]: They proposed values for (total) AUC/MIC of 80-120 for "higher success rates" for LZD for bacteraemia, but also for lower respiratory tract and skin and skin structure infections. Whilst the breakpoint for blood of 83 again matches considerably well to the present work, the infection-site specific breakpoints for skin (110), lower respiratory tract (99) and bone (164) are higher indicating the relevance of considering tissue distribution [157]. Rayner also investigated %T$_{>\mathrm{MIC}}$ and found that bacterial eradication was higher if total LZD concentrations exceeded the MIC for 82% (bacteraemia) to 99% (skin), which also is in good agreement with the determined PK/PD breakpoint of 80%-85% from the present study.

Vancomycin. The *in silico* dose fractionation study for VAN was less clear-cut regarding the correlation of any PK/PD index and the effect, which was inferior to the correlations obtained with both LZD or MER. When R² was evaluated, $f\mathrm{AUC}/\mathrm{MIC}$ in the log-phase scenario correlated slightly better than the other competing PK/PD indices. Moreover, the differences between lag- and log-phase drastically influenced the obtained PK/PD indices. Whilst e.g. the bacteriostatic or bactericidal $f\mathrm{AUC}/\mathrm{MIC}$ was 59 or 94 in lag-phase *S. aureus*, the bacteriostatic breakpoint was 160 in log-phase *S. aureus* and no bactericidal effect was attained. As for MER, the population PK/PD model for VAN

also contained an adaption submodel; the use of higher doses in the clinical trial simulation led to higher VAN concentrations and in turn faster adaption of *S. aureus* to VAN, which resulted in higher *f*AUC/MIC indices of 200-250 for the maximum effect of VAN. Rybak reported a bacteriostatic total AUC/MIC of 200-300 in a mouse thigh infection model [96]. Clinical investigations by Bosso [248] and Moise-Broder [249,250] set total AUC/MIC breakpoints of 125-400. Thus, those clinical breakpoints rather fit to the log-phase breakpoint of the present work. Even if a plasma protein binding ranging from 30% [155] to 55% [99] is assumed, the total AUC/MIC breakpoints from the clinical studies tend to be somewhat higher than the calculated values of the present work, which could originate from the partly impaired tissue distribution of VAN [96]. Although the unprocessed time-kill curves displayed different killing patterns in lag- and log-phase *S. aureus* for all studied antibiotics, a substantially different PK/PD breakpoint between lag- and log-phase *S. aureus* was only determined for VAN. For VAN, the value of *f*AUC/MIC for log-phase *S. aureus* was much closer to the clinically determined breakpoint(s) which indicates that bacteria might be actively replicating (i.e. in log-phase) in patients with symptomatic infections. Yet, also lag-phase bacteria might be clinically relevant, e.g. in prophylactic or perioperative antibiotic treatment to prevent infections.

Limitations and future considerations. Although the agreement of the PK/PD breakpoint of the present work and published animal and clinical PK/PD studies was considerable, some limitations of the presented approach have to be discussed: A major limitation is that solely time-kill curve studies with static drug concentrations were experimentally performed, but dynamic, i.e. changing concentrations were simulated in the population PK/PD model. As a consequence, the semi-mechanistic PD model was not informed about persistent antibiotic effects after declining antibiotic concentrations such as the so-called post-antibiotic effect. Yet, this major limitation in general turns out to be minor for the present study, as the post-antibiotic effects for MER, LZD and VAN against *S. aureus* are known to be considerably short up to 1.7 h [240], 2.2 h [251] and 1.2 h [205], respectively. For future studies with antibiotics displaying considerably longer persistent antibiotic effects, dynamic time-kill curve studies [22] should be performed to inform the semi-mechanistic PD model accordingly.

As the semi-mechanistic PD model represents the PD directly at the target-site and the utilised population PK models describe the PK of (unbound) antibiotic solely in plasma, no information about tissue distribution was included in the present approach. This formally limits the approach to the assessment of bloodstream infections. However, the use of microdialysis [252] could elucidate the target-site PK of an antibiotic which could be included in PK model development [253]. This would allow assessment of target-site specific population PK/PD analyses in future studies. A fundamental assumption in antimicrobial PK/PD studies is that only unbound drug concentrations can exert their antibiotic effects, formulated in the so called "free drug hypothesis" [254]. Although the PK models were corrected for unbound concentrations assuming linear plasma protein binding, the determination

of protein binding is susceptible to experimental conditions [155,245,246], as discussed earlier, and a biased estimate of the unbound fractions might result in biased PK/PD simulations. To further add complexity, plasma protein binding might be saturable and follow a non-linear pattern [47], which needs to be considered when analysing antibiotics displaying such binding behaviour in future studies. Another limitation originates from the determined MIC value in the denominator of the PK/PD index. A one tier higher or lower MIC will consequently shift the determined PK/PD indices substantially, which should be generally considered when interpreting PK/PD indices. Moreover, the effects of the immune system are not considered in the present work and hence the population PK/PD model might reflect a 'worst-case' situation, e.g. cancer patients suffering from neutropenia. Yet, it is assumed that particularly those patients benefit from an optimised bactericidal therapy, whilst for non-neutropenic patients, the immune system blurs differences between bacteriostatic and bactericidal antibiotics [126]. The investigated drugs LZD, MER and VAN are ultima-ratio antibiotics and particularly used in critically ill patients. Consequently, neutropenia might not be as rare as in community-based antibacterial therapy and an optimal appropriate treatment might be particularly important for the treatment of the critically ill patient [72]. Furthermore, in addition to the reduction of viable bacteria, other factors may contribute to the therapeutic success, e.g. the inhibition of toxin synthesis. LZD and clindamycin, another protein synthesis inhibitor, were found to suppress the toxin Panton-Valentine leucocidin, whereas oxacillin, a beta lactam antibiotic, even led to increased secretion of this toxin *in vitro* [255]. There is some initial clinical evidence that protein synthesis inhibitors are associated with a better clinical outcome in the case of invasive infections with toxin-producing bacteria [256,257], but more clinical data on this potential beneficial effect of protein synthesis inhibitors is necessary. Lastly, although the MICs and interaction profiles were similar in the three utilised *S. aureus* isolates, the time-kill curve studies and the semi-mechanistic PD model is based upon a single *S. aureus* isolate. Hence, further studies are required to investigate generalisability of the findings.

In summary, the *in silico* dose fractionation study did not only qualitatively identify the *in vivo* PK/PD indices correctly; also the quantitative PK/PD breakpoints of the present work well agreed with the *in vivo* PK/PD breakpoints found in published literature. This is insofar remarkable, as the present work determined the PK/PD breakpoints solely from simple, resource-saving and cost-effective *in vitro* studies and published literature on the PK of the studied antibiotics. In contrast to this efficient approach in the present work, conservative PK/PD breakpoint determination relies on resource-intense *in vivo* animal studies or even clinical trials in patients suffering from severe infections. Hence, the present work provides an integrated quantitative pharmacometric approach to translate *in vitro* studies with antibiotics into a clinical setting so as to comprehensively elucidate the PK/PD relationship of an antibiotic in a resource-saving manner. Future studies could also investigate and derive PK/PD indices and breakpoints of combination therapies by this approach.

4.4.3 Clinical trial simulation

The previously discussed *in silico* dose fractionation study yielded PK/PD indices being overall in accordance with the clinically used PK/PD breakpoints of MER, LZD and VAN. Hence the developed population PK/PD model was considered reliable to answer questions arising from 'what-if-scenarios' assessing the single and combined use of the antibiotics and potential impact of patient covariates informed from the utilised population PK models (3.3.2.2.2). For those translational simulations of clinical scenarios, both the interindividual variability in the PK of the studied patient population as well as the uncertainty of the semi-mechanistic PD model was considered in stochastic simulations using a Monte-Carlo approach [158]. Monte-Carlo methods are useful when the impact of several variables on a system is explored, but the mathematical analytical solution is unknown – as in the present work – or difficult to derive. The utilised number of 1000 simulations provided a reasonable compromise between accuracy of the obtained distributions [258] and the required simulation time of ca. 1 simulation per second.

Evaluation of single and combined standard dosing regimens. In a first step, standard dosing regimens were explored with a representative virtual patient population that overall represented the population on which the population PK models were built [150,153,154]. The entire time course of 24 h was presented allowing for detailed and continuous assessment of the PK/PD relationship of the MER, LZD and VAN. As previously, both bacterial growth phases were explored. Based on the results of the clinical trial simulation, the standard dosing regimen of 1000 mg TID for MER and 600 mg BID for LZD could be considered reliably bactericidal or bacteriostatic, respectively, in the investigated patient population for *S. aureus* with MIC values of 0.125 (MER) and 2 mg/L (LZD). The impact of the growth phase in those translational clinical studies was visible in the PK/PD plots for MER (Figure 46) and LZD (Figure 48), but the clinical impact of this rather fine-scale difference might not be relevant in clinical practice. Conversely, the standard dosing regimen of VAN 1000 mg BID was not reliable for *S. aureus* with a MIC of 1 mg/L in the presumably more relevant log-phase scenario for VAN (Figure 50).

The combinations of LZD or VAN with MER were evaluated solely against lag-phase *S. aureus* as the log-phase PK/PD model was not informed with (sufficient) experimental data. The clinical trial simulation revealed that the antagonistic interaction was also translated into the clinical setting and both MER alone, but also the combination of VAN and MER were superior to the combination of LZD and MER. The dosing regimens for both LZD and MER are designed to provide sustained plasma concentrations above the MIC. For the comparatively low MICs of the *S. aureus* strain in the present work, standard doses of both LZD and MER provided inhibitory concentrations and thus pharmacodynamic antagonism throughout the entire dosing interval.

Impact of patient covariates. In a second step, standard and alternative dosing regimens from the investigated antibiotics were explored in dependence of patient covariates of the population PK model.

This approach represents a comprehensive translational assessment of antibiotic dosing strategies learning most from *in vitro* experiments for the clinical setting and could be used for hypothesis generation of upcoming clinical studies with the antibiotics. For the sake of simplicity, in the present work, the impact of covariates was evaluated solely in a univariate way. If CLCR was assessed, WT was set to 75 kg. If WT was explored, CLCR was set to 120 mL/min to shed light on the covariate relationship that might be masked from the PTA perspective for lower CLCR values. Yet, if an investigator aims to assess a specific 'what-if' scenario, e.g. a worst case situation of augmented renal clearance accompanied by a high or low body weight, simulation of this scenario is trivial and of course possible with the presented approach.

Meropenem. For MER, the standard dosing regimens of 500 and 1000 mg TID administered as 1 h infusion provided high bacteriostatic PTA ranging >80% (lag-phase) or >94% (log-phase) depending on body weight (60-105 kg) and creatinine clearance (60-160 mL/min). The appropriateness of the standard dosing regimen of MER for the investigated *S. aureus* strain with a MIC of 0.125 mg/L is in accordance with the EUCAST clinical susceptibility breakpoint, which defines bacteria with a MIC ≤2 mg/L as susceptible to MER [20,79]. The PTA – counterintuitively – slightly increased with higher WT: This might originate from the adaptive resistance submodel of MER. Higher WT leads to lower (peak) concentrations in the virtual patient and consequently to slower adaption of *S. aureus* to MER and hence to a slightly better PTA. Continuous infusion of 1500 mg MER over 24 h provided higher PTA, particularly when exploring the bactericidal PTA, which was 100% even at presence of augmented renal clearance with CLCR of 160 mL/min. Continuous infusion of MER might be particularly beneficial for infections with *S. aureus* isolates with higher MIC values closer to the EUCAST susceptibility breakpoint of 2 mg/L. For instance, Roberts and coworkers have investigated continuous infusion of up to 6 g MER per day in the clinical setting, and found sufficient target attainment even for isolates with MIC values of 8-16 mg/L when applied as continuous infusion in septic patients [259]. In a randomised controlled clinical trial, Dulhunty and colleagues could also demonstrate that continuous infusion of MER improved the clinical cure rate from 43% to 70% in their patient population [83]. Hence, continuous infusion might be beneficial in the clinical setting, particularly for patients suffering from infections with considerably 'high' MIC values. Yet, Carlier and colleagues showed that stability (solutions retaining >90%) of reconstituted MER in isotonic 0.9% NaCl solution is limited at 25° C to 12 h or 8 h at MER concentrations up to 20 or 40 mg/mL, respectively [260], which possesses some handling issues and awareness of the medical personnel to adopt continuous infusion of MER in clinical practice.

Linezolid. For LZD, the standard dosing regimen of 600 mg BID provided bacteriostatic PTA values >79% depending on WT, CLCR or liver cirrhosis. Increasing WT and CLCR decreased the PTA whereas presence of liver cirrhosis reduced the clearance of LZD leading to higher exposure and in turn also higher PTA values. Hence, the standard dosing regimen provided reasonable PTA values for

Discussion

the investigated *S. aureus* strain with a MIC of 2 mg/L being also formally susceptible to LZD according to EUCAST (MIC ≤4 mg/L) [20,183]. As the effect of LZD was limited to a bacteriostatic effect, alternative regimens comprising continuous infusion with the same total daily dose (1200 mg), intensified TID dosing (3x 600 mg) and 'front-loading' (1200 mg -> 600 mg BID) were assessed on their potential as a more effective alternative to the standard regimen: The regimen with continuous infusion of LZD was inferior to the standard regimen in both growth phases of *S. aureus*. This could be explained by the slower increase of LZD concentrations in the continuous regimen than in the short-term infusion which could allow some bacterial growth at the beginning of the treatment which cannot be compensated by the considerably slow killing effect of LZD due to growth arrest of *S. aureus*. Adembri and colleagues compared continuous to intermittent infusion of LZD and found comparable clinical outcome, AUC/MIC values, but slightly higher $\%T_{>MIC}$ in the continuous infusion group [261]. The authors suggested continuous infusion as an alternative with comprehensible 'theoretical advantages' of the continuous infusion regimen. Jacqueline and co-authors found continuous infusion of LZD superior to intermittent dosing in rabbit endocarditis model [262]. However, the concentrations they simulated in the rabbits in the continuous infusion group increased from 10.4 to 32.5 mg/L from day 1 to day 5 were substantially higher than the concentrations observed in humans of ca. 6 to 14 mg/L up to 2 days [261,263] and from the translational PK/PD studies in the present work (median: 10.1 mg/L, 2.5[th] percentile: 5.5 mg/L, 97.5[th] percentile: 16.9 mg/L). Those higher LZD concentrations and the presence of an intact immune system in the animals might explain the superiority of continuous infusion in the study of Jacqueline et al. The present work rather questions the benefit of continuous infusion of LZD and elucidated the value of 'front-loaded' LZD regimen following the strategy of achieving high LZD concentrations at a very early stage of antibiotic treatment. Front-loading 1200 mg – 600 mg LZD was also superior to intensified TID dosing with 600 mg LZD and even stimulated a bactericidal effect for 8-29% of the patients (log-phase scenario) depending on CLCR. This result is primarily driven by the initial concentration-dependency of the effect of LZD in the first 4-6 h from the log-phase scenario, in which higher LZD concentrations can augment the effect. In contrast to that, at later time point the growth-arrest of LZD might render higher LZD concentrations ineffective. Hence, 'front-loaded' LZD regimen might be a promising alternative to the standard regimen to augment the antibacterial effect of LZD. A potential benefit of increased killing and suppression of resistance development for 'front-loading' of LZD was also described by Tsuji and colleagues when assessing the PK/PD relationship of LZD against enterococci [231] and *S. aureus* [264] in a dynamic *in vitro* infection model. However, the safety profile and also the impact on clinical outcome of this alternative intensified dosing regimen must be carefully evaluated in prospective clinical trials before adopting such a regimen in clinical practice.

Vancomycin. For the investigated *S. aureus* strain with a MIC of 1 mg/L, EUCAST would define this strain as susceptible to VAN [20,184]. However, the present work questions this general MIC

150

breakpoint and tremendous differences between both investigated growth phases were observed: Whilst the standard dosing regimen of 1 g VAN BID administered as short-term infusion provided considerably high bactericidal PTA values even for augmented renal function with a CLCR of 160 mL/min (PTA: 63%) and increased WT of 105 kg (PTA: 77%) for lag-phase *S. aureus,* the bacteriostatic PTA <60% for the lowest studied CLCR of 60 mL/min and no bactericidal effect was attained at all for log-phase *S. aureus*. As the *in silico* dose fractionation study revealed that log-phase *S. aureus* might be better reflected in the clinical setting for VAN, the discussion of alternative dosing regimens will focus on log-phase *S. aureus*. As suggested by guidelines, VAN dosing in current clinical practice is rather based on WT-adjusted dosing of 15 mg/kg BID with an optional loading dose of 25-30 mg/kg BID [102] than a fixed dose of 1000 mg BID as suggested in the label [99]. After initial dosing, also individual dose adjustment is suggested based on therapeutic drug monitoring [102]. WT-adjusted dosing did not only level out the influence of WT in the present work, but inverted the WT-effect relationship leading to even higher PTA values with increasing WT. Yet, only in few scenarios with WT of 75 kg and CLCR ≤80 mL/min and a dose of 30 mg/kg followed by 15 mg/kg, the PTA was considered sufficient (> 90%). In contrast to LZD and MER, CLCR had an enormous influence in the present work on the PTA also within the first 24 h; hence it might be beneficial to consider *both* WT and CLCR already for initialisation of antimicrobial therapy with VAN. To facilitate this two-dimensional dose adaption in clinical practice, pharmacometric models could be used rather than less precise nomograms [265]. User-friendly software is certainly a key prerequisite to implement pharmacometric techniques in the clinical setting. It shall be mentioned here that the author has developed an easy-to-use web application for this purpose to foster model-supported therapeutic drug monitoring in clinical practice (available at: www.tdmx.eu) [266]. An intensified dosing interval of 500 mg QID, also suggested in the label of VAN [99], provided higher PTAs than the front-loaded BID regimen with a higher total daily dose of 30 mg/kg followed by 15 mg/kg. Continuous infusion of 2000 mg VAN BID further improved the PTA which was found sufficient even up to CLCR of 160 mL/min. Waieno and co-authors very recently published a review on VAN administered via continuous infusion [267]: Although there was a trend to improved outcomes in some studies [268,269], no study found significantly better outcomes associated with continuous infusion [267]. It should be mentioned that Waino recommends maintaining (total) VAN steady state concentrations between 17.5 and 27.5 mg/L by administering higher doses determined by renal function (e.g. 27×CLCR+140 to achieve 27.5 mg/L) [267] than in the present work where 2000 mg over 24 h provided sufficient PTAs for all covariate scenarios. This might be due to the impaired tissue distribution of VAN [96] which is not implemented in the present work due to the unavailability of suitable population PK models that also account for tissue distribution. For example, Georges investigated penetration of VAN into epithelial lining fluid in the lung and found that for patients with plasma trough concentrations below 20 mg/L, no VAN was detected in the lining fluid whilst patients

with VAN concentrations >20 mg/L, the concomitant VAN concentrations in the lining fluid were as low as 1.38-2.77 mg/L [270]. Lamer and co-workers determined similarly low concentrations in the epithelial lining fluid and found that penetration was also altered by lung inflammation [239]. Hence, further clinical studies, e.g. using microdialysis [252] are required for VAN to build up predictive pharmacometric models integrating unbound tissue concentrations. In presence of this highly variable tissue distribution of VAN, the application of the developed population PK/PD model of the present work is limited to bloodstream infections.

In summary, the presented approach translated the results of *in vitro* experiments into a clinical setting. The obtained results agreed in a substantial portion with the results obtained from clinical trials providing evidence for the translational validity of the presented findings also for the evaluated monotherapy regimens of LZD, MER and VAN. Clinical studies evaluating the proposed dosing regimens with respect to their efficacy and safety would next be desirable.

5 Conclusion and Perspectives

The aim of the present thesis was to investigate and compare the mono- and combination therapy of LZD or VAN combined with MER against methicillin-susceptible *S. aureus* in an integrated *in vitro* and *in silico* approach under consideration of PK and PD. Thereby, the present work advanced both the knowledge on the (combined) use of the utilised antibiotics as well as methodological aspects on the *in vitro* and *in silico* studies.

The most prominent result on the combined use was that the rapid bactericidal effect of MER against methicillin-susceptible *S. aureus* was fully antagonised by LZD at concentrations above the MIC. The clinical trial simulation indicated that the antagonistic interaction between LZD and MER might also translate into a clinical setting. The comparator drug VAN resulted in an overall additive interaction with MER and even protracted the adaption process of *S. aureus* to MER, indicating a beneficial interaction between VAN and MER. The present work also assessed the approved and recently recommended single drug dosing regimens of the antibiotics in the virtual patient population. For MER, the standard dosing regimen of 1000 mg TID administered as 1 h infusion was sufficient up to CLCR of 140 mL/min (bacteriostatic) or 100 mL/min (bactericidal). Yet, continuous infusion of 1500 mg MER over 24 h was superior to intermittent dosing and provided sufficient bactericidal PTAs up to the highest studied CLCR value of 160 mL/min. For LZD, the standard dosing regimen of 600 mg BID as 1 h infusion was solely bacteriostatic and PTA was sufficient up to CLCR of 120 mL/min. The present work identified 'front-loaded' therapy with 1200 mg LZD followed by 600 mg as BID being beneficial to augment the antibacterial effect of LZD to an even bactericidal effect in a fraction of patients (8-23% depending on CLCR). Yet, the safety profile of such an intensified regimen must be evaluated before adopting such dosing recommendations in clinical practice. For VAN, standard dosing with 1000 mg BID was found unreliable for the majority of the patients. The present work underlines the value of a loading dose of 30 mg/kg which substantially increased the bacteriostatic PTA which was sufficient for CLCR <80 mL/min. However, the use of intensified dosing intervals (500 mg VAN QID) or continuous infusion of 2000 mg VAN over 24 h was comparable or superior, respectively, at a lower total daily dose than the regimen with the loading doses. Prospective clinical trials that evaluate the proposed alternative dosing regimens for LZD, MER and VAN are warranted.

The hypotheses for the novel dosing strategies for MER, LZD and VAN are based on a clinical trial simulation that used a population PK/PD model that was developed in the present work. This approach represents a methodological advancement to gain utmost information from *in vitro* experiments and to translate the obtained *in vitro* results into the clinical setting. Moreover, drug concentrations were measured *in vitro* in the present work and the different stability profiles of MER, LZD and VAN were quantified by HPLC, which were considered for PK/PD modelling dissecting loss of effect into the sources drug degradation and adaption of *S. aureus*. The elaborated adaptive optimal design approach

of iterative mathematical modelling and experiment conduct yielded a sole basis of quantitative PD data. Future studies could further exploit this approach to reduce the experimental workload to most-informative scenarios. The population PK/PD model was extensively internally and externally evaluated and demonstrated its translational validity by successful prediction of PK/PD indices generated from animal and clinical studies. Future studies on the (combined) use of MER, LZD and VAN should include experiments in dynamic *in vitro* infection models mimicking the PK profiles in plasma and at the target site. With this experimental setup, a potential schedule-dependency of the observed interactions could be assessed. Moreover, the use of dynamic *in vitro* infection models is a prerequisite to study other antibiotics that exhibit a longer post-antibiotic effect than the antibiotics used in the present work to account for persistent drug effects. Future studies should also go beyond measuring viable bacteria expressed as CFU/mL: Quantification of bacterial subpopulations with different susceptibility and persisting cells would provide further mechanistic insight into the interaction between antibiotic and bacterium that could be considered in a further refined PK/PD model.

Apart from the clinical implications, the present work shed light on some methodological issues on frequently used methods for determining the single and combined effect of antibiotics *in vitro*: (i) The conventional checkerboard method based on turbidity, frequently used for PD drug interaction screening, was unable to detect the antagonism between LZD and MER due to the insensitive turbidity threshold ($>10^7$CFU/mL). (ii) The 'dynamic' checkerboard with quantification of bacteria in combination with the elaborated response surface analysis, as applied in the present work, was a powerful tool for screening, evaluation of the nature of the drug interaction and ultimately hypotheses generation for the time-kill curve studies. Hence, future studies should rely on the 'dynamic' checkerboard and interaction results from conventional checkerboard studies should be interpreted with caution and respect to the underlying limitations of the turbidity read-out. (iii) For the time-kill curve studies, the growth-state of the inoculum was highly influential on the obtained *in vitro* antibacterial effect of all investigated antibiotics. Moreover, the influence of the growth-state on the effect did not follow a uniform pattern: Whilst LZD and MER were more active against exponentially growing (i.e. log-phase *S. aureus*) than against resting (i.e. lag-phase *S. aureus*), VAN behaved vice versa and differences were most pronounced leading to a much-less intense antibacterial effect in log-phase compared to lag-phase *S. aureus*. Current literature suggests that this influential factor is currently not considered in many studies and both proper reporting of the inoculum preparation as well as strict standardisation of the experimental procedures seem imperative to increase the comparability of time-kill curve studies in the scientific literature. Further experiments with different inoculum preparation methods (e.g. early vs. late log phase, colony-suspension vs. planktonic dilution) should be systematically evaluated and eventually standardised.

6 Bibliography

[1]   GBD 2013 Mortality and Causes of Death Collaborators. Global , regional and national levels of age-specific mortality and 240 causes of death, 1990-2013 : a systematic analysis for the Global Burden of Disease Study 2013. *Lancet*, 385: 117–171 (2015).

[2]   A. Fleming. On the antibacterial action of cultures of a Penicillium, with special reference to their use in the isolation of B. influenzae. *Brit. J. Exp. Pathol.*, 10: 226–236 (1929).

[3]   C.K. Murray, M.K. Hinkle, H.C. Yun. History of infections associated with combat-related injuries. *J. Trauma*, 64: S221–S231 (2008).

[4]   S.B. Singh. Confronting the challenges of discovery of novel antibacterial agents. *Bioorg. Med. Chem. Lett.*, 24: 3683–3689 (2014).

[5]   C.T. Walsh, T.A. Wencewicz. Prospects for new antibiotics: a molecule-centered perspective. *J. Antibiot. (Tokyo).*, 67: 7–22 (2014).

[6]   M.S. Kinch, E. Patridge, M. Plummer, D. Hoyer. An analysis of FDA-approved drugs for infectious disease: antibacterial agents. *Drug Discov. Today*, 19: 1283–1287 (2014).

[7]   M.A. Cooper, D. Shlaes. Fix the antibiotics pipeline. *Nature*, 472: 32 (2011).

[8]   D.M. Shlaes. Antibiotics. 1st ed., Springer Science & Business Media (2010).

[9]   World Health Organization. Antimicrobial Resistance Global Report on Surveillance. (2014). [http://www.who.int/mediacentre/news/releases/2014/amr-report/en/ - accessed: 2015 May 1]

[10] U. Theuretzbacher. Future antibiotics scenarios: is the tide starting to turn? *Int. J. Antimicrob. Agents*, 34: 15–20 (2009).

[11] E. Meyer, F. Schwab, B. Schroeren-Boersch, P. Gastmeier. Increasing consumption of MRSA-active drugs without increasing MRSA in German ICUs. *Intensive Care Med.*, 37: 1628–32 (2011).

[12] Clinical and Laboratory Standards Institute. Methods for Dilution Antimicrobial Susceptibility Tests for Bacteria That Grow Aerobically: Approved Standard, Seventh Edition M7-A9. (2012).

[13] J. McFarland. The nephelometer: an instrument for estimating the number of bacteria in suspensions used for calculating the opsonic index and for vaccines. *J. Am. Med. Assoc.*, XLIX: 1176–1178 (1907).

[14] J.H. Mueller, J. Hinton. A Protein-Free Medium for Primary Isolation of the Gonococcus and Meningococcus. *Exp. Biol. Med.*, 48: 330–333 (1941).

[15] Clinical and Laboratory Standards Institute. Performance Standards for Antimicrobial Disk Susceptibility Tests; Approved Standard, Eleventh Edition. 32: 76 (2012).

[16] J.D. Tunidge, J.M. Bell. Antimicrobial Susceptibility on Solid Media. In: V. Lorian (Ed.) *Antibiotics in Laboratory Medicine*. 5th ed., Philadelphia, PA, USA, Lippincott Williams & Wilkins: 8–60 (2005).

[17] J.M. Schuurmans, A.S. Nuri Hayali, B.B. Koenders, B.H. ter Kuile. Variations in MIC value caused by differences in experimental protocol. *J. Microbiol. Methods*, 79: 44–47 (2009).

[18] Clinical and Laboratory Standards Institute. Performance Standards for Antimicrobial Susceptibility Testing; Seventeenth Informational Supplement M100-S17. 27: 182 (2007).

[19] M. Mueller, A. De La Peña, H. Derendorf. Issues in pharmacokinetics and pharmacodynamics of anti-infective agents: kill curves versus MIC. *Antimicrob. Agents Chemother.*, 48: 369–377 (2004).

[20] EUCAST. Breakpoint tables on antimicrobial susceptibility testing, version 5.0. (2015). [www.eucast.org - accessed: 2015 May 5]

[21] D. Amsterdam. Susceptibility Testing of Antimicrobials in Liquid Media. In: V. Lorian (Ed.) *Antibiotics in Laboratory Medicine*. 5th ed., Philadelphia, PA, USA, Lippincott Williams & Wilkins: 61–143 (2005).

[22] J. Gloede, C. Scheerans, H. Derendorf, C. Kloft. In vitro pharmacodynamic models to determine the effect of antibacterial drugs. *J. Antimicrob. Chemother.*, 65: 186–201 (2010).

[23] W. Fang. Quantification of Staphylococcus aureus and Escherichia coli in the liquid medium by fluorimetry and its use in phagocytosis assay. *J. Appl. Bacteriol.*, 80: 577–582 (1996).

[24] H. Hanberger, E. Svensson, M. Nilsson, L.E. Nilsson, E.G. Hörnsten, R. Maller. Effects of imipenem on Escherichia coli studied using bioluminescence, viable counting and microscopy. *J. Antimicrob. Chemother.*, 31: 245–60 (1993).

[25] G. Drews. Mikrobiologisches Praktikum. 3rd ed., Berlin, Germany, Springer (2013).

[26] K.L. Laplante, M.J. Rybak. Impact of high-inoculum Staphylococcus aureus on the activities of nafcillin, alone and in combination with gentamicin, in an in vitro pharmacodynamic model. *Antimicrob. Agents Chemother.*, 48: 4665–4672 (2004).

[27] C. Jacqueline, J. Caillon, V. Le Mabecque, A.-F. Miegeville, P.-Y. Donnio, D. Bugnon, G. Potel. In vitro activity of linezolid alone and in combination with gentamicin, vancomycin or rifampicin against methicillin-resistant Staphylococcus aureus by time-kill curve methods. *J. Antimicrob. Chemother.*, 51: 857–64 (2003).

[28]   R. Schwameis, M. Fille, M. Manafi, M. Zeitlinger, R. Sauermann. Enhanced activity of linezolid against Staphylococcus aureus in cerebrospinal fluid. *Res. Microbiol.*, 163: 157–60 (2012).

[29]   P. Grohs, M.-D. Kitzis, L. Gutmann. In Vitro Bactericidal Activities of Linezolid in Combination with Vancomycin, Gentamicin, Ciprofloxacin, Fusidic Acid, and Rifampin against Staphylococcus aureus. *Antimicrob. Agents Chemother.*, 47: 418–420 (2003).

[30]   S. Schmidt, S.N. Sabarinath, D. Abbanat, P. Manitpisitkul, S. Sha, H. Derendorf. Modeling of the In Vitro Activities of Oxazolidinone Antimicrobial Agents against Methicillin-Resistant Staphylococcus aureus. *Antimicrob. Agents Chemother.*, 53: 5039–45 (2009).

[31]   C. Scheerans. PhD thesis. Martin-Luther-Universitaet, Halle-Wittenberg, Germany (2010).

[32]   S.K. Pillai, R.C. Moellering Jr, G.M. Eliopoulos. Antimicrobial Combinations. In: V. Lorian (Ed.) *Antibiotics in Laboratory Medicine*. 5th ed., Philadelphia, PA, USA, Lippincott Williams & Wilkins: 365–440 (2005).

[33]   C.R. Bonapace, J.A. Bosso, L. V Friedrich, R.L. White. Comparison of methods of interpretation of checkerboard synergy testing. *Diagn. Microbiol. Infect. Dis.*, 44: 363–366 (2002).

[34]   F.C. Odds. Synergy, antagonism, and what the chequerboard puts between them. *J. Antimicrob. Chemother.*, 52: 1 (2003).

[35]   K.H. Rand, H.J. Houck, P. Brown, D. Bennett. Reproducibility of the microdilution checkerboard method for antibiotic synergy. *Antimicrob. Agents Chemother.*, 37: 613–5 (1993).

[36]   B. Balke, M. Hogardt, S. Schmoldt, L. Hoy, H. Weissbrodt, S. Häussler. Evaluation of the E test for the assessment of synergy of antibiotic combinations against multiresistant Pseudomonas aeruginosa isolates from cystic fibrosis patients. *Eur. J. Clin. Microbiol. Infect. Dis.*, 25: 25–30 (2006).

[37]   C. Jacqueline, D. Navas, E. Batard, A.-F. Miegeville, V. Le Mabecque, M.-F. Kergueris, D. Bugnon, G. Potel, J. Caillon. In vitro and in vivo synergistic activities of linezolid combined with subinhibitory concentrations of imipenem against methicillin-resistant Staphylococcus aureus. *Antimicrob. Agents Chemother.*, 49: 45–51 (2005).

[38]   C. Jacqueline, J. Caillon, O. Grossi, V. Le Mabecque, A.-F. Miegeville, D. Bugnon, E. Batard, G. Potel. In vitro and in vivo assessment of linezolid combined with ertapenem: a highly synergistic combination against methicillin-resistant Staphylococcus aureus. *Antimicrob. Agents Chemother.*, 50: 2547–9 (2006).

[39] J.S. Barrett, M.J. Fossler, K.D. Cadieu, M.R. Gastonguay. Pharmacometrics: a multidisciplinary field to facilitate critical thinking in drug development and translational research settings. *J. Clin. Pharmacol.*, 48: 632–649 (2008).

[40] E. Nelson. Kinetics of drug absorption, distribution, metabolism, and excretion. *J. Pharm. Sci.*, 50: 181–192 (1961).

[41] J. Gabrielsson, D. Weiner. Non-compartmental analysis. *Methods Mol. Biol.*, 929: 377–389 (2012).

[42] P.L. Bonate. Pharmacokinetic-Pharmacodynamic Modeling and Simulation. Boston, MA, Springer US (2011).

[43] M. Rowland, C. Peck, G. Tucker. Physiologically-based pharmacokinetics in drug development and regulatory science. *Annu. Rev. Pharmacol. Toxicol.*, 51: 45–73 (2011).

[44] L.B. Sheiner, S.L. Beal. Evaluation of methods for estimating population pharmacokinetics parameters. I. Michaelis-Menten model: routine clinical pharmacokinetic data. *J. Pharmacokinet. Biopharm.*, 8: 553–571 (1980).

[45] L.B. Sheiner, S.L. Beal. Evaluation of methods for estimating population pharmacokinetic parameters. II. Biexponential model and experimental pharmacokinetic data. *J. Pharmacokinet. Biopharm.*, 9: 635–651 (1981).

[46] N. Safdar, J. Handelsman, D.G. Maki. Does combination antimicrobial therapy reduce mortality in Gram-negative bacteraemia ? A meta-analysis. *Lancet Infect. Dis.*, 4: 519–527 (2004).

[47] L. Michaelis, M. Menten. Die Kinetik der Invertinwirkung. *Biochem. Z.*, 49: 333–369 (1913).

[48] A.A. Firsov, V.M. Chernykh, S.M. Navashin. Quantitative analysis of antimicrobial effect kinetics in an in vitro dynamic model. *Antimicrob. Agents Chemother.*, 34: 1312–1317 (1990).

[49] J.E. Tisdale, M.T. Pasko, J.M. Mylotte. Antipseudomonal activity of simulated infusions of gentamicin alone or with piperacillin assessed by serum bactericidal rate and area under the killing curve. *Antimicrob. Agents Chemother.*, 33: 1500–1505 (1989).

[50] A.A. Firsov, S.N. Vostrov, A.A. Shevchenko, G. Cornaglia. Parameters of bacterial killing and regrowth kinetics and antimicrobial effect examined in terms of area under the concentration-time curve relationships: action of ciprofloxacin against Escherichia coli in an in vitro dynamic model. *Antimicrob. Agents Chemother.*, 41: 1281–7 (1997).

[51] E.B. Hirsch, K.R. Ledesma, K.-T. Chang, M.S. Schwartz, M.R. Motyl, V.H. Tam. In vitro activity of MK-7655, a novel β-lactamase inhibitor, in combination with

imipenem against carbapenem-resistant Gram-negative bacteria. *Antimicrob. Agents Chemother.*, 56: 3753–7 (2012).

[52] A.N. Boucher, V.H. Tam. Mathematical formulation of additivity for antimicrobial agents. *Diagn. Microbiol. Infect. Dis.*, 55: 319–325 (2006).

[53] W.R. Greco, G. Bravo, J.C. Parsons. The search for synergy: a critical review from a response surface perspective. *Pharmacol. Rev.*, 47: 331–85 (1995).

[54] S. Loewe. The problem of synergism and antagonism of combined drugs. *Arzneimittelforschung*, 3: 285–290 (1953).

[55] C.I. Bliss. The toxicity of poisons applied jointly. *Ann. Appl. Biol.*, 26: 585–615 (1939).

[56] E.I. Nielsen, L.E. Friberg. Pharmacokinetic-pharmacodynamic modeling of antibacterial drugs. *Pharmacol. Rev.*, 65: 1053–90 (2013).

[57] W.J. Jusko. Pharmacodynamics of chemotherapeutic effects: dose-time-response relationships for phase-nonspecific agents. *J. Pharm. Sci.*, 60: 892–895 (1971).

[58] E.I. Nielsen, A. Viberg, E. Löwdin, O. Cars, M.O. Karlsson, M. Sandström. Semimechanistic pharmacokinetic/pharmacodynamic model for assessment of activity of antibacterial agents from time-kill curve experiments. *Antimicrob. Agents Chemother.*, 51: 128–36 (2007).

[59] W. Craig. Basic pharmacodynamics of antibacterials with clinical applications to the use of β-lactams, glycopeptides, and linezolid. *Infect. Dis. Clin. North Am.*, 17: 479–501 (2003).

[60] H. Eagle, R. Fleischman, A.D. Musselman. Effect of schedule of administration on the therapeutic efficacy of penicillin. *Am. J. Med.*, 9: 280–299 (1950).

[61] B. Vogelman, S. Gudmundsson, J. Leggett, J. Turnidge, S. Ebert, W.A. Craig. Correlation of antimicrobial pharmacokinetic parameters with therapeutic efficacy in an animal model. *J. Infect. Dis.*, 158: 831–847 (1988).

[62] B. Vogelman, S. Gudmundsson, J. Turnidge, J. Leggett, W.A. Craig. In vivo postantibiotic effect in a thigh infection in neutropenic mice. *J. Infect. Dis.*, 157: 287–298 (1988).

[63] W.A. Craig, J. Redington, S.C. Ebert. Pharmacodynamics of amikacin in vitro and in mouse thigh and lung infections. *J. Antimicrob. Chemother.*, 27 Suppl C: 29–40 (1991).

[64] M.A. Zeitlinger, R. Sauermann, F. Traunmüller, A. Georgopoulos, M. Müller, C. Joukhadar. Impact of plasma protein binding on antimicrobial activity using time-killing curves. *J. Antimicrob. Chemother.*, 54: 876–880 (2004).

[65] A. Barger, C. Fuhst, B. Wiedemann. Pharmacological indices in antibiotic therapy. *J. Antimicrob. Chemother.*, 52: 893–8 (2003).

[66] W.A. Craig. Interrelationship between pharmacokinetics and pharmacodynamics in determining dosage regimens for broad-spectrum cephalosporins. *Diagn. Microbiol. Infect. Dis.*, 22: 89–96 (1995).

[67] S. Beck, S.G. Wicha, C. Kloft, M.G. Kees. Pharmakokinetik und Pharmakodynamik in der Antibiotikatherapie. *Anaesthesist*,: 1–7 (2014).

[68] F. Scaglione. Can PK/PD be used in everyday clinical practice. *Int. J. Antimicrob. Agents*, 19: 349–53 (2002).

[69] V. Fedorov, S.L. Leonov. Optimal Design for Nonlinear Response Models. 1st ed., Boca Raton, Florida, CRC Press (2013).

[70] L.B. Sheiner. Learning versus confirming in clinical drug development. *Clin. Pharmacol. Ther.*, 61: 275–91 (1997).

[71] A. Maloney, M.O. Karlsson, U.S.H. Simonsson. Optimal adaptive design in clinical drug development: a simulation example. *J. Clin. Pharmacol.*, 47: 1231–1243 (2007).

[72] J.A. Roberts, M.H. Abdul-Aziz, J. Lipman, J.W. Mouton, A.A. Vinks, T.W. Felton, W.W. Hope, A. Farkas, M.N. Neely, J.J. Schentag, G. Drusano, O.R. Frey, U. Theuretzbacher, J.L. Kuti. Individualised antibiotic dosing for patients who are critically ill: challenges and potential solutions. *Lancet. Infect. Dis.*, 14: 498–509 (2014).

[73] W.A. Craig. The pharmacology of meropenem, a new carbapenem antibiotic. *Clin. Infect. Dis.*, 24 Suppl 2: S266–S275 (1997).

[74] J.S. Kahan, F.M. Kahan, R. Goegelman, S.A. Currie, M. Jackson, E.O. Stapley, T.W. Miller, A.K. Miller, D. Hendlin, S. Mochales, S. Hernandez, H.B. Woodruff, J. Birnbaum. Thienamycin, a new beta-lactam antibiotic. I. Discovery, taxonomy, isolation and physical properties. *J. Antibiot. (Tokyo).*, 32: 1–12 (1979).

[75] A. Tomasz. The mechanism of the irreversible antimicrobial effects of penicillins: how the beta-lactam antibiotics kill and lyse bacteria. *Annu. Rev. Microbiol.*, 33: 113–37 (1979).

[76] H.C. Neu, T.D. Gootz. Antimicrobial Chemotherapy. Med. Microbiol. : 1–34 (1996). [http://www.ncbi.nlm.nih.gov/pubmed/21413283 - accessed: 2015 May 15]

[77] C.W. Stratton. Molecular Mechanisms of Action for Antimicrobial Agents: General Principles and Mechanisms for Selected Classes of Antibiotics. In: V. Lorian (Ed.) *Antibiotics in Laboratory Medicine*. 5th ed., Philadelphia, PA, USA, Lippincott Williams & Wilkins: 532–563 (2005).

[78] C.A. DeRyke, M.A. Banevicius, H.W. Fan, D.P. Nicolau. Bactericidal activities of meropenem and ertapenem against extended-spectrum-β-lactamase-producing Escherichia coli and Klebsiella pneumoniae in a neutropenic mouse thigh model. *Antimicrob. Agents Chemother.*, 51: 1481–1486 (2007).

[79] EUCAST. Meropenem - Rationale for the EUCAST clinical breakpoints, version 1.5. (2009).

[80] R. Bax, W. Bastain, A. Featherstone, D. Wilkinson, M. Hutchison. The pharmacokinetics of meropenem in volunteers. *J. Antimicrob. Chemother.*, 24: 311 (1989).

[81] Astra Zeneca. Meronem® - German summary of product characteristics (Fachinformation). (2011).

[82] F. Tomaselli, A. Maier, V. Matzi, F.M. Smolle-Jüttner, P. Dittrich. Penetration of meropenem into pneumonic human lung tissue as measured by in vivo microdialysis. *Antimicrob. Agents Chemother.*, 48: 2228–32 (2004).

[83] J.M. Dulhunty, J.A. Roberts, J.S. Davis, S.A.R. Webb, R. Bellomo, C. Gomersall, C. Shirwadkar, G.M. Eastwood, J. Myburgh, D.L. Paterson, J. Lipman. Continuous infusion of beta-lactam antibiotics in severe sepsis: A multicenter double-blind, randomized controlled trial. *Clin. Infect. Dis.*, 56: 236–244 (2013).

[84] G.L. Drusano, H. Lode, J.R. Edwards. Meropenem: clinical response in relation to in vitro susceptibility. *Clin. Microbiol. Infect.*, 6: 185–94 (2000).

[85] S. Swaney, H. Aoki. The oxazolidinone linezolid inhibits initiation of protein synthesis in bacteria. *Antimicrob. Agents Chemother.*, 42: 3251–3255 (1998).

[86] G.E. Zurenko, B.H. Yagi, R.D. Schaadt, J.W. Allison, J.O. Kilburn, S.E. Glickman, D.K. Hutchinson, M.R. Barbachyn, S.J. Brickner. In vitro activities of U-100592 and U-100766, novel oxazolidinone antibacterial agents. *Antimicrob. Agents Chemother.*, 40: 839–45 (1996).

[87] R. Wise, J.M. Andrews, F.J. Boswell, J.P. Ashby. The in-vitro activity of linezolid (U-100766) and tentative breakpoints. *J. Antimicrob. Chemother.*, 42: 721–8 (1998).

[88] R.N. Jones, D.M. Johnson, M.E. Erwin. In vitro antimicrobial activities and spectra of U-100592 and U-100766, two novel fluorinated oxazolidinones. *Antimicrob. Agents Chemother.*, 40: 720–726 (1996).

[89] A. Schumacher, R. Trittler, J.A. Bohnert, K. Kümmerer, J.M. Pagès, W. V. Kern. Intracellular accumulation of linezolid in Escherichia coli, Citrobacter freundii and Enterobacter aerogenes: Role of enhanced efflux pump activity and inactivation. *J. Antimicrob. Chemother.*, 59: 1261–1264 (2007).

[90] Pfizer. ZYVOXID® - German summary of product characteristics (Fachinformation). (2011).

[91] A.P. MacGowan. Pharmacokinetic and pharmacodynamic profile of linezolid in healthy volunteers and patients with Gram-positive infections. *J. Antimicrob. Chemother.*, 51 Suppl 2: ii17–ii25 (2003).

[92] P. Dehghanyar, C. Burger, M. Zeitlinger, F. Islinger, F. Kovar, M. Muller, C. Kloft, C. Joukhadar. Penetration of linezolid into soft tissues of healthy volunteers after single and multiple doses. *Antimicrob. Agents Chemother.*, 49: 2367 (2005).

[93] C. Buerger, N. Plock, P. Dehghanyar, C. Joukhadar, C. Kloft. Pharmacokinetics of unbound linezolid in plasma and tissue interstitium of critically ill patients after multiple dosing using microdialysis. *Antimicrob. Agents Chemother.*, 50: 2455–63 (2006).

[94] E. Boselli, D. Breilh, T. Rimmelé, S. Djabarouti, J. Toutain, D. Chassard, M.-C. Saux, B. Allaouchiche. Pharmacokinetics and intrapulmonary concentrations of linezolid administered to critically ill patients with ventilator-associated pneumonia. *Crit. Care Med.*, 33: 1529–1533 (2005).

[95] M.S. Dryden. Linezolid pharmacokinetics and pharmacodynamics in clinical treatment. *J. Antimicrob. Chemother.*, 66 Suppl 4: iv7–iv15 (2011).

[96] M. Rybak. The pharmacokinetic and pharmacodynamic properties of vancomycin. *Clin. Infect. Dis.*, 42: 35–39 (2006).

[97] P.M. Small, H.F. Chambers. Vancomycin for Staphylococcus aureus endocarditis in intravenous drug users. *Antimicrob. Agents Chemother.*, 34: 1227–1231 (1990).

[98] D.P. Healy, R.E. Polk, M.L. Garson, D.T. Rock, T.J. Comstock. Comparison of steady-state pharmacokinetics of two dosage regimens of vancomycin in normal volunteers. *Antimicrob. Agents Chemother.*, 31: 393–397 (1987).

[99] Riemser Arzneimittel AG. Vancomycin "Lederle"- German summary of product characteristics (Fachinformation). (2003).

[100] K. Skhirtladze, D. Hutschala, T. Fleck, F. Thalhammer, M. Ehrlich, T. Vukovich, M. Mu, E.M. Tschernko. Impaired Target Site Penetration of Vancomycin in Diabetic Patients following Cardiac Surgery. 50: 1372–1375 (2006).

[101] H. Georges, O. Leroy, S. Alfandari, B. Guery, M. Roussel-Delvallez, C. Dhennain, G. Beaucaire. Pulmonary disposition of vancomycin in critically ill patients. *Eur. J. Clin. Microbiol. Infect. Dis.*, 16: 385–8 (1997).

[102] M. Rybak, B. Lomaestro, J.C. Rotschafer, R. Moellering, W. Craig, M. Billeter, J.R. Dalovisio, D.P. Levine, C. Reilly. Therapeutic monitoring of vancomycin in adult patients: A consensus review of the American Society of Health-System Pharmacists, the Infectious Diseases Society of America, and the Society of Infectious Diseases Pharmacists. *Am. J. Heal. Pharm.*, 66: 82–98 (2009).

[103] G.M. Eliopoulos, C.T. Eliopoulos. Antibiotic combinations : Should they be tested? *Clin. Microbiol. Rev.*, 1: 139–156 (1988).

[104] A. Kumar, P. Ellis, Y. Arabi, D. Roberts, B. Light, J.E. Parrillo, P. Dodek, G. Wood, A. Kumar, D. Simon, C. Peters, M. Ahsan, D. Chateau. Initiation of inappropriate antimicrobial therapy results in a fivefold reduction of survival in human septic shock. *Chest*, 136: 1237–48 (2009).

[105] American Thoracic Society. Guidelines for the management of adults with hospital-acquired, ventilator-associated, and healthcare-associated pneumonia. *Am. J. Respir. Crit. Care Med.*, 171: 388–416 (2005).

[106] P. Yeh, A.I. Tschumi, R. Kishony. Functional classification of drugs by properties of their pairwise interactions. *Nat. Genet.*, 38: 489–94 (2006).

[107] G. Miranda-Novales, B.E. Leaños-Miranda, M. Vilchis-Pérez, F. Solórzano-Santos. In vitro activity effects of combinations of cephalothin , dicloxacillin , imipenem , vancomycin and amikacin against methicillin-resistant Staphylococcus spp . strains. *Ann. Clin. Microbiol. Antimicrob.*, 5: 1–5 (2006).

[108] R. Chait, A. Craney, R. Kishony. Antibiotic interactions that select against resistance. *Nature*, 446: 668–71 (2007).

[109] R. Pena-Miller, D. Laehnemann, G. Jansen, A. Fuentes-Hernandez, P. Rosenstiel, H. Schulenburg, R. Beardmore. When the most potent combination of antibiotics selects for the greatest bacterial load: the smile-frown transition. *PLoS Biol.*, 11: e1001540 (2013).

[110] R.A. Harvey. Lippincott's Illustrated Reviews: Microbiology. 3rd ed., Baltimore, MD, USA, Lippincott Williams & Wilkins (2013).

[111] J.F. Barrett. MRSA-what is it, and how do we deal with the problem? *Expert Opin. Ther. Targets*, 9: 253–65 (2005).

[112] T.J. Foster. Immune evasion by staphylococci. *Nat. Rev. Microbiol.*, 3: 948–958 (2005).

[113] D.C. (Pitt) Angus, T. van der Poll. Severe sepsis and septic shock. *N. Engl. J. Med.*, 369: 840–51 (2013).

[114] M.M. Dinges, P.M. Orwin, P.M. Schlievert. Exotoxins of Staphylococcus aureus. *Clin. Microbiol. Rev.*, 13: 16–34 (2000).

[115] R.P. Dellinger, M.M. Levy, A. Rhodes, D. Annane, H. Gerlach, S.M. Opal, J.E. Sevransky, C.L. Sprung, I.S. Douglas, R. Jaeschke, T.M. Osborn, M.E. Nunnally, S.R. Townsend, K. Reinhart, R.M. Kleinpell, *et al.* Surviving Sepsis Campaign. *Crit. Care Med.*, 41: 580–637 (2013).

[116] C.-I. Kang, S.-H. Kim, W.B. Park, K.-D. Lee, H.-B. Kim, E.-C. Kim, M.-D. Oh, K.-W. Choe. Bloodstream infections caused by antibiotic-resistant gram-negative bacilli: risk factors for mortality and impact of inappropriate initial antimicrobial therapy on outcome. *Antimicrob. Agents Chemother.*, 49: 760–6 (2005).

[117] European Antimicrobial Resistance Surveillance System. Susceptibility of Staphylococcus aureus Isolates to Methicillin in Participating Countries in 2012. (2012). [http://www.ecdc.europa.eu/en/healthtopics/antimicrobial_resistance/database/pages/table_reports.aspx - accessed: 2015 Jan 23]

[118] R. Wise, J.P. Ashby, J.M. Andrews. The antibacterial activity of meropenem in combination with gentamicin or vancomycin. *J. Antimicrob. Chemother.*, 24 Suppl A: 233–8 (1989).

[119] A.L. Koch. Growth measurement. In: P. Gerhardt, R.G.E. Murray, W.A. Wood, N.R. Krieg (Eds.) *Methods for general and molecular bacteriology.* 1st ed., Washington, ASM Press: 248–277 (1994).

[120] EMA. Guideline on bioanalytical method validation. (2012).

[121] C. Scheerans, S.G. Wicha, J. Michael, H. Derendorf, C. Kloft. Concentration-response studies and modelling of the pharmacodynamics of linezolid: Staphylococcus aureus versus Enterococcus faecium. *Int. J. Antimicrob. Agents*, 45: 54–60 (2015).

[122] J. Michael. PhD thesis. Martin-Luther-Universitaet, Halle-Wittenberg, Germany (2011).

[123] Pro-Lab Diagnostics. Microbank - Bacterial and Fungal Storage System (Manual). (2011).

[124] V. Lorian. Antibiotics in Laboratory Medicine. 5th ed., Lippincott Williams & Wilkins (2005).

[125] D.P. Nicolau. Pharmacokinetic and pharmacodynamic properties of meropenem. *Clin. Infect. Dis.*, 47 Suppl 1: S32–40 (2008).

[126] G.A. Pankey, L.D. Sabath. Clinical relevance of bacteriostatic versus bactericidal mechanisms of action in the treatment of Gram-positive bacterial infections. *Clin. Infect. Dis.*, 38: 864–70 (2004).

[127] R Core Team. R. A language and Environment for Statistical Computing. R 3.1.1, Vienna, Austria, R Foundation for Statistical Computing (2015).

[128] K. Soetaert, T. Petzoldt, R.W. Setzer. Solving differential equations in R. *R J.*, 2: 5–15 (2010).

[129] W.N. Venables, B.D. Ripley. Modern Applied Statistics with S. 4th ed., Springer (2003).

[130] H. Wickman. ggplot2: Elegant graphics for data analysis. 0.9.3.1, New York, Springer (2009). [http://had.co.nz/ggplot2/book

[131] E. Limpert, W.A. Stahel, M. Abbt. Log-normal Distributions across the Sciences: Keys and Clues. *Bioscience*, 51: 341 (2001).

[132] W.K. Newey, D. McFadden. Large sample estimation and hypothesis testing. *Handb. Econom.*, 4: 2111–2245 (1994).

[133] B.Y.B. Efron, D. V. Hinkley. Assessing the accuracy of the maximum likelihood estimator: Observed versus expected Fisher information. *Biometrika*, 65: 457–483 (1978).

[134] D.R. Mould, R.N. Upton. Basic concepts in population modeling, simulation, and model-based drug development-part 2: introduction to pharmacokinetic modeling methods. *CPT pharmacometrics Syst. Pharmacol.*, 2: e38 (2013).

[135] H. Akaike. A new look at the statistical model identification. *IEEE Trans. Automat. Contr.*, 19: 716–723 (1974).

[136] C.M. Hurvich, C.-L. Tai. Regression and time series model selection in small samples. *Biometrika*, 76: 297–307 (1989).

[137] A.V. Hill. The possible effects of the aggregations of the molecules of haemoglobin on its dissociation curves. *J. Physiol.*, 40: 4–7 (1910).

[138] M.N. Prichard, C. Shipman. A three-dimensional model to analyze drug-drug interactions. *Antiviral Res.*, 14: 181–205 (1990).

[139] C.H. Jackson. Multi-State Models for Panel Data: The {msm} Package for "R." *J. Stat. Softw.*, 38: 1–29 (2011).

[140] J. Bland, D. Altman. Multiple significance tests: the Bonferroni method. *Brithish Med. J.*, 310: 170 (1995).

[141] J.B. Bulitta, N.S. Ly, J.C. Yang, A. Forrest, W.J. Jusko, B.T. Tsuji. Development and qualification of a pharmacodynamic model for the pronounced inoculum effect of ceftazidime against Pseudomonas aeruginosa. *Antimicrob. Agents Chemother.*, 53: 46–56 (2009).

[142] A.F. Mohamed, E.I. Nielsen, O. Cars, L.E. Friberg. Pharmacokinetic-pharmacodynamic model for gentamicin and its adaptive resistance with predictions of dosing schedules in newborn infants. *Antimicrob. Agents Chemother.*, 56: 179–88 (2012).

[143] V.H. Tam, A.N. Schilling, M. Nikolaou. Modelling time-kill studies to discern the pharmacodynamics of meropenem. *J. Antimicrob. Chemother.*, 55: 699–706 (2005).

[144] B. Efron. The Jackknife, the Bootstrap and Other Resampling Plans. Society for Industrial and Applied Mathematics (1982).

[145] A.C. Davison, D.V. Hinkley. Bootstrap Methods and Their Applications. Cambridge, Cambrigde University Press (1997).

[146] S.R. Singh, A.E. Bacon, D.C. Young, K.A. Couch. In vitro 24-hour time-kill studies of vancomycin and linezolid in combination versus methicillin-resistant Staphylococcus aureus. *Antimicrob. Agents Chemother.*, 53: 4495–7 (2009).

[147] H.K. Johansen, G.J. Jensen, R.B. Dessau, B. Lundgren, Frimodt-Moller. Antagonism between penicillin and erythromycin against Streptococcus pneumoniae in vitro and in vivo. *J. Antimicrob. Chemother.*, 46: 973–980 (2000).

[148] J.L. Weeks, E.O. Mason, C.J. Baker. Antagonism of ampicillin and chloramphenicol for meningeal isolates of group B streptococci. *Antimicrob. Agents Chemother.*, 20: 281–285 (1981).

[149] E.I. Nielsen, O. Cars, L.E. Friberg. Pharmacokinetic/pharmacodynamic (PK/PD) indices of antibiotics predicted by a semimechanistic PKPD model: a step toward model-based dose optimization. *Antimicrob. Agents Chemother.*, 55: 4619–30 (2011).

[150] T. Sasaki, H. Takane, K. Ogawa, S. Isagawa, T. Hirota, S. Higuchi, T. Horii, K. Otsubo, I. Ieiri. Population pharmacokinetic and pharmacodynamic analysis of linezolid and a hematologic side effect, thrombocytopenia, in Japanese patients. *Antimicrob. Agents Chemother.*, 55: 1867–73 (2011).

[151] D.W. Cockcroft, M.H. Gault. Prediction of creatinine clearance from serum creatinine. *Nephron*, 16: 31–41 (1976).

[152] E. Cholongitas, G. V. Papatheodoridis, M. Vangeli, N. Terreni, D. Patch, A.K. Burroughs. Systematic review: The model for end-stage liver disease - Should it replace Child-Pugh's classification for assessing prognosis in cirrhosis? *Aliment. Pharmacol. Ther.*, 22: 1079–1089 (2005).

[153] C. Li, J.L. Kuti, C.H. Nightingale, D.P. Nicolau. Population pharmacokinetic analysis and dosing regimen optimization of meropenem in adult patients. *J. Clin. Pharmacol.*, 46: 1171–8 (2006).

[154] P. Llopis-Salvia, N. V. Jiménez-Torres. Population pharmacokinetic parameters of vancomycin in critically ill patients. *J. Clin. Pharm. Ther.*, 31: 447–454 (2006).

[155] M.G. Kees, S.G. Wicha, A. Seefeld, F. Kees, C. Kloft. Unbound fraction of vancomycin in intensive care unit patients. *J. Clin. Pharmacol.*, 54: 318–23 (2014).

[156] J.W. Mouton, M.N. Dudley, O. Cars, H. Derendorf, G.L. Drusano. Standardization of pharmacokinetic/pharmacodynamic (PK/PD) terminology for anti-infective drugs: an update. *J. Antimicrob. Chemother.*, 55: 601–7 (2005).

[157] C.R. Rayner, A. Forrest, A.K. Meagher, M.C. Birmingham, J.J. Schentag. Clinical Pharmacodynamics of Linezolid in Seriously Ill Patients Treated in a Compassionate Use Programme. *Clin. Pharmacokinet.*, 42: 1411–1423 (2003).

[158] N. Metropolis, S. Ulam. The Monte Carlo method. In: *Journal of the American Statistical Association*. : 335–341 (1949).

[159] NIH open chemistry database. Compound summary for meropenem. [http://pubchem.ncbi.nlm.nih.gov/compound/meropenem - accessed: 2015 Aug 14]

[160] NIH open chemistry database. Compound summary for linezolid. [http://pubchem.ncbi.nlm.nih.gov/compound/441401 - accessed: 2015 Aug 14]

[161] NIH open chemistry database. Compound summary for vancomycin. [http://pubchem.ncbi.nlm.nih.gov/compound/vancomycin - accessed: 2015 Aug 14]

[162] J.A. Nelder, R. Mead. A Simplex Method for Function Minimization. *Comput. J.*, 7: 308–313 (1965).

[163] R. Fletcher, C.M. Reeves. Function minimization by conjugate gradients. *Comput. J.*, 7: 149–154 (1964).

[164] H. Eagle, A.D. Musselman. The rate of bactericidal action of penicillin in vitro as a function of its concentration, and its paradoxically reduced activity at high concentrations against certain organisms. *J. Exp. Med.*, 88: 99–131 (1948).

[165] M. Friendly. Corrgrams: Exploratory displays for correlation matrices. *Am. Stat.*, 34: 1447–9 (2002).

[166] K. Kipper, K. Anier, I. Leito, J. Karjagin, K. Oselin, K. Herodes. Rapid Determination of Meropenem in Biological Fluids by LC: Comparison of Various Methods for Sample Preparation and Investigation of Meropenem Stability. *Chromatographia*, 70: 1423–1427 (2009).

[167] B.C. McWhinney, S.C. Wallis, T. Hillister, J. a. Roberts, J. Lipman, J.P.J. Ungerer. Analysis of 12 beta-lactam antibiotics in human plasma by HPLC with ultraviolet detection. *J. Chromatogr. B Anal. Technol. Biomed. Life Sci.*, 878: 2039–2043 (2010).

[168] M.C. Verdier, O. Tribut, P. Tattevin, Y. Le Tulzo, C. Michelet, D. Bentué-Ferrer. Simultaneous Determination of 12 {beta}-Lactam Antibiotics in Human Plasma by High-Performance Liquid Chromatography with UV Detection: Application to Therapeutic Drug Monitoring. *Antimicrob. Agents Chemother.*, 55: 4873–4879 (2011).

[169] T. Ohmori, A. Suzuki, T. Niwa, H. Ushikoshi, K. Shirai, S. Yoshida, S. Ogura, Y. Itoh. Simultaneous determination of eight β-lactam antibiotics in human serum by liquid chromatography-tandem mass spectrometry. *J. Chromatogr. B Anal. Technol. Biomed. Life Sci.*, 879: 1038–1042 (2011).

[170] B.B. Ba, C. Arpin, B. Bikie Bi Nso, V. Dubois, M.-C. Saux, C. Quentin. Activity of Linezolid in an In Vitro Pharmacokinetic-Pharmacodynamic Model Using Different Dosages and Staphylococcus aureus and Enterococcus faecalis Strains with and without a Hypermutator Phenotype. *Antimicrob. Agents Chemother.*, 54: 1443–52 (2010).

[171] M. Hagihara, C. Sutherland, D.P. Nicolau. Development of HPLC methods for the determination of vancomycin in human plasma, mouse serum and bronchoalveolar lavage fluid. *J. Chromatogr. Sci.*, 51: 201–207 (2013).

[172] D.W. Backes, H.I. Aboleneen, J.A. Simpson. Quantitation of vancomycin and its crystalline degradation product (CDP-1) in human serum by high performance liquid chromatography. *J. Pharm. Biomed. Anal.*, 16: 1281–1287 (1998).

[173] S. Swoboda, M. Ober, K. Anagnostakos, H.K. Geiss, M.A. Weigand, T. Hoppe-Tichy. A simple isocratic HPLC assay to determine linezolid concentrations in different biomatrices for in vivo and in vitro studies. *Clin. Chem. Lab. Med.*, 45: 1019–22 (2007).

[174] C. Buerger, C. Joukhadar, M. Muller, C. Kloft. Development of a liquid chromatography method for the determination of linezolid and its application to in vitro and human microdialysis samples. *J. Chromatogr. B*, 796: 155–164 (2003).

[175] T. Satyanarayana Raju, O. Vishweshwari Kutty, V. Ganesh, P. Yadagiri Swamy, T.S. Raju, O.V. Kutty, P.Y. Swamy. A validated stability-indicating LC method for the separation of enantiomer and potential impurities of Linezolid using polar organic mode. *J. Pharm. Anal.*, 2: 272–278 (2012).

[176] C.W. Stratton, L.S. Weeks. Effect of human serum on the bactericidal activity of daptomycin and vancomycin against staphylococcal and enterococcal isolates as determined by time-kill kinetic studies. *Diagn. Microbiol. Infect. Dis.*, 13: 245–52 (1990).

[177] S. Lemaire, F. Van Bambeke, M.P. Mingeot-Leclercq, P.M. Tulkens. Activity of three β-lactams (ertapenem, meropenem and ampicillin) against intraphagocytic Listeria monocytogenes and Staphylococcus aureus. *J. Antimicrob. Chemother.*, 55: 897–904 (2005).

[178] E. Viaene, H. Chanteux, H. Servais, M.P. Mingeot-Leclercq, P.M. Tulkens. Comparative stability studies of antipseudomonal β-lactams for potential administration through portable elastomeric pumps (home therapy for cystic fibrosis patients) and motor-operated syringes (intensive care units). *Antimicrob. Agents Chemother.*, 46: 2327–2332 (2002).

[179] T. Katsube, Y. Yano, Y. Yamano, T. Munekage, N. Kuroda, M. Takano. Pharmacokinetic-pharmacodynamic modeling and simulation for bactericidal effect in an in vitro dynamic model. *J. Pharm. Sci.*, 97: 4108–4117 (2008).

[180] A. Fey, S. Eichler, R. Christen, M.G. Ho, C.A. Guzma. Establishment of a Real-Time PCR-Based Approach for Accurate Quanti cation of Bacterial RNA Targets in Water, Using. *Microbiology*, 70: 3618–3623 (2004).

[181] C.J. Smith, A.M. Osborn. Advantages and limitations of quantitative PCR (Q-PCR)-based approaches in microbial ecology. *FEMS Microbiol. Ecol.*, 67: 6–20 (2009).

[182] E. Goebgen. Diploma thesis. Martin-Luther-Universitaet, Halle-Wittenberg, Germany (2014).

[183] EUCAST. Linezolid - Rationale for the EUCAST clinical breakpoints, version 1.0. (2005).

[184] EUCAST. Vancomycin - Rationale for the EUCAST clinical breakpoints, version 2.1. (2010).

[185] Clinical and Laboratory Standards Institute. Methods for determining bactericidal activity of antimicrobial agents: approved guideline. (1999).

[186] M.T. Sweeney, G.E. Zurenko. In Vitro Activities of Linezolid Combined with Other Antimicrobial Agents against Staphylococci, Enterococci, Pneumococci, and Selected Gram-Negative Organisms. *Antimicrob. Agents Chemother.*, 47: 1902–1906 (2003).

[187] U. Zeidler, M.E. Bougnoux, A. Lupan, O. Helynck, A. Doyen, Z. Garcia, N. Sertour, C. Clavaud, H. Munier-Lehmann, C. Saveanu, C. d'Enfert. Synergy of the antibiotic colistin with echinocandin antifungals in candida species. *J. Antimicrob. Chemother.*, 68: 1285–1296 (2013).

[188] R. Pereira, M.J. Cole, C.A. Ison. Combination therapy for gonorrhoea: In vitro synergy testing. *J. Antimicrob. Chemother.*, 68: 640–643 (2013).

[189] X. Gonzalo, F. Drobniewski. Is there a place for ß-lactams in the treatment of multidrug-resistant/extensively drug-resistant tuberculosis? Synergy between meropenem and amoxicillin/clavulanate. *J. Antimicrob. Chemother.*, 68: 366–369 (2013).

[190] C. Biswas, T.C. Sorrell, J.T. Djordjevic, X. Zuo, K.A. Jolliffe, S.C.A. Chen. In vitro activity of miltefosine as a single agent and in combination with voriconazole or posaconazole against uncommon filamentous fungal pathogens. *J. Antimicrob. Chemother.*, 68: 2842–2846 (2013).

[191] D.M. Livermore, M. Warner, S. Mushtaq. Activity of MK-7655 combined with imipenem against enterobacteriaceae and Pseudomonas aeruginosa. *J. Antimicrob. Chemother.*, 68: 2286–2290 (2013).

[192] D.M. Livermore, S. Mushtaq, A. Morinaka, T. Ida, K. Maebashi, R. Hope. Activity of carbapenems with ME1071 (disodium 2,3-diethylmaleate) against Enterobacteriaceae and Acinetobacter spp. With carbapenemases, including NDM enzymes. *J. Antimicrob. Chemother.*, 68: 153–158 (2013).

[193] D.M. Livermore, S. Mushtaq. Activity of biapenem (RPX2003) combined with the boronate β-lactamase inhibitor RPX7009 against carbapenem-resistant Enterobacteriaceae. *J. Antimicrob. Chemother.*, 68: 1825–1831 (2013).

[194] E.C. Calabrese, S. Castellano, M. Santoriello, C. Sgherri, M.F. Quartacci, L. Calucci, A.G.S. Warrilow, D.C. Lamb, S.L. Kelly, C. Milite, I. Granata, G. Sbardella, G. Stefancich, B. Maresca, A. Porta. Antifungal activity of azole compounds CPA18 and CPA109 against azole-susceptible and -resistant strains of Candida albicans. *J. Antimicrob. Chemother.*, 68: 1111–1119 (2013).

[195] W. Schröder, C. Goerke, C. Wolz. Opposing effects of aminocoumarins and fluoroquinolones on the sos response and adaptability in staphylococcus aureus. *J. Antimicrob. Chemother.*, 68: 529–538 (2013).

[196] S. Mushtaq, N. Woodford, R. Hope, R. Adkin, D.M. Livermore. Activity of BAL30072 alone or combined with ß -lactamase inhibitors or with meropenem against carbapenem-resistant Enterobacteriaceae and non-fermenters. *J. Antimicrob. Chemother.*, 68: 1601–1608 (2013).

[197] G.L. Hobby, M.H. Dawson. Effect of Rate of Growth of Bacteria on Action of Penicillin. *Exp. Biol. Med.*, 56: 181–184 (1944).

[198] I. Odenholt, E. Löwdin, O. Cars. Comparative in vitro pharmacodynamics of BO-2727, meropenem and imipenem against Gram-positive and Gram-negative bacteria. *Clin. Microbiol. Infect.*, 3: 73–81 (1997).

[199] T. Nishino, S. Nakazawa. Bacteriological study on effects of beta-lactam group antibiotics in high concentrations. *Antimicrob. Agents Chemother.*, 9: 1033–1042 (1976).

[200] M. Mychajlonka, T.D. McDowell, G.D. Shockman. Inhibition of Peptidoglycan, Ribonucleic Acid, and Protein Synthesis in Tolerant Strains of Streptococcus mutans. *Antimicrob. Agents Chemother.*, 17: 572–582 (1980).

[201] R. Fontana, M. Boaretti, A. Grossato, E.A. Tonin, M.M. Lleò, G. Satta. Paradoxical response of Enterococcus faecalis to the bactericidal activity of penicillin is associated with reduced activity of one autolysin. *Antimicrob. Agents Chemother.*, 34: 314–20 (1990).

[202] A. Ferrara, F. Grassi. Bactericidal activity of meropenem and interactions with other antibiotics. *J. Antimicrob. Chemother.*,: 239–250 (1989).

[203] G.A. McKay, S. Beaulieu, F.F. Arhin, A. Belley, I. Sarmiento, T. Parr, G. Moeck. Time-kill kinetics of oritavancin and comparator agents against Staphylococcus aureus, Enterococcus faecalis and Enterococcus faecium. *J. Antimicrob. Chemother.*, 63: 1191–9 (2009).

[204] D. Honeybourne, C. Tobin, G. Jevons, J. Andrews, R. Wise. Intrapulmonary penetration of linezolid. *J. Antimicrob. Chemother.*, 51: 1431–4 (2003).

[205] E. Löwdin, I. Odenholt, O. Cars. In Vitro Studies of Pharmacodynamic Properties of Vancomycin against Staphylococcus aureus andStaphylococcus epidermidis. *Antimicrob. agents …*, 42: 2739–2744 (1998).

[206] H.-S. Lim, Y.P. Chong, Y.-H. Noh, J. Jung, Y.S. Kim. Exploration of optimal dosing regimens of vancomycin in patients infected with methicillin-resistant Staphylococcus aureus by modeling and simulation. *J. Clin. Pharm. Ther.*, 39: 196–203 (2014).

[207] E. Coyle, R. Cha, M. Rybak. Influences of linezolid, penicillin, and clindamycin, alone and in combination, on streptococcal pyrogenic exotoxin a release. *Antimicrob. Agents Chemother.*, 47: 1752–1755 (2003).

[208] K.L. LaPlante, G. Sakoulas. Evaluating aztreonam and ceftazidime pharmacodynamics with Escherichia coli in combination with daptomycin, linezolid, or vancomycin in an in vitro pharmacodynamic model. *Antimicrob. Agents Chemother.*, 53: 4549–55 (2009).

[209] P.J. Yeh, M.J. Hegreness, A.P. Aiden, R. Kishony. Drug interactions and the evolution of antibiotic resistance. *Nat. Rev. Microbiol.*, 7: 460–6 (2009).

[210] K. Sieradzki, A. Tomasz. Inhibition of the autolytic system by vancomycin causes mimicry of vancomycin-intermediate Staphylococcus aureus-type resistance, cell concentration dependence of. *Antimicrob. Agents Chemother.*, 50: 527–533 (2006).

[211] C.B. Inderlied, M.G. Lancero, L.S. Young. Bacteriostatic and bactericidal in-vitro activity of meropenem against clinical isolates, including Mycobacterium avium complex. *J. Antimicrob. Chemother.*, 24 Suppl A: 85–99 (1989).

[212] R.-C. Mercier. Effect of growth phase and pH on the in vitro activity of a new glycopeptide, oritavancin (LY333328), against Staphylococcus aureus and Enterococcus faecium. *J. Antimicrob. Chemother.*, 50: 19–24 (2002).

[213] S. Mizunaga, T. Kamiyama, Y. Fukuda, M. Takahata, J. Mitsuyama. Influence of inoculum size of Staphylococcus aureus and Pseudomonas aeruginosa on in vitro activities and in vivo efficacy of fluoroquinolones and carbapenems. *J. Antimicrob. Chemother.*, 56: 91–6 (2005).

[214] A. Louie, H.S. Heine, K. Kim, D.L. Brown, B. Vanscoy, F. Sörgel, G.L. Drusano, W. Liu, F. So. Use of an In Vitro Pharmacodynamic Model To Derive a Linezolid Regimen That Optimizes Bacterial Kill and Prevents Emergence of Resistance in Bacillus anthracis Use of an In Vitro Pharmacodynamic Model To Derive a Linezolid Regimen That Optimizes Bacterial. *Antimicrob. Agents Chemother.*, 52: 2486–96 (2008).

[215] R.A. Proctor, C. von Eiff, B.C. Kahl, K. Becker, P. McNamara, M. Herrmann, G. Peters. Small colony variants: a pathogenic form of bacteria that facilitates persistent and recurrent infections. *Nat. Rev. Microbiol.*, 4: 295–305 (2006).

[216] M.N. Prichard, L.E. Prichard, C. Shipman. Strategic design and three-dimensional analysis of antiviral drug combinations. *Antimicrob. Agents Chemother.*, 37: 540–545 (1993).

[217] J.B. Fitzgerald, B. Schoeberl, U.B. Nielsen, P.K. Sorger. Systems biology and combination therapy in the quest for clinical efficacy. *Nat. Chem. Biol.*, 2: 458–66 (2006).

[218] M. Goldoni, C. Johansson. A mathematical approach to study combined effects of toxicants in vitro: evaluation of the Bliss independence criterion and the Loewe additivity model. *Toxicol. In Vitro*, 21: 759–69 (2007).

[219] J. Martinez-Irujo, M. Villahermosa. A checkerboard method to evaluate interactions between drugs. *Biochem. Pharmacol.*, 51: 635–644 (1996).

[220] G.L. Drusano, D.Z. D'Argenio, W. Symonds, P.A. Bilello, J. McDowell, B. Sadler, A. Bye, J.A. Bilello. Nucleoside analog 1592U89 and human immunodeficiency virus protease inhibitor 141W94 are synergistic in vitro. *Antimicrob. Agents Chemother.*, 42: 2153–9 (1998).

[221] D.M. Jonker, S.A.G. Visser, P.H. van der Graaf, R.A. Voskuyl, M. Danhof. Towards a mechanism-based analysis of pharmacodynamic drug-drug interactions in vivo. *Pharmacol. Ther.*, 106: 1–18 (2005).

[222] J. Meletiadis, J.W. Mouton, J.F.G.M. Meis, P.E. Verweij. In Vitro Drug Interaction Modeling of Combinations of Azoles with Terbinafine against Clinical Scedosporium prolificans Isolates In Vitro Drug Interaction Modeling of Combinations of Azoles with Terbinafine against Clinical Scedosporium prolificans Isolat. *Antimicrob. Agents Chemother.*, 47: 106–117 (2003).

[223] W.R. Greco, H.S. Park, Y.M. Rustum. Application of a new approach for the quantitation of drug synergism to the combination of cis-diamminedichloroplatinum and 1-beta-D-arabinofuranosylcytosine. *Cancer Res.*, 50: 5318–27 (1990).

[224] D. Czock, F. Keller. Mechanism-based pharmacokinetic-pharmacodynamic modeling of antimicrobial drug effects. *J. Pharmacokinet. Pharmacodyn.*, 34: 727–51 (2007).

[225] A.K. Meagher, A. Forrest, A. Dalhoff, H. Stass, J.J. Schentag. Novel pharmacokinetic-pharmacodynamic model for prediction of outcomes with an extended-release formulation of ciprofloxacin. *Antimicrob. Agents Chemother.*, 48: 2061–2068 (2004).

[226] W. Treyaprasert, S. Schmidt, K.H. Rand, U. Suvanakoot, H. Derendorf. Pharmacokinetic/pharmacodynamic modeling of in vitro activity of azithromycin against four different bacterial strains. *Int. J. Antimicrob. Agents*, 29: 263–70 (2007).

[227] N. Jumbe, A. Louie, R. Leary, W. Liu, M.R. Deziel, V.H. Tam, R. Bachhawat, C. Freeman, J.B. Kahn, K. Bush, M.N. Dudley, M.H. Miller, G.L. Drusano. Application of a mathematical model to prevent in vivo amplification of antibiotic-resistant bacterial populations during therapy. *J. Clin. Invest.*, 112: 275–285 (2003).

[228] J. Mouton, A. Vinks, N. Punt. Pharmacokinetic-pharmacodynamic modeling of activity of ceftazidime during continuous and intermittent infusion. *Antimicrob. Agents Chemother.*, 41: 733–738 (1997).

[229] Y. Yano, T. Oguma, H. Nagata, S. Sasaki. Application of logistic growth model to pharmacodynamic analysis of in vitro bactericidal kinetics. *J. Pharm. Sci.*, 87: 1177–1183 (1998).

[230] O.O. Okusanya, B.T. Tsuji, J.B. Bulitta, A. Forrest, C.C. Bulik, S.M. Bhavnani, P. Fernandes, P.G. Ambrose. Evaluation of the pharmacokinetics-pharmacodynamics of fusidic acid against Staphylococcus aureus and Streptococcus pyogenes using in vitro infection models: implications for dose selection. *Diagn. Microbiol. Infect. Dis.*, 70: 101–11 (2011).

[231] B.T. Tsuji, J.B. Bulitta, T. Brown, A. Forrest, P.A. Kelchlin, P.N. Holden, C.A. Peloquin, L. Skerlos, D. Hanna. Pharmacodynamics of early, high-dose linezolid against vancomycin-resistant enterococci with elevated MICs and pre-existing genetic mutations. *J. Antimicrob. Chemother.*, 67: 2182–90 (2012).

[232] N.Q. Balaban, J. Merrin, R. Chait, L. Kowalik, S. Leibler. Bacterial persistence as a phenotypic switch. *Science*, 305: 1622–1625 (2004).

[233] A. de Haro Moreno, H. Regina Nunes Salgado. Stability Study and Degradation Kinetics of Ceftazidime in Pharmaceutical Preparations. *Adv. Anal. Chem. Sci. Acad. Publ.*, 2: 1–5 (2012).

[234] E.L. Schuck, A. Dalhoff, H. Stass, H. Derendorf. Pharmacokinetic/pharmacodynamic (PK/PD) evaluation of a once-daily treatment using ciprofloxacin in an extended-release dosage form. *Infection*, 33 Suppl 2: 22–8 (2005).

[235] A. Kristoffersson, A.C. Hooker, M.O. Karlsson, L.E. Friberg. Optimal design of in vitro time kill curve experiments for the evaluation of antibiotic effects. In: *20th Population Approach Group Europe (PAGE) Meeting*. Athens, Greece: I–07 (2011). [http://www.page-meeting.org/default.asp?abstract=2243

[236] S.G. Wicha, A. Solms, W. Huisinga, C. Kloft. Adaptive optimal design for the concentration tiers in time-kill curve experiments. In: *23rd Population Approach Group Europe (PAGE) Meeting*. Alicante, Spain: IV–47 (2014). [http://www.page-meeting.org/default.asp?abstract=3202

[237] J.E. Conte, J.A. Golden, M.G. Kelley, E. Zurlinden. Intrapulmonary pharmacokinetics and pharmacodynamics of meropenem. *Int. J. Antimicrob. Agents*, 26: 449–456 (2005).

[238] J.G. Slatter, D.J. Stalker, K.L. Feenstra, I.R. Welshman, J.B. Bruss, J.P. Sams, M.G. Johnson, P.E. Sanders, M.J. Hauer, P.E. Fagerness, R.P. Stryd, G.W. Peng, E.M. Shobe. Pharmacokinetics, metabolism, and excretion of linezolid following an oral dose of [(14)C]linezolid to healthy human subjects. *Drug Metab. Dispos.*, 29: 1136–1145 (2001).

[239] C. Lamer, V. de Beco, P. Soler, S. Calvat, J.Y. Fagon, M.C. Dombret, R. Farinotti, J. Chastre, C. Gibert. Analysis of vancomycin entry into pulmonary lining fluid by bronchoalveolar lavage in critically ill patients. *Antimicrob. Agents Chemother.*, 37: 281–286 (1993).

[240] H.L. Nadler, D.H. Pitkin, W. Sheikh. The postantibiotic effect of meropenem and imipenem on selected bacteria. *J. Antimicrob. Chemother.*, 24 Suppl A: 225–31 (1989).

[241] C. Li, X. Du, J.L. Kuti, D.P. Nicolau. Clinical pharmacodynamics of meropenem in patients with lower respiratory tract infections. *Antimicrob. Agents Chemother.*, 51: 1725–30 (2007).

[242] T. Takata, K. Aizawa, A. Shimizu, S. Sakakibara, H. Watabe, K. Totsuka. Optimization of dose and dose regimen of biapenem based on pharmacokinetic and pharmacodynamic analysis. *J. Infect. Chemother.*, 10: 76–85 (2004).

[243] D. Maglio, M.A. Banevicius, C. Sutherland, C. Babalola, C.H. Nightingale, D.P. Nicolau. Pharmacodynamic profile of ertapenem against Klebsiella pneumoniae and Escherichia coli in a murine thigh model. *Antimicrob. Agents Chemother.*, 49: 276–280 (2005).

[244] D. Xuan, M. Banevicius, B. Capitano, M.K. Kim, C. Nightingale, D. Nicolau. Pharmacodynamic assessment of ertapenem (MK-0826) against Streptococcus pneumoniae in a murine neutropenic thigh infection model. *Antimicrob. Agents Chemother.*, 46: 2990–2995 (2002).

[245] U. Liebchen, A. Kratzer, S.G. Wicha, F. Kees, C. Kloft, M.G. Kees. Unbound fraction of ertapenem in intensive care unit patients. *J. Antimicrob. Chemother.*, 54: 2–5 (2014).

[246] A. Kratzer, U. Liebchen, M. Schleibinger, M.G. Kees, F. Kees. Determination of free vancomycin, ceftriaxone, cefazolin and ertapenem in plasma by ultrafiltration: Impact of experimental conditions. *J. Chromatogr. B Anal. Technol. Biomed. Life Sci.*, 961: 97–102 (2014).

[247] D. Andes, M.L. van Ogtrop, J. Peng, W.A. Craig. In vivo pharmacodynamics of a new oxazolidinone (linezolid). *Antimicrob. Agents Chemother.*, 46: 3484–9 (2002).

[248] J.A. Bosso, J. Nappi, C. Rudisill, M. Wellein, P.B. Bookstaver, J. Swindler, P.D. Mauldin. Relationship between vancomycin trough concentrations and nephrotoxicity: A prospective multicenter trial. *Antimicrob. Agents Chemother.*, 55: 5475–5479 (2011).

[249] P.A. Moise, A. Forrest, S.M. Bhavnani, M.C. Birmingham, J.J. Schentag. Area under the inhibitory curve and a pneumonia scoring system for predicting outcomes of vancomycin therapy for respiratory infections by Staphylococcus aureus. *Am. J. Heal. Pharm.*, 57: (2000).

[250] P.A. Moise-Broder, A. Forrest, M.C. Birmingham, J.J. Schentag. Pharmacodynamics of vancomycin and other antimicrobials in patients with Staphylococcus aureus lower respiratory tract infections. *Clin. Pharmacokinet.*, 43: 925–942 (2004).

[251] W.J. Munckhof, C. Giles, J.D. Turnidge. Post-antibiotic growth suppression of linezolid against Gram-positive bacteria. *J. Antimicrob. Chemother.*, 47: 879–83 (2001).

[252] N. Plock, C. Kloft. Microdialysis–theoretical background and recent implementation in applied life-sciences. *Eur. J. Pharm. Sci.*, 25: 1–24 (2005).

[253] I.K. Minichmayr, A. Schaeftlein, M. Zeitlinger, C. Kloft. Impact of patient- and disease-related characteristics on plasma and target site pharmacokinetics of linezolid in four heterogeneous populations. In: *24th European Congress of Clinical Microbiology and Infectious Diseases (ECCMID).* Barcelona, Spain (2014).

[254] M.A. Zeitlinger, H. Derendorf, J.W. Mouton, O. Cars, W.A. Craig, D. Andes, U. Theuretzbacher. Protein binding: do we ever learn? *Antimicrob. Agents Chemother.*, 55: 3067–74 (2011).

[255] O. Dumitrescu, S. Boisset, C. Badiou, M. Bes, Y. Benito, M.-E. Reverdy, F. Vandenesch, J. Etienne, G. Lina. Effect of antibiotics on Staphylococcus aureus producing Panton-Valentine leukocidin. *Antimicrob. Agents Chemother.*, 51: 1515–9 (2007).

[256] J. Zimbelmann, A. Palmer, J. Todd. Improved outcome of clindamycin compared with beta-lactam antibiotic treatment for invasive Streptococcus pyogenes infection. *Pediatr. Infect. Dis. J.*, 18: 1096–1100 (1999).

[257] Z.D. Mulla, P.E. Leaverton, S.T. Wiersma. Invasive group A streptococcal infections in Florida. *South. Med. J.*, 96: 968–73 (2003).

[258] D.R. Mould, R.N. Upton. Basic Concepts in Population Modeling, Simulation, and Model-Based Drug Development. *CPT Pharmacometrics Syst. Pharmacol.*, 1: e6 (2012).

[259] J.A. Roberts, C.M.J. Kirkpatrick, M.S. Roberts, T.A. Robertson, A.J. Dalley, J. Lipman. Meropenem dosing in critically ill patients with sepsis and without renal dysfunction: intermittent bolus versus continuous administration? Monte Carlo dosing simulations and subcutaneous tissue distribution. *J. Antimicrob. Chemother.*, 64: 142–50 (2009).

[260] M. Carlier, V. Stove, A.G. Verstraete, J.J. De Waele. Stability of generic brands of meropenem reconstituted in isotonic saline. *Minerva Anestesiol.*, 81: 283–7 (2015).

[261] C. Adembri, S. Fallani, M.I. Cassetta, S. Arrigucci, A. Ottaviano, P. Pecile, T. Mazzei, R. De Gaudio, A. Novelli. Linezolid pharmacokinetic/pharmacodynamic profile in critically ill septic patients: intermittent versus continuous infusion. *Int. J. Antimicrob. Agents*, 31: 122–9 (2008).

[262] C. Jacqueline, E. Batard, L. Perez, D. Boutoille, A. Hamel, J. Caillon, M.F. Kergueris, G. Potel, D. Bugnon. In vivo efficacy of continuous infusion versus intermittent dosing

of linezolid compared to vancomycin in a methicillin-resistant Staphylococcus aureus rabbit endocarditis model. *Antimicrob. Agents Chemother.*, 46: 3706–3711 (2002).

[263] E. Boselli, D. Breilh, A. Caillault-Sergent, S. Djabarouti, C. Guillaume, F. Xuereb, L. Bouvet, T. Rimmelé, M.C. Saux, B. Allaouchiche. Alveolar diffusion and pharmacokinetics of linezolid administered in continuous infusion to critically ill patients with ventilator-associated pneumonia. *J. Antimicrob. Chemother.*, 67: 1207–1210 (2012).

[264] B.T. Tsuji, T. Brown, R. Parasrampuria, D.A. Brazeau, A. Forrest, P.A. Kelchlin, P.N. Holden, C.A. Peloquin, D. Hanna, J.B. Bulitta. Front-loaded linezolid regimens result in increased killing and suppression of the accessory gene regulator system of Staphylococcus aureus. *Antimicrob. Agents Chemother.*, 56: 3712–3719 (2012).

[265] M. Neely, R. Jelliffe. Practical, individualized dosing: 21st century therapeutics and the clinical pharmacometrician. *J. Clin. Pharmacol.*, 50: 842–7 (2010).

[266] S.G. Wicha, M.G. Kees, A. Solms, I.K. Minichmayr, A. Kratzer, C. Kloft. TDMx: A novel web-based open-access support tool for optimising antimicrobial dosing regimens in clinical routine. *Int. J. Antimicrob. Agents*, 45: 442–444 (2015).

[267] M.F. Waineo, T.C. Kuhn, D.L. Brown. The pharmacokinetic/pharmacodynamic rationale for administering vancomycin via continuous infusion. *J. Clin. Pharm. Ther.*, 40: 259–265 (2015).

[268] J. Rello, J. Sole-Violan, M. Sa-Borges, J. Garnacho-Montero, E. Muñoz, G. Sirgo, M. Olona, E. Diaz. Pneumonia caused by oxacillin-resistant Staphylococcus aureus treated with glycopeptides. *Crit. Care Med.*, 33: 1983–1987 (2005).

[269] A.J. Verrall, R. Llorin, V.H. Tam, D.C. Lye, Z. Sulaiman, L. Zhong, S. Archuleta, D. a. Fisher. Efficacy of continuous infusion of vancomycin for the outpatient treatment of methicillin-resistant staphylococcus aureus infections. *J. Antimicrob. Chemother.*, 67: 2970–2973 (2012).

[270] H. Georges, O. Leroy, S. Alfandari, B. Guery, M. Roussel-Delvallez, C. Dhennain, G. Beaucaire. Pulmonary disposition of vancomycin in critically ill patients. *Eur. J. Clin. Microbiol. Infect. Dis.*, 16: 385–8 (1997).

7 Appendix

7.1 Supplementary Figures
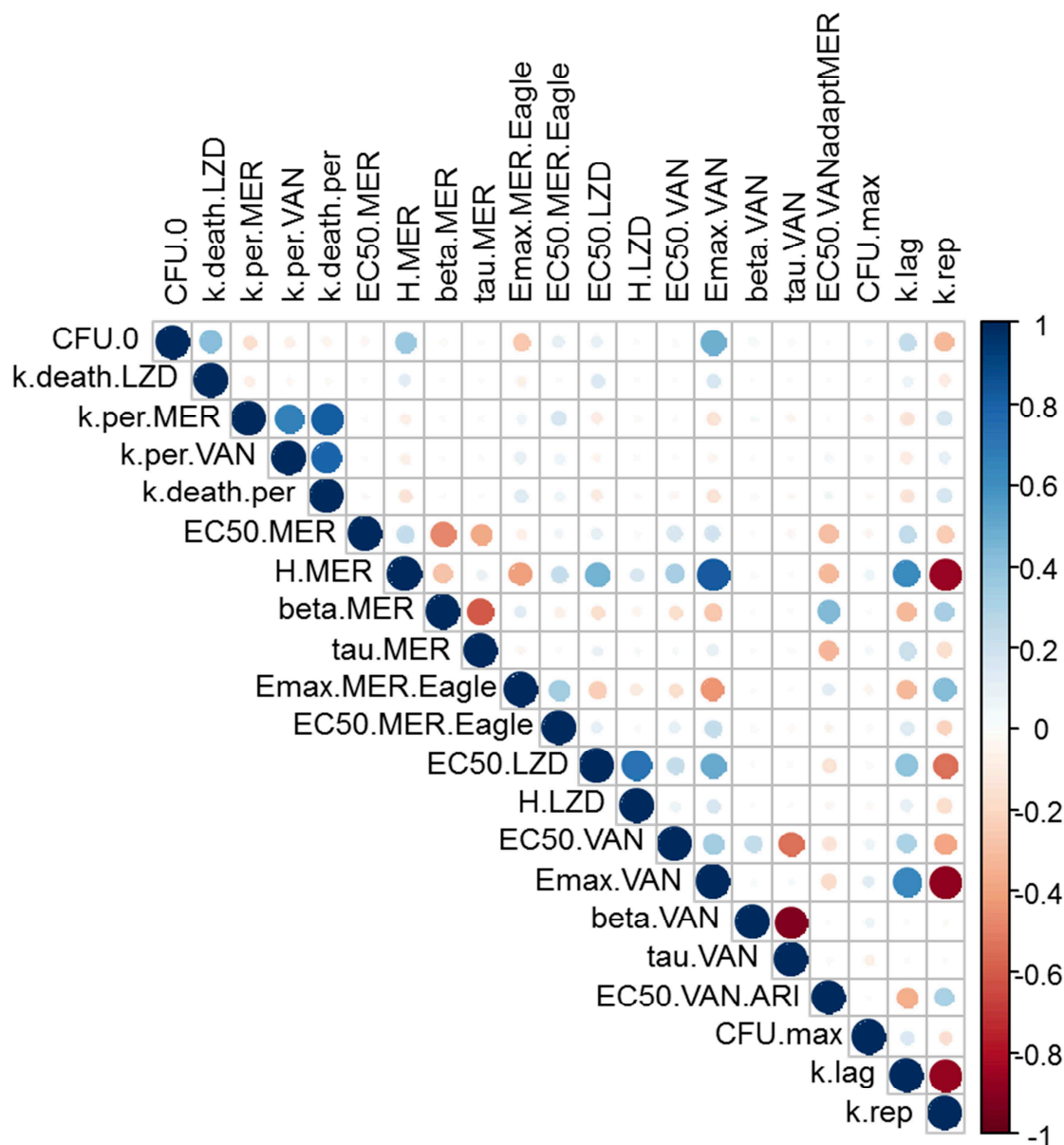
Figure 73: Correlation plot for the structural parameters of the final semi-mechanistic PD model for *S. aureus* in lag-phase at drug exposure. Positive correlation is indicated by blue, negative correlation by red circles. Circle size and colour gradient indicate the magnitude of correlation.
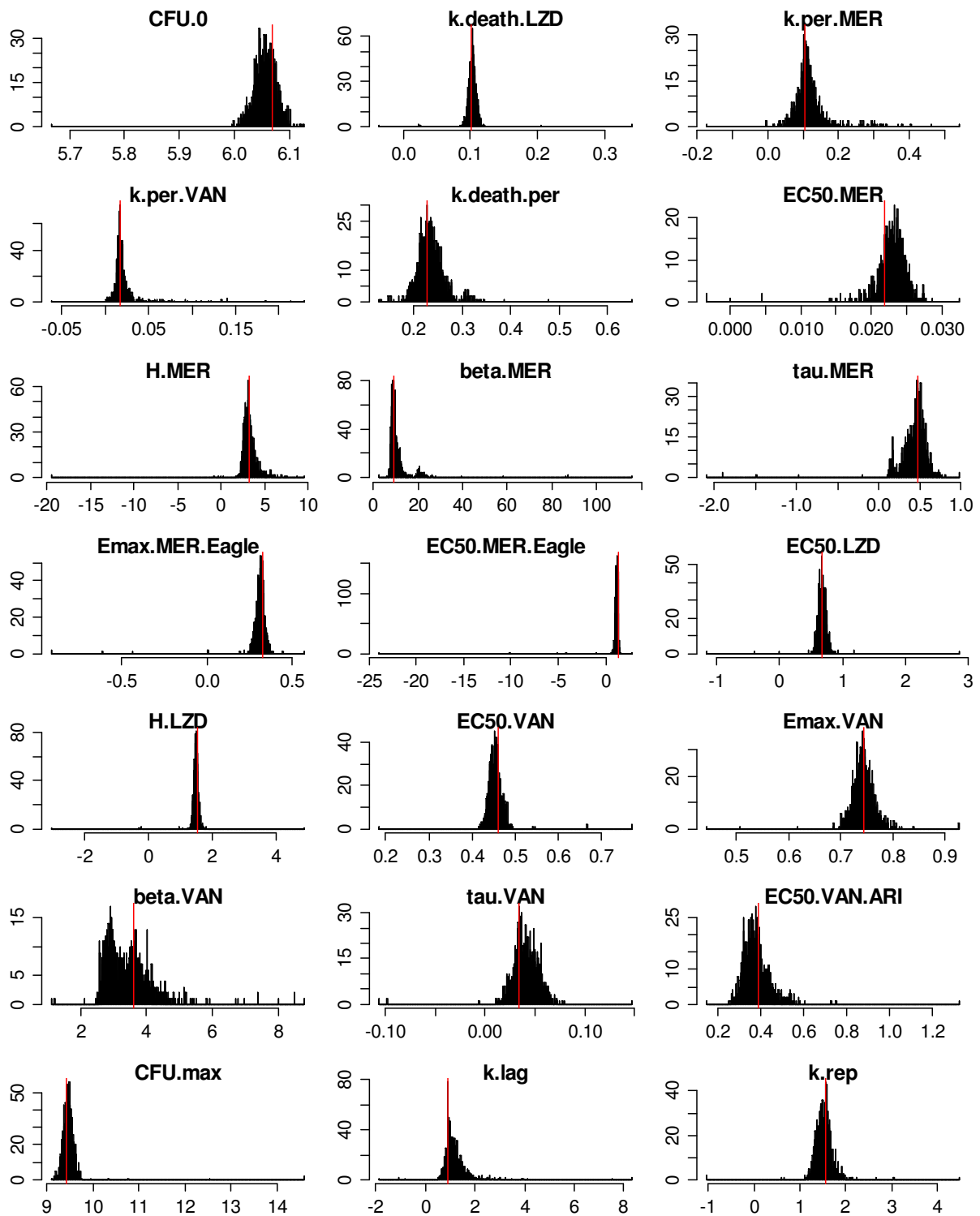
Figure 74: Frequency (y-axis) distribution of the bootstrap estimates (x-axis) for the semi-mechanistic PD model for *S. aureus* in lag-phase obtained from n=1198 bootstrap datasets, red lines indicate final parameter estimates.
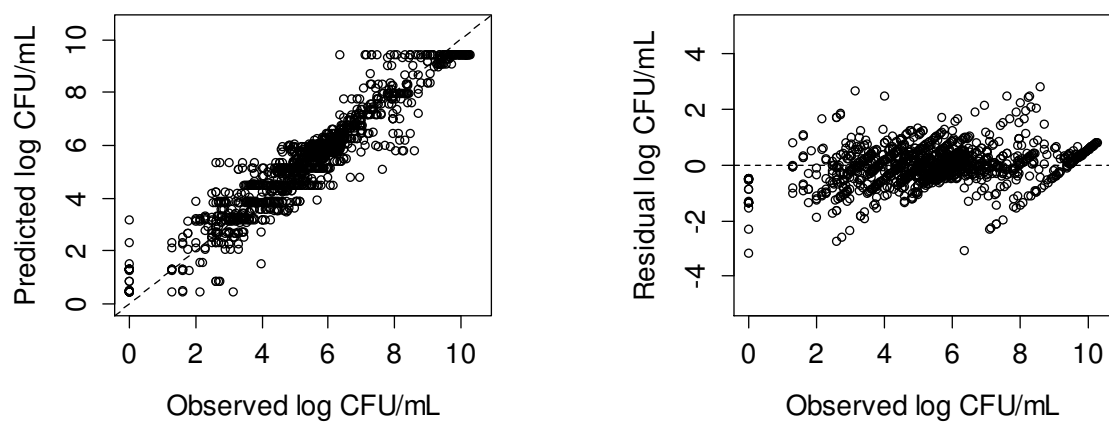
Figure 75: Goodness-of-fit plots illustrating observed vs. predicted log10 CFU/mL (left) and residual vs. predicted log10 CFU/mL for semi-mechanistic PD model for *S. aureus* in lag-phase.
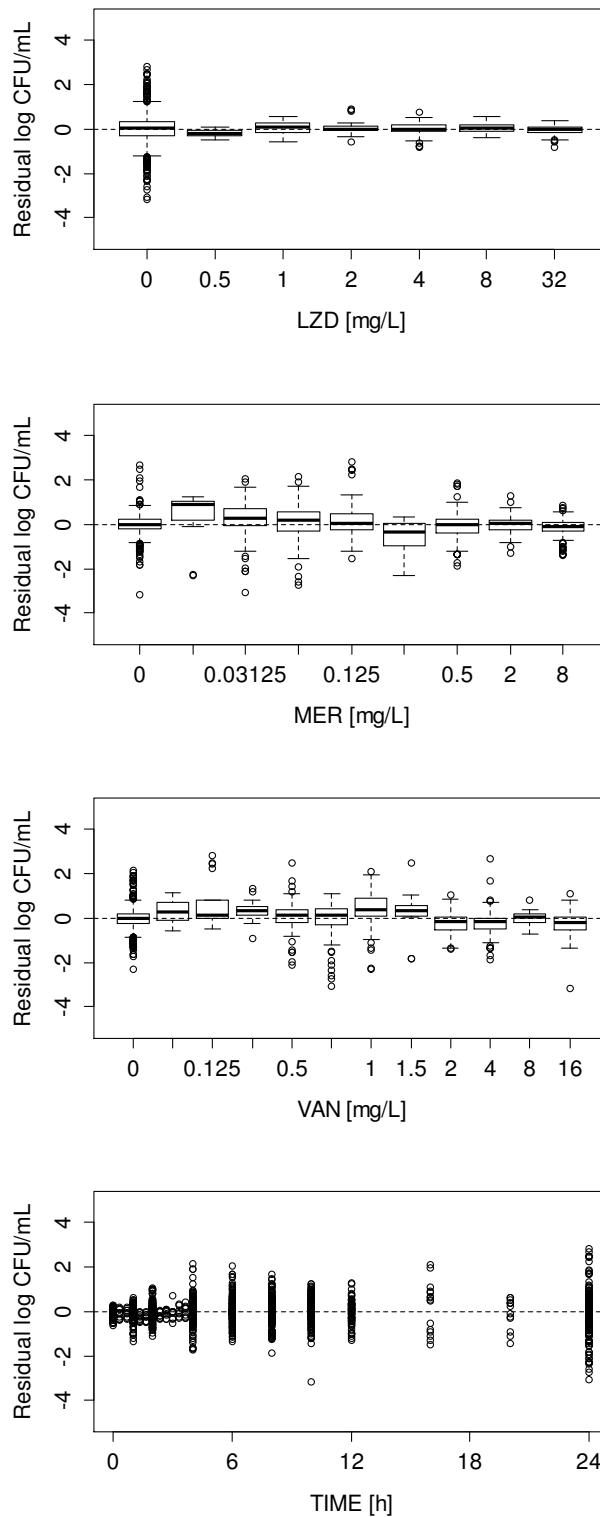
Figure 76: Residuals between observed and predicted log10 CFU/mL vs. investigated concentrations of LZD, MER and VAN for the semi-mechanistic PD model for lag-phase *S. aureus*. Boxplots illustrate median (horizontal line), 25th to 75th quantile (box), 1.5 fold inter-quartile range from box edge (whiskers) and points outside the whiskers.
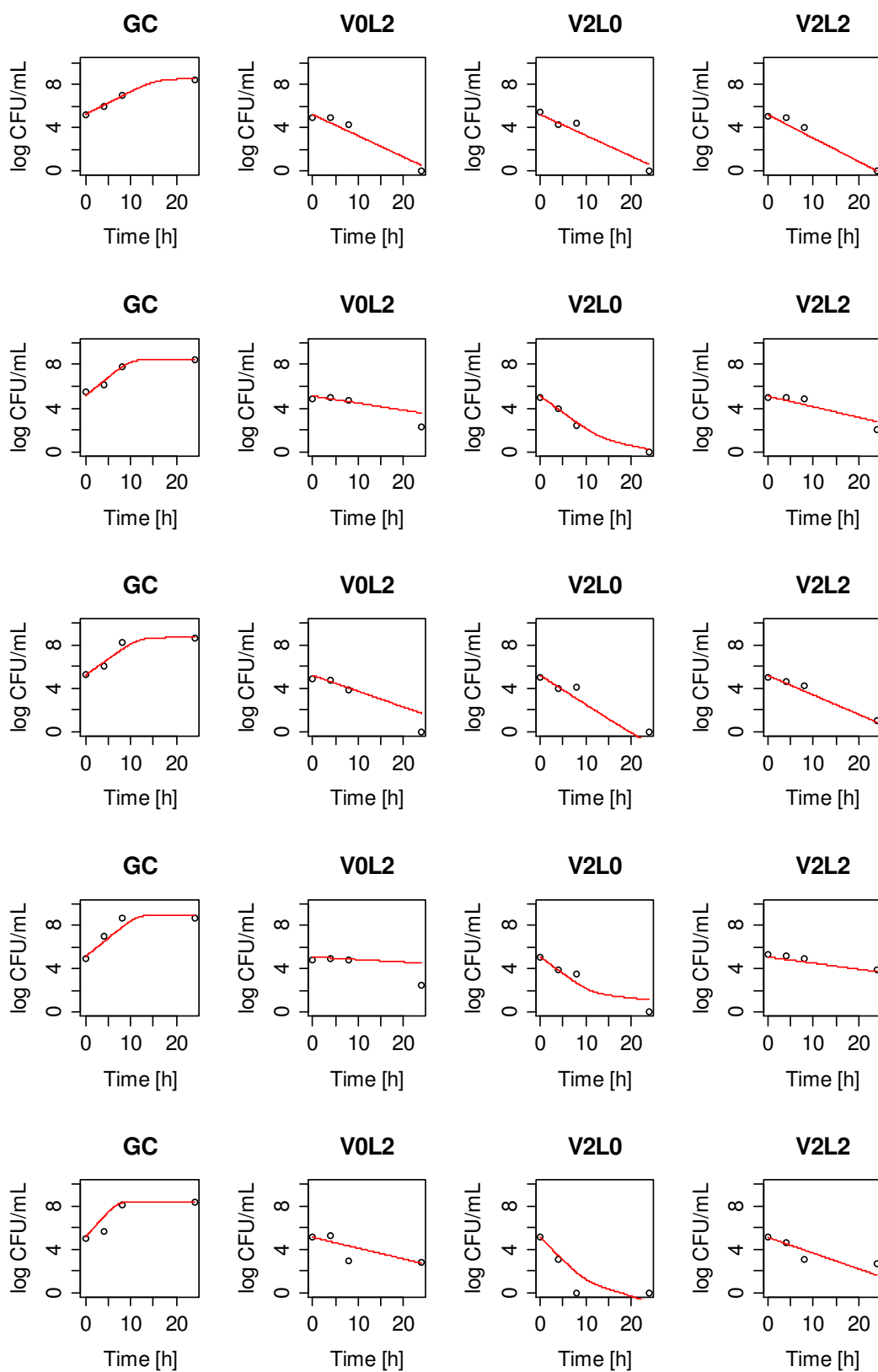
Figure 77: External model evaluation for the semi-mechanistic PD model for *S. aureus* (3.3.1.3.1) for vancomycin (V) and linezolid (L) vs. five MRSA strains (rows). Numbers indicate concentration of antibiotic (fold MIC).
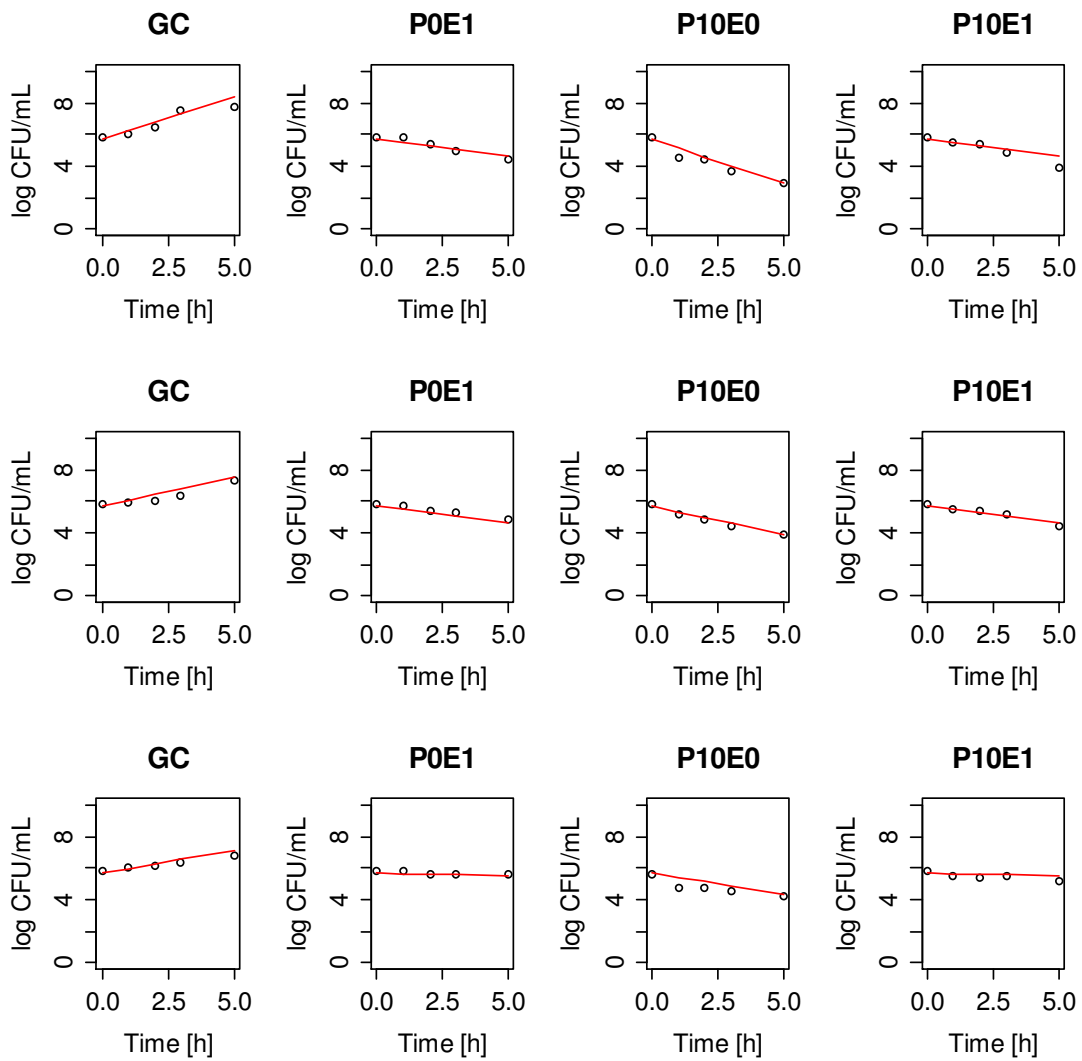
Figure 78: External model evaluation for the semi-mechanistic PD model for *S. aureus* (3.3.1.3.1) for penicillin (P) and erythromycin (E) vs. three strains of S. pneumoniae (rows). Numbers indicate concentration of antibiotic (fold MIC).
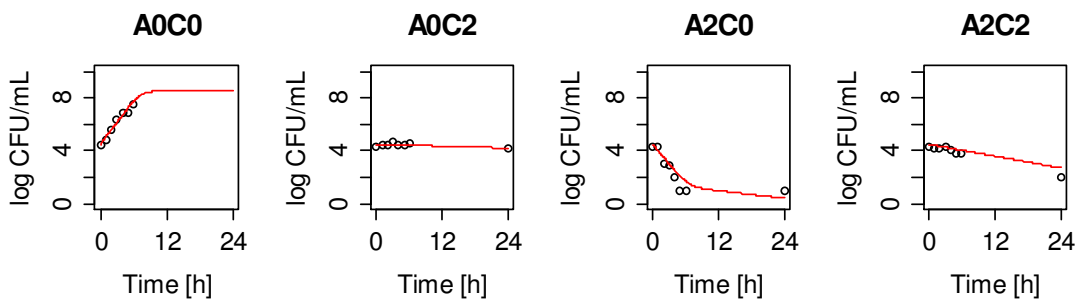
Figure 79: External model evaluation for the semi-mechanistic PD model for *S. aureus* (3.3.1.3.1) for ampicillin (A) and chloramphenicol (C) vs. an meningeal isolate of group B streptococci (rows). Numbers indicate concentration of antibiotic (fold MIC).
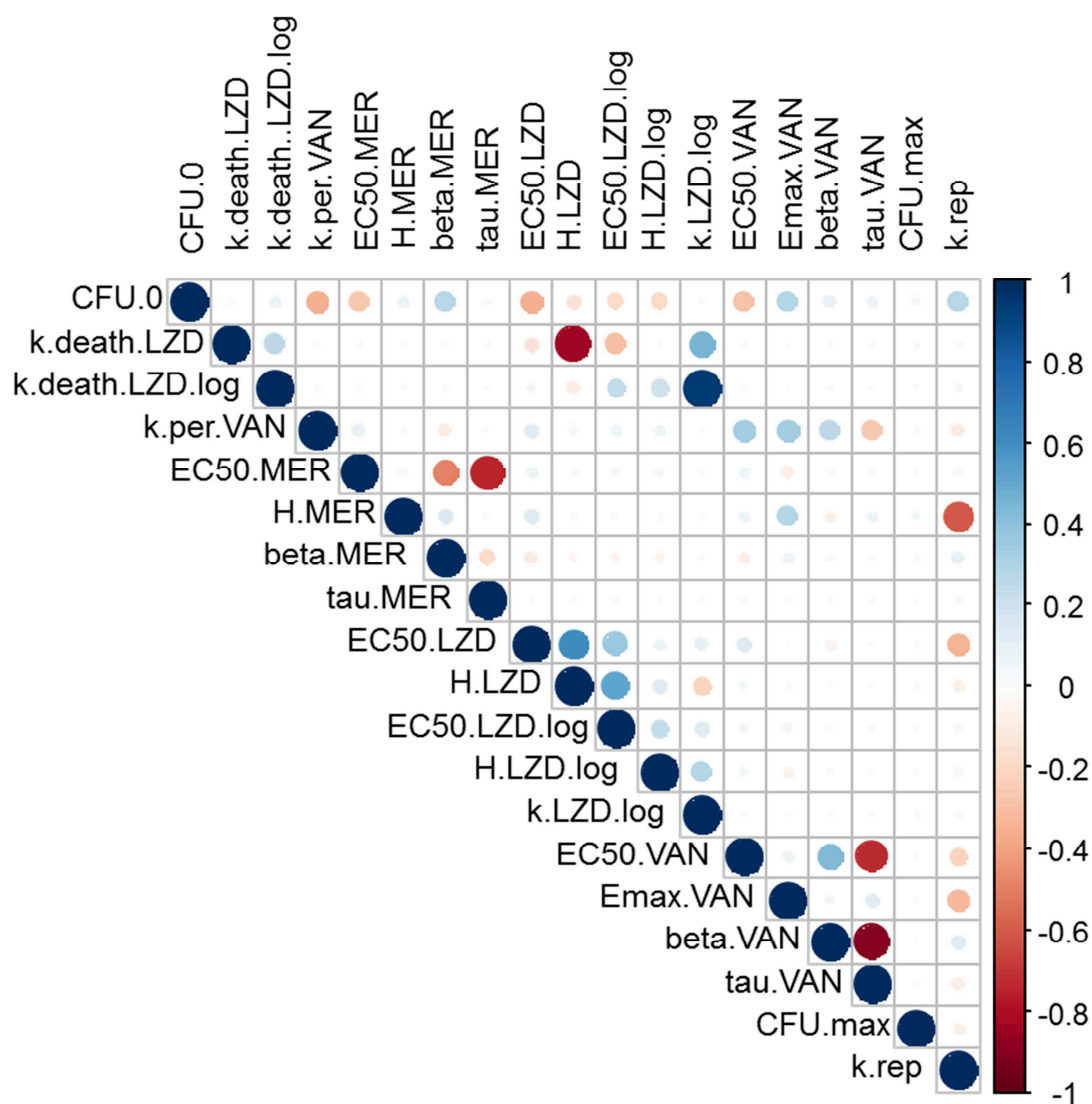
Figure 80: Correlation plot for the structural parameters of the final semi-mechanistic PD model for *S. aureus* in log-phase at drug exposure. Positive correlation is indicated by blue circles, negative correlation by red circles. Circle size and colour gradient indicates magnitude of correlation.
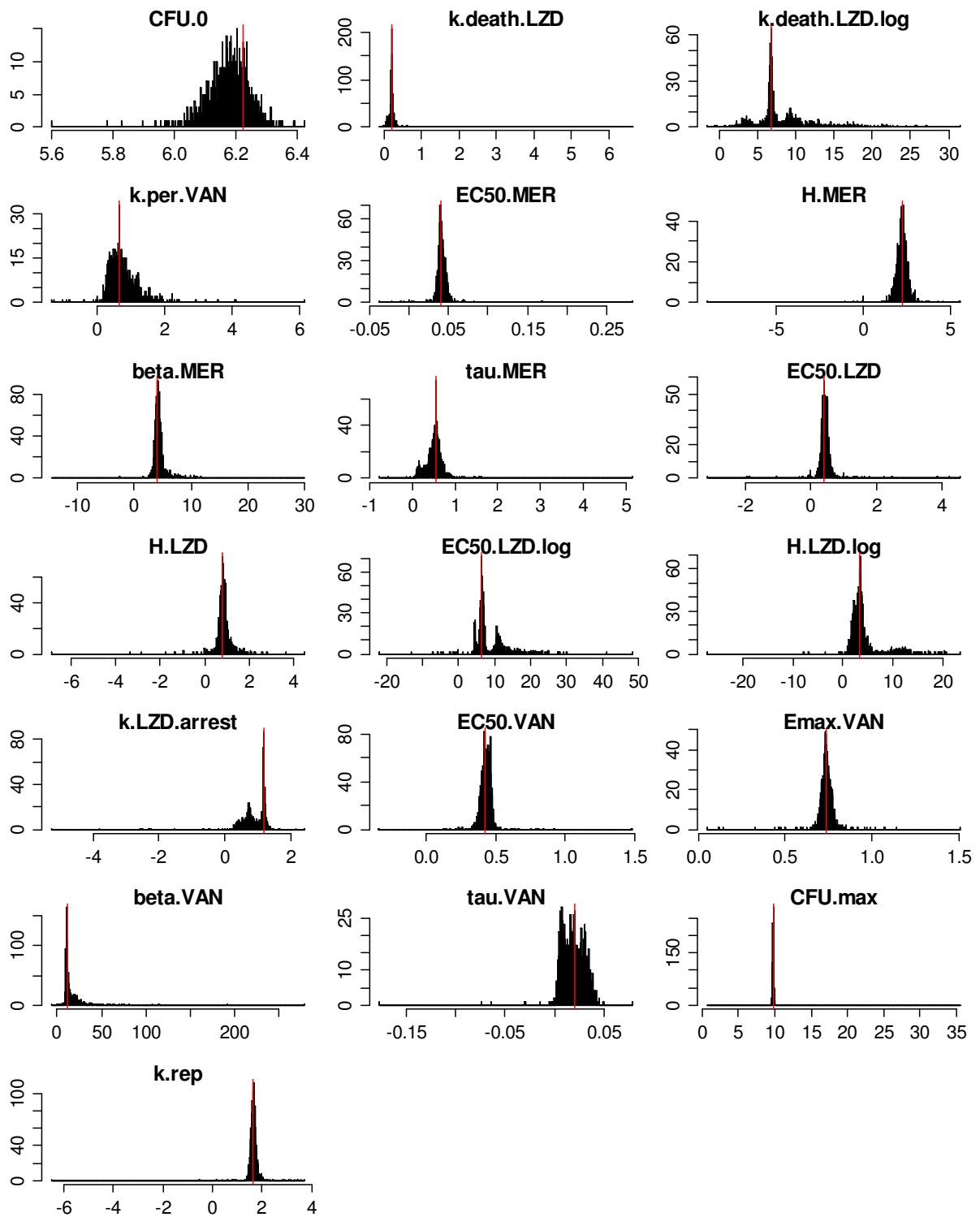
Figure 81: Frequency (y-axis) distribution of the bootstrap estimates (x-axis) for the semi-mechanistic PD model for *S. aureus* in log-phase obtained from n=1190 bootstrap datasets, red lines indicate final parameter estimates.
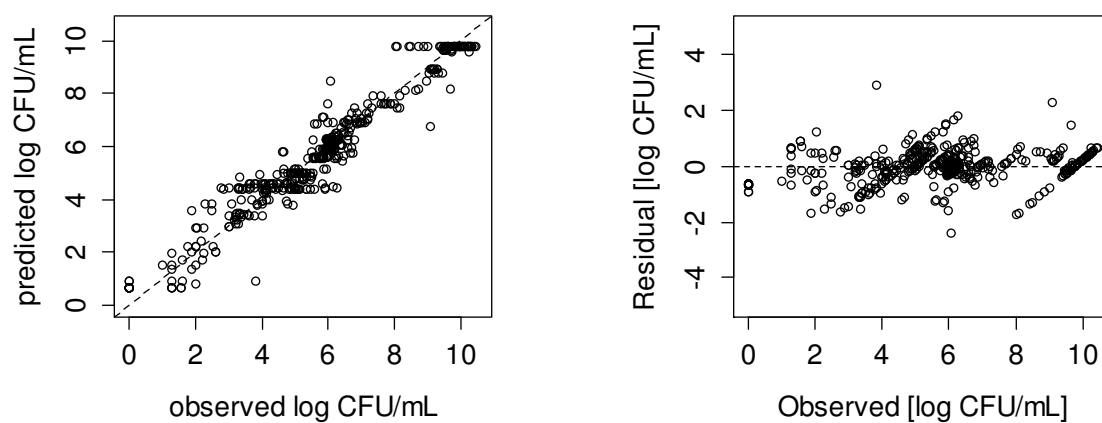
Figure 82: Goodness-of-fit plots illustrating observed vs. predicted log10 CFU/mL (left) and residual vs. predicted log10 CFU/mL for semi-mechanistic PD model for *S. aureus* in log-phase.
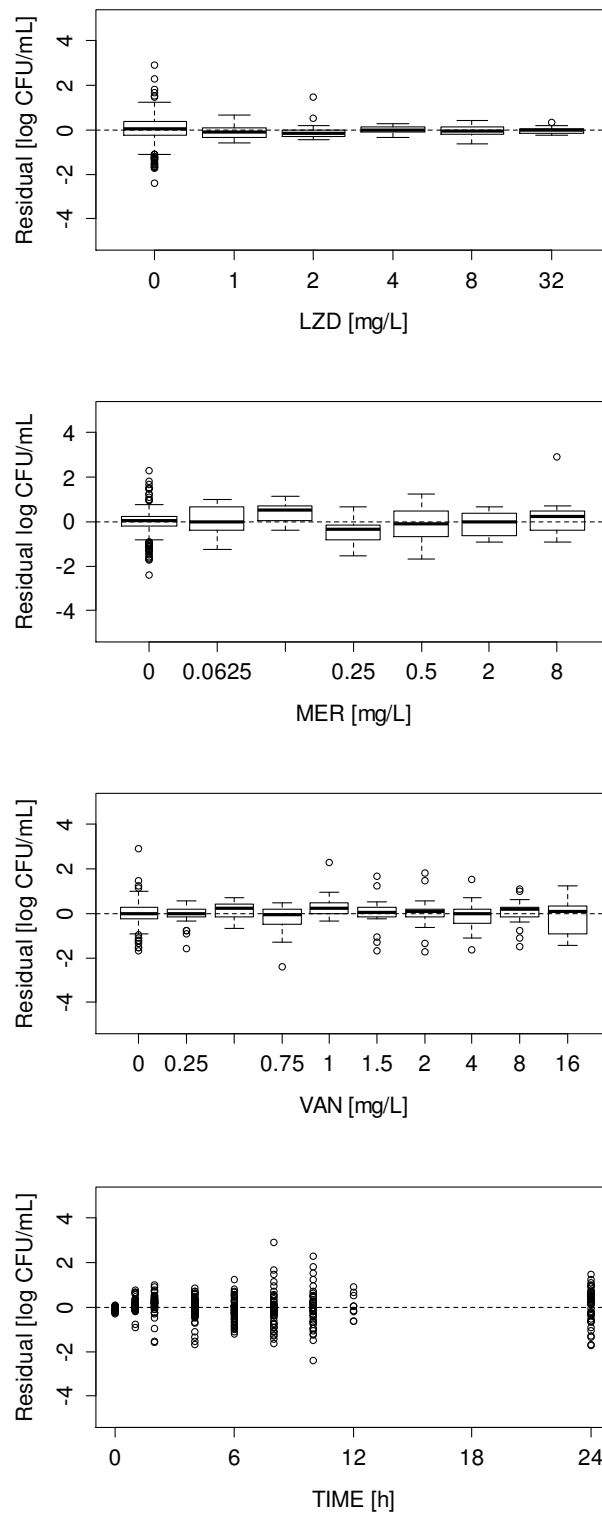
Figure 83: Residuals between observed and predicted log10 CFU/mL vs. investigated concentrations of LZD, MER, VAN and time for the semi-mechanistic PD model for log-phase *S. aureus*. Boxplots illustrate median (horizontal line), 25th to 75th quantile (box), 1.5 fold inter-quartile range from box edge (whiskers) and points outside the whiskers.
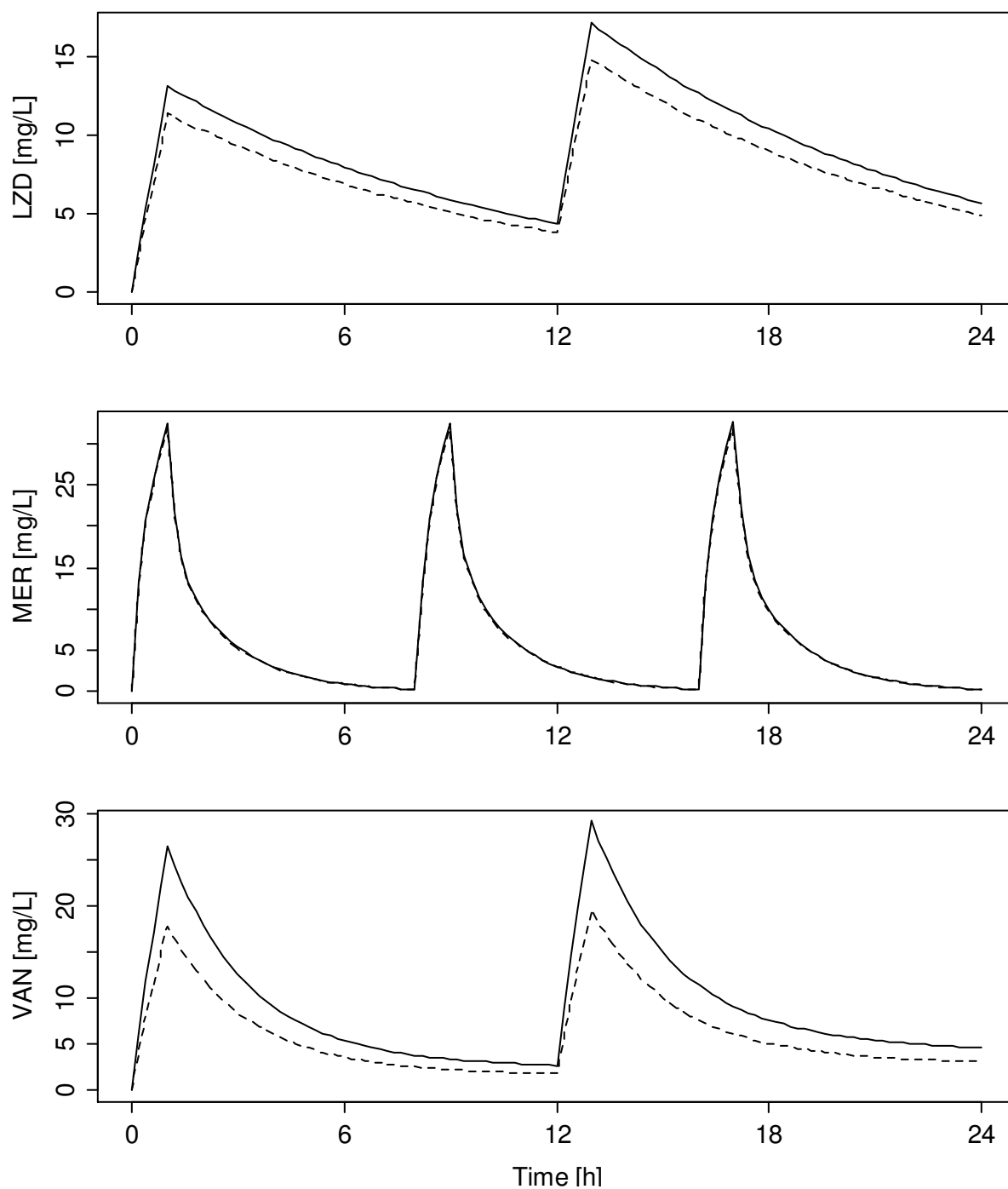
Figure 84: Typical PK profiles for LZD 600 mg BID (upper panel), MER 1000 mg TID (middle) and VAN 1000 mg BID (lower panel), administered as 1 h intravenous infusion; total drug concentrations (solid lines) and unbound concentrations (dashed lines) are presented for a typical 35 year old male patient with total body weight of 75 kg, creatinine clearance of 120 mL/min, and no liver cirrhosis.

7.2 Supplementary Tables

Table 19: Model selection criteria for the final semi-mechanistic PD model for lag-phase *S. aureus* (first row) vs. key models obtained during model development. OLS: ordinary least squares at objective function minimum; k: number of model parameters; AIC: Akaike information criterion; AICc: corrected AIC for n/p < 40; -2LL: minus 2 times log likelihood. Bold: Criterion used for comparison; -2LL was used for comparison of nested models, AIC was used for comparison of non-nested models. Positive difference indicates statistical superiority of the final model, negative difference of the respective key model.

Model	OLS	k	AIC	AICc	-2LL	ΔAIC	ΔAICc	Δ(-2LL)
Final model	549.92	21	-1700.02	-1699.39	2844.82	0.00	0.00	0.00
w/o $k_{per,MER}$	572.44	20	-1637.13	-1636.55	2909.72	+62.89	+62.84	**+64.89**
w/o $k_{per,VAN}$	566.42	20	-1654.22	-1653.64	2892.63	+45.80	+45.75	**+47.80**
w/o Eagle effect for MER	588.14	19	-1595.39	-1594.86	2953.46	**+104.64**	+104.53	+108.64
w/o $Emax_{VAN}$	570.12	20	-1643.68	-1643.10	2903.17	+56.34	+56.29	**+58.34**
w. $EC50_{MER,ARI}$	556.19	22	-1679.7	-1679.01	2863.15	+20.32	+20.38	**+18.32**
w/o $EC50_{VAN,ARI}$	828.75	20	-1038.82	-1038.24	3508.03	+661.20	+661.15	**+663.20**
vs. biphasic growth model	543.16	22	-1718.04	-1717.35	2824.81	**-18.01**	-17.96	-20.01

Table 20: Model selection criteria for the final semi-mechanistic PD model for log-phase *S. aureus* (first row) vs. key models obtained during model development. OLS: ordinary least squares at objective function minimum; k: number of model parameters; AIC: Akaike information criterion; AICc: corrected AIC for n/p < 40; -2LL: minus 2 times log likelihood. Bold: Criterion used for comparison; -2LL was used for comparison of nested models, AIC was used for comparison of non-nested models. Positive difference indicates statistical superiority of the final model, negative difference of the respective key model.

Model	OLS	k	AIC	AICc	-2LL	ΔAIC	ΔAICc	Δ(-2LL)
Final model	149.31	19	-443.86	-441.87	776.16	0.00	0.00	0.00
w. Eagle-effect for MER	149.32	21	-439.86	-437.45	776.16	+4.00	**+4.42**	0.00
w/o $k_{per,MER}$	261.81	19	-194.53	-192.54	1025.49	+249.33	+249.33	**+249.33**
w/o $k_{per,VAN}$	212.53	18	-289.11	-287.31	932.91	+154.75	+154.56	**+156.75**
w. $k_{death,per}$	149.36	20	-441.71	-439.52	776.31	+2.15	+2.35	**+0.15**
w/o $Emax_{VAN}$	163.81	18	-404.73	-402.94	817.29	+39.13	+38.93	**+41.13**
w/o $k_{death,LZD,log}$, $EC_{LZD,log}$, $H_{LZD,log}$, $k_{LZD,log}(t)$	189.56	15	-345.91	-344.63	882.11	+97.95	**+97.24**	+105.95
vs. model with initial replication dependent effect of LZD	174.75	17	-378.01	-376.40	846.01	+65.85	**+65.47**	+69.85

7.3 'R'-Scripts

7.3.1 Empiric PD modelling and response surface analysis

```
#- RSA of Checkerboard for LZD and MER
#- Read data -----------------------------------------------------------------
data_checkerb=read.csv("~.csv")
data_checkerb$LOGCFU=log10(data_checkerb$CFU)
data_checkerb$LOGCFU[data_checkerb$LOGCFU==("-Inf")]<-0

#- Calculate descriptive statistics of experimental data --------------------
data=cbind(summarize(data_checkerb$LOGCFU, by=llist(data_checkerb$LZD,
                                                    data_checkerb$MER), mean),
          summarize(data_checkerb$LOGCFU, by=llist(data_checkerb$LZD,
                                                    data_checkerb$MER), min)[,3],
          summarize(data_checkerb$LOGCFU, by=llist(data_checkerb$LZD,
                                                    data_checkerb$MER), max)[,3],
          summarize(data_checkerb$LOGCFU, by=llist(data_checkerb$LZD,
                                                    data_checkerb$MER), sd)[,3])
colnames(data)=c("LZD","MER","LOGCFU","LOGCFU_MIN","LOGCFU_MAX","LOGCFU_SD")

# CI 95 calculation for sample mean of n<30 (here n = 3) --> t-distribution
# with df = n (=3) - 1 --> more conservative than 1.96 * SEM !
data$CI95_LOW  = data$LOGCFU + data$LOGCFU_SD/sqrt(3) * qt(0.025, df = 2)
data$CI95_UP   = data$LOGCFU + data$LOGCFU_SD/sqrt(3) * qt(0.975, df = 2)

#- Individual effects --------------------------------------------------------
#- Sigmoidal Emax model
E.ind = function(Emax, EC50, H, c){

  # growth control                        # drug effect reduces bacterial load
  data$LOGCFU[data$LZD==0&data$MER==0] - ((Emax*c^H)/(EC50^H+c^H))

}

#- Individual analysis of MER ------------------------------------------------
OBJ_OLS_MER = function(parms,
                       c){

  Emax      = parms[1]
  EC50      = parms[2]
  H         = parms[3]

  # Ordinary least squares
      # predicted log10 CFU/mL                  # observed log10 CFU/mL
  sum((E.ind(Emax,EC50,H,data$MER[data$LZD==0]) - data$LOGCFU[data$LZD==0])^2)
}

#- Minimise OBJ_OLS
OBJ_min_MER =    optim(start.MER,
                       OBJ_OLS_MER,
                       method="L-BFGS-B",
                       lower=0,
                       control=list(trace=T,
                                    maxit=500,
                                    factr=1e-5,
                                    parscale=start.MER,
                                    fnscale=OBJ_OLS_MER(start.MER)),
                       hessian=T)

#- calculate residual variance using MLE for sig2
sig2 = OBJ_min_MER$value/length(data$LOGCFU[data$LZD==0])

#- invert Hessian (observed Fisher information matrix) to obtain variance-
#- covariance matrix; correct Hessian by 1/(2*sig2) as OLS was used instead of MLE!
var_cov_mat<-solve(OBJ_min_MER$hessian/(2*sig2))
```

```
#- calculate standard errors of the estimates from diagonal elements of
#- var_covar_mat
prop_sigma<-sqrt(diag(var_cov_mat))

# calculation of 95% CIs of parameter estimates; since n < 30 --> t-distribution!
# degrees of freedom = n-p
upper<-OBJ_min_MER$par+qt(0.975,
                          df = (length(data$LOGCFU[data$LZD==0])-3))*prop_sigma
lower<-OBJ_min_MER$par+qt(0.025,
                          df = (length(data$LOGCFU[data$LZD==0])-3))*prop_sigma
interval.MER<-data.frame(value=OBJ_min_MER$par,
                         upper=upper,
                         lower=lower,
                         RSE=(prop_sigma/OBJ_min_MER$par*100))

#- Individual analysis of LZD ------------------------------------------------
OBJ_OLS_LZD = function...
{dto. analogous to MER}
...


#- Response Surface Analysis -------------------------------------------------
E.comb.LZDMER = function(Emax.MER,EC50.MER,H.MER, # parameters from ind. analyis
                         Emax.LZD,EC50.LZD,H.LZD, # parameters from ind. analyis
                         MER,LZD) {               # Drug concentrations

  # Bliss independence model: Ecomb = Ea + Eb + Ea*Eb
  # --> modified to account for differences in Emax between MER and LZD

  EMERLZD  = Emax.MER*(
    ((MER^H.MER)/(EC50.MER^H.MER+MER^H.MER)) + # EMER is normalised to max. 100%
    (( (Emax.LZD/Emax.MER) * LZD^H.LZD)/
       (EC50.LZD^H.LZD+LZD^H.LZD)) -  # Emax LZD as fraction of max effect of MER

    (((MER^H.MER)/(EC50.MER^H.MER+MER^H.MER)) *
    (( (Emax.LZD/Emax.MER) * LZD^H.LZD)/(EC50.LZD^H.LZD+LZD^H.LZD)))  )

  return(EMERLZD)
}

#- Calculate uncertainty (SD) of additivity surface from residuals of individual
#- effect models

#- residual analysis
resid_MER= E.ind(OBJ_min_MER$par[1],
                 OBJ_min_MER$par[2],
                 OBJ_min_MER$par[3],
                 data$MER[data$LZD==0]) - data$LOGCFU[data$LZD==0]

resid_LZD= E.ind(OBJ_min_LZD$par[1],
                 OBJ_min_LZD$par[2],
                 OBJ_min_LZD$par[3],
                 data$LZD[data$MER==0]) - data$LOGCFU[data$MER==0]

#- compute 'joint' residual variance of response surface with delta method
#-
resid_LZDMER_SD = deltamethod(~x1+x2,          # transformation independent of E as
                                               additive residual sigma2
                              mean=c(0,0),  # exp. mean of residuals for large n
                              cov=matrix(data=c(sum(resid_MER^2)/length(resid_MER),
                                                0,
                                                0,
                                                sum(resid_LZD^2)/length(resid_LZD)),
                                         nrow=2,ncol=2),
                              ses=T) # compute standard error
```

```
# Test for significant deviation of experimental data from BI-RSA -----------------
p_values=NULL
delta_LOGCFU=NULL

for (i in 1:length(data$LOGCFU)){

  i_MER=data$MER[i]
  i_LZD=data$LZD[i]


  delta_LOGCFU[i] = data$LOGCFU[data$LZD==0&data$MER==0] -
    E.comb.LZDMER(OBJ_min_MER$par[1],OBJ_min_MER$par[2],OBJ_min_MER$par[3],
                  OBJ_min_LZD$par[1],OBJ_min_LZD$par[2],OBJ_min_LZD$par[3],
                  MER=i_MER,LZD=i_LZD) -
data$LOGCFU[data$LZD==i_LZD&data$MER==i_MER]
  p_values[i] =
  tsum.test(mean.x=data$LOGCFU[data$LZD==0&data$MER==0] -
            E.comb.LZDMER(OBJ_min_MER$par[1],OBJ_min_MER$par[2],OBJ_min_MER$par[3],

OBJ_min_LZD$par[1],OBJ_min_LZD$par[2],OBJ_min_LZD$par[3],
                            MER=i_MER,LZD=i_LZD),
        s.x=resid_LZDMER_SD,
        n.x=length(resid_LZD)+length(resid_MER),

        mean.y=data$LOGCFU[data$LZD==i_LZD&data$MER==i_MER],
        s.y=data$LOGCFU_SD[data$LZD==i_LZD&data$MER==i_MER],
        n.y=3)$p.value

}

# Bonferoni correction for multiple testing alpha/n
alpha = 0.05
n = length(data$LOGCFU)

cbind(data, delta_LOGCFU, p_values, p_values<.05, p_values<.05/n)
```

7.3.2 Final semi-mechanistic PD model for lag-phase *S. aureus*

```
#- PD model  ---------------------------------------------------------------
PD.model = function(t, cLZD, cMER, cVAN,
                    parms,logp.operator
){
  if(logp.operator==T){parms=exp(parms)}

  CFU.0 = 10^(parms[1])

  out=lsoda(c(CFU.0,0,0,      #init of bacterial concentrations
              1,0,1,0),   #init of adaption system --> all bacteria in AR_off
          t,
          function(t,S,parms){
            k.death.LZD     = parms[2]
            k.doub          = 100
            kper.MER        = parms[3]
            kper.VAN        = parms[4]
            k.death.per     = parms[5]
            EC50.MER        = parms[6]
            H.MER           = parms[7]
            beta.MER        = parms[8]
            tau.MER         = parms[9]
            Emax.MER.Eagle  = parms[10]
            EC50.MER.Eagle  = parms[11]
            H.MER.Eagle     = 4
            EC50.LZD        = parms[12]
```

```
                H.LZD            = parms[13]
                EC50.VAN        = parms[14]
                H.VAN           = 20
                Emax.VAN        = parms[15]
                beta.VAN        = parms[16]
                tau.VAN         = parms[17]
                EC50.VAN.ARI    = parms[18]
                CFU.MAX         = 10^(parms[19])
                k.deg.MER       = 0.01898    #Determined by HPLC
                k.deg.VAN       = 0.003898   #Determined by HPLC
                k.lag           = parms[20]
                k.rep           = parms[21]


                k12=k.rep*(1-exp(-k.lag*t)) *(1-(S[1]+S[2]+S[3])/(CFU.MAX))


                alpha.MER = 1 + beta.MER*S[5]

                alpha.VAN = 1 + beta.VAN*S[7]

                cMER_t = cMER*(exp(-k.deg.MER*t))
                cVAN_t = cVAN*(exp(-k.deg.VAN*t))

                MER = (1*cMER_t^H.MER)/
                        ((alpha.MER*EC50.MER)^H.MER + cMER_t^H.MER)

                MER.Eagle = (Emax.MER.Eagle * cMER_t^ H.MER.Eagle)/
                             (EC50.MER.Eagle^H.MER.Eagle + cMER_t^H.MER.Eagle)

                VAN = (1*cVAN_t^H.VAN)/
                        ((alpha.VAN*EC50.VAN)^H.VAN + cVAN_t^H.VAN)

                VANadaptonMER = ((1*cVAN_t)/(EC50.VAN.ARI + cVAN_t))

                LZD = (1*cLZD^H.LZD)/
                        (EC50.LZD^H.LZD + cLZD^H.LZD)

                dSdt=vector(len=7)
                dSdt[1] =- k.death.LZD*LZD*S[1]
                        - k12*(1-LZD)*S[1]
                        + k.doub*(1-MER*(1-MER.Eagle)*(1-VAN))
                                *(1-Emax.VAN*VAN)*S[2]*2 #GRO
                dSdt[2] = k12*(1-LZD)*S[1] - k.doub*S[2] - kper.MER*MER*S[2]
                          - kper.VAN*VAN*S[2] #REP
                dSdt[3] = kper.MER*MER*S[2] + kper.VAN*VAN*S[2]
                          - k.death.per*S[3] #PER

                #adaption model MER
                dSdt[4] =-(1-VANadaptonMER)*tau.MER*cMER_t*S[4]     #AR_off
                dSdt[5] = (1-VANadaptonMER)*tau.MER*cMER_t*S[4]     #AR_on

                #adaption model VAN
                dSdt[6] =-tau.VAN*cVAN_t*S[6]        #AR_off
                dSdt[7] = tau.VAN*cVAN_t*S[6]        #AR_on

                log10CFU.apparent=log10(S[1]+S[2]+S[3])

                list(dSdt, log10CFU.apparent)
              }
            , parms, rtol=1e-10)

  return(out[,9])  #return log10CFU.apparent
}

#- least squares OBJ -------------------------------------------------------
```

```r
#- function of parameter vector and operator to log-transform parameters
OBJ_OLS = function(parms,logp.operator){

  estdata=NULL
  i=0
  k=NULL

  for(k in 1:length(levels(factor(data_lag$FLAG_SOLVE)))){

    i = i + length(data_lag[,"TIME"][data_lag$FLAG_SOLVE==(k-1)])

    estdata[(i+1):(i+(length(data_lag[,"TIME"][data_lag$FLAG_SOLVE==k])))] =

      PD.model(data_lag[,"TIME"][data_lag$FLAG_SOLVE==(k)],
               data_lag[,"LZD"][data_lag$FLAG_SOLVE==(k)][1],
               data_lag[,"MER"][data_lag$FLAG_SOLVE==(k)][1],
               data_lag[,"VAN"][data_lag$FLAG_SOLVE==(k)][1],
               parms,logp.operator)
  }

  sum((data_lag[,"LOGCFU"] - estdata)^2, na.rm=T)

}

#- minimise OBJ_OLS_logp ------------------------------------------------------
OBJ_OLS(log(initials),logp.operator=TRUE) #check OBJ at initial estimates
OBJ_OLS_logp_min = optim(par = log(initials),
                    fn  = OBJ_OLS,
                    logp.operator=T,
                    method = "Nelder-Mead",
                    control = list(trace=T,
                                   maxit=3500,
                                   reltol=1e-3,
                                   parscale=log(initials),
                                   fnscale=OBJ_OLS(log(initials),logp.operator=T)),
                    hessian = F)


#- check parameter estimates
exp(OBJ_OLS_logp_min$par)

#- minimise OBJ_OLS using estimates of OBJ_OLS_logp_min as initial estimates ------
OBJ_OLS(exp(OBJ_OLS_logp_min$par),logp.operator=FALSE) #check OBJ at initials

OBJ_OLS_min = optim(par = exp(OBJ_OLS_logp_min$par),
                    fn  = OBJ_OLS,
                    logp.operator=FALSE,
                    method = "BFGS",
                    control = list(trace=T,
                                   maxit=300,
                                   reltol=1e-4,
                                   parscale=exp(OBJ_OLS_logp_min$par),
                                   fnscale=OBJ_OLS_logp_min$value),
                    hessian = T)
#- check parameter estimates
OBJ_OLS_min$par

#- calculate residual variance using MLE for sig2
sig2 = OBJ_OLS_min$value/ length(data_lag$LOGCFU)

#- invert Hessian (observed Fisher information matrix) to obtain variance-
#- covariance matrix; correct Hessian by 1/(2*sig2) as OLS was used instead of MLE!
var_covar_mat<-solve(OBJ_OLS_min$hessian/(2*sig2))

#- calculate standard errors of the estimates from diagonal elements of
#- var_covar_mat
```

```
prop_sigma<-sqrt(diag(var_covar_mat))

#- calculate 95% confidence intervals for parameter estimates(1.96 as n is large)
upper<-OBJ_OLS_min$par+1.96*prop_sigma
lower<-OBJ_OLS_min$par-1.96*prop_sigma

interval<-data.frame(value=OBJ_OLS_min$par,
                     lower=lower,
                     upper=upper)

#- Model diagnostics ----------------------------------------------------------
#- AIC formula
AIC = length(data_lag$LOGCFU) *
      log(OBJ_OLS_min$value/length(data_lag$LOGCFU)) +
      2*(length(OBJ_OLS_min$par)+1)

#- AICc fomula
AICc = AIC + (2*(length(OBJ_OLS_min$par)+1)*(length(OBJ_OLS_min$par)+2))/
             (length(data_lag$LOGCFU)-(length(OBJ_OLS_min$par)+1)-1)

#- minus 2* log-likelihood function
m2LogLik = -2*(-(length(data_lag$LOGCFU)/2)*log(2*pi) -
               (length(data_lag$LOGCFU)/2)*log(sig2) - 1/(2*sig2)*OBJ_OLS_min$value)

# VPC ------------------------------------------------------------------------
timepoints=seq(0,24,by=.1)
VPC=function(cLZD,cMER,cVAN,n,alpha){
  VPC_data = matrix(nrow=length(timepoints),ncol=n+1)
  VPC_data[,1] = timepoints
  for(i in 1:n){
      VPC_data[,i+1] = PD.model(timepoints,
                                cLZD=cLZD,
                                cMER=cMER,
                                cVAN=cVAN,
                                parms=mvrnorm(mu=OBJ_OLS_min$par, #parm uncertainty
                                              Sigma=var_covar_mat),
                                logp.operator=F) +
                       rnorm(n=1,mean=0,sd=sqrt(sig2)) #residual variability

}
VPC_out=rbind(TIME=timepoints,
              apply(VPC_data,1,
                    quantile,
                    probs=c((alpha/2),.5,1-(alpha/2)),na.rm=T))

return(VPC_out)
}

#- VPC execution ------------------------------------------------------------
VPC_plot=NULL
for (i in levels(factor(data_lag$FLAG2))){
VPC_plot[[paste(i)]] = VPC(cLZD=data_lag$LZD[data_lag$FLAG2==i][1],
                           cMER=data_lag$MER[data_lag$FLAG2==i][1],
                           cVAN=data_lag$VAN[data_lag$FLAG2==i][1],
                           1000,
                           .1)
print(paste("Processing currently:",i))
}


VPC_plot_df = NULL
for (i in levels(factor(data_lag$FLAG2))){
 VPC_plot_df_append = as.data.frame(t(VPC_plot[[paste(i)]]))
 VPC_plot_df = rbind(VPC_plot_df,cbind(VPC_plot_df_append,"FLAG2"=i))
}
```

```r
VPC_plot_df[1,]
colnames(VPC_plot_df) = c("TIME","lower","median","upper","FLAG2")

ggplot() +
  geom_ribbon(data=VPC_plot_df,aes(x=TIME,ymin=lower,ymax=upper),
               fill="black",alpha=.2) +
  geom_point(data=data_lag,aes(TIME, LOGCFU),shape=1) +
  geom_line(data=VPC_plot_df,aes(TIME, median),color="red") +
  facet_wrap( ~ FLAG2) +
  scale_x_continuous(name="Time [h]", breaks=c(0,6,12,18,24)) +
  scale_y_continuous(name="Log10 CFU/mL", breaks=c(0,2,4,6,8,10))

# Bootstrap ---------------------------------------------------------------
N_boot = 1200
Boot_pars = matrix(data=NA,nrow=N_boot,ncol=length(OBJ_OLS_min$par))
colnames(Boot_pars)=rownames(estimates_RSE)

for(j in 1:N_boot){

  data_lag_boot = data_lag[sample(seq(1:length(data_lag$LOGCFU)),
                                  size=length(data_lag$LOGCFU),
                                  replace=T),]

  data_lag_boot = data_lag_boot[order(data_lag_boot$TIME),]
  data_lag_boot = data_lag_boot[order(data_lag_boot$FLAG_SOLVE),]

OBJ_OLS_boot = function(parms,logp.operator){

  estdata=NULL
  i=0
  k=NULL

  for(k in 1:length(levels(factor(data_lag_boot$FLAG_SOLVE)))){

    i = i + length(data_lag_boot[,"TIME"][data_lag_boot$FLAG_SOLVE==(k-1)])


estdata[(i+1):(i+(length(data_lag_boot[,"TIME"][data_lag_boot$FLAG_SOLVE==k])))] =

      PD.model(data_lag_boot[,"TIME"][data_lag_boot$FLAG_SOLVE==(k)],
               data_lag_boot[,"LZD"][data_lag_boot$FLAG_SOLVE==(k)][1],
               data_lag_boot[,"MER"][data_lag_boot$FLAG_SOLVE==(k)][1],
               data_lag_boot[,"VAN"][data_lag_boot$FLAG_SOLVE==(k)][1],
               parms,logp.operator)
  }

  sum((data_lag_boot[,"LOGCFU"] - estdata)^2, na.rm=T)

}

print(paste("Bootstrap sample #",j))
OBJ_OLS_logp_boot_min = optim(par = log(OBJ_OLS_min$par),
                              fn  = OBJ_OLS_boot,
                              logp.operator=TRUE,
                              method = "Nelder-Mead",
                              control = list(trace=T,
                                             maxit=120,
                                             reltol=1e-3,
                                             parscale=log(OBJ_OLS_min$par),
                                             fnscale=OBJ_OLS_min$value),
                              hessian = F)

OBJ_OLS_boot_min = optim(par = exp(OBJ_OLS_logp_boot_min$par),
                         fn  = OBJ_OLS_boot,
                         logp.operator=FALSE,
                         method = "BFGS",
```

```
                     control = list(trace=T,
                                     maxit=300,
                                     reltol=1e-4,
                                     parscale=exp(OBJ_OLS_logp_min$par),
                                     fnscale=OBJ_OLS_logp_min$value),
                  hessian = F)
Boot_pars[j,] = OBJ_OLS_boot_min$par


}
```

7.3.3   Final semi-mechanistic PD model for log-phase *S. aureus*

```
#- PD model using non-transformed parms ------------------------------------------
PD.model = function(t, cLZD, cMER, cVAN,
                    parms,logp.operator
){
  if(logp.operator==T){parms=exp(parms)}

  CFU.0 = 10^(parms[1])

  out=lsoda(c(CFU.0,0,0,      #init of bacterial concentrations
              1,0,1,0),   #init of adaption system --> all bacteria in AR_off
            t,
            function(t,S,parms){
              k.death.LZD    = parms[2]
              k.death.log.LZD= parms[3]
              k.doub         = 100
              k.per.MER      = 2.651608e-04 #fixed to final est. to increase stab.
              k.per.VAN      = parms[4]
              k.death.per    = 0 #fixed to final est. to increase stab.
              EC50.MER       = parms[5]
              H.MER          = parms[6]
              beta.MER       = parms[7]
              tau.MER        = parms[8]
              EC50.LZD       = parms[9]
              H.LZD          = parms[10]
              EC50.LZD.log   = parms[11]
              H.LZD.log      = parms[12]
              k.LZD.arrest   = parms[13]
              EC50.VAN       = parms[14]
              H.VAN          = 20
              Emax.VAN       = parms[15]
              beta.VAN       = parms[16]
              tau.VAN        = parms[17]
              CFU.MAX        = 10^(parms[18])
              k.deg.MER      = 0.01898    #Determined by HPLC
              k.deg.VAN      = 0.003898   #Determined by HPLC
              k.rep          = parms[19]


              k12=k.rep*(1-(S[1]+S[2]+S[3])/(CFU.MAX))


              alpha.MER = 1 + beta.MER*S[5]

              alpha.VAN = 1 + beta.VAN*S[7]

              cMER_t = cMER*(exp(-k.deg.MER*t))
              cVAN_t = cVAN*(exp(-k.deg.VAN*t))

              MER = ((1*cMER_t^H.MER)/
                     ((alpha.MER*EC50.MER)^H.MER + cMER_t^H.MER) )

              VAN = ((1*cVAN_t^H.VAN)/
```

```
                          ((alpha.VAN*EC50.VAN)^H.VAN + cVAN_t^H.VAN) )

            LZD = ((1*cLZD^H.LZD)/(EC50.LZD^H.LZD + cLZD^H.LZD))
            LZD.log = ((1*cLZD^H.LZD.log)/(EC50.LZD.log^H.LZD.log +
                                                 cLZD^H.LZD.log))

            dSdt=vector(len=7)
            dSdt[1] = -k.death.LZD*LZD*S[1]
                    -k.death.log.LZD*LZD.log*exp(-k.LZD.arrest*t)*S[1]
                    -k12*(1-LZD)*S[1]
                    +k.doub*(1-MER)*(1-Emax.VAN*VAN)*S[2]*2 #GRO
            dSdt[2] = k12*(1-LZD)*S[1] - k.doub*S[2]
                    -k.per.MER*MER*S[2] - k.per.VAN*VAN*S[2] #REP
            dSdt[3] = k.per.MER*MER*S[2] + k.per.VAN*VAN*S[2]
                    -k.death.per*S[3] #PER

            #adaption model MER (Mohamed 2009 AAC)
            dSdt[4] = -tau.MER*cMER_t*S[4]      #AR_off
            dSdt[5] = tau.MER*cMER_t*S[4]       #AR_on

            #adaption model VAN (Mohamed 2009 AAC)
            dSdt[6] = -tau.VAN*cVAN_t*S[6]       #AR_off
            dSdt[7] = tau.VAN*cVAN_t*S[6]        #AR_on

            log10CFU.apparent=log10(S[1]+S[2]+S[3])

            list(dSdt, log10CFU.apparent)
          }
          , parms, rtol=1e-10)

  return(out[,9])
}

[further steps are similar as for lag-phase model (7.3.2)]
[...]
```

7.3.4   Adaptive optimal design

```
#- Compute anticipated RSE based on provided design --------------------------------
#- required:
#- * dataframe 'data_lag' with design columns:
#-    - TIME (sampling points in 'h' incl. anticipated replicates)
#-    - LZD (LZD concentration in 'mg/L')
#-    - MER (MER concentration in 'mg/L')
#-    - VAN (VAN concentration in 'mg/L')
#- * parameter vector 'parms' with anticipated values for model parameters
#- * anticipated residual variance 'sig2'

OD_PDMODEL_SEs = function(parms,sig2){

  # first 'parms'-derivatives of PD model (Jacobian)
  df      = jacobian(func = function(parms,logp.operator){

    estdata=NULL
    i=0
    k=NULL

    for(k in 1:length(levels(factor(data_lag$FLAG_SOLVE)))){

      i = i + length(data_lag[,"TIME"][data_lag$FLAG_SOLVE==(k-1)])

      estdata[(i+1):(i+(length(data_lag[,"TIME"][data_lag$FLAG_SOLVE==k])))] =

        # semi-mechanistic PD model
        PD.model(data_lag[,"TIME"][data_lag$FLAG_SOLVE==(k)],
```

```
                data_lag[,"LZD"][data_lag$FLAG_SOLVE==(k)][1],
                data_lag[,"MER"][data_lag$FLAG_SOLVE==(k)][1],
                data_lag[,"VAN"][data_lag$FLAG_SOLVE==(k)][1],
                parms,logp.operator=F)
    }

    estdata
  },
  x = parms,
  method = "simple")

  # expected Fisher information matrix
  FishInf  = 1/sig2 * (t(df)%*%df)

  # expected relative standard errors
  out      = sqrt(diag(solve(FishInf))) / initials *100
  out

}
```

7.3.5   Generation of the virtual patient population for clinical trial simulation

```
set.seed(1)
WT   = rlnorm(1000, meanlog = log(75), sdlog = .1)         # Total body weight
SEX  = rbinom(1000, 1, 0.5)                                # Sex (female = 1)
AGE  = round(rlnorm(1000, meanlog = log(35), sdlog = .1),0)# Age (yrs.)
CIR  = rbinom(1000, 1, 0.05)                               # Liver cirrhosis
                                                           # 0 = no, 1 = yes
SCR  = rlnorm(1000, meanlog = log(1.0), sdlog = .1)        # Serum creatinine
CLCR = (140-AGE)*WT/72/SCR * ifelse(SEX==1,0.85,1)         # Creatinine Clearance
                                                           # Cockcroft Gault


write.csv(cbind(WT,SEX,AGE,CIR,SCR,CLCR),
          "LMV01_virtual_population.csv",
          row.names=F)
```

7.3.6   Clinical trial simulation model (lag-phase example)

```
#- Load virtual patient population --------------------------------------------
virt_pat=read.csv("LMV01_virtual_population_20150502.csv")
var_covar_mat=read.csv("var-covar-mat_mod06.csv")
parms = read.csv("Estimates_mod06.csv")[,2]
names(parms) = read.csv("Estimates_mod06.csv")[,1]


CLCR = virt_pat$CLCR      # Creatinine clearance mL/min
WT   = virt_pat$WT        # Total body weight
AGE  = virt_pat$AGE       # Age (yrs.)
CIR  = virt_pat$CIR       # Liver cirrosis (LZD model; 0 = no, 1 = yes)

#- PK models (cf. analytical solutions presented in Monolix PK/PD Library
#-          http://www.lixoft.eu/wp-content/uploads/2015/06/PKPDlibrary.pdf)
#-=============================================================================
#- Meropenem Population PK model (Li et al JCP 2006) ---------------------------
MEROPENEM_PK=function(t,Inf_Dose,Inf_Dur,t_Dose,ETA,AGE,WT,CLCR){

  CL_i = 14.6 * (CLCR/83)^0.62 * (AGE/35)^-0.34 * exp(ETA[1])
  V1_i = 10.8 * (WT/70)^0.99                    * exp(ETA[2])
  Q_i  = 18.6                                   * exp(ETA[3])
  V2_i = 12.6                                   * exp(ETA[4])

  #convert parameters to rate constants
  k10 = CL_i/V1_i
```

```
  k12 = Q_i/V1_i
  k21 = Q_i/V2_i

  beta = 0.5 * (k12 + k21 + k10 - sqrt((k12 + k21 + k10)^2 - 4 * k21 * k10))
  alpha = (k21 * k10) / beta
  A = 1/V1_i * (alpha - k21)/(alpha - beta)
  B = 1/V1_i * (beta - k21)/(beta - alpha)

  if(t==0){cp=0}else{

    #infusion phase
    if(t-tail(t_Dose[t_Dose<t],1)<=tail(Inf_Dur[t_Dose<t],1)){
      cp = sum(
        ( Inf_Dose[t_Dose<t][-length(Inf_Dose[t_Dose<t])]/Inf_Dur[t_Dose<t][-
length(Inf_Dose[t_Dose<t])] *
            (A/alpha * (1-exp(-alpha*Inf_Dur[t_Dose<t][-
length(Inf_Dose[t_Dose<t])])) * exp(-alpha*(t-t_Dose[t_Dose<t][-
length(Inf_Dose[t_Dose<t])]-Inf_Dur[t_Dose<t][-length(Inf_Dose[t_Dose<t])])) +
              B/beta  * (1-exp(-beta*Inf_Dur[t_Dose<t][-
length(Inf_Dose[t_Dose<t])]))  * exp(-beta*(t-t_Dose[t_Dose<t][-
length(Inf_Dose[t_Dose<t])]-Inf_Dur[t_Dose<t][-length(Inf_Dose[t_Dose<t])]))) ) ) +
        ( tail(Inf_Dose[t_Dose<t],1)/tail(Inf_Dur[t_Dose<t],1) * (A/alpha * (1-
exp(-alpha*(t-tail(t_Dose[t_Dose<t],1)))) + B/beta * (1-exp(-beta*(t-
tail(t_Dose[t_Dose<t],1)))))))
    }
    # elimination phase
    if(t-tail(t_Dose[t_Dose<t],1)>tail(Inf_Dur[t_Dose<t],1)){
      cp = sum(

        Inf_Dose[t_Dose<t]/Inf_Dur[t_Dose<t] * (A/alpha * (1-exp(-
alpha*Inf_Dur[t_Dose<t])) * exp(-alpha*(t-t_Dose[t_Dose<t]-Inf_Dur[t_Dose<t])) +
                                    B/beta  * (1-exp(-
beta*Inf_Dur[t_Dose<t]))  * exp(-beta*(t-t_Dose[t_Dose<t]-Inf_Dur[t_Dose<t]))) )
    }
  }
  return(cp)
}

#- Vancomycin Population PK model (Llopis-Salvia et al J. Clin. Pharm. Ther. 2006)
-------------------------------------------------------
VANCOMYCIN_PK=function(t,Inf_Dose,Inf_Dur,t_Dose,ETA,WT,CLCR){

  CL_i = (0.034 * CLCR + 0.015 * WT) * (1 + ifelse(ETA[1]<= -1,0,ETA[1]))
  V1_i = (0.414 * WT)                * (1 + ifelse(ETA[2]<= -1,0,ETA[2]))
  Q_i  =  7.48
  V2_i = (1.32  * WT)                * (1 + ifelse(ETA[4]<= -1,0,ETA[4]))

  #convert parameters to rate constants
  k10 = CL_i/V1_i
  k12 = Q_i/V1_i
  k21 = Q_i/V2_i

  beta = 0.5 * (k12 + k21 + k10 - sqrt((k12 + k21 + k10)^2 - 4 * k21 * k10))
  alpha = (k21 * k10) / beta
  A = 1/V1_i * (alpha - k21)/(alpha - beta)
  B = 1/V1_i * (beta - k21)/(beta - alpha)

  if(t==0){cp=0}else{

    #infusion phase
    if(t-tail(t_Dose[t_Dose<t],1)<=tail(Inf_Dur[t_Dose<t],1)){
      cp = sum(
        ( Inf_Dose[t_Dose<t][-length(Inf_Dose[t_Dose<t])]/Inf_Dur[t_Dose<t][-
length(Inf_Dose[t_Dose<t])] *
            (A/alpha * (1-exp(-alpha*Inf_Dur[t_Dose<t][-
length(Inf_Dose[t_Dose<t])])) * exp(-alpha*(t-t_Dose[t_Dose<t][-
```

```
length(Inf_Dose[t_Dose<t]))]-Inf_Dur[t_Dose<t][-length(Inf_Dose[t_Dose<t]))])) +
               B/beta  * (1-exp(-beta*Inf_Dur[t_Dose<t][-
length(Inf_Dose[t_Dose<t]))]))  * exp(-beta*(t-t_Dose[t_Dose<t][-
length(Inf_Dose[t_Dose<t]))]-Inf_Dur[t_Dose<t][-length(Inf_Dose[t_Dose<t])]))) ) ) +
        ( tail(Inf_Dose[t_Dose<t],1)/tail(Inf_Dur[t_Dose<t],1) * (A/alpha * (1-
exp(-alpha*(t-tail(t_Dose[t_Dose<t],1)))) + B/beta * (1-exp(-beta*(t-
tail(t_Dose[t_Dose<t],1))))))
    }
    # elimination phase
    if(t-tail(t_Dose[t_Dose<t],1)>tail(Inf_Dur[t_Dose<t],1)){
      cp = sum(

        Inf_Dose[t_Dose<t]/Inf_Dur[t_Dose<t] * (A/alpha * (1-exp(-
alpha*Inf_Dur[t_Dose<t])) * exp(-alpha*(t-t_Dose[t_Dose<t]-Inf_Dur[t_Dose<t])) +
                                     B/beta  * (1-exp(-
beta*Inf_Dur[t_Dose<t]))  * exp(-beta*(t-t_Dose[t_Dose<t]-Inf_Dur[t_Dose<t]))) )
    }
  }
  return(cp)
}


#- Linezolid Population PK model (Sasaki et al AAC 2011) -------------------------
------------------------
LINEZOLID_PK = function(t,Inf_Dose,Inf_Dur,t_Dose,ETA,WT,CLCR,CIR){

  CL_i = (2.85 * (CLCR/60.9)^0.618 * 0.472^CIR) * exp(ETA[1])
  V1_i = (33.6 * WT/57.9)                       * exp(ETA[2])

  #convert parameters to rate constants
  kel = CL_i/V1_i
  Vd  = V1_i

  if(t==0){cp=0}else{
    if(t-tail(t_Dose[t_Dose<t],1)<=tail(Inf_Dur[t_Dose<t],1)){
      cp = sum(
        ( Inf_Dose[t_Dose<t][-length(Inf_Dose[t_Dose<t])]/Inf_Dur[t_Dose<t][-
length(Inf_Dose[t_Dose<t])] * 1/(kel*Vd) *
            (1-exp(-kel*Inf_Dur[t_Dose<t][-length(Inf_Dose[t_Dose<t])]))*exp(-
kel*(t-t_Dose[t_Dose<t][-length(Inf_Dose[t_Dose<t])]-Inf_Dur[t_Dose<t][-
length(Inf_Dose[t_Dose<t])])) )) +
        tail(Inf_Dose[t_Dose<t],1)/tail(Inf_Dur[t_Dose<t],1)*1/(kel*Vd)*(1-exp(-
kel*(t-tail(t_Dose[t_Dose<t],1)))))

    }

    if(t-tail(t_Dose[t_Dose<t],1)>tail(Inf_Dur[t_Dose<t],1)){
      cp = sum(
        ( Inf_Dose[t_Dose<t]/Inf_Dur[t_Dose<t] * 1/(kel*Vd) *
            (1-exp(-kel*Inf_Dur[t_Dose<t]))*exp(-kel*(t-t_Dose[t_Dose<t]-
Inf_Dur[t_Dose<t])) ))
    }}
  return(cp)
}


#-=============================================================================
#-Covariates for virtual patient population -----------------------------------

CLCR = virt_pat$CLCR      # Creatinine clearance mL/min
WT   = virt_pat$WT        # Total body weight
AGE  = virt_pat$AGE       # Age (yrs.)
CIR  = virt_pat$CIR       # Liver cirrosis (LZD model; 0 = no, 1 = yes)

#-Nr of stochastic simulations ------------------------------------------------

N_sim = 1000
```

```
#- population PK/PD model  -----------------------------------------------
PKPD.model = function(t,
                      parms,
                      PKparms.MER,
                      PKparms.VAN,
                      PKparms.LZD,
                      init.cond,
                      MIC_MER,
                      MIC_VAN,
                      MIC_LZD
){

  GRO      =init.cond[1]
  REP      =init.cond[2]
  PER      =init.cond[3]
  ARoff.MER=init.cond[4]
  ARon.MER =init.cond[5]
  ARoff.VAN=init.cond[6]
  ARon.VAN =init.cond[7]

  out=lsoda(c(GRO,REP,PER,                           #init of bacteria
            ARoff.MER,ARon.MER,ARoff.VAN,ARon.VAN,   #init of adaption system
                                                     #--> all bacteria in AR_off
            fAUC_MER=0,fTMIC_MER=0,                  #init of fAUC and T>MIC
            fAUC_LZD=0,fTMIC_LZD=0,                  #init of fAUC and T>MIC
            fAUC_VAN=0,fTMIC_VAN=0),                 #init of fAUC and T>MIC
          t,
          function(t,S,parms){

              k.death.LZD    = parms[2]
              k.doub         = 100
              kper.MER       = parms[3]
              kper.VAN       = parms[4]
              k.death.per    = parms[5]
              EC50.MER       = parms[6]
              H.MER          = parms[7]
              beta.MER       = parms[8]
              tau.MER        = parms[9]
              Emax.MER.Eagle = parms[10]
              EC50.MER.Eagle = parms[11]
              H.MER.Eagle    = 4
              EC50.LZD       = parms[12]
              H.LZD          = parms[13]
              EC50.VAN       = parms[14]
              H.VAN          = 20
              Emax.VAN       = parms[15]
              beta.VAN       = parms[16]
              tau.VAN        = parms[17]
              EC50.VAN.ARI   = parms[18]
              CFU.MAX        = 10^(parms[19])
              k.deg.MER      = 0.01898    #Determined by HPLC
              k.deg.VAN      = 0.003898   #Determined by HPLC
              k.lag          = parms[20]
              k.rep          = parms[21]

              k12=k.rep*(1-exp(-k.lag*t)) *(1-(S[1]+S[2]+S[3])/(CFU.MAX))


              alpha.MER = 1 + beta.MER*S[5]

              alpha.VAN = 1 + beta.VAN*S[7]

              cMER_t = MEROPENEM_PK(t,
                                    PKparms.MER$Inf_Dose,
                                    PKparms.MER$Inf_Dur,
                                    PKparms.MER$t_Dose,
```

```
                            PKparms.MER$ETA,
                            PKparms.MER$AGE,
                            PKparms.MER$WT,
                            PKparms.MER$CLCR) *0.98 #--> correction for
                                                   #protein binding (FI)
        cVAN_t = VANCOMYCIN_PK(t,
                            PKparms.VAN$Inf_Dose,
                            PKparms.VAN$Inf_Dur,
                            PKparms.VAN$t_Dose,
                            PKparms.VAN$ETA,
                            PKparms.VAN$WT,
                            PKparms.VAN$CLCR) *0.672 #--> correction for
                                                    #protein binding
                                                    #(Kees JCP 2014)
        cLZD_t = LINEZOLID_PK(t,
                            PKparms.LZD$Inf_Dose,
                            PKparms.LZD$Inf_Dur,
                            PKparms.LZD$t_Dose,
                            PKparms.LZD$ETA,
                            PKparms.LZD$WT,
                            PKparms.LZD$CLCR,
                            PKparms.LZD$CIR) *0.866 #--> correction for
                                                   #protein binding
                                                   #Buerger AAC 2006

        MER = ((1*(cMER_t*1)^H.MER)/ #--> no correction for penetration
              ((alpha.MER*EC50.MER)^H.MER + (cMER_t*1)^H.MER) )

        LZD = ((1*cLZD_t^H.LZD)/ #--> no correction for penetration
              (EC50.LZD^H.LZD + cLZD_t^H.LZD) )

        VAN = ((1*(cVAN_t*1)^H.VAN)/ #--> no correction for penetration
              ((alpha.VAN*EC50.VAN)^H.VAN + (cVAN_t*1)^H.VAN) )

        VANadaptonMER = ((1*cVAN_t)/( EC50.VAN.ARI + cVAN_t))

        MER.Eagle = (Emax.MER.Eagle * cMER_t^ H.MER.Eagle)/
                    (EC50.MER.Eagle^H.MER.Eagle + cMER_t^H.MER.Eagle)

        dSdt=vector(len=13)
        dSdt[1] =- k.death.LZD*LZD*S[1]
                - k12*(1-LZD)*S[1]
                + k.doub*(1-MER*(1-MER.Eagle)*(1-VAN))
                    *(1-Emax.VAN*VAN)*S[2]*2
        dSdt[2] = k12*(1-LZD)*S[1] - k.doub*S[2] - kper.MER*MER*S[2]
                - kper.VAN*VAN*S[2]
        dSdt[3] = kper.MER*MER*S[2] + kper.VAN*VAN*S[2] - k.death.per*S[3]

        #adaption model MER
        dSdt[4] =-(1-VANadaptonMER)*tau.MER*cMER_t*S[4]     #AR_off
        dSdt[5] = (1-VANadaptonMER)*tau.MER*cMER_t*S[4]     #AR_on

        #adaption model VAN
        dSdt[6] =-tau.VAN*cVAN_t*S[6]       #AR_off
        dSdt[7] = tau.VAN*cVAN_t*S[6]       #AR_on

        FMER=ifelse(cMER_t>MIC_MER,1,0)
        dSdt[8] = cMER_t                    #fAUC MER in plasma
        dSdt[9] = FMER                      #fTMIC MER calculation in plasma

        FLZD=ifelse(cLZD_t>MIC_LZD,1,0)
        dSdt[10] = cLZD_t                    #fAUC LZD in plasma
        dSdt[11] = FLZD                      #fTMIC LZD calculation in plasma

        FVAN=ifelse(cVAN_t>MIC_VAN,1,0)
        dSdt[12] = cVAN_t                    #fAUC VAN in plasma
```

```
                dSdt[13] = FVAN                         #fTMIC VAN calculation in plasma

                log10CFU.apparent=log10(S[1]+S[2]+S[3])

                list(dSdt, cMER_t=cMER_t, cVAN_t=cVAN_t, cLZD_t=cLZD_t,
                    Ntot=log10CFU.apparent)
            }
            , parms, rtol=1e-10)

  return(out)
}

# Stochastic simulations MER 500 mg TID
init.cond=c(
  GRO       =10^6,
  REP       =0,
  PER       =0,
  ARoff.MER=1,
  ARon.MER =0,
  ARoff.VAN=1,
  ARon.VAN =0)

MER_500_TID = data.frame(NULL)
MER_500_TID_append = data.frame(NULL)
for (i in 1:N_sim){
  MER_500_TID_append =
    PKPD.model(c(0,.001,seq(0.2,24,.2)),
              parms=mvrnorm(n=1,mu=parms,Sigma=var_covar_mat),
              PKparms.MER=list(Inf_Dose=c(500,500,500),
                              Inf_Dur=c(1,1,1),
                              t_Dose=c(0,8,16),
                              ETA=c(rnorm(1,mean=0,sd=sqrt(0.118)), #iiv CL
                                    rnorm(1,mean=0,sd=sqrt(0.143)), #iiv V1
                                    rnorm(1,mean=0,sd=sqrt(0.290)), #iiv Q
                                    rnorm(1,mean=0,sd=sqrt(0.102))),#iiv V2
                              AGE=AGE[i],
                              WT=WT[i],
                              CLCR=CLCR[i]),
              PKparms.VAN=PKparms.VAN.dummy,
              PKparms.LZD=PKparms.LZD.dummy,
              init.cond,
              MIC_MER=0.125,MIC_VAN=1,MIC_LZD=2)

  MER_500_TID = rbind(MER_500_TID,MER_500_TID_append)

  print(i)
}
```

8 Publications

8.1 Original articles

M.G. Kees, **S.G. Wicha**, A. Seefeld, F. Kees, C. Kloft
Unbound fraction of vancomycin in intensive care unit patients.
J. Clin. Pharmacol. 54: 318-323 (2014).
doi: 10.1002/jcph.175

U. Liebchen, A. Kratzer, **S.G. Wicha**, F. Kees, C. Kloft, M.G. Kees
Unbound fraction of ertapenem in intensive care unit patients.
J. Antimicrob. Chemother. 69: 3108-3111 (2014).
doi: 10.1093/jac/dku226

C. Scheerans[§], **S.G. Wicha**[§], J. Michael, H. Derendorf, C. Kloft
Concentration–response studies and modelling of the pharmacodynamics of linezolid: Staphylococcus aureus versus Enterococcus faecium.
Int. J. Antimicrob. Agents. 45: 54-60 (2015). ([§] equal contribution)
doi: 10.1016/j.ijantimicag.2014.07.028

S.G. Wicha, M.G. Kees, A. Solms, I.K. Minichmayr, A. Kratzer, C. Kloft
TDMx – a novel web-based open-access support tool for optimising antimicrobial dosing regimens in clinical routine.
Int. J. Antimicrob. Agents. 45: 442-444 (2015).
doi: 10.1016/j.ijantimicag.2014.12.010

S.G. Wicha, M.G. Kees, J. Kuss, C. Kloft
Pharmacodynamic and response surface analysis of linezolid or vancomycin combined with meropenem against Staphylococcus aureus.
Pharm. Res. 32: 2410-2418 (2015).
doi: 10.1007/s11095-015-1632-3

S.G. Wicha, K. Zink, T. Haak, F. Kees, C. Kloft , M.G. Kees
Pharmacokinetic/pharmacodynamic analysis of moxifloxacin in patients with diabetic foot infections.
J. Clin. Pharmacol. 55: 639-646 (2015).
doi: 10.1002/jcph.464

M.G. Kees, I.K. Minichmayr, S. Moritz, S. Beck, **S.G. Wicha**, F. Kees, C. Kloft, T. Steinke
Population pharmacokinetics of meropenem during continuous infusion in surgical ICU patients.
J. Clin. Pharmacol. Epub ahead of print (2015).
doi: 10.1002/jcph.600

S.G. Wicha, C. Kloft
Simultaneous determination and stability studies of linezolid, meropenem and vancomycin in bacterial growth medium by high-performance liquid chromatography.
(in manuscript)

S.G. Wicha, E. Goebgen, J. Kuss, C. Kloft
Beyond the inoculum effect: The growth state at drug exposure influences the effect of various antibiotics against Staphylococcus aureus.
(in manuscript)

S.G. Wicha, R.G. Mundkowski, A. Klock, U.T. Hopt, B. Drewelow, C. Kloft, T. Keck, U.A. Wittel
Pharmacokinetics of moxifloxacin in serum and pancreatic juice following pancreaticoduodenectomy.
(in manuscript)

S.G. Wicha, W. Huisinga, A. Solms, C. Kloft
Semi-mechanistic PK/PD modelling of drug interactions between vancomycin or linezolid combined with meropenem against Staphylococcus aureus.
(in preparation)

8.2   Review articles

S. Beck[§], **S.G. Wicha**[§], M.G. Kees C. Kloft
Pharmakokinetik und Pharmakodynamik der Antibiotikatherapie.
Der Anaesthesist. 63: 775-782 (2014) ([§] equal contribution)
doi: 10.1007/s00101-014-2369-9

8.3   Conference abstracts (oral/poster)

L. Klopp-Schulze, M. Joerger, Z. P. Parra-Guillen, **S. G. Wicha**, C. Kloft
Making use of modelling and simulations: Towards individualised tamoxifen therapy in breast cancer.
Annual Meeting of the Central European Society of Anticancer Drug Research (CESAR), Innsbruck, Austria, 17-19 September 2015.
(oral presentation)

E.B. Goebgen, **S.G. Wicha**, C. Kloft
Rapid bacterial cell counting method: proof-of-principle with a batch culture of E. coli.
Annual Meeting of the German Pharmaceutical Society (DPhG), Düsseldorf, Germany, 23-25 September 2015.
(poster presentation)

S.G. Wicha, R. Mundkowski, A. Klock, U. Wittel, U. Wellner, T. Keck, C. Kloft
Suitability of Moxifloxacin to Treat Pancreatic Infections from a Pharmacokinetic Perspective.
55th Interscience Conference on Antimicrobial Agents and Chemotherapy (ICAAC), San Diego, USA, 17-21 September 2015.
(poster presentation)

S.G. Wicha, M.G. Kees, A. Solms, I. K. Minichmayr, A. Kratzer, C. Kloft
TDMx: A web-application for therapeutic drug monitoring enhanced by Pharmacometrics.
24th Population Approach Group Europe (PAGE), Hersonissos, Crete, 2-5 June 2015.
[http://www.page-meeting.org/?abstract=3622]
(software demonstration)

S.G. Wicha, A. Solms, W. Huisinga, C. Kloft
Evaluation of the delta-method to efficiently compute probability of target attainment of antibiotics.
24th Population Approach Group Europe (PAGE), Hersonissos, Crete, 2-5 June 2015.
[http://www.page-meeting.org/?abstract=3445]
(poster presentation)

S.G. Wicha, A. Kratzer, C. Kloft
TDMx: Eine Web-Applikation zur Dosierungsoptimierung von Antiinfektiva.
40th Congress of the German Association of Hospital Pharmacists (ADKA), Mannheim, Germany, 28.-30. Mai 2015.
(poster and oral presentation)

S.G. Wicha, M.G. Kees, A. Solms, I.K. Minichmayr, A. Kratzer, C. Kloft
TDMx: A web application for bedside model-supported therapeutic drug monitoring to improve antibiotic therapy.
25th European Congress of Clinical Microbiology and Infectious Diseases, Copenhagen, Denmark, 25.-28 April 2015.
(poster presentation)

S.G. Wicha, E. Goebgen, J. Kuss, C. Kloft
Growth state at drug exposure highly influences the pharmacodynamics of linezolid, levofloxacin, meropenem and vancomycin in time-kill studies with Staphylococcus aureus.
25th European Congress of Clinical Microbiology and Infectious Diseases, Copenhagen, Denmark, 25.-28 April 2015.
(poster presentation)

E. Goebgen, **S.G. Wicha**, C. Kloft
Assessing the antibiotic effect with a simple, rapid and reliable quantification assay for counting clinically relevant strains with a CASY coulter counter.
25th European Congress of Clinical Microbiology and Infectious Diseases, Copenhagen, Denmark, 25.-28 April 2015.
(poster presentation)

I.K. Minichmayr, T. Steinke, S. Moritz, S. Beck, **S.G. Wicha**, M.G. Kees, C. Kloft
Determinants of piperacillin clearance in critically ill patients receiving continuous infusion: Comparison of cystatin C-based and alternative markers of renal function.
25th European Congress of Clinical Microbiology and Infectious Diseases, Copenhagen, Denmark, 25.-28 April 2015.
(poster presentation)

A.K. Appelt, D. Kauzor, **S.G. Wicha**, H. Brosig, M. Zeitlinger, C. Kloft
HPLC method development for the determination of linezolid and cefuroxime in synovial fluidsite microdialysis samples of arthritis patients
Annual Meeting of the Deutsche Pharmazeutische Gesellschaft (DPhG), Frankfurt, 24.-26. September 2014.
(poster presentation)

S.G. Wicha, A. Solms, W. Huisinga, C. Kloft
Adaptive optimal design for the concentration tiers in time-kill curve experiments.
23rd Population Approach Group Europe (PAGE), Alicante, Spain, 10-13 June 2014.
[http://www.page-meeting.org/default.asp?abstract=3202]
(poster presentation)

S.G. Wicha, K. Zink, T. Haak, F. Kees, C. Kloft, M.G. Kees
Pharmacokinetic/pharmacodynamic analysis of moxifloxacin in patients with diabetic foot infections.
24th European Congress of Clinical Microbiology and Infectious Diseases, Barcelona, Spain, 10.-13. May 2014.
(poster presentation)

S.G. Wicha, J. Kuss, W. Huisinga, C. Kloft
Semi-mechanistic PK/PD modelling of drug interactions between vancomycin or linezolid combined with meropenem against Staphylococcus aureus.
24th European Congress of Clinical Microbiology and Infectious Diseases, Barcelona, Spain, 10.-13 May 2014.
(poster presentation)

Kratzer, U. Liebchen, **S.G. Wicha**, F. Kees, M.G. Kees
Protein binding of ertapenem in plasma from healthy volunteers and from ICU patients
24th European Congress of Clinical Microbiology and Infectious Diseases, Barcelona, Spain, 10.-13. May 2014.
(poster presentation)

S.G. Wicha, W. Huisinga, C. Kloft
Mechanism-based PK/PD modelling of antagonistic drug-drug interactions exemplified by linezolid and meropenem against S. aureus.
Annual Meeting of the Deutsche Pharmazeutische Gesellschaft (DPhG), Freiburg, 09.-11. October 2013.
(poster and oral presentation)

S.G. Wicha, M.G. Kees, C. Kloft
In vitro time kill curve studies of linezolid and meropenem in combination against methicillin susceptible Staphylococcus aureus in different growth phases.
23rd European Congress of Clinical Microbiology and Infectious Diseases, Berlin, Germany, 27.-30. April 2013.
(poster presentation)

S.G. Wicha, C. Kloft
Evaluation of combinatory use of linezolid and meropenem against methicillin susceptible S. aureus by dynamic checkerboard testing.
Annual Meeting of the Deutsche Pharmazeutische Gesellschaft (DPhG), Greifswald, Deutschland, 11.-13. October 2012.
(poster presentation)

E. Goebgen, **S.G. Wicha**, C. Kloft
Development of a simple, rapid and reliable assay to count enterococcus faecium with a CASY coulter counter to assess antibiotic therapy.
Annual Meeting of the Deutsche Pharmazeutische Gesellschaft (DPhG), Greifswald, Deutschland, 11.-13. October 2012.
(poster presentation)

8.4 Presentations without abstract

S.G. Wicha
TDMx: A bedside web-based support tool to guide intermittent vs. continuous infusion of beta-lactams.
25th Meeting of the International Society of Antiifective Pharmacology, San Diego, USA 21. September 2015.

S.G. Wicha, C. Kloft
Does linezolid antagonise the bactericidal effect of meropenem?
Tag der Pharmazie, Berlin, Germany, 6. June 2012.

H. Derendorf, D. Gonzalez, D. Conrado, **S. G. Wicha**
Benefits and risks of pharmacokinetic and pharmacodynamic drug-drug interactions in anti-infective therapy
DDI 2011 – 2nd International workshop on regulatory requirements and current scientific aspects on preclinical and clinical of drug-drug interactions, Schloss Marbach, Germany, 1.-3. May 2011.

9 Curriculum vitae

For reasons of data protection, the curriculum vitae is not published in
the electronic version